River temperature under change: understanding the potential of riparian forest and landscape properties for climate adaptation

By

Dominic Eardly

A thesis submitted to

the University of Birmingham

for the degree of

DOCTOR OF PHILOSOPHY

School of Geography, Earth and Environmental Sciences

College of Life and Environmental Sciences

University of Birmingham

October 2024

Abstract

Climate change has driven global stream temperature increases in recent decades and poses a challenge to cold water adapted fish such as Atlantic salmon (*Salmo* salar) and Brown trout (*Salmo* trutta) whose populations are in decline. Beyond fish populations, elevated stream temperatures also pose risks to electric power generation (Van Vliet et al., 2013) and the production of drinking water (Delpla et al., 2009), making the mitigation of rising temperatures associated with climate change of socioeconomic importance (Hannah & Garner, 2015). Riparian tree planting is one of a limited number of mitigation strategies available to freshwater fisheries and river management, limiting summer stream temperature increases by providing shade to channels. Research indicates that planting in small headwater streams is most effective, but larger rivers, where adult salmonids are often found in summer, remain vulnerable. Previous studies using process-based stream temperature models have typically been limited to small scale stream reaches and as a result, are unable to capture the impact of cooled tributary inflows on larger rivers. The aim of this thesis was to further inform riparian planting strategies by elucidating the impact of cooled tributary inflows and the influence of heat advection on larger mainstem rivers. These research gaps were addressed by increasing the scale of modelling from reaches and sub-catchments to larger nested catchments with the following four-step methodology: (1), a six-point energy balance study was undertaken within a nested headwater catchment, using high-temporal-resolution hydrometeorological data at a novel spatial resolution of six locations across three sub-catchments to identify spatiotemporal patterns in energy fluxes within and between catchments; (2) these data were interpolated from point observations to 50m intervals along river networks, complemented with hydrometeorological data obtained from a novel roving weather station measuring for discrete 24 hour periods at a higher sub-km spatial resolution within the study area; (3) these newly-developed datasets were then incorporated into process-based stream temperature models to assess their influence on model performances; and (4) three sub-catchment models were

combined to assess the immediate and downstream temperature influence of a series of riparian planting strategies across stream networks and at catchment outlets.

The key findings are: (1) within a Scottish headwater catchment, controlled for land-use, observed stream energy fluxes show spatiotemporal variation within and between sub-catchments, with the presence of a shallow loch disrupting longitudinal patterns in stream temperature; (2) inverse distance weighting using Euclidean distances was shown to be the most effective method for scaling micrometeorology within and between nested catchments of a Scottish headwater catchment; (3) the use of scaled micrometeorology improved the performance of process-based stream temperature models when compared with standard model inputs; and (4) within the study area, the largest catchment scale stream temperature reductions were obtained by planting headwaters and upstream tributaries but largest stream temperature reductions at the mainstem outlet were achieved by planting at the mainstem outlet locality itself. Within the scale of study area investigated, the diminishing returns in stream temperature reduction when planting in larger rivers were not large enough to overcome the diminishing stream temperature reductions observed in the advection of upstream cooling. These results represent new insights into the best-use of riparian tree planting when looking to mitigate elevated summer stream temperatures with climate change.

Acknowledgements

I would first like to thank David Hannah, Faye Jackson, Iain Malcolm, Steve Dugdale and Stefan Krause for their supervision over the past four years. Beginning the PhD during COVID lockdown, it took longer than I'd have liked to meet many of you in person but with these constraints among others, I was always impressed with the time you made for me alongside hectic schedules. Peers were always surprised and often alarmed when I told them I had five supervisors but the expertise you each provided for the PhD project was always harmonious and invaluable.

I thank the Royal Society for funding this PhD. I also thank the University of Birmingham, Marine Directorate and University of Nottingham for providing support.

I would also like to thank my friends spread across the Geography building, be they Nine and Adria helping me take my first steps with R, old Grace for joining me in the gym, young Grace and Andrea for joining me at the CBS, the true Cathedral of Football, Gianni and Manon always providing positive vibes, Alex and Aaron standing in for Statler and Waldorf, Jess for introducing me to the best wild swim spots, Hannah never failing to impress me with her crocheting skills and Lisa baking me vegan friendly treats. I don't know half of you half as well as I should like; and I like less than half of you half as well as you deserve.

A special mention goes to my very good friend, Joe, for allowing me to move in for a couple of weeks…months…years during a very difficult time for me. I wouldn't have been able to finish this PhD without your support and generosity. Warne out. Mentions, too, go to Third Team BBB for the regular footballing lessons we provided down at power league on a cold and rainy Tuesday night.

I'd like to thank my parents, too, for allowing me to move back home to finish the write up once funding had run out. I'll be out of your hair soon enough.
Finally, I'd like to thank Fleur for tolerating me throughout the PhD. You've been so patient with me as I go into too much forensic detail about rivers when you ask how my day has been and you've put up with me postponing our travels time and time again. We can go soon, I promise!

Contents

List of Figures

List of Tables

1. Introduction

1.1. Context

Climate change will impact river ecosystems as a consequence of extreme low flows and increasing air temperatures leading to high river water temperature events (Hannah & Garner, 2015; Garner et al., 2017; White et al., 2023). In recent decades, stream temperature has been recognised increasingly in the freshwater science community as an important variable controlling physical, chemical and biological conditions (Hannah, et al., 2008). As well as being an important water quality parameter in its own right, it is a major influence on biogeochemical cycles in river ecosystems, acting as a primary control on the rates of gross primary production and ecosystem respiration within the carbon cycle (Comer-Warner et al., 2018). Stream temperature is strongly associated with the distribution (Isaak & Young, 2023), abundance (Gallagher et al., 2022), competition between species (Skoglund et al., 2024), growth (Elliot & Elliot, 2010), demographic structure (Gurney *et al*., 2008) and phenology (Otero *et al*., 2014) of salmonid fish. With global stream water quality deteriorating under extreme temperatures associated with climate change (van Vliet, et al., 2023) and the potential for negative synergistic relationships with other pressures including excess nutrients (Vagheei *et al*., 2023), there are growing concerns for the present and future environmental health of freshwater habitats (Ficklin et al., 2023).

Atlantic salmon (*Salmo* salar) and brown trout (*Salmo* trutta) are native species that are widespread across Scotland, important to rural communities and environmentally as a keystone species for freshwater environments. Atlantic salmon also have a strong cultural significance as a feature of Scottish mythology; and economic significance as a source of international angling tourism. The most recent economic assessment indicated that £135 m of angler expenditure and 4,300 full-time jobs are connected to wild fisheries, which primarily concern salmon and trout angling (PACEC, 2017).

Salmon face a wide range of pressures which often act in combination. These include, but are not limited to angling, predation, disease and parasites, genetic introgression, freshwater quality and quantity, barriers to migration, and thermal habitat (Marine Directorate, 2021). As a result, the number of salmon returning to Scotland's coasts has declined since the early 1970s. Initial declines were offset by reductions in exploitation in the coastal, estuarine and in-river environments. However, with these mechanisms exhausted, spawner numbers have also begun to decline since ca. 2010 (Marine Directorate, 2021). The primary cause of this decline is thought to be poor marine survival. Although the exact causes are unknown, marine climate change is thought to be a potential driver, altering marine habitat suitability and feeding opportunities (Strom et al., 2023; Tyldesley *et al*., 2024). Unfortunately, pressures in the marine environment are not readily susceptible to management due to the limited jurisdiction associated with trans-national ranges. Consequently, fisheries managers have focussed their attention on managing pressures in freshwater with the aim of maximising production and quality of wild salmon smolts from freshwaters (Thorstad *et al*., 2021).

As a species protected under the EU Habitats Directive (European Union, 1992), the Scottish Biodiversity List, the OSPAR list of threatened or declining habitats and species (OSPAR, 2015) and the UN Convention for the Conservation of Salmon in the North Atlantic Ocean (North Atlantic Salmon Convservation Organization, 2020), the Scottish government has international obligations and legal requirements to conserve and protect its Atlantic salmon populations and their habitats in Scottish marine and freshwaters.

Scientific research and monitoring play a crucial role in the management of Scotland's Atlantic salmon populations. The Scottish and UK governments, in conjunction with charities, industry, EU and UK Research Councils, support a range of initiatives to build a scientific evidence base for management decisions. The Marine Directorate programme focuses on the provision of essential data for national policy and local management actions, that includes climate change adaptation strategies, working closely with other parts of government and external stakeholders including fisheries trusts and boards (Marine Directorate, 2022).

1.2. Research gaps

River managers have advocated bankside tree planting to help river ecosystems adapt to climate change - by providing increased shading, especially in summer (DeWalle, 2008; Fuller et al., 2022; Johnson & Wilby, 2015; Malcolm et al., 2004a; Roth et al., 2010; Swartz et al., 2020; Trimmel et al., 2018). Recent research has led to the development of statistical models that identify broad regions of Scotland where rivers are hottest and most sensitive to climate change (Jackson et al., 2018) and complimentary process-based models that identify the reaches where riparian planting would be most effective in reducing river temperatures (Jackson et al., 2021a). When combined these models provide a strong scientific basis for prioritising riparian tree planting, forming a central component of the Scottish Government's efforts in relation to climate change adaptation in support of salmon.

Despite these major scientific developments, there remain a number of challenges in the provision of tree planting advice. In particular, it is unclear which strategies are likely to be most effective in reducing temperature in larger rivers, where effective shading is harder to achieve, water volumes are greater and residence times shorter (Jackson *et al*., 2021). In these circumstances it remains unclear whether planting should be undertaken on larger rivers or focussed on contributing tributaries, to either reduce overall temperatures on the larger rivers or to create localised thermal refugia (Dugdale et al., 2013).

Given this context, there remains an urgent need for research on optimal tree planting to understand the resilience of rivers to climate change and yield applied management tools for resource managers, with a particular focus on intermediate and larger rivers and the role that tree planting in tributary streams could play. Answering these questions requires models that are able to adequately represent heat advection and straddle spatial scales, moving from smaller to larger rivers. These scientific challenges are likely to be most readily addressed through process-based, rather than statistical modelling approaches.

Dugdale et al (2017) provided a comprehensive review of process-based models, which simulate river temperature by accounting for physical processes such as heat exchange between the river and its surroundings. It also identified which models comprised routines capable of representing the effects of riparian woodland, and thereby allow for virtual experiments for assessing the potential effects of riparian planting scenarios on stream temperatures. This review highlighted (a) the strengths and weaknesses of existing models, underscoring the necessity for more precise and dependable predictions and (b) stressed the importance of high-quality meteorological and physiographic input data for model calibration and validation. The review states that the scarcity of such data can significantly hinder the effectiveness of these models when attempting to make accurate predictions.

However, the acquisition of high-quality meteorological input data presents its own challenges. Many stream temperature studies, particularly those investigating headwater catchments, are conducted in remote locations where there are no high-quality meteorological data available (Dugdale, et al., 2017). Where existing data can be found, they are typically in the form of point data from a single weather station which can be located outside of the study area in question (Benyahya et al., 2012). Such data would be incapable of representing the variability of hydrometeorology observed along stream networks, particularly in the topographically complex environments of the Scottish Highlands. Some stream temperature models have proven scaling routines for inputs such as solar radiation, where solar time and position relative to the Earth and a given stream's geographic coordinates are incorporated to provide estimates of radiation receipt (Boyd & Kasper, 2003), but for other meteorological inputs for stream temperature models, particularly those related to turbulent heat fluxes, scaling methods remain limited, especially at the sub-daily temporal scale.

Due to limitations in the availability of meteorological input data, previous studies including process-based stream temperature models have been typically limited to the reach and smaller sub-catchment scales (Jackson, et al., 2016). There is a paucity of spatial distributed river energy budget observations across connected river networks and lack of understanding about how to extrapolate such point observations across catchments (especially in headwaters) over space and time. At the reach to point scale, studies suggest that shading from riparian trees is less likely to influence water temperatures in wider channels with high water volumes and short residence times relative to narrow headwater channels with longer residence times (Jackson, et al., 2021). However, water temperature at a given point is the result of cumulative energy exchanges between the stream and its surrounding environment occurring upstream across space and time and their advection downstream (Hannah & Garner, 2015). Because these studies have been constrained to reach and sub-catchment scales, they can only provide insight into the effects of riparian tree planting on water temperature at small scales and are unable to elucidate the cumulative effect of riparian planting across entire stream networks and how temperatures downstream in wider channels can be affected. This is especially limiting for stream temperature modelling within the context of salmonid fisheries management as adult salmonids are likely to be found in the larger streams during the summer months (Milner et al., 2012).

Considering this, there is a need to increase the scale at which process-based stream temperature models are used from the reach and sub-catchment scale to larger rivers and riverscapes to investigate the cumulative downstream impacts of riparian planting on stream temperatures. Within this challenge, there is another inherent challenge of increasing the provision and spatial resolution of input meteorological data.

Within this research, when scaling stream temperature models there is a particular emphasis on the latent heat flux. During the day, this flux typically acts as an energy source to rivers as condensation in winter months and an energy sink as evaporation in summer months (Malcolm et al., 2008a). Within the context of the high-temperature, low-flow conditions in upland headwaters that this study investigates, the latent heat flux will act as an energy sink, removing energy from the river system. A number of previous stream energy balance studies have found that the latent heat flux is the largest energy sink to rivers during these conditions with mean daily losses from the latent heat flux accounting for 73-84 % of total losses (Webb & Zhang, 1997; Hannah, et al., 2008; Leach & Moore, 2010; MacDonald, et al., 2014; Garner, et al., 2014; Dugdale, et al., 2018; Ouellet & Caissie, 2023; Evans, et al., 1998).

The microclimate parameters which drive this flux aside from water temperature itself are air temperature, relative humidity and wind speed (Oke, 1987). The latter two variables are known to show a high degree of spatiotemporal variation, making them particularly difficult to predict across river networks, especially when meteorological observations are limited. As a result, few stream temperature modelling studies have investigated the spatiotemporal variation in latent heat fluxes. Where models have incorporated the latent heat flux, it has been characterised by uncertainty and identified as a modelling limitation. (Dugdale, et al., 2017).

1.3. Aims and objectives

To address these research gaps, the primary aim of this PhD thesis was to use process-based stream temperature models to determine the relative importance of tributary and mainstem shading in protecting larger streams from elevated summer stream temperatures- incorporating the effects of channel hydraulics, residence times and heat advection between stream reaches. This research could inform future guidance on optimal riparian planting strategies to reduce temperatures in larger rivers.

Specific objectives within the thesis are as follows:

(1) To identify spatiotemporal variability in stream energy fluxes governing water temperatures at the catchment scale making use of high spatial and temporal resolution hydrometeorological data within nested catchments (Chapter 2)

(2) To scale conventional hydrometeorological data from point locations along stream networks, creating spatiotemporally continuous datasets for use in process-based stream temperature modelling (Chapter 3)

(3) To examine the representation of the latent heat flux in conventional stream energy balance and temperature model studies by constraining evaporation rates to field-observations (Chapter 3)

(4) To investigate spatiotemporal patterns in energy fluxes and how they cumulatively impact downstream water temperatures using process-based stream temperature models (Chapter 4)

(5) To compare the benefits of contrasting riparian planting strategies in mitigating extreme high summer stream temperatures using hierarchically nested process-based stream temperature models (Chapter 5)

Figures 1-1 and 1-2 illustrate how the chapters collectively address the objectives. Figure 1-1 provides a schematic representation of the thesis structure, detailing the data acquisition and methodologies employed throughout the project. Figure 1-2 offers a conceptual diagram that highlights the progression of knowledge across chapters, demonstrating how each chapter builds upon the findings of the previous one to advance the overall understanding of stream temperature dynamics and riparian planting strategies.

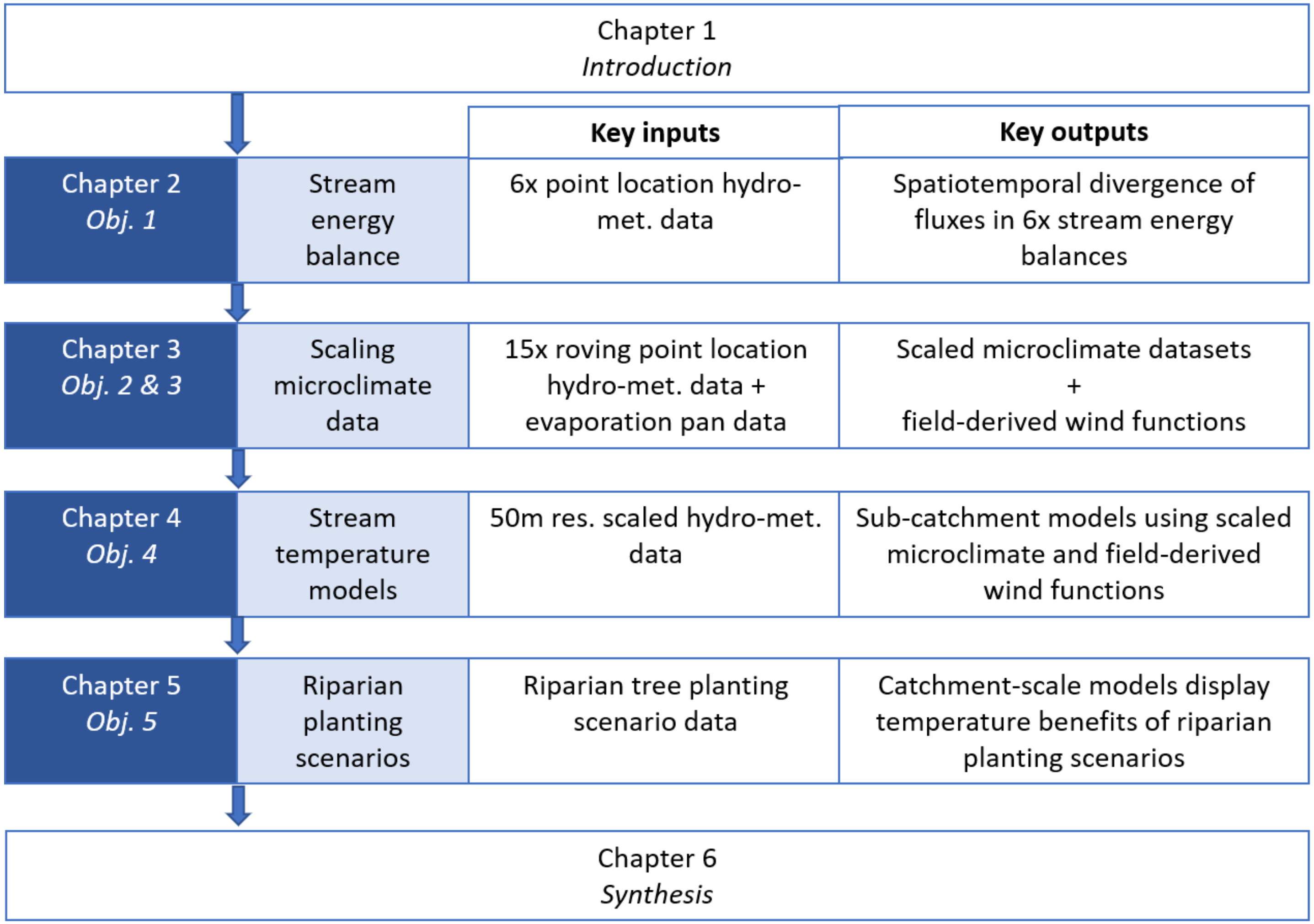

Figure 1-1 Thesis structure, identifying where thesis objectives are discussed, the theme of each chapter, key data inputs and outputs and how these feed into one another

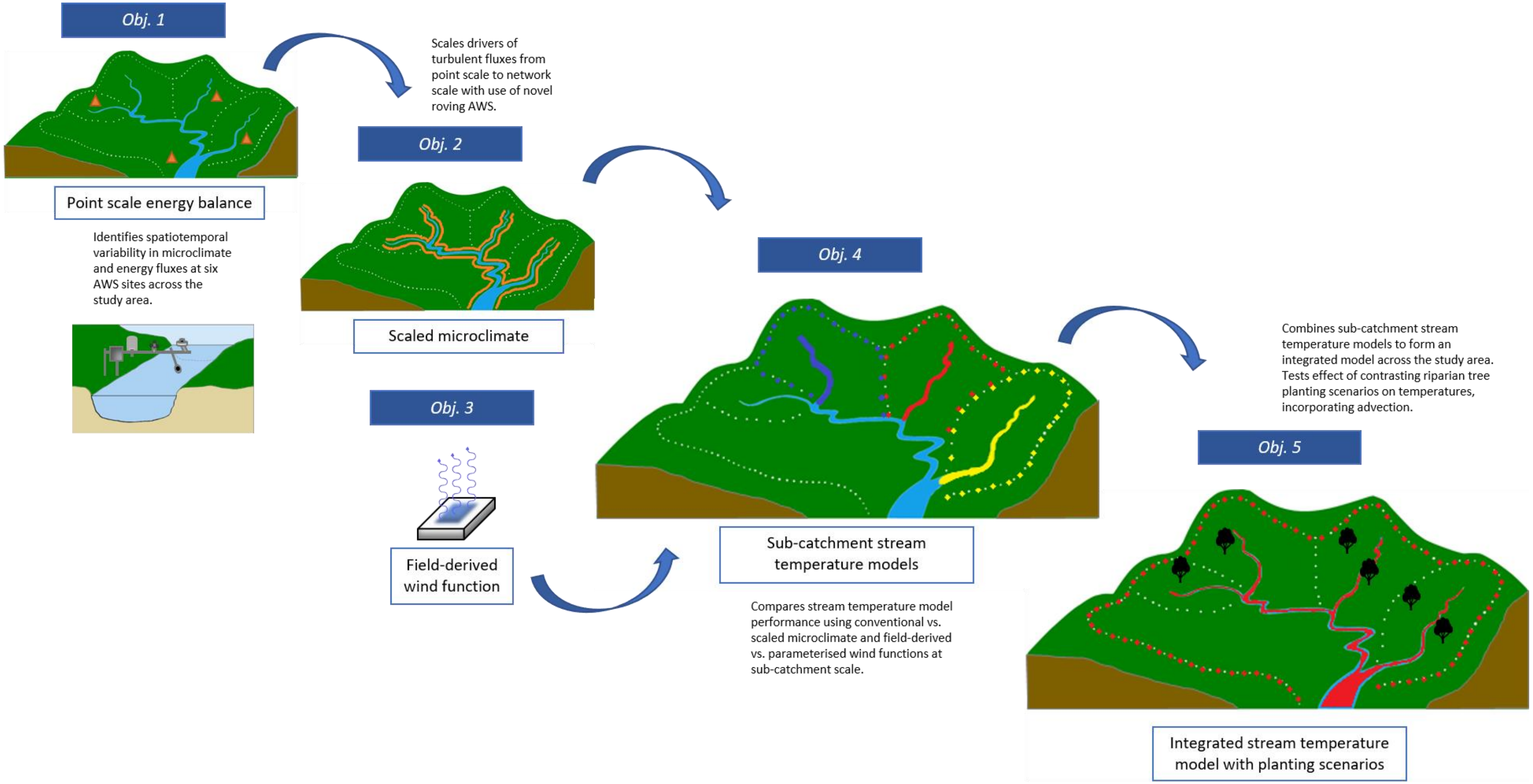

Figure 1-2 Conceptual diagram identifying how each thesis objective builds on the previous to produce an integrated stream temperature model with riparian planting scenarios.

1.4. Thesis structure

The following research design was used to address the objectives and so explore the relative importance of tributary and main-stem shading in protecting larger rivers from high river temperatures- incorporating the effects of channel hydraulics, residence times and heat advection.

The research is presented in the format of four self-contained journal-article type chapters (Chapters 2 to 5), followed by a synthesis wherein key findings are summarised and implications for future research as well as river and fisheries management are discussed (Chapter 6). Each chapter identifies and summarises the relevant literature, describes the data acquisition process and research methodology. Because some datasets, maps and data descriptions feature in multiple chapters, to prevent redundancy, the reader is provided with the relevant location where the data were first described.

To address the first objective of identifying spatiotemporal variability in stream energy fluxes governing water temperatures at the catchment scale, an energy balance study was conducted using six automatic weather stations (AWS) installed both within and between nested catchments of Clunie Water, a fifth order tributary of the Aberdeenshire Dee located in the Scottish Cairngorms (Chapter 2). The chapter characterised spatiotemporal variability within and between sub-catchments for stream temperature, microclimate and stream energy fluxes at a novel spatial resolution. It also identified the key influences on stream temperature during summer low-flow, high-temperature conditions.

The spatiotemporal variability of stream energy fluxes observed within the study catchment were then considered in Chapter 3, which addressed thesis objectives two and three: scaling conventional hydrometeorological data from point locations along stream networks, and using field-observed evaporation rates to examine the representation of the latent heat flux in stream energy balance and temperature model studies, respectively. Here, the observed microclimate metrics of air temperature, relative humidity and windspeed were scaled from point locations to the catchment scale using a series of scaling methods to create spatially continuous microclimate datasets at a 50 m resolution. These datasets were then tested against temporally discrete microclimate observations captured using a novel roving weather station installed at 15 points along a longitudinal stream gradient. They were also tested against the original observations of the six stationary weather stations using leave-one-out cross-validation. Bespoke wind function coefficients were then derived from evaporation rates measured using a floating evaporation pan. Coefficients derived from this research were compared with existing values from the literature to assess the potential error in conventional representation of latent heat fluxes in stream energy balance studies.

Having determined the best-performing method for scaling microclimate across the study area as well as assessing the potential value of field-observed evaporation rates in calculating latent heat fluxes in Chapter 3, these findings were carried into Chapter 4, which considered the fourth thesis objective of using process-based stream temperature models to investigate spatiotemporal patterns in energy fluxes and how they cumulatively impact downstream water temperatures. The best-performing scaled microclimate dataset and wind function coefficients derived from field observations of evaporation rates were used in hierarchically nested series of process-based stream temperature models built to simulate stream temperatures within the study area's sub-catchments. The accuracy of model predictions were then tested against more conventional microclimate data derived from a single location. The impacts of different microclimate inputs on model performance in simulating observed stream temperatures were then compared. The influence of bespoke wind function coefficient inputs derived from field observations of evaporation rates were also compared against coefficients generated from model calibration.

In Chapter 5, the fifth and final thesis objective was addressed. Here the stream temperature models developed in Chapter 4 were integrated within a spatial hierarchy, with sub-catchment models flowing into a larger mainstem model. A series of riparian planting scenarios were then simulated to assess the benefits of contrasting riparian planting strategies in mitigating extreme high summer stream temperatures.

In Chapter 6, the key findings within the thesis were synthesised, implications for river management were discussed and suggestions were made for future research opportunities.

2. Spatiotemporal variation in stream energy fluxes within and between spatially nested catchments

Abstract

Stream temperature during summer is likely to be impacted both directly and indirectly by climate change, with alterations in energy exchange and hydrological regimes causing direct impacts and changes in anthropogenic land and water use having indirect impacts. Due to their complex, multifaceted nature, it is difficult to predict future trends in stream temperatures associated with projected climate change. However, potential rises in stream temperature poses a significant threat to stream ecosystems, particularly for cold water adapted salmonid species, raising concerns for freshwater fisheries. To plan effectively and develop adaptations to potential rising summer stream temperatures, it is crucial to understand the processes that control stream temperature dynamics. Process-based stream temperature models are commonly used to study these processes by simulating energy transfer between the stream and its environment. However, the use of these models requires extensive hydrometeorological data, which can be challenging to collect. Consequently, existing process-based stream temperature models are often limited to short reaches or relying on data from a single meteorological station to represent the microclimate of an entire study area.

To overcome these limitations and gain a better understanding of stream temperature dynamics, this study compares summer stream temperatures, microclimatic conditions, and energy exchanges at six different locations within three nested catchments of a headwater stream in the Scottish Cairngorms, UK. The findings of this study revealed that in the absence of lakes, the daily means, minima, maxima, and ranges of stream temperatures increased downstream throughout the summer. Mean and minimum stream temperatures observed at the outlet of a shallow loch (lake) consistently showed higher values than those observed 1.5 km downstream, and daily temperature ranges were substantially lower at the loch outlet.

The study also investigated the sources of energy contributing to stream temperature changes throughout the summer. The results showed that net radiation was the dominant source of energy for all sites, accounting for 96.4% to 98.6% of total summer energy gains. Latent heat fluxes were the primary energy loss from all sites, accounting for 83.4% to 96% of losses throughout the summer. Sensible heat, fluid friction, and bed heat fluxes were found to be negligible for the majority of sites, except for the site close to a loch outlet, where sensible heat accounted for 16.6% of total summer losses. These findings provide new insights into the spatiotemporal heterogeneity of stream energy fluxes across catchments with uniform land uses. Due to the spatiotemporal variations in fluxes observed between sites within and between nested catchments, the findings also highlight the benefit of installing multiple micrometeorological sensors to capture these variations within a study area when developing process-based stream temperature models for catchment-scale studies.

Key words: stream temperature; river temperature; energy balance; energy budget; hydrometeorology; Cairngorms; Scotland

2.1. Introduction

Stream temperature plays a crucial role in stream ecosystem health and impacts biogeochemical processes throughout stream networks (Hannah & Garner, 2015; Durance & Ormerod, 2009). It is a primary factor influencing gross primary production and ecosystem respiration in the carbon cycle (Comer-Warner et al., 2018). It also has strong influences on the distribution, abundance, demographics, and production of freshwater fish, with recent studies focusing on thermally-sensitive salmonids (Dugdale, et al., 2017; Jackson, et al., 2018; Caissie, 2006). Stream ecosystems are therefore vulnerable to the impacts of climate change, with recent studies finding a 1 °C increase in stream temperature can result in 23% decline in net ecosystem productivity and increased carbon emissions from streams (Song, et al., 2018). Global river temperatures may increase by 1.0-3.0 °C within the century, due largely to the impacts of rising air temperatures (van Vliet, et al., 2013). However, the mechanisms controlling stream temperature are complex, varying spatially and temporally under the influence of their local environmental conditions and regional climate (Hannah & Garner, 2015). As a result, the way in which thermal regimes of river networks respond to climate change will vary in response to local influences from the environment. One specific type of environment which is suspected to be more susceptible to warming includes exposed upland streams such as those in the Scottish Cairngorms, UK (Dugdale, et al., 2018). Due to the low thermal inertia in comparison with larger rivers and the limited availability of riparian canopy to shade from solar radiation, upland environments could experience above-average temperature increases which would have harmful effects on the local thermally-sensitive salmonid populations (Hrachowitz, et al., 2010; Jackson, et al., 2018). It is therefore increasingly important to improve the understanding of the processes governing stream temperature regimes and the landscape characteristics which drive these processes.

Many studies in the 21st century have investigated the processes governing stream temperatures, identifying their relative contributions to thermal regimes (Caissie, 2006; Webb, et al., 2008; Dugdale, et al., 2018; Leach, et al., 2022; Hannah, et al., 2008). At a given location, water temperature is determined first by the combination of its sources, be they surface and shallow sub-surface flows, groundwater or snowmelt. Secondly, water temperature is controlled by energy exchanges at the air-water interface and water-riverbed interface (Kedra, 2020; Hannah, et al., 2008; Hannah & Garner, 2015). Energy exchange occurs through radiation, conduction, convection, evaporation, condensation, advection, and fluid friction (Webb & Zhang, 1997), with the radiative and evaporative components typically dominating relative gains and losses from the system (Caissie, 2006; Webb & Zhang, 1999; Garner, et al., 2017). The principal influence of these energy exchanges on stream temperatures has been well-documented within the literature. However, these processes can be influenced in turn by the landscape characteristics of a catchment, with neighbouring catchments subjected to uniform regional climate forcing producing divergent stream thermal regimes (Dugdale, et al., 2018).

Due to the complex nature of stream thermal regimes, identifying the influences of landscape characteristics on energy exchange processes is a challenging task. As a result of the multidimensional nature of landscape-energy exchange interactions, many studies have looked to limit landscape characteristics to a single variable, whilst controlling all others. A prime example of such single variable impact assessment is the analysis of riparian vegetation, where studies have investigated energy exchanges in the presence and absence of a riparian canopy (Hannah, et al., 2008; Garner, et al., 2017; Dugdale, et al., 2018). The influence of riparian vegetation on stream temperatures has been known for many years, with numerous studies initially investigating changes in stream temperature following the harvesting of plantation conifers in the Pacific Northwest (Swift & Messer, 1971; Burton & Likens, 1973; Feller, 1981). The presence of riparian canopies can reduce extreme temperatures in summers by providing streams with shade, reducing the energy gains from solar shortwave radiation. Their removal during forest harvesting can therefore lead to increases in maximum stream temperatures which has been confirmed by direct measurements of radiative forcing at the air-water interface in forested and un-forested reaches (Hannah, et al., 2008; Garner, et al., 2017). However, because these studies have looked to constrain the inter-site variabilities with the exception of riparian land use, they have often been limited to small reaches of stream networks. Stream temperature at a given point is the result of energy exchanges between the stream and local environment advected downstream along the stream network. To better understand the interactions between a stream and its local environment, there is therefore a need to increase the scale at which energy fluxes are observed from the reach scale to the catchment scale.

To address this research gap, this study deployed six stationary automatic weather stations (AWS) across the three nested catchments of Baddoch Burn, Callater Burn and Clunie Water in the Scottish Cairngorms to explore the spatiotemporal patterns and dynamics of hydrometeorological controls of stream temperature at the catchment-scale. It aims to:

(1) Characterise stream microclimate, heat exchange and dynamics across a summer period;

(2) Compare the different drivers of stream temperature dynamics observed at six locations across a nested headwater catchment; and

(3) Explain the temporal and spatial differences of stream temperature dynamics as a function of relevant meteorological and hydrological drivers.

The use of six automated weather stations enables coverage of a considerably larger spatial scale across which energy fluxes can be compared, with previous river energy balance studies typically making use of one or two weather stations installed at the reach scale. With this increased spatial scale, this chapter will focus on inter-site dynamics across a range of environments, varying in altitude, aspect and riparian topographic relief. This study expands on previous research into stream energy fluxes within a catchment (Dugdale et al., 2018), where contrasting vegetation influences were compared between catchments. In this study, the influence of riparian topography is investigated in place of vegetation. Although riparian topography has been acknowledged as an influence on both microclimate and stream energy fluxes, the existing body of stream energy balance literature has not quantified this influence. In doing so, the insights gained from this study aim to provide a knowledge base on which to begin scaling process-based stream temperature models from reach scales to catchment scales.

2.2. Methodology

The area chosen for this study was the Clunie Water catchment. Nested within the Clunie Water catchment are the two main tributaries of the Baddoch Burn and Callater Burn, which have different characteristics to one another. In order to capture the inter-site variabilities within the Clunie catchment, these sub-catchments were also investigated. With thermally-sensitive fish being most vulnerable to elevated stream temperatures during the summer months, this study focused on energy exchanges across a three-month summer period from June to August.

The following sections provide more detail on the methods deployed in this study. Firstly, the characteristics of sites chosen for investigation are described, followed by a summary of the hydrometeorological metrics measured and the sensors installed to capture these metrics. Finally, the methods used for deriving stream energy fluxes from observed hydrometeorology are then discussed.

2.2.1. Study area and site characteristics

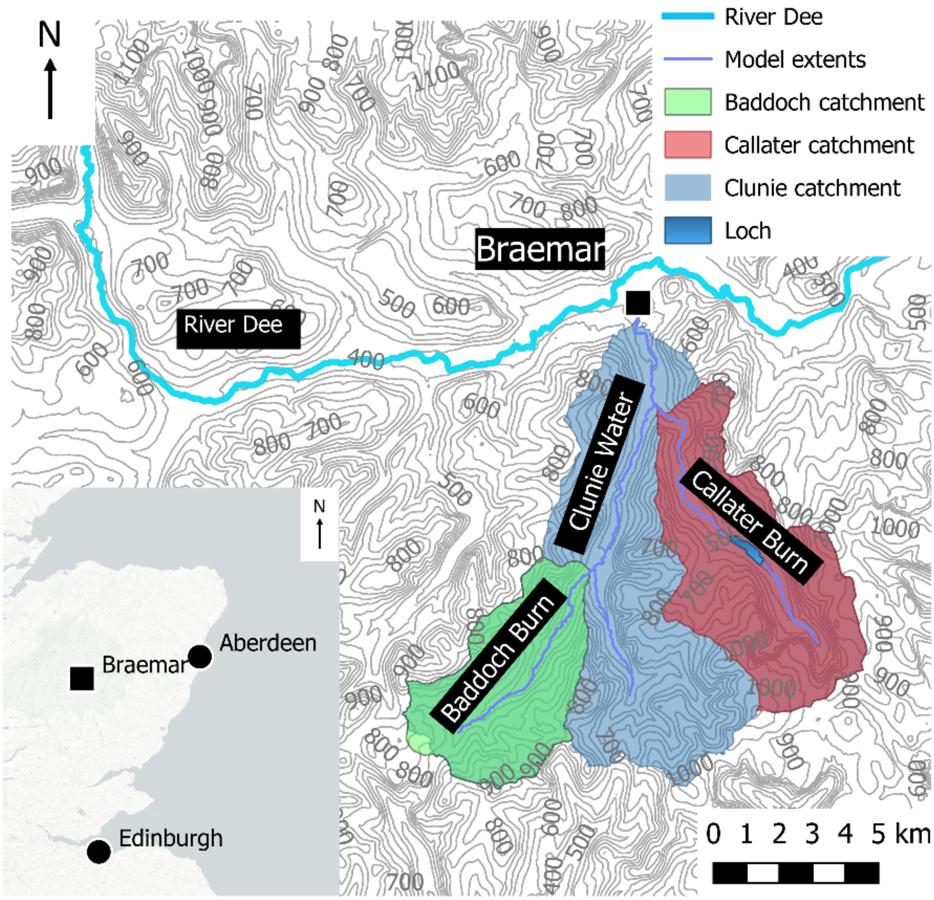

Figure 2-1 Location of Braemar in north-east Scotland, displaying the River Dee and the catchments of Clunie Water and its tributaries

Clunie Water is located in the central Cairngorm Mountain range. Its catchment ranges in altitude from 338 to 1062 mAOD and spans an area of 104 km^2. The stream flows in a south-to-north direction, merging with the Aberdeenshire Dee in Braemar. The Baddoch Burn and Callater Burn serve as major tributaries, flowing from southwest-to-northeast and southeast-to-northwest respectively. The contributing catchments for these tributaries have areas of 23 and 35 km^2, respectively (Figure 2-1). Higher discharges occur during autumn and spring due to seasonal precipitation and snowmelt, with lower discharges observed in summer. Land cover primarily consists of open heather moorland used for sheep grazing, with two sections of pine plantation forest situated at the confluence of Clunie Water and Baddoch Burn and to the west of Clunie Water between its confluences with Baddoch Burn and Callater Burn. The local geology mainly comprises granite, low-permeability metamorphic rock overlain with peat, till, and glaciofluvial deposits. Callater Burn flows from Loch Callater, a shallow freshwater loch with a length of 1.6 km and an average depth of 3.7 m.

Study locations for installing AWS (Figure 2-2) were selected to represent the range of elevations, stream channel orientations, geomorphologies, land uses, and the thermal influence of Loch Callater (Table 2-1). AWS locations were micro-sited, wherein once arriving at a specific coordinated location, the eventual AWS site would be chosen within a range of ~10 m upstream or downstream of said location, with site selection based on ease of access for maintenance and data downloads as well as capturing well-mixed channel water.

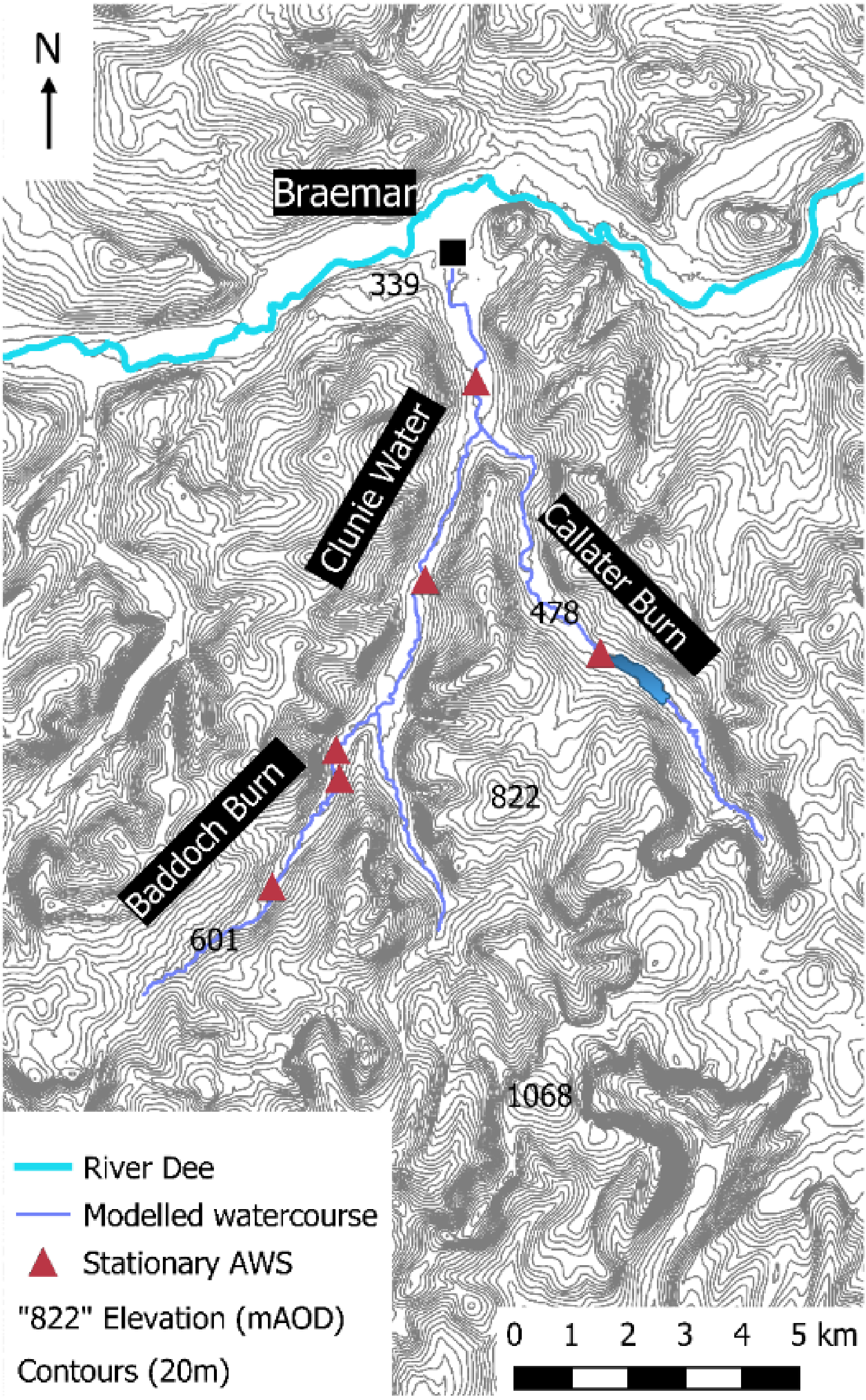

Figure 2-2 Stationary AWS locations within the study catchment, with three existing AWS along Baddoch Burn, two additional AWS installed along Clunie Water upstream and downstream of the Callater Burn confluence, and one additional AWS installed on Callater Burn at the outlet of Loch Callater.

*Table 2-1 Stationary AWS location characteristics. * Area weighted discharge is calculated as the mean scaled discharge for a characteristic low-flow period during the study period, with values scaled from observations from the stream gauge located in the lower reaches of Baddoch Burn.*

Site	***Area weighted discharge (m^3s^{-1})**	**Contributing catchment (km^2)**	**Altitude (mAOD)**	**Chainage (distance upstream)**	**Width (m)**	**Mean slope (m)**	**Channel orientation**	**Sheltering from topography and land use**	**Geomorphology/ sediment**	**Land use**
Baddoch 1	0.045	14	486	4.35	6.97	0.0278	SW → NE	Very little sheltering	East bankside incised, west bank exposed boulders in low discharge.	Pasture, some heather on west bank.
Baddoch 2	0.07	21	436	1.65	7.23	0.0084	SSW → NNE	Greater sheltering than Baddoch-1, more extreme relief	East bankside raised after 5 or 6 m, uniform channel, limited stream incision	Pasture, 20-25 m of riparian planting, still saplings.
Baddoch 3	0.07	21	429	1.05	6.47	0.0144	S → N	More exposed than Baddoch-2 but within 160 m of conifer plantation	Deposited sediment on east bank. No large boulders.	Pasture and heather
Clunie 1	0.186	56	419	6.5	11.29	0.01	SSE → NNW	Sheltering from stream incision and topography, limited riparian trees nearby	Deepest of sites, non-wadable, largest boulders, some exposed in low discharge	Pasture and heather. Some deciduous trees upstream and downstream on east bank.
Clunie 2	0.33	100	350	2.5	16.68	0.0076	S → N	Little sheltering, conifer plantation 35 m west, no riparian vegetation	No exposed sediment, uniform, relatively deep channel	Pasture and heather. Conifer plantation 35 m to west.
Callater	0.06	19	497	5.8	7.12	0.023	ESE → WNW	Very little topographic sheltering, some juvenile trees	Shallow, several small, exposed boulders	Heather moorland. Some riparian planting but canopy yet to mature.
Callater_SRTMN		22	471	4.35	9.20	0.0196	ESE → WNW	Little topographic shading, no trees	Shallow, exposed boulders	Heather moorland

2.2.2. Stream energy balance estimation

Stream water temperature is determined firstly by its sources and secondly by energy exchanges at the air-water interface and water-riverbed interface (Kedra, 2020; Hannah, et al., 2008; Hannah & Garner, 2015). The energy exchanges occur through radiation, conduction, convection, evaporation, condensation, advection, and fluid friction (Webb & Zhang, 1997). By observing and estimating these energy exchanges, the net energy available for heating or cooling a stream can be calculated and temperature changes can be modelled. The equation for determining this net available energy is known as the energy balance equation. For a short river reach without tributaries and a constant flow rate, this can be expressed as:

$$Qn = Qa + Q^* + Qe + Qh + Qbhf + Qf \qquad [2\text{-}1]$$

Where:

Qn = the total energy available to heat or cool a river.

Qa = advected heat from groundwater discharge, hyporheic exchange, tributaries, precipitation, and longitudinal advection.

Q* = net radiation

Qe = latent heat

Qh = sensible heat

Qbhf = bed heat exchange

Qf = friction at the bed and banks

To measure real-time components of the energy balance equation, studies use AWS along riverbanks, with sensors on a cross-arm extending over the water to measure conditions at the air-water interface and further sensors installed in the stream channel and streambed to measure conditions at the water-riverbed interface.

2.2.3. Automatic weather station instrumentation

Summer field data were collected at a 15-minute resolution between 21st June and 9th September 2022, with stationary AWS installed at the locations shown in Figure 2-2. Stream temperatures in the water column were measured using thermistors installed within PVC tubing to protect the sensor from direct radiative heating. Streambed water temperatures were measured using thermistors inserted into the streambed at depths of 5, 20 and 40 cm (Table 2-2). The bed heat flux was captured using a heat flux plate attached to the underside of a flat cobble at a depth of 5 cm below the streambed. The following measurements were taken from the AWS cross-arm at an approximate height of 1.5 m above the water surface: air temperature and relative humidity were measured with an air temperature and relative humidity probe; wind speed was measured using an anemometer; incoming and reflected solar shortwave radiation measured by upward and downward-facing pyranometers; and net all-wave radiation was measured using a net radiometer. The instruments used and their associated instrument error are detailed in Table 2-2. Precipitation was not measured during this study. Although it can be an important influence on stream energy balances, due to this study's focus on low-flow periods during the summer of 2022 which saw limited precipitation events in what is a characteristically flashy headwater catchment, precipitation is omitted from energy balance calculations.

Table 2-2 Hydrometeorological variables measured at stationary automated weather stations (AWS).

Variable	**Instrument**	**Location**	**Instrument error**
Stream temperature (Tw)	Campbell Scientific 107 thermistor	0.05 m above streambed	±0.2 °C
SRTMN_Tw Site*	Gemini Tinytag Aquatic 2 logger	0.2m above streambed	±0.5 °C

Stream bed temperature (Tb)	Campbell Scientific 107 thermistor	0.05, 0.20, 0.40 m below stream bed	±0.2 °C
Air temperature (Ta) and relative humidity (RH)	Vaisala HMP45C / Rotronic HC2S3 temperature and relative humidity probe	~1.50 m above stream surface	Temp ±0.2 °C, RH ± 3% / Temp ±0.1 °C, RH ± 0.8%
Wind speed (WS)	Vector Instruments A100R 3-cup anemometer	~1.50 m above stream surface	±1% + 0.1 m s^{-1}
Incoming ($K_s\downarrow$) and reflected ($K_s\uparrow$) solar shortwave radiation	Skye SKS 1110 pyranometer	~1.50 m above stream surface	±5%
Net all-wave radiation (Q*)	Kipp & Zonen NR-LITE /NR-LITE2 net radiometer	~1.50 m above stream surface	±5%
Bed heat flux (Qbhf)	Hukseflux HFP01 soil heat flux plate	0.05 m below stream bed	3%

Water column temperatures at Clunie 2 were erroneous for periods during the summer as the thermistor was displaced from the water column and deposited on the bank during high flow events. Water column temperatures at Callater were also erroneous during the summer, caused by the thermistor drying up during very low discharge events. As a result, final stream water column temperatures at both sites were measured using temperature and pressure loggers placed in the water column just above the stream bed. The same logger was installed at Clunie 1 site and showed very strong agreement with the water column thermistor here.

The temperature and pressure logger at Clunie 2 was lost during a high flow event in September, with temperature data were last retrieved on 11th August 2022.

There is some uncertainty surrounding the water column temperatures measured at the Callater site. A large discrepancy is observed between the temperatures at Callater, just downstream of the outlet of loch Callater, and another sensor (Callater_SRTMN) situated 1.5 km downstream, with the downstream logger experiencing substantial warming over a short distance. The water column temperature at Callater could be unrepresentative of the channel mean due to hyporheic exchange cooling the water column at the logger location. It could, however be a true representation of the loch outlet temperatures, displaying an influence on water column temperatures. The values from the temperature logger 1.5 km downstream of the Callater AWS site are included in the results section, labelled as Callater_SRTMN, to show fluxes which could be closer to the true mean for the Callater site if water temperatures here were unrepresentative for a well-mixed reach. The Callater_SRTMN site consists of a single Gemini Tinytag Aquatic 2 logger installed 0.2m above the streambed in white PVC tubing following standard operating procedures used by Marine Directorate (Marine Directorate, 2017). The logger records stream temperatures at a 15-minute resolution. Net radiation was not measured at the Baddoch 1 site due to a defective net radiometer. As a result, Baddoch 1 total summer energy gains and losses were not calculated in the energy flux results section. Radiation at the stream bed was not used as a component in the net energy balance as a streambed pyranometer was not used in the AWS configuration. Previous research within a comparable environment has shown this flux to be negligible in comparison with other fluxes (Hannah, et al., 2008).

To allow for the statistical analysis of environmental variables against stream energy fluxes and their meteorological drivers, topographic sheltering was quantitatively described using GIS spatial analysis. A 250 m round buffer zone was created for reaches 250 m upstream and 250 m downstream of each stationary AWS. Digital terrain models (DTM) in each of these buffer zones were analysed to produce means of slope, aspect and topographic roughness. Before analysing the influence of topography on stationary AWS, the following hypotheses were made:

Comparing between the six stationary AWS sites,

(1) A stationary AWS site with above-average shelter will have an above-average mean slope value and TRI;

(2) On a cloudless day, a stationary AWS site with above-average shelter will have below average total incoming radiation; and

(3) A stationary AWS site with above-average shelter will experience lower than average wind speeds and higher than average relative humidity.

2.2.4. Deriving energy fluxes

As stated in Table 2-2, Q* and Qbhf fluxes were measured directly. The following terms were not directly measured, but estimated: latent heat flux (Qe); sensible heat flux (Qh) and fluid friction (Qf).

Latent heat fluxes were estimated using the empirical Penman-style equation adopted by Webb & Zhang (1997), which uses water and air temperatures, relative humidity and wind speed to calculate the amount of heat lost or gained through evaporation or condensation respectively. The sensible heat flux was derived using the latent heat flux in combination with the Bowen ratio, as described by Bowen (1926). Fluid friction was derived using an equation described in Theurer et al. (1984) which calculates the flux using stream discharge, channel width and slope.

Stream discharges for sites were calculated using aerial weighting of stage observations at a gauging station installed and maintained by Marine Directorate within the catchment in the lower reaches of Baddoch Burn. A stage-discharge relationship curve was developed by Marine Directorate at this gauge using 26 observations of discharge measured using an ADCP over a period spanning from 2011 to 2018. Observed discharges ranged from low flow (< 0.2 m^3s^{-1}) to high flow (> 4 m^3s^{-1}) events. Aerially weighted discharges were verified against discharges measured at sites throughout the study period. The flux values reported in this paper are in $MJm^{-2}d^{-1}$, with positive fluxes representing net energy gains to the stream and negative fluxes representing losses.

When comparing the microclimate timeseries data of air temperature, relative humidity and wind speed, large and stochastic differences made it difficult to interpret temporal variabilities between sites. In order to assess inter-site variability, a Loess smoothing function was applied to the time series data (Figure 2-5). The function used for this analysis was the loess method, which uses locally weighted scatterplot smoothing. It performs a local regression on small subsets of data, assigning weights to each data point within the subset based on their distance to the regression target. A span parameter determined the size of the data subsets to be analysed. When choosing a span value, a balance must be struck between improving the interpretability of the data and conserving the nature of the time series. A larger span is easier to interpret but the resulting time series will be less representative of the original data (NIST/SEMATECH, 2024). In this instance, the span was 0.1, accounting for 10% of the total summer study period. Each subset of the time series covered 5 days and 14 hours. All data displayed in Figure 2-5 have been treated with this loess smoothing.

2.2.5. Timeseries data quality control and assurance procedures

The following steps were taken to ensure accuracy and consistency of the timeseries data collected during the study. Firstly, a visual inspection was taken of timeseries data, with a "sense check" taken, taking into account the nature of a given timeseries. For example, detecting outliers in water temperature data such as those associated with a sensor being taken out of the water column, would be easier to identify than erroneous air temperatures due to the relatively more gradual changes likely to occur to water temperature as a result of its greater thermal capacity than air. Where unrealistic outliers in water temperature occurred, and they lasted for a single timestep (15 minutes) or two (30 minutes), these values would be removed and replaced with interpolated values calculated using the hour of observations prior to and following the outlier. For more temporally variable data such as wind speed or shortwave and longwave radiation data, interpolations were not used to replace any outliers as there would be less confidence in adjacent conditions representing those removed.

Data were also inspected for the occurrence of sensor drift. Sensor drift can occur gradually, where a sensor's measurements slowly deviate from true values over time, or in the form of a plateau, where values suddenly shift to a new mean. With the high level of sensor instrumentation, there was a large body of data against which to test for these deviations, but no such observations were found in the stream temperature or meteorological data.

2.3. Results

Spatial and temporal variability in summer water temperature, discharge, microclimate and energy flux data are presented using time series difference plots and probability-density-functions. Time series plots highlight the temporal variability between sites, with the probability density functions displaying the distribution of data between sites across the summer period, their central tendencies and outliers. Relationships between environmental characteristics and energy fluxes are displayed in a correlation matrix, consisting of linear regression plots between mean summer fluxes and environmental characteristics and their corresponding correlation coefficients. Spearman correlation was used in this analysis due to the non-linear relationships between energy fluxes and environmental variables and small sample size (n = 6).

2.3.1. Water column temperatures

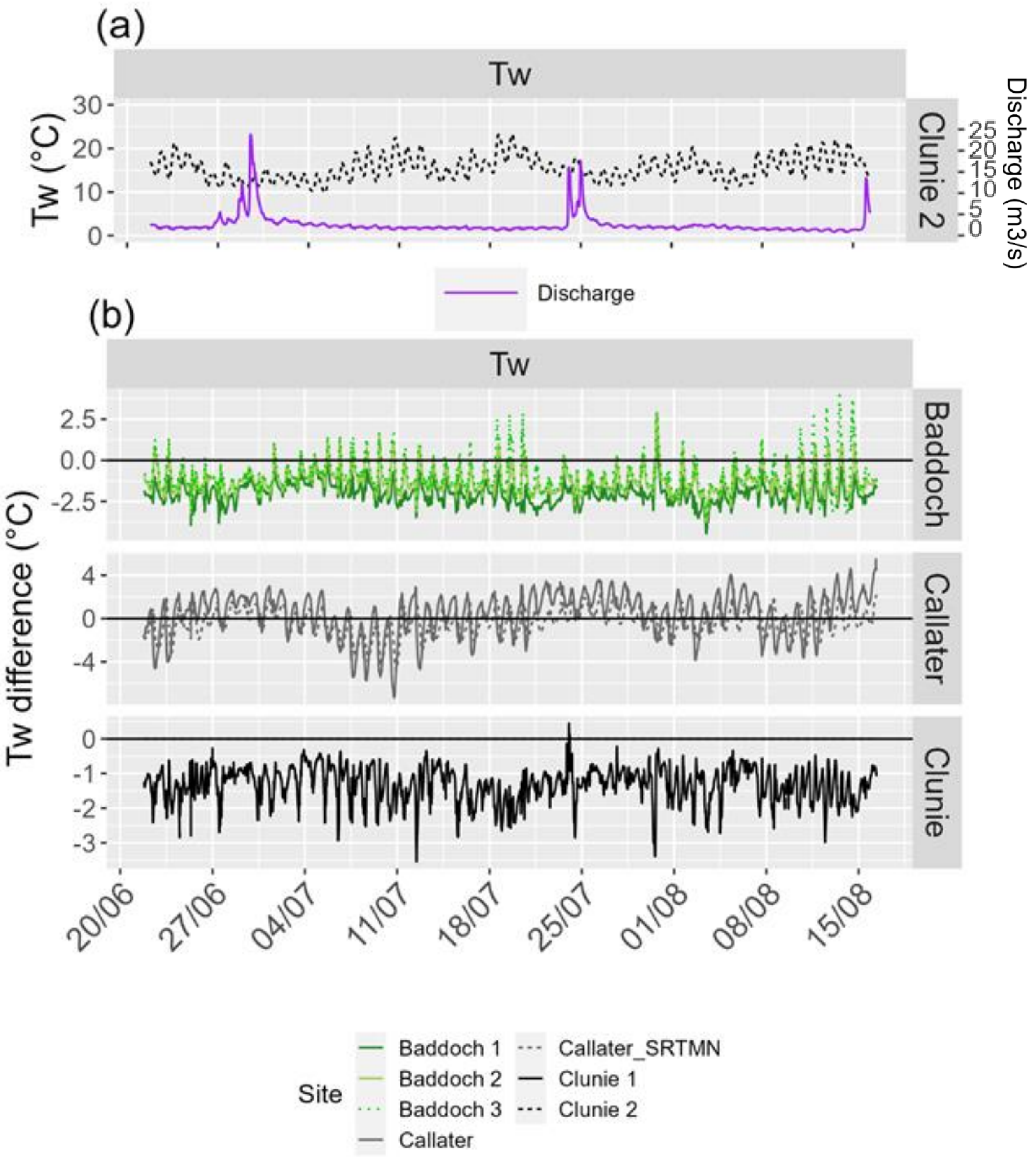

Figure 2-3 (a) Summer water column temperatures at reference site (Clunie 2) and (b) Differences in water column temperature between each site and the reference site. Colours denote different sites and panels denote different sub-catchments. The black horizontal line is at 0 where points above the line are warmer than the reference and points below the line are cooler.

Water column temperatures varied both within and between catchments throughout the study period. Mean water column temperatures, daily minima, maxima and range typically increased downstream (Figure 2-3b, 2-4). However, this downstream warming pattern was not observed along Callater Burn. Here, mean water column temperatures and daily minima decreased downstream, whereas maxima increased. There are broadly consistent patterns between the Baddoch and Clunie catchments. Across the study period the Baddoch was typically cooler than the Clunie with temperature increasing in a downstream direction from Baddoch 1 (most upstream) to Clunie 2 (most downstream). However, under warmer conditions (18/07/22-20/7/22, Figure 2-3b Tw, 2-5a Ta) patterns became more variable, with Baddoch 2 and 3 daily maximum water temperatures consistently exceeding those of Clunie 2.

The temperature profiles of both Callater sites are more muted than those of the Baddoch and Clunie across the study period. As a result, temperatures are typically higher along Callater than Clunie during cooler periods (21/06/2022 - 30/06/2022, Figure 2-4, 2-5a Ta) and lower during warmer periods (08/07/22 - 11/7/22, Figure 2-3b Tw, 2-5a Ta).

Although variable between sub-catchments, there is generally consistence within sub-catchment spatial patterns in absolute temperatures and diurnal variability. For the Baddoch and Clunie this is a downstream increase in temperature and diurnal range (Baddoch 1 is coolest and least variable of the 3 Baddoch sites, with a daily mean of 12.9 °C and mean daily range of 4.9 °C; Baddoch 3 warmest and most variable in Baddoch with daily mean of 13.9 °C and mean daily range of 6.1 °C). In contrast, Callater typically shows a pattern of cooling from the upstream site (Callater 1) to the downstream site (Callater_SRTMN), with daily means reducing downstream from 15.7 °C to 14.8 °C. Mean daily range still increases downstream along the Callater, with mean daily ranges increasing markedly from 2.5 °C to 4.9 °C. The downstream increase in water temperature variability can be observed in Figure 2-4, where the density of the modal temperature (highest point in the plot) reduces downstream.

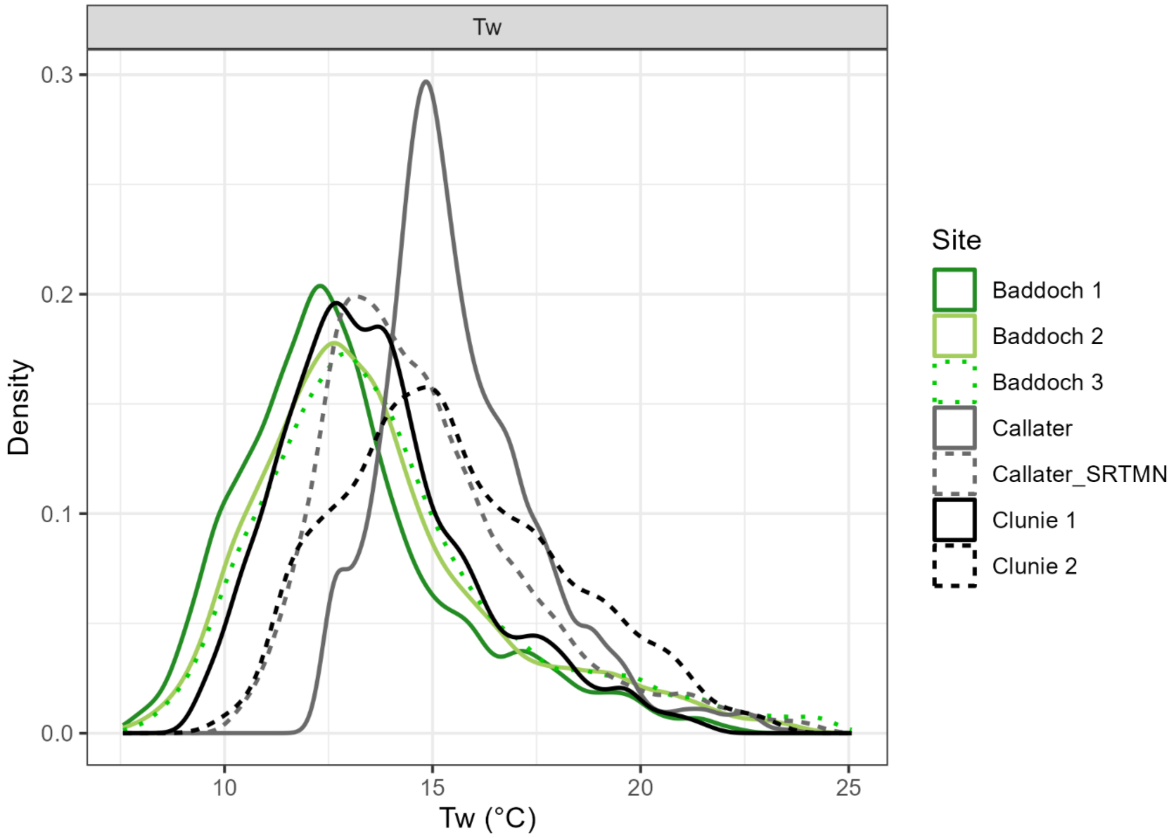

Figure 2-4 Probability density functions of summer water column temperature data. Colours denote different sites

2.3.2. Microclimatic drivers

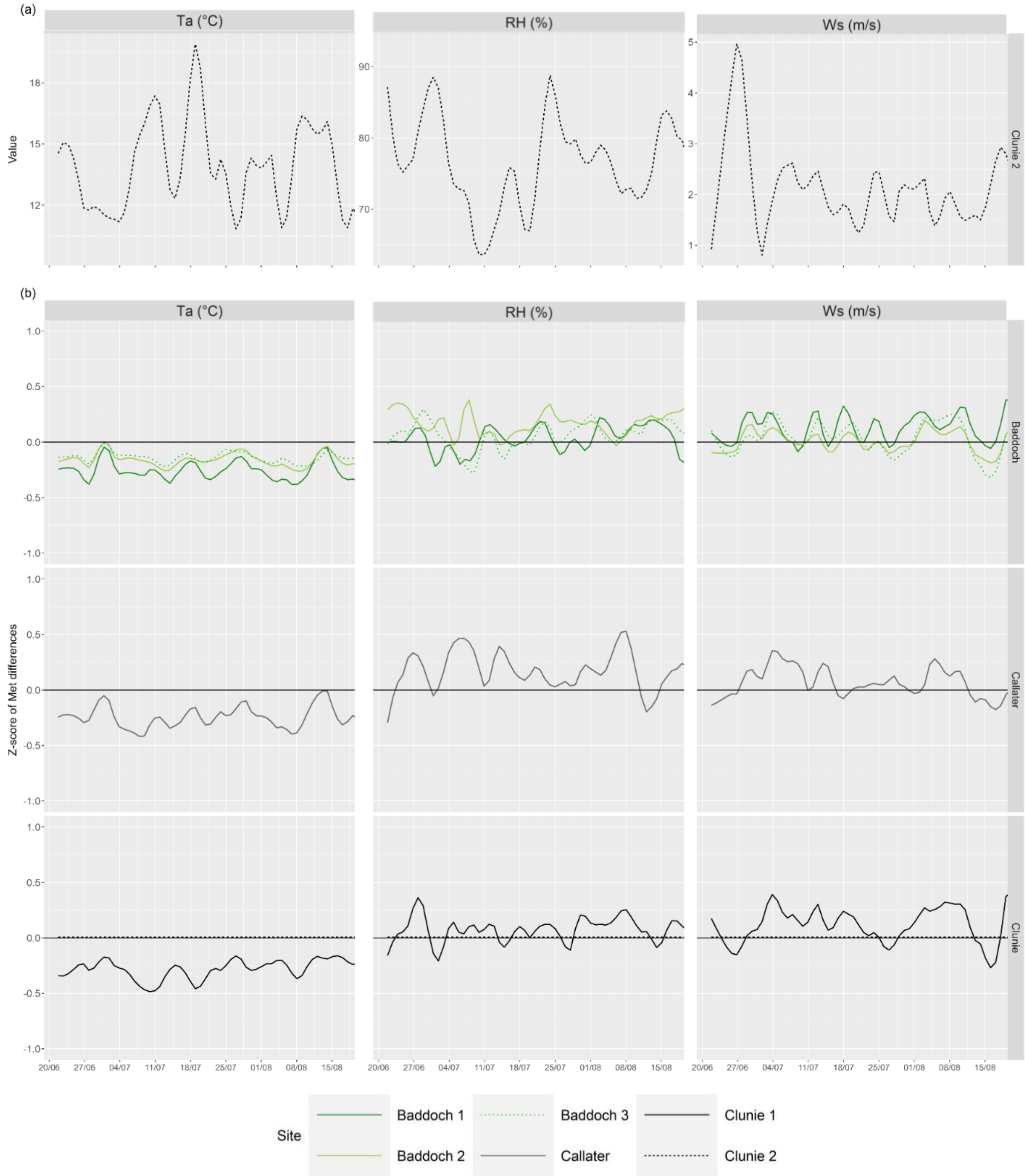

Figure 2-5 (a) Observed microclimate (air temperature, relative humidity and wind speed) at reference site with a Loess (locally weighted) regression applied to remove noise from instantaneous inter-site differences.(b) Z-scores of differences in microclimate between each site and reference site. Line colours denote different sites. Vertical panels denote microclimate metrics and horizontal panels denote different sub-catchments. The black horizontal line is at 0 where points above the line are higher than the reference and points below the line are lower. Rotronic sensors are used for measuring RH and Ta at all Baddoch AWS sites, Callater and Clunie 2, with the Clunie 1 site using a Vaisala sensor. In-situ comparisons between Vaisala and Rotronic sensor readings were made between Clunie 1 and Clunie 2 sites respectively using the roving AWS with good agreement observed between sensors.

As with water column temperatures, microclimate data varied both spatially and temporally between sites. The metrics focused on in this section are relative humidity, air temperature and wind speed. Across the study periods, these metrics all showed much higher variability than water temperatures, with large fluctuations in differences observed between sites in the instantaneous (15-minute) time series.

Relative humidity at the reference site during the study period ranged from 35% to 100%, with a mean relative humidity of 79%. When the observed relative humidity at the reference site was low (05/07/2022 – 07/07/22), inter-site variabilities diminished. This is observed in the probability density function plot, where the left tails of sites showed good agreement for relative humidity up to 50%, beyond which, diversions begin (Figure 2-6). Across the study period similarities in the distribution of relative humidity values are observed between Baddoch 1 and Callater sites, with both sites having most values clustering around their respective modal values. Another grouping can be found between Clunie 1, 2 and Baddoch 3, which all display a smaller clustering around their respective modal values, resulting in a greater number of low and high values. Unlike with water temperatures, there is no relationship between relative humidity and stream chainage.

Differences in relative humidity between sites peaked during periods of transition at the reference site (from low to high RH). For instance, when smoothed relative humidity at the reference site rose from 75% to 90% during late June (27/06/2022 – 30/06/2022 Figure 2-5a), inter-site differences peaked at the majority of sites, with differences at all sites changing from negative to positive.

Air temperature showed much closer similarity between sites than relative humidity, as shown in the metric’s probability density function plot where distributions are much more tightly grouped and more normally distributed (Figure 2-6). Air temperature typically increased downstream during the study period, with the lowest mean air temperatures recorded at Clunie 1 and Baddoch 1 observing means of 12.81 °C and 12.97 °C respectively. The same observations were found for daily minima, maxima and range, with all air temperature metrics increasing downstream.

As seen with relative humidity, inter-site variation during the study period tended to peak during periods of transition from cooler to warmer weather (06/07/2022 – 11/07/2022 Figure 2-5a, 2-5b), with differences between the reference site and other sites showing general agreement. Inter-site variation in air temperatures tended to diminish during extended periods of warm weather (08/08/22 – 15/08/22 Figure 2-5a, 2-5b).

Wind speeds during the study period showed large instantaneous differences between sites as well as relatively large differences in means, with mean wind speeds varying from 1.97 m/s at Baddoch 2 to 2.48 m/s at Baddoch 1. There were no observed relationships between inter-site variability in wind speeds and the magnitude of wind speed observed at the reference site. There was a weak relationship observed between wind speeds and stream chainage, with higher wind speeds typically observed further upstream (Figure 2-6). However, wind speed was the most spatiotemporally stochastic microclimate metric, with no strong patterns observed between sites.

Inter-site variations in relative humidity and wind speed were highly variable within the Baddoch catchment and more spatially pronounced between Baddoch 2 and Baddoch 3 sites.

Baddoch 2 observed high relative humidity values much more frequently than Baddoch 3 (Figure 2-6, right tails of RH (%)) but also observed both low and high wind speed values more frequently than Baddoch 3 (Figure 2-6, both tails of Ws (m/s)).

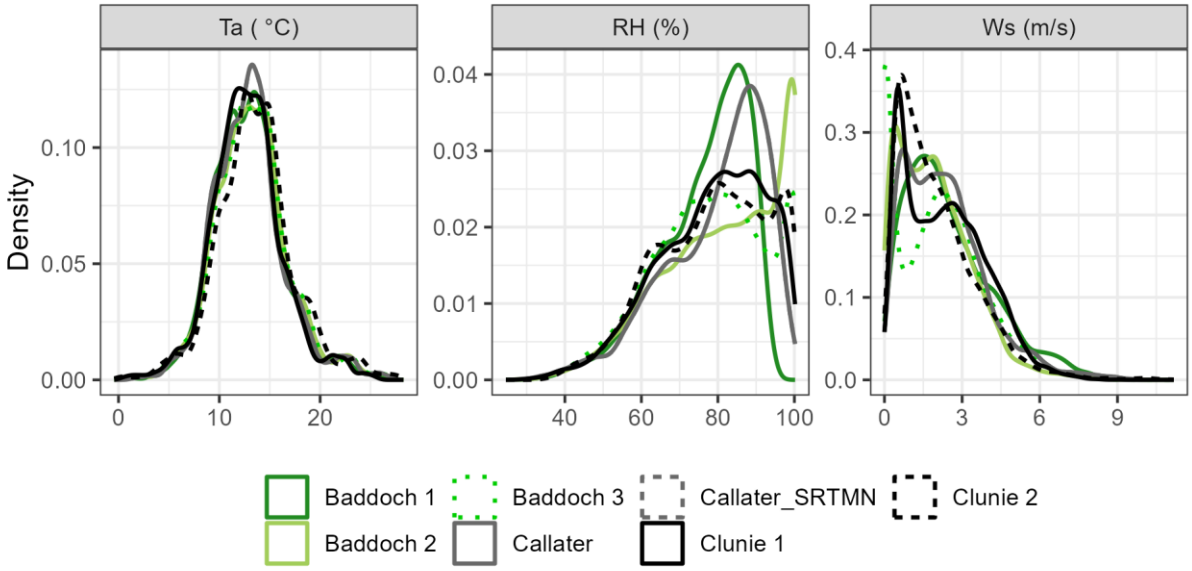

Figure 2-6 Probability density functions of summer microclimate data, (air temperature (Ta), relative humidity (RH) and wind speed (Ws)).

2.3.3. Energy fluxes

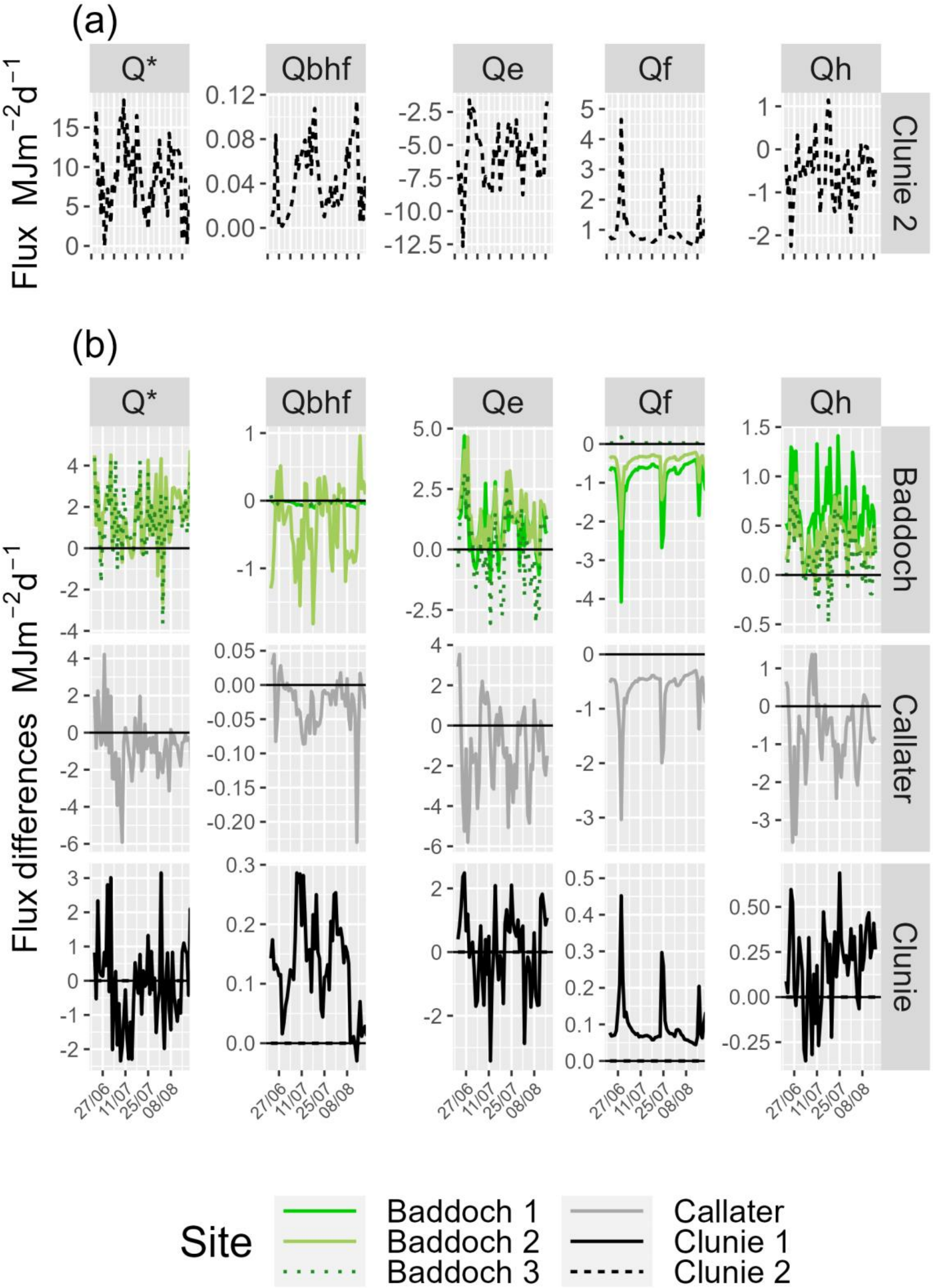

Figure 2-7 (a) Observed daily energy fluxes (net radiation (Q), bed heat flux (Qbhf), latent heat flux (Qe), friction (Qf) and sensible heat flux (Qh) (b) Differences in daily energy fluxes between each site and reference site Line colours denote different sites. Vertical panels denote microclimate metrics and horizontal panels denote different sub-catchments. The black horizontal line is at 0 where points above the line are higher than the reference and points below the line are lower. Note that Baddoch 1 Q* data is unavailable and the scales of y axes vary between plots.*

As with water temperatures and microclimate, energy fluxes showed both spatial and temporal variations across the study area during the summer period. At the reference site, net radiation (Q*), bed heat fluxes (Qbhf), latent (Qe) and sensible (Qh) heat fluxes were all highly variable across time (Figure 2-7a). Fluid friction displayed a higher degree of stability, with fluxes closely reflecting discharge (Figures 2-7a and 2-3a).

Q* throughout the study period was typically higher across the Baddoch sites than Clunie or Callater (Figure 2-9), with mean daily fluxes of 9.19 $MJm^{-2}d^{-1}$ and 8.87 $MJm^{-2}d^{-1}$ for Baddoch 2 and Baddoch 3 respectively, compared with 7.59 $MJm^{-2}d^{-1}$ and 7.57 $MJm^{-2}d^{-1}$ for Clunie sites 1 and 2 and 6.93 $MJm^{-2}d^{-1}$ for Callater. The difference in mean daily flux between sites with the smallest and greatest fluxes was 21%. The Baddoch sites experienced higher Q* fluxes for the majority of the study period, with inter-site variations typically diminishing during periods where Q* values were elevated across the study area (17/07/2022 – 18/07/2022 Figure 2-7). Maximum inter-site variations would occur during periods of transition from high to low Q* fluxes at the reference site (08/07/2022 – 09/07/2022 Figure 2-7).

Q* observations throughout the study period tended to be grouped to catchments, with the Baddoch sites experiencing the greatest Q* followed by Clunie sites, with the Callater site experiencing the smallest Q* fluxes (Figure 2-9).

Bed heat fluxes were variable both spatially and temporally across the study period. At the reference site, bed heat fluxes steadily increased during periods of low discharge, with daily fluxes rising from near zero to peaks of 0.1 $MJm^{-2}d^{-1}$ shortly before elevated flow events, after which fluxes would reduce dramatically (Figure 2-7a and 2-3a). Spatial variation in Qbhf was high but did not follow any trends. Daily Qbhf for Clunie 2, Callater, Baddoch 1 and Baddoch 3 were minimal, with a largest mean daily flux of 0.038 $MJm^{-2}d^{-1}$ observed at Clunie 2. However, Qbhf observed at Baddoch 2 and Clunie 1 were an order of magnitude larger, with mean daily fluxes of -0.25 $MJm^{-2}d^{-1}$ and 0.14 $MJm^{-2}d^{-1}$ respectively (Figure 2-7b).

Latent heat fluxes were highly variable across both space and time. They were negative across the study area through the summer, with daily flux totals ranging from -12.6 $MJm^{-2}d^{-1}$ to -1.5 $MJm^{-2}d^{-1}$ at the reference site (Figure 2-7a). Across the summer, mean daily fluxes varied from -4.4319 $MJm^{-2}d^{-1}$ at Baddoch 2 to -6.9258 $MJm^{-2}d^{-1}$ at Callater, representing a 36% difference in mean fluxes- a greater variation than for Q* (Figure 2-9). Latent heat fluxes were typically higher (lower losses) for Baddoch sites, with a large variability observed between Baddoch 2 and Baddoch 3 sites (Figure 2-9). There were no strong longitudinal patterns observed between latent heat fluxes at sites throughout the study period.

Fluid friction was the most temporally stable of fluxes throughout the study period with fluxes remaining low for the vast majority of the summer (Figure 2-7a). Although fluxes were temporally stable, they were highly variable spatially, with mean daily fluxes ranging from 0.15 $MJm^{-2}d^{-1}$ at Baddoch 1 to 1.31 $MJm^{-2}d^{-1}$ at Clunie 1. A longitudinal pattern in fluid friction was observed along the Baddoch sites, with fluid friction increasing downstream (Figure 2-9). However, this observation was not observed along Clunie, with energy gained from fluid friction reducing from Clunie 1 to Clunie 2.

Daily totals of sensible heat fluxes at the reference site were mostly negative throughout the summer, with all but seven days experiencing net energy losses from sensible heat. Mean daily losses from the sensible heat flux ranged from -1.25 $MJm^{-2}d^{-1}$ at Callater to +0.1 $MJm^{-2}d^{-1}$ at Baddoch 1. Baddoch 1 was the only site to experience a net gain from the sensible heat flux throughout the study period. A longitudinal trend was observed for sensible heat fluxes across the study area with mean daily losses increasing downstream in both the Baddoch and Clunie throughout the summer (Figure 2-9). As well as mean losses changing downstream, so too did the variability in observed sensible heat fluxes. Observations of the sensible heat flux typically became less variable downstream during the study period (Figure 2-9). The distribution of the sensible heat flux at Callater was markedly different from the other sites, with a more negative modal value as well as a larger range of values throughout the summer

(Figure 2-9). Inter-site variabilities between the reference site and other sites were largest during periods of extremes. When the reference site observed greater losses or gains from sensible heat, differences at the other sites were more pronounced (24/06/2022 Figure 2-7); whereas when gains or losses were lower at the reference site, there was more agreement between sites (17/07/2022 Figure 2-7).

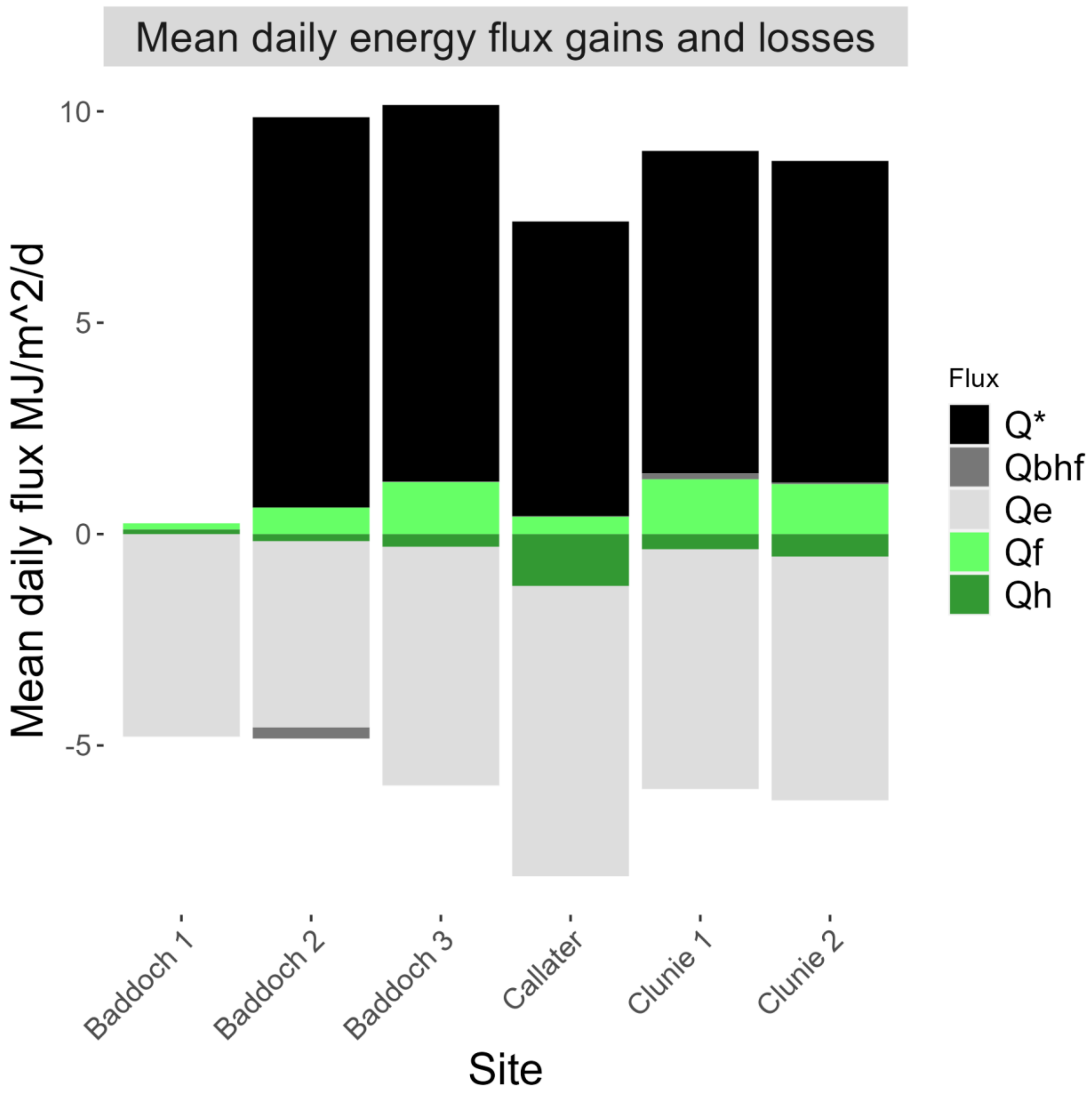

Figure 2-8 Mean daily totals of each flux for each site across the summer. Q is omitted from Baddoch 1 site due to erroneous net radiometer at AWS site*

Q* was the largest source of energy for all sites throughout the summer period, with relative contributions to mean daily fluxes ranging from 84% at Clunie 1 to 94% at Callater (Figure 2-8). Qe was the largest sink across all sites, with contributions to mean daily losses ranging from 85% at Callater to over 99% at Baddoch 1 (Figure 2-8). The contributions of Qf and Qh were substantially lower than Q* or Qe. Qf percentage contributions to gains ranged from 6% at Baddoch 2 to 14% at Clunie 1 and Qh contributions to losses ranged from 4% at Baddoch

2 to 15% at Callater. The relative contributions of Qbhf to the net energy balance were negligible for most sites, with highest contributions of 5% to losses at Baddoch 2 and gains of 2% at Clunie 1 (2- 8). The Baddoch 1 site was omitted from the analysis of relative contributions to mean daily energy gains due to the absence of the Q* measurements at this site.

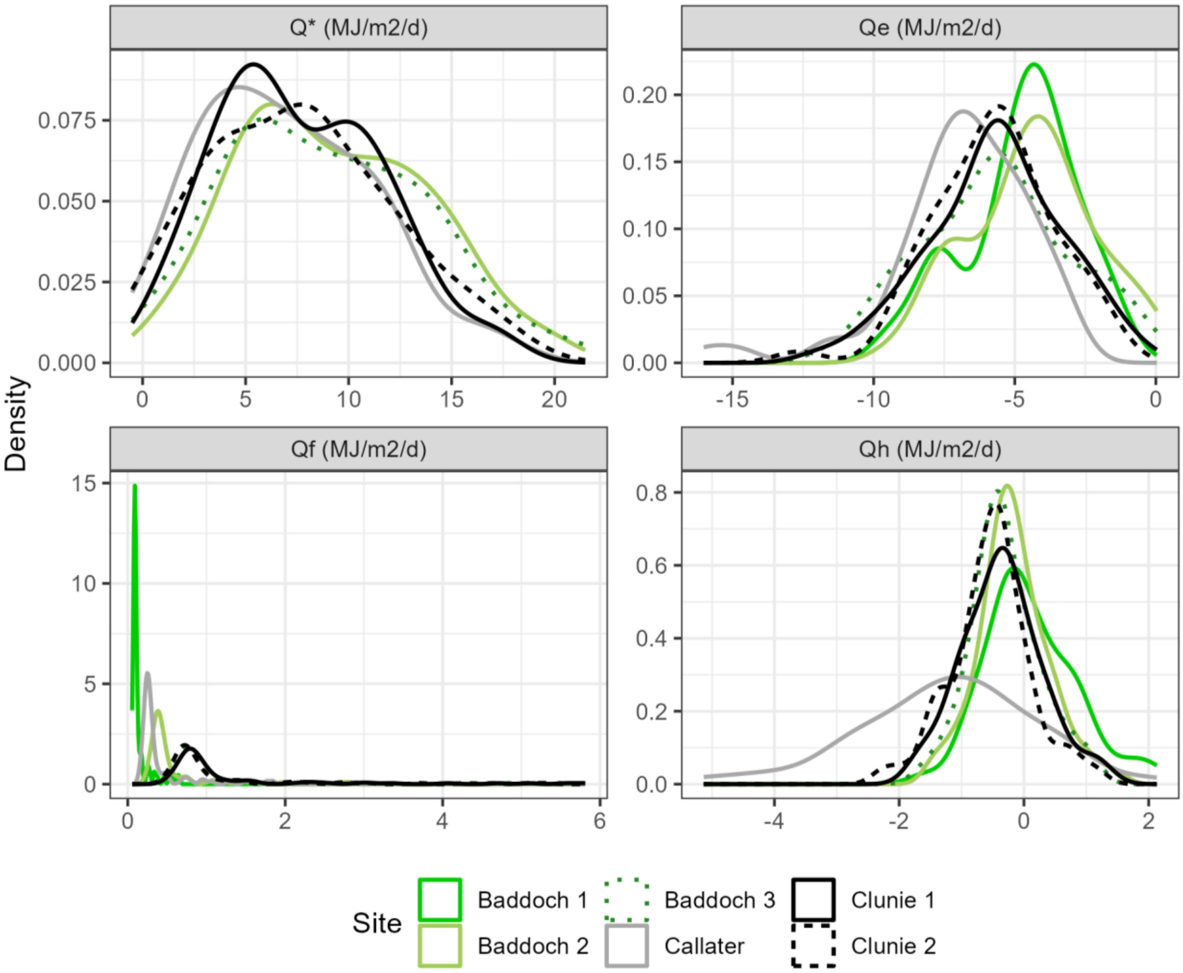

Figure 2-9 Probability density functions of summer daily energy flux data (net radiation (Q), latent heat flux (Qe), fluid friction (Qf) and sensible heat flux (Qh). Line colours denote sites and panels denote energy flux metrics.*

2.3.4. Energy fluxes in relation to environmental characteristics

To understand the environmental drivers of variations in energy fluxes, summer means of the main fluxes (demonstrated by the proportion of total fluxes in Figure 2-8), Qn, Q*, Qe and Qh, were plotted in linear regressions against site altitude, mean slope of riparian topography, mean topographic roughness index of riparian topography and mean aspect. The fluxes of bed heat flux and fluid friction were omitted from analysis due to their limited influence on net energy exchange between the stream and the environment (see Figure 2-8). These linear regression plots can be observed in a correlation matrix, along with the correlation coefficients of each corresponding plot (Figure 2-10).

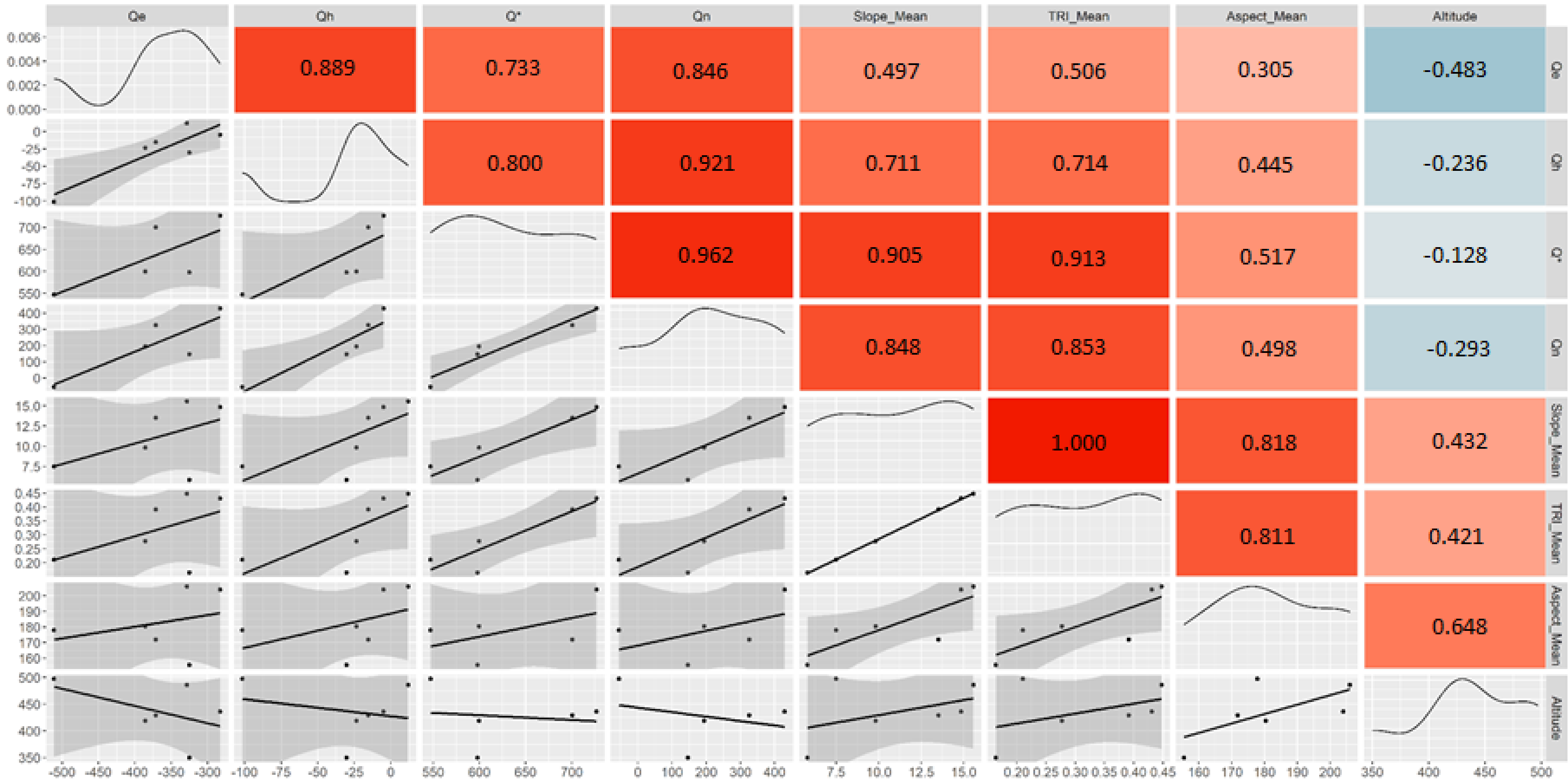

Figure 2-10 Correlation matrix of summer totals for net energy exchange (Qn), latent heat flux (Qe), sensible heat flux (Qh) and net radiation (NR), altitude, mean slope topographic roughness (TR), and aspect. Blue squares denote negative correlation coefficients; red denote positive. Spearman correlation was used for calulating correlation coefficients.

The correlation matrix identifies strong positive correlations between major fluxes and the environmental characteristic metrics of slope, topographic roughness (TRI) and aspect. Of the major fluxes, the strongest correlations were found with Q*, which had correlation coefficients of 0.905, 0.913 and 0.517 for slope, TRI and aspect respectively. Out of the non-radiative fluxes of Qe and Qh, Qh displayed the stronger correlation with all environmental metrics, averaging correlation coefficients 0.19 greater than Qe. Contrary to the correlation coefficients between major fluxes and the metrics of slope, TRI and aspect, altitude displayed negative correlations with fluxes. The strengths of relationships between altitude and the major fluxes were typically weaker than for the other metrics. The strongest negative correlation was between Qe and altitude, which had a coefficient of -0.483. This shows a departure from the relationships between Qe and other metrics, where Qe showed the weakest correlation. Another departure from those relationships can be found between altitude and Q*. Here, Q* had the weakest correlation of all fluxes, with a coefficient of -0.128.

As shown in the regression plots (Figure 2-10, bottom right corner), the confidence bounds of these regressions were very large. Regression plots for the non-radiative heat fluxes also showed one site to be a strong outlier from the remaining sites, considerably altering the relationships between environmental characteristic metrics and fluxes. There is very little statistical power in this analysis, with $n = 6$. This lack of statistical power further exacerbates the influence of the single outlier in the regression analysis for non-radiative fluxes.

There was also very strong agreement between mean slope and mean topographic roughness, with a correlation coefficient of 1. This result shows that between the six sites, no additional information is gained as to the relationships between environmental characteristics and energy fluxes by including both of these metrics.

2.4. Discussion

This section includes the following: it first outlines the novel aspects of the study; discusses the inter site spatio-temporal variabilities in water column temperature, microclimate and energy fluxes, inferring the mechanisms behind the observed patterns and comparing said observations with those found in other studies; it then discusses the limitations of the study; then the implications of the study for river management and future research before concluding on the findings of the study.

The collection of microclimate data at a high temporal resolution using AWS is expensive. High costs are involved both in the initial purchasing of sensors and in the ongoing maintenance of equipment, especially if sensors are deployed in remote regions. As a result, previous studies into stream energy fluxes have typically made use of a small number of AWS. With limited spatial coverage, studies with a single AWS have typically focused on temporal variations in energy budgets (Evans, et al., 1998; MacDonald, et al., 2014; Ouellet & Caissie, 2023) or influence of land use (Webb & Zhang, 1997; Hannah, et al., 2008; Leach & Moore, 2010; Garner, et al., 2014; Dugdale, et al., 2018) with some studies controlling for other landscape characteristics including upstream catchment area, altitude and geomorphology (Dugdale, et al., 2018). This experimental design allows binary comparisons to be made when trying to understand a particular control or influence; for example, a woodland effect where the site selection captures one site as forested and another un-forested.

However, a number of stream energy balance studies have not controlled for these characteristics. Although this is identified as a limitation in said studies, where variables such as spatial proximity and altitude discrepancies are large, it is then difficult to separate land use influences from spatial influences (Webb & Zhang, 1997; Hannah, et al., 2008). Some studies also use discontinuous data collection periods, subjecting sites to different microclimate conditions. Due to its design, such a study is unable to separate spatial variability from temporal variability (Webb & Zhang, 1997). As seen in this study, inter-site variability in microclimate and energy fluxes can be highly temporally variable between days. This has been controlled by gathering continuous data between the six stationary AWS sites during a fixed time period.

This study increases the number of observation sites with the use of six AWS, allowing for an improved understanding of spatial variability in microclimate and energy fluxes within and between nested headwater catchments. Because the study area is dominated by heather moorland and grassland, it is controlled for land-use, allowing for a focus on the influence of other environmental characteristics including riparian topography and altitude on microclimate and energy fluxes. Previous studies at this spatial scale have been spatially disconnected, with instrumented sites not being nested within a larger catchment (Webb & Zhang, 1997). The use of nested catchments allows an observation of fluxes within sub-catchments which compound to influence water temperatures downstream of confluences. Previous studies which have instrumented sites along a river network have not done so at this spatial scale (Hannah, et al., 2008).

2.4.1. Inter-site spatio-temporal variabilities in water column temperatures, microclimate and energy fluxes

2.4.1.1. Water column temperatures

The diurnal variability observed in inter-site differences (Figure 2-3b) is likely a feature of the lag associated with the downstream advection of heat. In this energy balance study, with the use of fixed locations, energy fluxes are viewed in a eulerian framework, where the fluxes vary at a fixed point through time. However, the water temperature metric lends itself more readily to a lagrangian framework, wherein the parcel of water pulses through the stream network. This diurnal water temperature difference between sites can be seen as the interaction of the water parcel pulsing through the network and being recorded at different locations throughout the day. The use of probability density functions better represents the inter-site variability in water temperatures (Figure 2-4).

Water temperatures within the Baddoch catchment were typically cooler than the reference site (Clunie 2). This was to be expected as the headwaters of Baddoch Burn are closer to their groundwater sources which are typically cooler than surface waters during summer periods (Caissie, 2006). As the time of exposure to solar forcing increases downstream, so too does water column temperature. This is observed in the downstream warming between Baddoch sites as well as Clunie sites. This longitudinal gradient of warming during summers in in agreement with previous water temperature studies in the absence of significant groundwater-surface water interactions (Sinokrot & Stefan, 1993; Caissie, 2006; Malcolm, et al., 2008).

Although mean temperatures during the study period were lower for the Baddoch sites than the reference site, Baddoch 2 and 3 daily maxima would exceed that of the reference site, especially during warm periods (18/07/22-20/7/22, Figure 2-3b Tw, 2-5a Ta). This is also to be expected as the Baddoch Burn, being a smaller stream than Clunie Water, has a lower thermal capacity. As a result, during especially warm days, Baddoch Burn would be expected to be more responsive to alterations in the energy budget than Clunie Water (Webb, 1996).

The longitudinal thermal gradient of Callater Burn from the Callater AWS site to the Callater_SRTMN logger displays the reverse relationship to that of Baddoch Burn and Clunie Water, with the downstream site typically measuring lower water column temperatures than the upstream site (Figure 2-3b). This is likely due to the influence of loch Callater on the thermal regime of Callater Burn. A shallow loch with a large retention time and large surface are for radiative forcing at the air-water interface allows water to warm during the summer. The large thermal capacity of Loch Callater also has an influence on the amplitude of daily water column temperature fluctuations at the Callater site, typically dampening maxima and minima (Figure 2-4). The warm waters at the loch outlet are exposed to the environment as they flow downstream to the Callater_SRTMN site. With a reduced thermal capacity in comparison to the loch, the water cools as it travels further from the loch. Large bodies of water have been shown to disrupt downstream thermal regimes, with the degree of disruption varying as a result of regional climates as well as characteristics of the water bodies in question (Evans, et al., 1998; Caissie, 2006).

2.4.1.2. Microclimatic forcings

Observations of relative humidity throughout the study period showed that when relative humidity was low, inter-site variabilities diminished. This is likely due to the influence of regional pressure systems. When a high-pressure system dominated the region, lower relative humidity would be consistent throughout the study area. Further evidence to support this claim is found in when inter-site variability was largest; during transitions from low to high relative humidity. This observation suggests a temporal lag as a lower pressure system approached the study area. The system, having arrived at one site, would increase the relative humidity here relative to other sites, resulting in large differences during transitions from low to high relative humidity.

Spatial variabilities in relative humidity were not as consistent as with water column temperatures. For instance, relative humidity was seen to increase downstream from Baddoch 1 to Baddoch 2, before decreasing from Baddoch 2 to Baddoch 3. This is not unexpected as the influence of local environment on relative humidity is multifaceted. The observed downstream increase can be due in part to the increase in atmospheric pressure with decreasing altitude, as higher-pressure air is capable of holding more moisture relative to lower pressure air. The increase in stream size downstream can also contribute to increases in relative humidity, as a larger body of water is available for providing moisture locally through evaporation (Oke, 1987). The influence of locally available water on relative humidity can be observed at the Callater site, which observed a higher relative humidity than the reference site on occasion throughout the study period, with the presence of Loch Callater providing additional moisture to the local environment. However, this elevated relative humidity at Callater was not prevalent throughout the entire study period, likely due to increases in wind speed at Callater relative to the reference site. Increases in wind speeds can lower above-stream relative humidity by increasing the rate at which evaporated water is removed from the local environment (Oke, 1987). Inter-site variabilities in relative humidity are typically more marked within the literature (Leach & Moore, 2010). This is likely due to the presence and absence of riparian forests between sites studied, where forest canopies provide streams with shelter from high winds, allowing evaporated moisture to remain in the air column above the stream (Georges, et al., 2021).

The reference site typically observed the highest air temperatures of the six sites during the study period. This was to be expected, with the reference site being the most-downstream of sites and air temperature typically increasing as altitude decreases. As with relative humidity, inter-site variations in air temperature tended to be most pronounced during periods of transition from cooler to warmer summer weather (06/07/2022 – 11/07/2022 Figure 2-5a, 2-5b). Once warmer weather was set in, inter-site variations typically diminished (08/08/22 – 15/08/22 Figure 2-5a, 2-5b). This could be due to the uniform radiative forcing during warmer periods. With little to no cloud cover across the catchment during warmer weather, radiative forcing would be more uniform between sites. The stronger agreement in air temperatures between sites during warmer weather could also be due in part to increased atmospheric mixing at higher temperatures. The atmosphere, receiving more energy during a warm period, is more likely to experience vertical mixing through convection, reducing the inter-site variability (Di Cecco & Gouhier, 2018).

Downstream trends in air temperature are difficult to compare with the literature. This is due to the open moorland sites and sheltered forested sites being typically upstream and downstream respectively. Air temperature differences between sites within the literature also tend to be less pronounced than those observed in this study due to their closer proximity to one another (Leach & Moore, 2010).

Wind speed was shown to be the most spatiotemporally stochastic of all microclimate metrics. As a result, any trends identified across space and time were difficult to ascertain. Wind speeds tended to increase upstream during the study period but this relationship was weaker than others. As with relative humidity, studies into the influence of land use on river microclimate typically observe larger inter-site variabilities in wind speed due to the significant influence of established canopies on reducing above-stream wind speeds (Dugdale, et al., 2018; Leach & Moore, 2010; Hannah, et al., 2008).

2.4.1.3. Quantification of energy fluxes

Net radiation (Q*) represents the most substantial energy input to the stream, an observation that is consistent with findings from prior studies examining energy balances during summer periods (Webb & Zhang, 1997; Hannah, et al., 2008; Leach & Moore, 2010; MacDonald, et al., 2014; Garner, et al., 2014; Dugdale, et al., 2018; Ouellet & Caissie, 2023) This emphasises the significance of Q* in driving a headwater stream's energy dynamics.

Additionally, observations revealed high temporal variability in Q* across the catchment, which can be primarily attributed to fluctuations in cloud cover. Cloud cover within the study area exhibited considerable variability throughout the summer months. Furthermore, inter-site variabilities in Q* exhibited a mechanistic pattern, with Q* totals closely mirroring the orientation of respective catchments. The Callater catchment, orientated from southeast to northwest, displayed the lowest mean daily Q* across the summer period, the Clunie catchment, with a south-north orientation, exhibited intermediate Q* and the Baddoch, orientated from southwest to northeast, registered the highest mean daily Q*. This relationship between catchment orientation and Q* during the summer months stems from the more direct alignment of northeast-facing catchments with incoming solar radiation.

The mean daily flux difference between the smallest and greatest Q* flux amounted to 21%. This value is lower than what has been typically observed in the existing literature (Webb & Zhang, 1997; Hannah, et al., 2008; Garner, et al., 2014; Dugdale, et al., 2018), but this discontinuity is expected, given that most previous energy balance studies have compared fluxes under contrasting riparian land uses, with developed riparian canopies reducing the influence of Q* on the stream energy balance. The only previous study which compared spatial variation in Q* fluxes across sites without existing riparian canopies was that of Webb & Zhang, (1997). However, these inter-site variabilities cannot be compared with those observed in this study as data were gathered over discontinuous timeframes.

The largest mean daily loss of energy throughout the study period was from the latent heat flux (Qe). This is consistent with summer observations within the literature (Webb & Zhang, 1997; Hannah, et al., 2008; Leach & Moore, 2010; MacDonald, et al., 2014; Garner, et al., 2014; Dugdale, et al., 2018; Ouellet & Caissie, 2023; Evans, et al., 1998). However, mean daily losses from Qe observed in this study were larger than were observed in similar studies. Hannah et al., (2008) and Dugdale et al., (2018) observed mean daily losses at their respective open moorland sites of -3.44 MJm-2d-1 and -3.1 $MJm^{-2}d^{-1}$ whereas in this study, mean daily losses range from -4.4 $MJm^{-2}d^{-1}$ to -6.9 $MJm^{-2}d^{-1}$.

As with Q* this flux had a high temporal variability across the study area. This is also to be expected as Qe is governed in part by water temperature but also wind speed and relative humidity, microclimate metrics which were also found to be high temporally variable during the study period.

Inter-site variability was greater for Qe than for Q*, with differences in mean daily flux varying by 36% between the smallest and largest fluxes. The influence of water column temperature can be seen when comparing this flux between catchments. The greatest losses during the study period were observed at the Callater site, which also experienced the highest water column temperature. The smallest losses were observed within the Baddoch catchment, which also had the lowest water column temperatures.

Inter-site variations in Qe were also larger within most of the literature (Hannah, et al., 2008; Dugdale, et al., 2018), due primarily to the influence of riparian forests on wind speeds and relative humidity. Here, the forested sites experienced much lower losses from the latent heat flux during summer, with mean daily losses of less than 1 $MJm^{-2}d^{-1}$ (Hannah, et al., 2008; Dugdale, et al., 2018)

Once more, sensible heat (Qh) fluxes were highly variable both within and between sites throughout the study period. Qh is calculated as a function of Qe and the Bowen ratio which is primarily governed by differences between air and water temperatures as well as wind speed. With wind speeds variable both within and between sites, Qh is also highly variable both spatially and temporally. Once more, this also maps onto water column temperatures. The Baddoch sites and Clunie 1 site typically observed lower water temperatures and as a result, had a greater Qh flux than the reference site. The warmer waters of the Callater site typically had lower Qh losses.

Although mean daily fluxes from Qh were much smaller than Qe and Q*, the inter-site variabilities were much larger as a percentage of values, varying by 123% between the smallest and largest fluxes. Inter-site differences observed in the literature varied between studies. Studies showing limited variation in mean daily Qh between sites also tended to have strong similarities in water column temperature during the same period (Dugdale, et al., 2018). Studies with larger inter-site variations also experienced larger differences in water temperature between sites, due in part to groundwater-surface water interactions (Hannah, et al., 2008; Webb & Zhang, 1997). Such variabilities in this study, due to the smaller size of the flux, are of less importance when discussing their influence on inter-site variabilities in net energy exchange.

The same could be said of the influence of the bed heat flux (Qbhf) on net energy exchanges across the study area. When a mean daily net flux was positive, Qbhf attributed for 0.6% of energy gains at sites and when a mean daily net flux was negative, it accounted for an average of 2.6% of losses. Most sites showed close agreement in Qbhf throughout the summer, with the exception of Baddoch 2 and, to a lesser extent, Clunie 1. The Qbhf at these sites were an order of magnitude greater than those of the other site with mean daily Qbhf at Baddoch 2 measuring -0.25 MJm^{-2}, compared to 0.04 MJm^{-2} observed at Clunie 2. As a result, the inter-site variation between fluxes was large as a percentage of their own value, showing high spatiotemporal variability across the study area. This is to be expected as Qbhf is a complex aggregate of conductive, radiative, convective and advective processes, driven in part by spatially discrete phenomena such as groundwater-surface water interactions. Qbhf variations within the literature were also substantial, with Dugdale et al. (2018) observing ranges in mean daily fluxes of -0.1 MJm^{-2} to -0.6 MJm^{-2} across the summer period, but as with Qh, the influence of this flux on the net energy exchange between streams and their environment in this study, as well as in the literature, is small (Webb & Zhang, 1997; Evans, et al., 1998; Dugdale, et al., 2018).

Heat gained from fluid friction displayed less variability than other fluxes throughout the study period. This was to be expected as the magnitude of energy gained from fluid friction is a result of discharge and local geomorphology, the latter typically being fixed at seasonal scales. Temporally, as discharge increased, Qf increased, with three peaks in Qf across sites coinciding with peaks in discharge during the study period (Figure 2-3a, Figure 2-7a & b). Regarding inter-site variability, sites with larger contributing catchments would experience larger discharges which, would increase Qf where channel slope and width were otherwise uniform. Sites with greater slope and smaller widths would also experience an increased Qf flux. Variations in Qf in parts of the literature showed similar patterns with this study during summer low discharge (Webb & Zhang, 1997), with other studies omitting Qf from their energy balance studies due to the equation of Theurer et al., (1984) yielding unrealistically high values compared with other fluxes (Hannah, et al., 2008; Dugdale, et al., 2018).

When analysing the influence of riparian topography and altitude on major energy fluxes, positive correlations were observed between major fluxes and slope mean, topographic roughness index (TRI) mean and aspect mean. The strongest associations were found with these spatial metrics and the Q* flux. This relationship was not expected, with increasing topographic roughness and slope thought to increase riparian topographic shading. However, this relationship can be explained in part by the positive correlation between mean aspect and the slope and TRI metrics. These results suggest that the mean aspect of the riparian topography local to a site and the related exposure to solar radiation from the pathway of the summer sun is more influential on the Q* flux than any shading from riparian topography. A limitation of the correlation analysis is that there is no correction for multiple comparisons within the same dataset, meaning there is an elevated chance of making a type I error, incorrectly rejecting the null hypothesis.

In conclusion, the two major fluxes influencing energy gains and losses from all sites across the summer period are Q* (gains) and Qe (losses). Comparing the inter-site variations in this study with those observed in other studies focusing on land-use influences, this study was found to have more agreement between the turbulent fluxes of Qe and Qh. However, the inter-site variabilities observed in this study are still sizeable enough to influence site-specific energy balances, especially with the observed thermal influence of Loch Callater on the Callater and Clunie 2 sites.

2.4.2. Implications for river management and future research

Process-based stream temperature models are a vital tool for informing land management actions, allowing stakeholders to mitigate the effects of climate change on summer stream temperatures. They can provide insight into how to best target tree planting strategies to have a maximum influence on stream energy fluxes. These models rely on spatially continuous inputs of hydrometeorological data in order to calculate the relevant energy fluxes and the influences the additions of riparian trees could have on stream thermal regimes. Due to financial constraints, it is not possible to produce spatially continuous observations of hydrometeorological data at the river network scale. As a result, process-based stream temperature models are typically constrained to the reach and sub-catchment scale. At these scales, riparian tree planting has been shown to reduce the magnitude of stream temperature increases in summer high-temperature, low discharge conditions in headwater catchments (Benyahya, et al., 2011; Garner, et al., 2017; Hannah, et al., 2008; Dugdale, et al., 2024). However, at small scales, stream temperature studies fail to incorporate the potentially significant effects of advection as a parcel of water travels along a stream network. There is therefore a need to increase the scale at which these stream temperature models are used. This is of particular importance for building an evidence base for reducing stream temperatures in larger order rivers where local riparian planting is considered to be less effective than the planting of headwaters due to the combination of wider channels reducing the extent of shading, greater stream velocities reducing residence times and larger thermal capacities reducing the impact of reduced shortwave radiation on stream temperatures (Jackson, et al., 2021).

There is also a need to understand the relative importance of different river processes and energy fluxes to determine where investments should be focused in scaling said fluxes. Methods for the scaling of some energy fluxes exist, such as solar routine simulations for scaling solar radiation. However, the scaling of turbulent fluxes (Qe and Qh) remains a challenge.

This study has highlighted the spatiotemporal variabilities observed in the non-radiative fluxes both within and between catchments, illustrating the potential risks associated with transferring values from remote AWS across space. Of these non-radiative fluxes, the latent heat flux (Qe) has the largest influence on stream energy balances during summer low discharge conditions. This energy balance study utilised the empirical Penman-style equation adopted by Webb & Zhang (1997) to estimate evaporation rates for the calculation of the latent heat flux (Webb & Zhang, 1997). This method uses empirically derived wind functions to represent the adiabatic portion of evaporation, of which there are many values in the literature. The values used in Webb & Zhang (1997) were developed for forested streams, which would typically experience substantially different evaporation rates compared to the open moorland sites investigated in this study (Hannah, et al., 2008). In order to improve energy flux representation, additional research is necessary to assess the suitability of these wind functions for calculating latent heat fluxes across open moorland catchments.

This study has also shown the variation in energy fluxes within and between nested catchments, along with the influence of large water bodies on disrupting longitudinal thermal gradients in rivers. Further study should be conducted into these variations in order to aid in the scaling of fluxes along river networks.

2.5. Conclusion

Previous studies into spatiotemporal variations in stream energy balances have tended to compare the inter-site variabilities in fluxes between sites with markedly different riparian land uses, such as open moorland/grassland versus riparian forests (Hannah, et al., 2008). This study shows that there are also substantial inter-site variabilities across six novel sites with uniform land uses of exposed moorland and grassland. These findings illustrate the limitations of using a single location for the representation of microclimate and energy fluxes across a temperate headwater catchment. In using a single AWS, spatiotemporally variable microclimate phenomena including cold air drainage and anabatic and katabatic wind patterns, which in-turn influence stream energy fluxes, are not captured.

The study also identified some structure within these variabilities, with correlations found with landscape controls. However, these correlations have very little statistical power and are not a basis upon which to scale energy fluxes against environmental characteristics. The correlations have also not been treated for multiple comparisons, increasing the risk of a type I error having occurred.

There is a need to expand upon these observations, scaling these six point-energy-balance studies to the catchment scale, with emphasis on understanding the turbulent fluxes of Qe and Qh; two fluxes with high spatiotemporal variability. Within this context there is also a need to further investigate the suitability of the wind functions used in calculating latent heat fluxes, with these empirically derived coefficients having the potential to significantly alter the magnitude of latent heat flux calculations in response to observed wind conditions.

Having six AWS makes this study novel in terms of spatial coverage of observations, but inter-site variabilities show that further spatial coverage is needed in order to develop quasicontinuous hydrometeorological inputs for improving process-based stream temperature models.

3. Scaling microclimate determinants of turbulent fluxes from point locations to river networks

Abstract:

Climate change poses significant threats to the suitability of rivers for thermally sensitive freshwater fish species. Consequently, rivers and fisheries managers have substantial interest in understanding and managing river thermal regimes to guide management actions. Process-based river temperature models are a useful tool for understanding how changes to heat and energy fluxes (for example by planting trees) can influence thermal regimes. However, such models can require large inputs of data, which can mean they are confined to smaller river reaches. With river temperatures at a given point being influenced by upstream energy exchanges between the river and its environment, there is a need to increase the spatial scale of these models and their inputs to capture these compounding longitudinal exchanges. Understanding of the variability and relative importance of controls on energy and heat fluxes, alongside knowledge of pre-existing 'proxies' or tools to predict these fluxes, can be used to prioritise modelling efforts to drive process-based river temperature models.

In this study, emphasis was placed on the drivers of latent and sensible heat fluxes, with these turbulent fluxes being highly spatiotemporally variable therefore difficult to scale and the latent heat flux often acting as the greatest energy sink during summer low-flow, high-temperature conditions. Six continuous automatic weather stations (AWS) were deployed across 3 nested sub-catchments during the summer of 2022, supplemented by 24-hour monitoring at 15 additional sites using a roving AWS. Comparing observations from the roving AWS with a stationary reference AWS showed both spatial and temporal patterns in inter-site variability in the micrometeorological determinants of turbulent heat fluxes (air temperature, relative

humidity and wind speeds). Furthermore, given the importance of evaporation on river energy budgets, floating evaporation pans were used to develop wind function estimates for the area, which were subsequently compared to those in the literature.

A number of methods for scaling air temperature, relative humidity and wind speeds were explored. Use of a single AWS for characterising microclimate across the study area was found to be insufficient, especially for predicting microclimate metrics in sub-catchments, with the single AWS introducing large prediction biases. When incorporating all six fixed weather stations across the three catchments in a leave-one-out-cross-validation (LOOCV), inverse distance weighting (IDW) of microclimate metrics using Euclidean distances was found to perform best in scaling air temperature and wind speeds across the study area, producing small root mean square errors and biases. For scaling relative humidity observations, Euclidean distance IDW was the second-best metric behind streamwise IDW.

A number of empirically derived wind functions from previous literature are typically used to calculate evaporation rates in physically based water temperature models. Often derived from lakes and cooling ponds rather than river environments, these values can be a major source of error in modelling turbulent fluxes. This study employed a floating evaporation pan to ground truth wind function estimates in observed river evaporation rates, constraining the wind function parameter for this environment. Wind functions developed for the study area performed best in reproducing observed evaporation rates, with substantial variability in the performance of other literature derived wind functions. However, the choice of wind function could be aided by having observed evaporation rates to compare against. The findings here illustrate the importance for understanding the spatial and temporal variability in the controls on river temperatures, which can inform the required resolution of monitoring to provide data for process-based river temperature models.

3.1. Introduction

Water temperature is a critical factor controlling the functioning of river ecosystems (Hannah & Garner, 2015; Durance & Ormerod, 2009). It governs rates of primary production and ecosystem respiration in the carbon cycle (Allen, et al., 2005) and has a strong influence on cold water adapted freshwater fish species, such as Atlantic salmon and brown trout, influencing their distribution, abundance, demographics and production (Dugdale, et al., 2017; Jackson, et al., 2018; Caissie, 2006).

In temperate uplands, such as the Scottish Cairngorms, significant climate-induced temperature changes are expected due to low thermal capacity and high exposure to solar radiation from the lack of shading by riparian trees (Hrachowitz, et al., 2010; Jackson, et al., 2018). There is a pressing need to manage riverscapes in the Scottish Cairngorms to build river temperature resilience against future climate scenarios which could harm salmonid populations.

To guide management action, it is important to understand the processes controlling river thermal regimes. One tool increasingly used is the process-based river temperature model, which predicts river temperatures by using empirical hydrometeorological measurements to derive the energy and water fluxes which occur between a river and its environment. Such models are useful in researching the response of river thermal regimes due to their ability to simulate different climate inputs (Dugdale, et al., 2017).

However, process-based river temperature models can be ‘data intensive’ requiring detailed information on heat and energy fluxes, which can exhibit substantial spatial and temporal variability, meaning that some models can be restricted to reach scales (Dugdale, et al., 2018; Garner, et al., 2017; Webb & Zhang, 1997). Furthermore, the number of continuous monitoring locations (e.g. weather stations) available to underpin such models is often limited (MacDonald, et al., 2014). There is thus a need to develop models of (or proxies for predicting) key fluxes to understand and predict spatio-temporal variability in fluxes, to underpin process-based river temperature models at larger spatial scales (e.g. sub-catchment, catchment).

Evaporation is a key control on river temperature and as stream temperatures rise during summer low-flow conditions, loss of energy from a river via evaporation (or the latent heat flux) is an important energy sink restricting further warming in the water column (Caissie, 2006). This is particularly true in exposed reaches with limited riparian vegetation such as those featured in this study (Hannah, et al., 2008). Results of the six-point energy balance study conducted in Chapter 2 found that the latent heat source was the largest energy sink across the study period with mean daily losses ranging from 4.4 $MJm^{-2}d^{-1}$ to 6.9 $MJ\ m^{-2}d^{-1}$. Similar studies in open moorland conducted by Hannah et al., (2008) and Dugdale et al., (2018), also found the latent heat flux to be the primary energy sink during low flow summer conditions, with observed mean daily losses of 3.44 and 3.1 $MJm^{-2}d^{-1}$ respectively (Dugdale, et al., 2018; Hannah, et al., 2008).

The primary microclimatic drivers of the latent heat flux, aside from water temperature, are air temperature, relative humidity, and wind speed. Of these, relative humidity and wind speed exhibit significant spatiotemporal variability, making them particularly challenging to predict across river networks, especially where meteorological observations are historically limited. Consequently, the representation of the latent heat flux in previous stream temperature models has been marked by considerable uncertainty and recognized as a key modelling limitation (Dugdale et al., 2017). This issue is discussed in the Section 1.2- Research Gaps, within the thesis introduction.

New methodologies using floating evaporation pans and adapted wind functions have provided insights into evaporation dynamics in mountainous streams (Maheu, et al., 2014; Szeitz & Moore, 2019). However, thus far these studies have typically featured well-developed riparian trees which are known to influence river evaporation rates through effects on air temperature, wind speed and humidity (Hannah et al., 2008). Within the current literature, observations of evaporation rates from floating evaporation pans in environments with little to no riparian vegetation is limited. Furthermore, although a number of wind functions have been developed for varying environments and objectives (Bowie et al., 1985; Harbeck, 1952; Harbeck et al., 1958; Marciano & Harbeck, 1952; Meyer, 1942; Morton, 1983), there are limited examples for river and riparian environments (Benner, 2000; Szeitz & Moore, 2019; Guenther, et al., 2012; Maheu, et al., 2014).

With this in mind, the aim of this paper is to incorporate short time-series of discontinuous and asynchronous microclimate and energy flux data from a large number of sites into a continuous series of data from a smaller number of sites, in order to understand and scale fluxes across riverscapes.

The objectives of this study are to:

(i) characterise the spatiotemporal variability in microclimate and energy exchanges across a physically diverse upland landscape with the use of a roving AWS;

(ii) explore options for scaling microclimate and energy fluxes from point locations to spatially distributed river networks; and

(iii) compare estimates of latent heat fluxes obtained from evaporation pan experiments with those derived from microclimate data to determine the accuracy and biases associated with commonly applied algorithms, investigating opportunities for calibration and correction.

3.2. Methods

This study focuses on three sub-catchments of the Aberdeenshire River Dee, Scotland. The Clunie Water catchment ranges in altitude from 338 to 1062 mAOD and spans an area of 104 km^2 (for further information, see Chapter 2, section 2.2.1, Study area and site characteristics).

3.2.1. Site locations and measurements

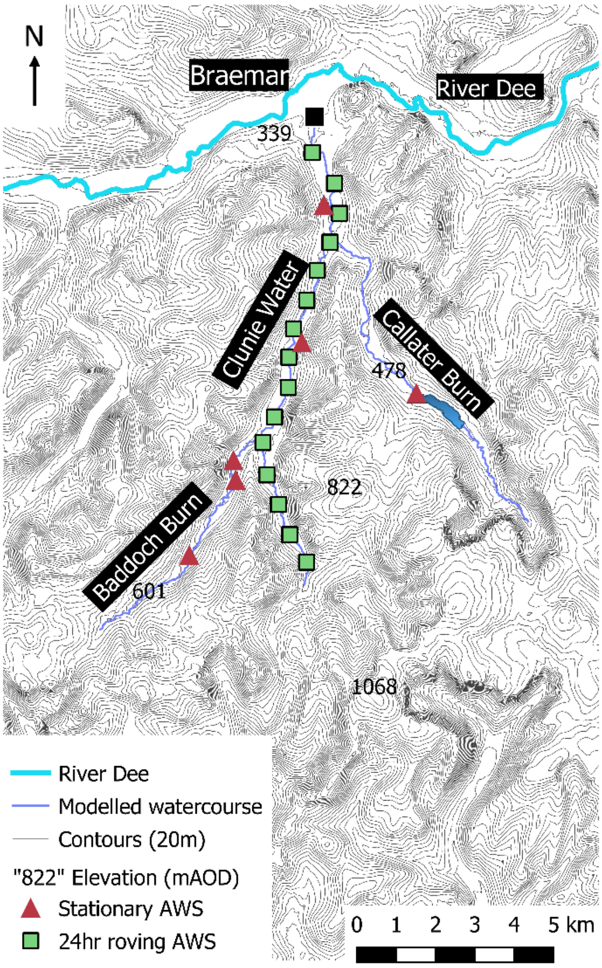

Figure 3-1 Stationary and roving AWS locations

Six stationary AWS (red triangles, Figure 3-1), collected continuous hydrometeorological data at a 15-minute resolution between 21st June and 9th September 2022. Sites were selected to represent various elevations, stream channel orientations, geomorphologies, land uses, and the thermal influence of Loch Callater.

Stationary weather stations were supplemented with the use of 15 sites using a novel roving weather station. The novelty of this roving weather station was in its lightweight design which allowed for rapid installation, whilst also using the majority of the sensors found on the stationary AWS. The same sensors were used on the roving AWS as the stationary AWS for air temperature, relative humidity, shortwave radiation, longwave radiation and wind speed. The only sensor deviance was for water temperature, where a Gemini Tinytag 2 sensor was used in place of CS 107 and Van Essen Cera Divers. The roving AWS was considerably lighter than the stationary AWS due to the use of a lightweight Campbell Scientific tripod and crossarm in place of the series of 3m and 4m scaffolding poles used to provide the base and crossarm for the stationary AWS design.

The lightweight design meant that microclimate observations could be taken at a very high spatial resolution (sub-1 km) with the roving AWS but for smaller periods (24 hours) and these observations could be anchored against those from the six spatially limited but temporally continuous stationary AWS. In doing so, insights could be gained into the spatiotemporal variability of microclimate between stationary AWS.

Data were collected for a single 24-hour period (at 15-minute resolution) over three separate weeks in June, August and September. In Figure 3-1 the green squares represent the 15 roving AWS locations. Roving AWS site 1 is the most upstream and 15 is the most downstream of roving sites. Relative to these numbers, the reference site is situated between roving sites 13 and 14.

The roving AWS sites were selected to capture the site variability across the length of Clunie Water, with sites occurring regularly (approximately every 850 m when accounting for micrositing). AWS locations were micro-sited for ease of access for maintenance and data downloads as well as capturing well-mixed channel water.

In this design, the stationary AWS provide a high temporal resolution to develop approaches for scaling fluxes. The roving AWS provides an increased spatial resolution and understanding of spatial variability in fluxes, which can also be used as validation for scaling approaches. The instruments used and their associated instrument error are detailed in Table 2-2 in Chapter 2. The roving AWS featured the same sensors with the exception of T107 sensors in the streambed and heat flux plates. Water column temperatures were monitored using a Gemini Tinytag Aquatic 2 sensor and no bed heat fluxes were measured from the roving AWS.

3.2.2. Deriving energy fluxes

The following equations are cited in the methodology document prepared by Boyd and Kasper (2003) to accompany the Heat Source model Version 7.0.

For the latent heat flux,

$$Q_e = E_v \bullet L \bullet p$$

Where

Qe = latent heat flux (W m^{-2}), Ev = evaporation/condensation rate (mmd^{-1}), L = latent heat of vaporisation (°CJg^{-1}) and p = specific weight of water (gcm^{-3}).

The evaporation/ condensation rate can be calculated using the following mass transfer method equation:

$$E_v = f(W) \bullet (e_s - e_a)$$

Where *f(W)* = a function of wind speed (km d^{-1}), e_s = saturation vapour pressure at water surface temperature, e_a = vapour pressure at air temperature based on saturation vapour pressure

$$e_s = 6.1275 \bullet e^{\left(\frac{17.27 \bullet Tw}{(237.3+Tw)}\right)}$$

$$e_a = (RH/100) \bullet e_s$$

Where T_w = water column temperature (°C) and RH = relative humidity (%)

The latent heat of vaporisation can be calculated as follows:

$$L = 1000 \bullet (2501.4 + (1.83 + T_w))$$

Sensible heat exchange can then be calculated as the product of the latent heat flux and the Bowen ratio. The Bowen ratio is estimated using the following equation:

$$B = [0.61P \bullet (T_w - T_a)/E_w - E_a)]/1000$$

Where B = Bowen ratio and P = air pressure (mbar)

The equations used to calculate the latent heat flux are often referred to in the literature as the Dalton method as they are based on Dalton's law of partial pressures, wherein the evaporation rate is proportional to the difference between the saturation vapour pressure at the water surface and the actual vapour pressure in the air above the water surface (Lim et al., 2012).

From this series of equations, the metrics determining the turbulent heat fluxes are air temperature, water temperature, relative humidity and wind speed and the wind functions associated with wind speed. Because the outputs of this scaling exercise will feed into water temperature models, water temperature cannot be scaled here as this creates a circular dependency. In this instance, only direct observations of water temperature can be used as inputs.

3.2.4. Evaporation pan methodology

To observe evaporation rates, an evaporation pan was built inspired by the methods outlined in Szeitz & Moore (2020).

Figure 3-2 Roving AWS and floating evaporation pan installed along Clunie Water

A plastic container with base dimensions of 180 mm x 155 mm was used as the pan to hold the water, and it was kept buoyant using a swimming aid float. The float was covered in white electric tape to reduce the absorption of solar radiation and any influence on the temperature of the water held in the pan. The design ensured that the bottom of the pan was in contact with stream water at all times. This was to reduce any potential warming of the pan water above that of the river water, as the small quantity of liquid would have a lower heat capacity than the river and would be susceptible to warming at a faster rate than the river. The evaporation pan was anchored by chaining it to a hessian sack filled with cobbles. Ideally, the pan would be placed in calm but flowing water downstream of a riffle, so it was well mixed but not turbulent enough to cause water to splash into or out of the pan.

Measuring rates in the field consisted of filling the pan with 250 ml of river water, placing the pan in the river for a set amount of time and measuring changes in mass every 30 mins or 1 hour between 12:00 and 16:00 reflecting evaporation rate being most influential on high summer river temperatures during the early afternoon. 250 ml was chosen as a compromise between having the largest quantity of water possible to reduce the likelihood of significant warming and having too much water so as to lose a quantity through spillages. A balance was used to measure out the initial 250 ml and any mass lost to evaporation. When removing the evaporation pan from the river for weighing, the bottom of the pan was dried to remove any additional river water attached. Measurements from the balance were sensitive to gusts of wind so measurements were taken from within a storage box which acted as a wind break. Each measurement was repeated three times with a mean mass loss calculated. Across repeat measurements, the mean standard deviation of mass loss was observed as 0.05g. To calculate the evaporation rate, the following equation was used:

$$E = -\frac{\Delta M \cdot c_f}{\rho_w \cdot A \cdot \Delta t}$$

Where:

E is evaporation rate (mm h^{-1});

ΔM is the change in mass over the measurement interval (kg);

cf is a conversion factor of $3.6*10^6$, to convert the result from m s^{-1} to mm h^{-1};

ρw is the density of water (kg m^{-3});

A is the surface area of the water in the pan (m^2); and

Δt is the length of time interval measured (s).

The wind function present in the evaporation rate equation was used to estimate the adiabatic portion (phase change between liquid and gas) of the latent heat flux. The wind function can be defined as follows:

$$f(W) = a + b \bullet W$$

Where a and b are coefficients which have been empirically derived and W is wind speed.

Plotting observed evaporation rates against wind speeds measured at the roving AWS and fitting a linear regression to the relationship provides the wind function coefficients for estimating evaporation (evaporation rate = a + b* wind speed). These wind function coefficients were then compared with a series of coefficients empirically derived from the literature (see Table 3-1) which cover a range of environments from Southern USA to Australia. The majority of functions were developed within the context of water resource management, estimating quantities of water to be lost from reservoirs to the atmosphere via evaporation. Other applications include estimating evaporation rates from arable crops to inform irrigation rate optimisation (Boyd & Kasper, 2003). Of the wind functions featured in this study, only those of Caissie (2016), Maheu (2014) and Szeitz (2019) were developed using floating evaporation pans in river environments. Further still, these river environments typically consisted of largely wooded areas. With headwater streams in open moorland environments such as those in this study differing in character to densely forested headwaters and differing significantly in their character to arable fields and reservoirs, there is therefore a need to test the suitability of these wind functions by comparing derived evaporation rates with observations in the field.

Table 3-1 Literature wind functions coefficients for Dalton style evaporation rate calculations

Author	a	b	Region	Site	Pan type
Meyer (1942)	4.18E-09	9.50E-10	USA	Lake	Floating pan
Marciano & Harbeck (1952)	0.00E+00	1.02E-09	Oklahoma	Lake	Land-based pan
Harbeck et al. (1958)	0.00E+00	1.51E-09	Arizona	Lake	Mixture of floating and land-based pans
Morton (1983)	3.45E-09	1.26E-09	Canada	Land evapo-transpiration	Land-based pan
Brady et al. (1969)	2.81E-09	1.40E-10	Southern USA	Cooling pond	NA
Brady et al. (1971)	2.21E-09	0.00E+00	Southern USA	Cooling pond	NA
Ryan & Harleman (1973)	2.83E-09	1.26E-09	Melbourne	Cooling pond	NA
Dunne & Leopold (1978)	1.51E-09	1.60E-09	NA	NA	NA
Bowie et al. (1985)	3.08E-09	5.85E-09	California	Lake	NA
Szeitz (2019)	1.94E-09	1.53E-09	New Brunswick	River	Floating pan
Benner (2000)	4.00E-09	2.36E-09	Oregon	River	Land-based pan
Guenther et al. (2012)	0.00E+00	1.18E-09	Vancouver	River	Land-based pan
Maheu et al. (2014)	3.06E-09	3.39E-09	New Brunswick	River	Floating pan
Caissie (2016)	0.00E+00	5.28E-09	Canada	River	Floating pan
Webb & Zhang (1997)	1.53E-09	1.64E-09	Southwest England	River	NA
This study	3.06E-09	7.28E-10	Cairngorms UK	River	Floating pan

3.2.5. Understanding spatio-temporal variability

Spatial and temporal variability in summer air temperature, relative humidity and wind speeds at the stationary and roving weather station sites are presented using time series difference plots and scatter plots. The time series plots highlight the temporal variability between the reference site (most downstream of stationary AWS) and roving sites. Difference plots are calculated as roving AWS observation minus stationary AWS observation, so a positive difference is where the roving AWS observes a higher value than the reference.

Scatter plots display the relationships between sites across the summer period. Relationships between environmental characteristics and micrometeorology are also displayed in a series of scatter plots, consisting of linear regression plots between mean summer fluxes and environmental characteristics and their corresponding correlation coefficients.

3.2.6. Scaling methods development and evaluation

Previous work (Chapter 2) demonstrated spatio-temporal variability and relative importance of energy fluxes on the river energy balance. This understanding, alongside knowledge of pre-existing ‘proxies’ or tools to predict these fluxes, can be used to prioritise modelling efforts to drive process-based river temperature models. Specifically, by focusing on the most variable and important fluxes where alternative information is not available.

For example, although net radiation is the most influential flux on net energy exchange, between rivers and their environment, there are established methods for scaling. In contrast latent and sensible fluxes are not readily available at larger spatial scales, as the drivers of turbulent fluxes, (namely air temperature, relative humidity and wind speed) do not currently have well established methods for scaling. Similarly, bed heat flux and fluid friction show large spatiotemporal variation between sites, but have a relatively small influence on the energy balance across sites. Consequently, this chapter focuses on scaling the variables which govern the turbulent heat.

When attributing data from six AWS to nodes along the river network (i.e. scaling from point observations to continuous across the network), the two methods chosen for comparison were: using the nearest stationary AWS data for a given location and using data from all six AWS and applying an inverse distance weighting (IDW) to each AWS. The IDW method uses temperatures from all six AWS for each location in question, assigning a weighting to the temperature of each stationary AWS which is inverse to its distance from the given point along the stream network. Thus, the AWS which are closer to a given location will be given a larger weighting than those further away.

As well as these two methods of attributing AWS data, two methods of calculating distances along the river network were tested: Euclidean distance and streamwise distance. The Euclidean distance is the straight-line distance between an AWS and a point along the river. This is the easiest method for calculating distances but does not consider the presence of topography and valley form, which will influence micrometeorology in a temperate headwater catchment. The streamwise distance is the distance along the river network between points. By measuring distances between sites as the distance along the river network, the streamwise method indirectly incorporates the influence of valleys on micrometeorology by increasing the distance between AWS in disparate valley systems. It also better represents the true distance the stream travels and the interaction time between the stream and surrounding environment.

To study the effects of using different methods for characterising the air temperature, relative and humidity and wind speeds across the catchment, the following plots were produced:

instantaneous values at 06:00, 12:00 noon, 18:00 and midnight during periods of high and low values for each metric (e.g. for Ta, days with the highest and lowest mean Ta at reference site); scatter plots of observed vs predicted measurements for each metric coloured firstly by time of day to observe diel patterns in predictions, and secondly by site to observe spatial patterns; and finally, spatial plots of the largest positive and negative differences in observed and predicted measurements for each roving site, with point sizes equalling the size of the difference and point colour being the time of day of the largest observed differences.

The performance of methods used for incorporating the data would be validated against the observed micrometeorology of the 15 roving AWS sites and 6 fixed AWS sites. The validation metrics chosen were the root mean square error (RMSE), bias and standard deviation (SD) of observations. Using SD instead of variance allowed for all three metrics to be compared on a uniform scale.

Furthermore, research efforts into river temperature modelling have typically been limited to a single AWS, the use of six stationary AWS was first be tested against the performance of a single AWS. The AWS chosen for this was the most downstream of the six (Clunie 2), as this is the easiest to access of the six sites and in a study with one AWS, would likely be the chosen location.

3.3. Results

The following results section explores the spatial and temporal variability of the microclimate metrics of air temperature, relative humidity and wind speed measured at the roving AWS sites along Clunie Water. Microclimate data from the six stationary AWS were then scaled to produce continuous observations along the stream network using nearest-neighbour and inverse distance weighting methods, with an additional lapse rate method tested for scaling air temperature. These scaled data were then validated against roving AWS observations and stationary AWS observations, with leave-one-out-cross-validation (LOOCV) used for testing against stationary AWS observations. Finally, observed evaporation rates recorded in the floating evaporation pan were compared with rates derived from microclimate metrics using a series of literature wind functions alongside bespoke wind functions calculated using the evaporation pan.

3.3.1. Observed roving AWS microclimate

Observed air temperature (Ta), relative humidity (RH) and windspeed (Ws) at the reference site (Clunie 2, most downstream of stationary AWS) and the difference between these observations and those at each roving AWS site illustrate spatial and temporal variability across the catchment (Figure 3-3). The figure is divided into three columns: a, b and c; one for each microclimate metric, with values displaying observations for the week of August. The figure is also divided into two rows: (i) and (ii), with the first row displaying observations at a reference site (Clunie 2 stationary AWS, most downstream in the study area) and the second row displaying differences between observations at a given roving AWS location and the reference site.

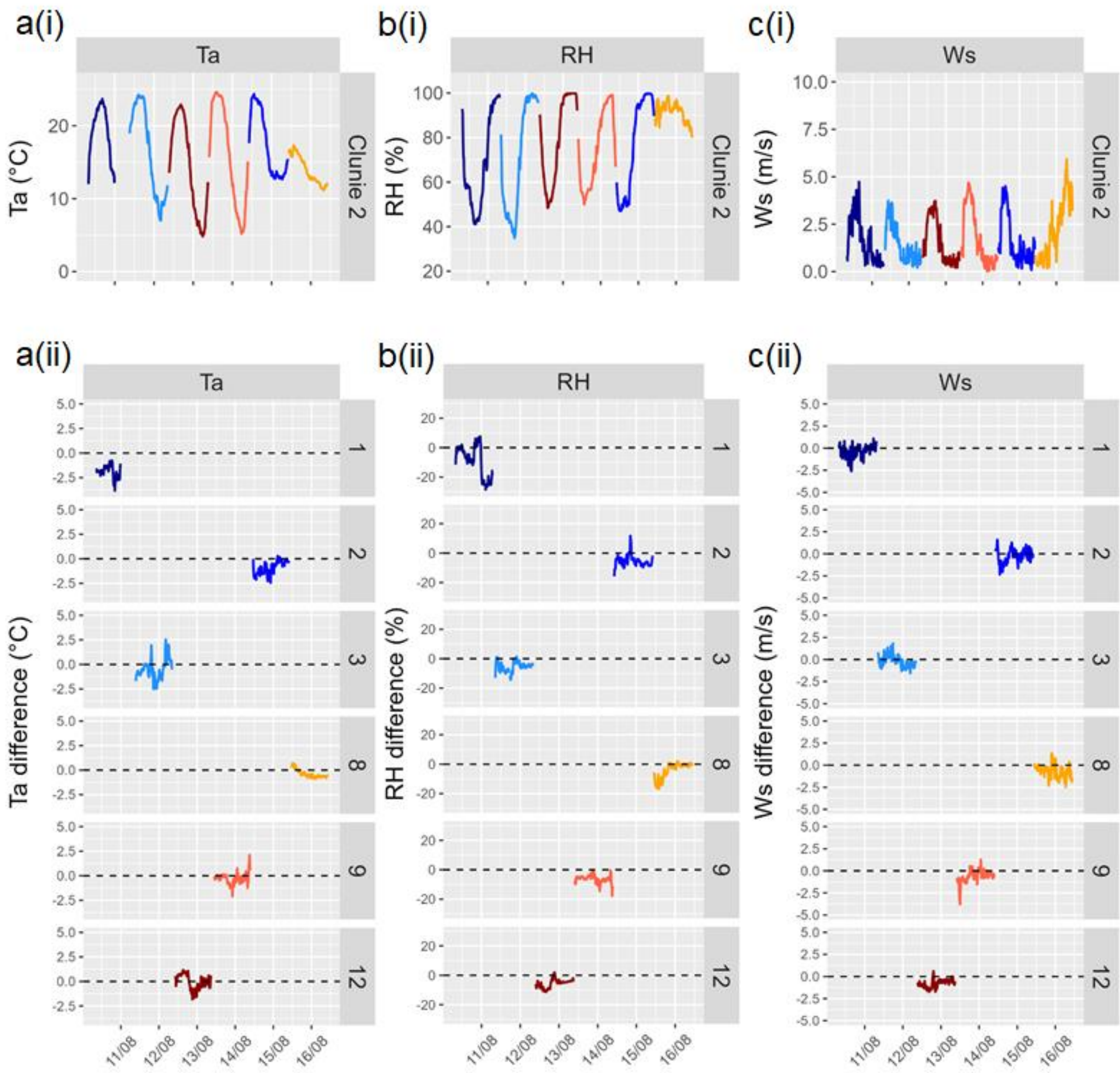

Figure 3-3 Observed air temperature (Ta, a(i)), relative humidity (RH, b(i)) and windspeed (Ws, c(i)) at the reference site (Clunie 2 stationary AWS) and differences (roving AWS minus reference AWS) between roving AWS and reference site (a(ii), b(ii), c(ii)). Difference panel numbers signify roving site number.

3.3.1.1. Air temperature

The Roving AWS was deployed for a week in June, August and September. The week of collecting measurements with the roving AWS in August differed from June and September, with the majority of days being conducted during clear skies. This coincided with the warmest period of roving data collection, measuring up to 24.5 °C, compared with the warmest roving days in June and September of 20.6 °C and 17.0 °C respectively (Figure 3-3, warmest roving AWS day 14/08 highlighted in orange). The 24-hour period with closest air temperature agreement with the reference site was at site 8 which displayed muted diurnal temperature fluctuations at both the reference site and roving site (Figure 3-3, highlighted in yellow). Sites further upstream (higher altitudes) typically had lower air temperatures than their downstream equivalents (Figure 3-3, sites 1, 2 and 3) and inter-site variations were greater during periods with larger diurnal ranges in air temperatures.

Compared to the August monitoring period, air temperatures were cooler during June and much cooler in September at the reference site, with temperatures ranging from 7 °C to 21 °C and 1.5 °C to 17.0 °C respectively. Diurnal ranges were also muted in these periods compared to August. Still, within these periods with more muted diurnal ranges in air temperature, on days where larger diurnal ranges were observed at the reference site, the larger differences between roving and stationary AWS air temperatures still occurred.

Air temperatures observed at each roving site across the summer were plotted against respective observations at the reference site. This scatterplot was coloured by a number of spatial environment characteristics including elevation, distance upstream, mean riparian slope, mean topographic roughness and mean aspect (see Chapter 3 Appendix- Scatterplots). Of these environmental characteristics, the only strong pattern observed was between elevation and air temperature. Sites with higher elevation typically observed lower air temperatures relative to the reference site. As a result, when scaling air temperature, a lapse rate method incorporating elevation was tested as one of the scaling methods.

3.3.1.2. Relative humidity

Figure 3-3 Column b displays diurnal fluctuations in relative humidity for a week in August. These were consistent throughout much of the summer, with highest measurements in the early morning and lowest in mid-afternoon. The range of values for relative humidity at the reference site were somewhat consistent, with values ranging from 37% to 100%. Differences between relative humidity at the reference site and roving sites were more stochastic than air temperature, with oscillations occurring to make relative humidity briefly higher at most roving sites than the reference site on occasion. However, when averaged, relative humidity readings at the roving sites were typically lower than at the reference site for most of the summer.

Diurnal ranges in relative humidity in August, as with air temperature, were greater than those of June and September. However, in contrast to air temperature, differences in relative humidity between the reference site and roving sites in August were lower than those observed in June. Across the sites visited in August there appeared to be a weak longitudinal pattern in relative humidity, with higher relative humidity observed in the headwaters than downstream.

Relative humidity at the reference site was relatively high during September, with observations ranging from 65% to 100%. Differences between the reference site and roving sites were more varied here than during the months of June and August, with stochastic readings at sites five and six. The final two roving sites showed a diurnal pattern in relative humidity difference, wherein the roving sites had greater relative humidity than the reference site in the evening. This pattern then reversed by the late morning and into midday.

To test for relationships between relative humidity and environmental characteristics, observed relative humidity was plotted against elevation, distance upstream, mean riparian slope, mean topographic roughness and mean aspect, but no patterns were observed (see Chapter 3 Appendix- Scatterplots).

3.3.1.3. Wind speed

Wind speed at the reference site is much more stochastic in nature than air temperature or relative humidity. Most days during the June roving period saw a diurnal fluctuation, with wind speeds typically elevated in the afternoon and reducing at night. A high degree of stochasticity in wind speeds was observed at roving sites too, with more agreement with the reference site at roving locations in closer proximity to the reference site (see Figure 3-3, panel c(ii), site 12).

Wind speeds at the reference site throughout the August roving period were more consistent than for the month of June. Once more, the diurnal pattern of high wind speeds during the afternoon and lower wind speeds at night was observed at the reference site. Wind speeds at the roving sites were also more consistent with the reference site than they had been during June, with differences between the roving site and reference site much more muted across the catchment.

Wind speeds were lower during the period of September at the reference site when compared to June and August, with wind speeds only exceeding 5 m/s for a brief period on 11/09. The diurnal pattern which was observed for much of the August roving week was also observed during September but only for two of the four days. It was during the calm nights of these two days that differences in wind speeds between the reference site and roving site were reduced.

For the wind speed metric, as with the relative humidity observations, no spatially consistent patterns were observed in relation to the environmental characteristics of elevation, distance upstream, mean riparian slope, mean topographic roughness or mean aspect.

3.3.2. Scaling microclimate

3.3.2.1. Air temperature

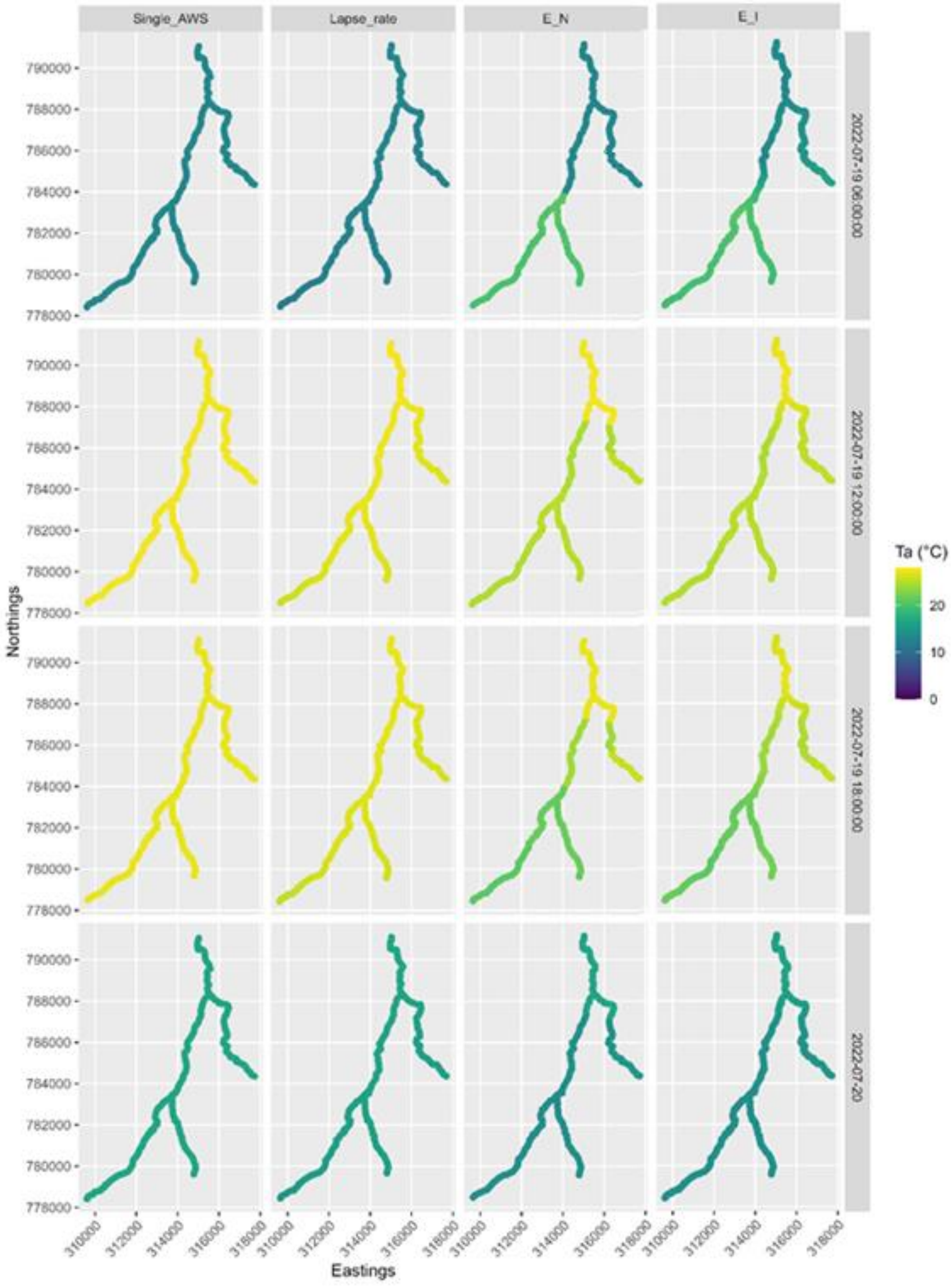

Figure 3-4 Instantaneous air temperature observations and estimates across the catchment on the hottest day of 2022 using observations of a single AWS (Single_AWS, far left), lapse rate estimates of a single AWS scaled (Lapse_rate, centre left) observations of 6x AWS scaled using nearest Euclidean distance (E_N, centre right) and inverse distance weighted Euclidean distance (E_I, far right).

There are large instantaneous differences in air temperature across the study area (Figure3-5 E_N column), which using only data from the single AWS (Figure 3-4 Single_AWS column) would fail to capture.

Spatial variation was incorporated into the lapse rate method (centre left column), with air temperatures reducing with increasing elevation at a rate of 6.5 °C km^{-1}. However, the instantaneous differences observed between the six AWS are more pronounced than those predicted using the lapse rate method.

Additionally, the observed air temperatures also do not follow a linear pattern along the river network, particularly between sub-catchments. Observations of the six AWS show that at both 06:00 and 12:00 noon, air temperatures observed upstream along the Baddoch Burn catchment were higher than those downstream within Clunie Water. As displayed in Figure 3-4, the lapse rate method is incapable of estimating warmer air temperatures at higher elevations and is therefore, in this instance, unable to reproduce the observed air temperatures within the study area shown in.

When comparing the spatiotemporal outputs of the air temperature scaling methods which incorporate data from all six stationary AWS (Figure 3-4, Euclidean nearest, Euclidean IDW, Streamwise nearest and Streamwise IDW), there is little to distinguish in spatiotemporal patterns between the methods, with all methods typically capturing similar patterns in air temperature throughout the day.

As seen in Figure 3-4, the point along a river at which the nearest AWS switches from one AWS to another will often cause a "jump" in observations, whereas the IDW method will produce a gradient of change between locations as the weightings of one AWS gradually overcomes the other.

One observed difference in patterns drawn from methods here is in the Euclidean nearest fixed method and its influence on the mid-reaches of Callater. In the mid-Callater, the Euclidean nearest AWS is Clunie 1, the most upstream Clunie site. At both 12:00 noon and 18:00, Clunie 1 has a lower air temperature than that of Callater. Because the Euclidean method does not account for changes in sub-catchment, this cooler Clunie 1 air temperature extends to the mid-Callater Burn reaches and is seen most visibly at 18:00.

Overall, each of the methods which use the six stationary AWS capture the non-linear spatiotemporal dynamics observed across the catchment for air temperature.

3.3.2.2. Relative humidity

Observing the patterns between the six AWS (Figure 3-5), relative humidity was typically higher downstream in the morning and lower relative to the headwaters by 18:00. As seen with air temperature, the patterns in relative humidity along the river network were not longitudinal or consistent throughout the 24-hour period, thus the use of a single AWS does not capture the instantaneous spatiotemporal dynamics along the network.

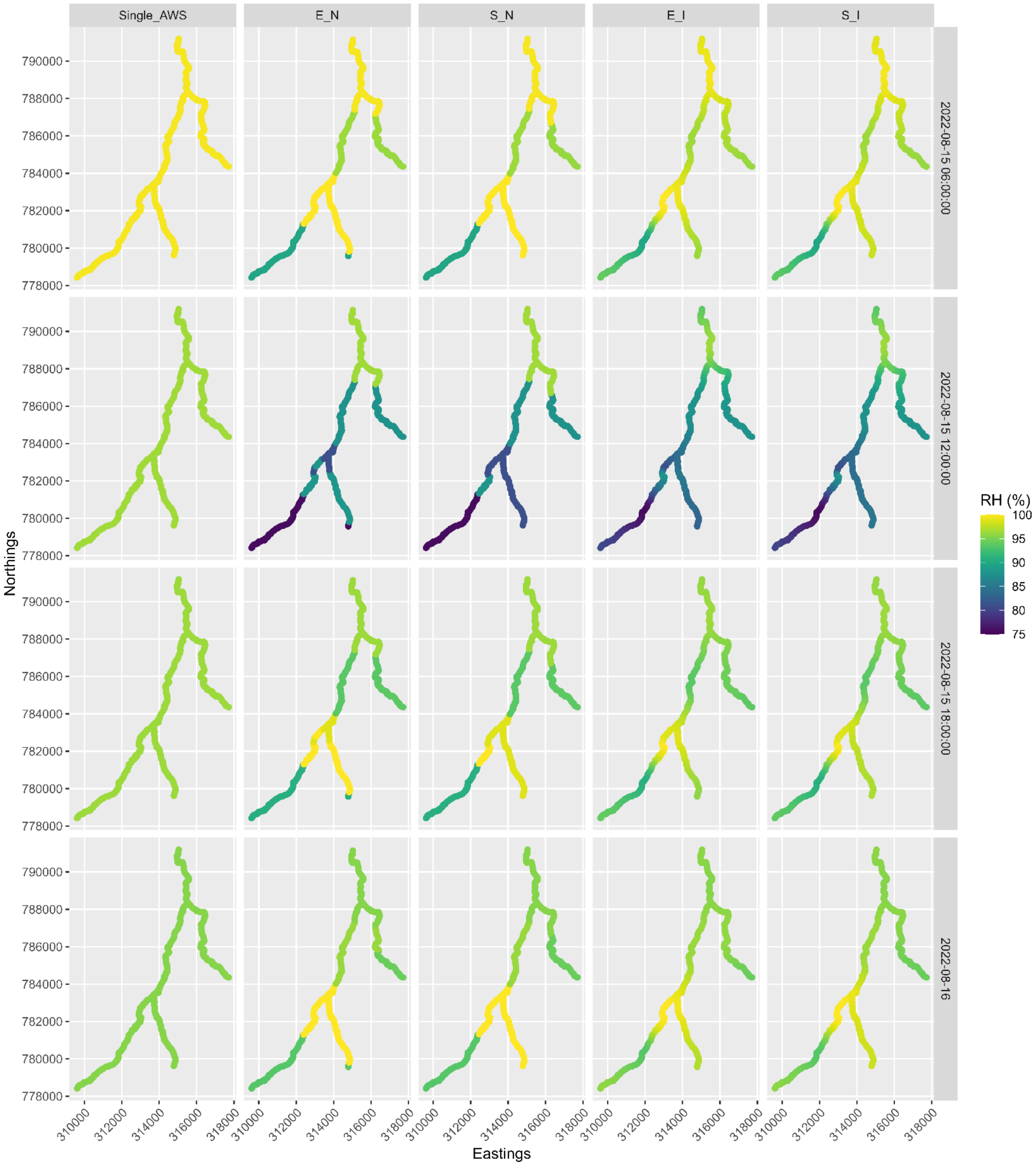

Figure 3-5 Instantaneous relative humidity observations and estimates across the catchment on the most humid day of summer 2022 using observations of a single AWS (Single_AWS, far left), and observations of 6x AWS scaled using nearest Euclidean nearest distance (E_N, centre left), Streamwise nearest distance (S_N, centre), Euclidean IDW (E_I, centre right) and Streamwise IDW (S_I, far right).

3.3.2.3. *Wind speed*

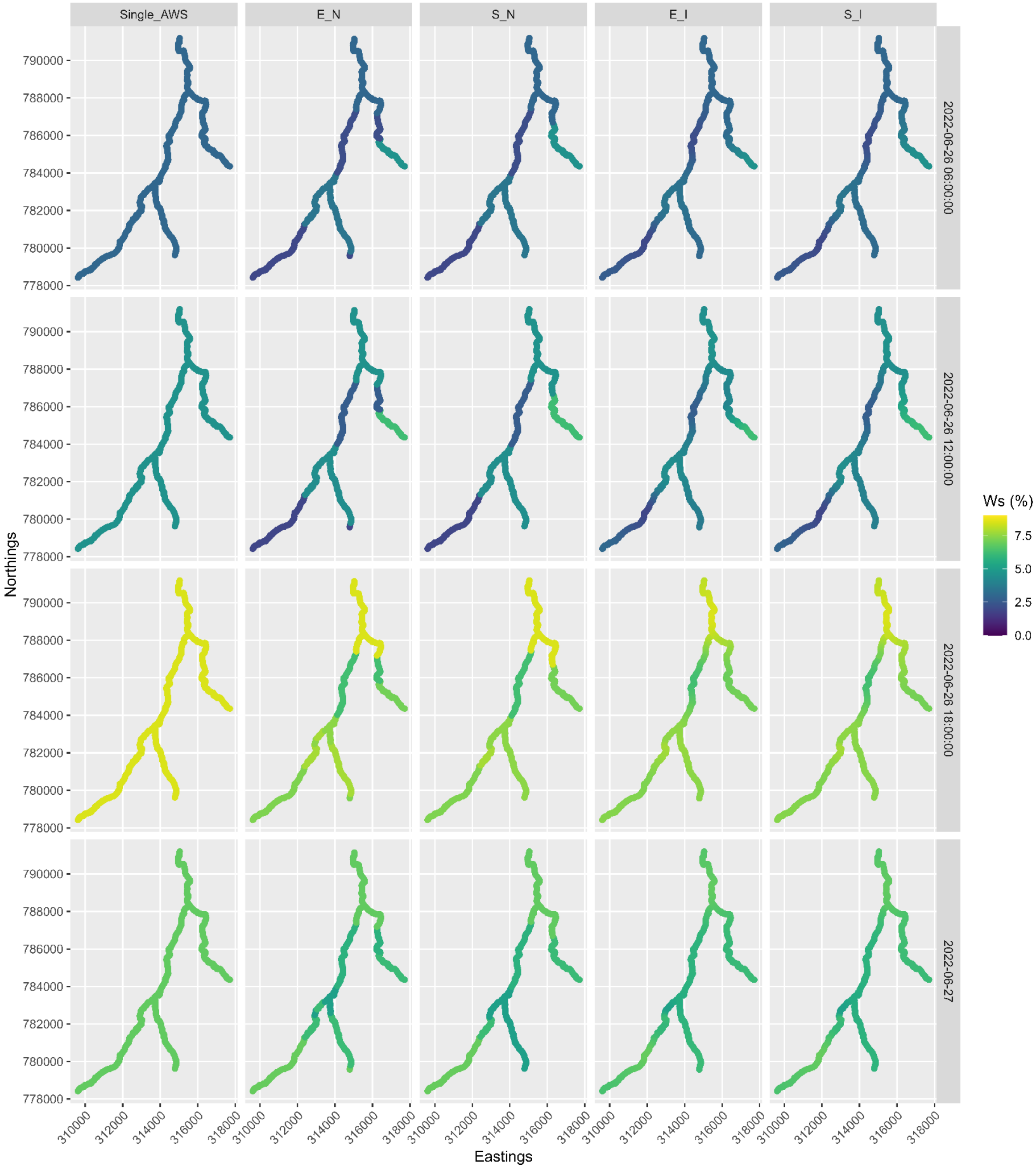

Figure 3-6 Instantaneous wind speed observations and estimates across the catchment on the windiest day of summer 2022 using observations of a single AWS (Single_AWS, far left), and observations of 6x AWS scaled using nearest Euclidean nearest distance (E_N, centre left), Streamwise nearest distance (S_N, centre), Euclidean IDW (E_I, centre right) and Streamwise IDW (S_I, far right).

Figure 3-6 shows the distribution of wind speeds across the catchment during the day where mean wind speeds were highest at the single AWS site. This day was chosen because, as with air temperature and warm days and relative humidity and humid days, wind speed shows elevated inter-site differences during more unsettled conditions. The spatiotemporal patterns observed here are similar to the relative humidity observations during the dry day, with areas experiencing low relative humidity also experiencing high wind speeds. Wind speeds are higher across the catchment at 18:00, with inter-site variabilities also at their greatest at this point.

As observed with relative humidity, there is no consistent longitudinal pattern observed for wind speeds. They are typically greater upstream during the morning and greater downstream in the afternoon.

Although these instantaneous differences displayed in figures 3-5, 3-6 and 3-7 have an impact on the energy exchanges across the catchment, any spatiotemporal patterns, if not observed over longer periods, will have a limited influence on resultant stream temperatures over time. The previous chapter identified long-term spatiotemporal trends across the summer, with the amplitude of instantaneous differences varying in response to larger regional changes in climate. To test these scaled observations against longer-term observations, the microclimate metrics were averaged by week of the year, with the warmest, most humid and windiest weeks assessed in the same fashion. These results averaged across the week showed similar spatiotemporal patterns, albeit slightly muted.

3.3.3. Validating microclimate scaling against roving AWS observations

Table 3-2 Validation results for scaled microclimate vs observed roving AWS microclimate

Method	Metric	RMSE	Bias	SD
Single AWS	Ta	1.15	0.18	1.14
Single AWS + lapse rate		1.16	-0.13	1.15
Euclidean IDW		0.96	-0.17	0.95
Euclidean nearest		1.04	-0.13	1.03
Streamwise IDW		0.92	-0.18	0.91
Streamwise nearest		1.13	-0.16	1.12
Single AWS	RH	7.21	4.96	5.23
Euclidean IDW		7.25	5.06	5.2
Euclidean nearest		8.25	5.43	6.22
Streamwise IDW		6.98	4.98	4.9
Streamwise nearest		7.48	4.94	5.61
Single AWS	Ws	1.17	0.52	1.05
Euclidean IDW		0.99	0.34	0.93
Euclidean nearest		1.07	0.25	1.04
Streamwise IDW		0.99	0.33	0.94
Streamwise nearest		1.11	0.22	1.09

Streamwise IDW had the smallest RMSE and SD for predicting temperatures across the 15 roving AWS locations (Table 3-2). The single AWS and single AWS + lapse rate methods were the least accurate for predicting air temperature. In addition, the single AWS had one of the largest biases, which was also in the opposite direction to all other methods (positive bias). Euclidean IDW scaling produced the second smallest RMSE and standard deviation, but a relatively large bias. The next best performing method after Euclidean IDW was Euclidean nearest, producing close to average RMSE and standard deviation alongside the smallest bias of any method. The streamwise nearest method performed worse than the Euclidean nearest, producing below average RMSE and standard deviation scores along with a reasonable bias.

As with air temperature, the streamwise IDW had the smallest RMSE of all methods, as well as the smallest standard deviation. The bias of the streamwise IDW was the median of the methods. The single AWS method outperformed the Euclidean nearest method in every metric, with Euclidean nearest performing the worst of all methods for all metrics. Controlling for interpolation method, the streamwise methods outperformed the nearest methods for both RMSE and standard deviation. However, the bias introduced by the streamwise IDW method was larger than that of the streamwise nearest.

For scaling wind speeds, the inverse distance weighting methods produced the smallest RMSE of the five methods. Euclidean IDW had the smallest RMSE and standard deviation of all methods, with streamwise IDW producing the second smallest RMSE and SD. However, the respective biases introduced by both IDW methods were larger than those of the nearest methods. The single AWS was the weakest performer regarding RMSE and bias, with the largest values for both.

3.3.4. Validating microclimate scaling against stationary AWS observations

The LOOCV validation provides insight into the performance of each scaling method for replicating observations at each stationary AWS within the sub-catchments (Figure 3-7). The following figure shows the RMSE and bias associated with each method for each stationary AWS.

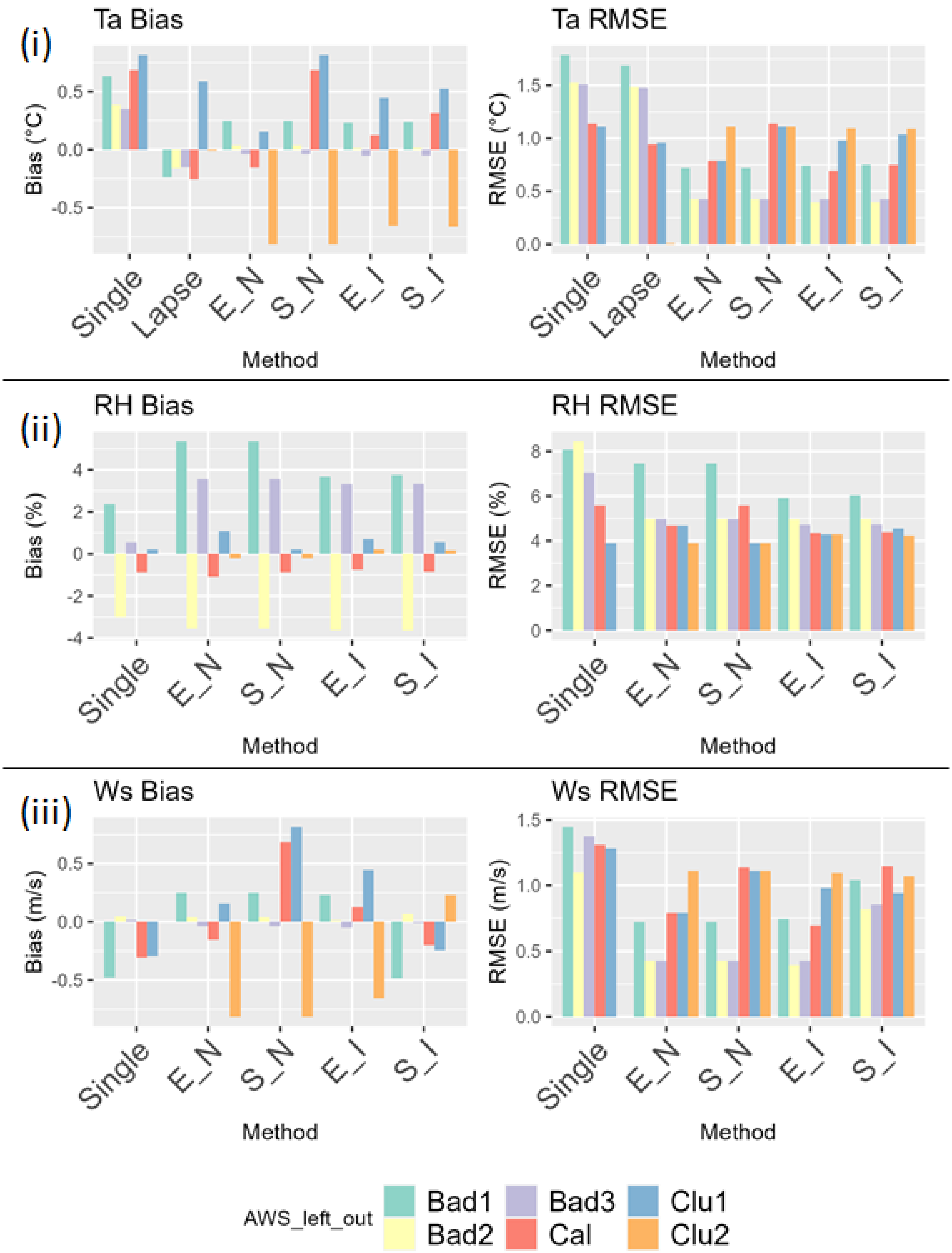

Figure 3-7 Bias and RMSE of LOOCV analysis for air temperature (i), relative humidity (ii) and windspeed (iii) predictions grouped by scaling method and coloured by stationary AWS site left out in the LOOCV. As the single AWS and lapse rate methods both utilised the Clunie 2 (Clu2) site, they have bias and RMSE values of zero and close to zero respectively for air temperature, relative humidity and wind speed.

For air temperature, LOOCV results showed a wider range of biases between sites. The single AWS method produced positive biases for all other sites, overestimating air temperature across the catchment. For all sites except for Clunie 1 (Figure 3-7, Clu1), the lapse rate method produced negative biases, systemically underestimating air temperatures for other sites. Of the methods which utilised six stationary AWS, the two Euclidean methods performed were least biased.

RMSE results showed that methods using data from the six AWS outperformed the single AWS and lapse rate methods. There was little difference in RMSE of each Euclidean and streamwise method with the exception of the streamwise nearest method, which produced an abnormally large RMSE for the Callater site (Figure 3-7, Cal) when comparing with RMSE values for other methods when removing Callater. However, there was variability in model performance depending on the site removed, with removal of Bad2 and Bad3 having the smallest impacts on model performance (e.g. lowest RMSE values).

The distribution of bias in predictions of relative humidity between stationary AWS sites showed more consistent results between methods than air temperature, with all methods producing positive biases for Bad1, Bad3 and Clu1 and negative biases for Bad2 and Cal sites. The single AWS performed was least biased, producing a substantially lower bias for reproducing Bad1 and Bad3 RH. The IDW interpolation methods were less biased than the nearest methods.

For RMSE, the single AWS method was the worst performer for most sites. RMSE scores between the methods utilising six AWS were mixed, with the two IDW methods performing better than nearest methods for most sites, except for Clu2, where both nearest sites had smaller RMSE than IDW.

The differences in bias between methods were less uniform for wind speed, with all methods introducing a large bias for at least one site. The single AWS introduced a negative bias for three of the sites, with a larger bias for Bad1 than both nearest methods and the Euclidean IDW method. The three Baddoch sites had similar biases produced from both nearest methods and the Euclidean IDW method, but biases diverged for the Callater and Clu1 sites. These three methods all produced large negative biases for Clu2. Although Streamwise IDW produced the largest bias for Bad1, it performed well for all other sites.

The single AWS method, produced the largest RMSE for all sites (excluding Clu2). RMSE results are more uniform across the four methods using six AWS than they were for bias. Of these methods, Euclidean IDW performs best overall, producing the smallest RMSE scores for three of the sites.

3.3.5. Deriving wind functions from observed evaporation

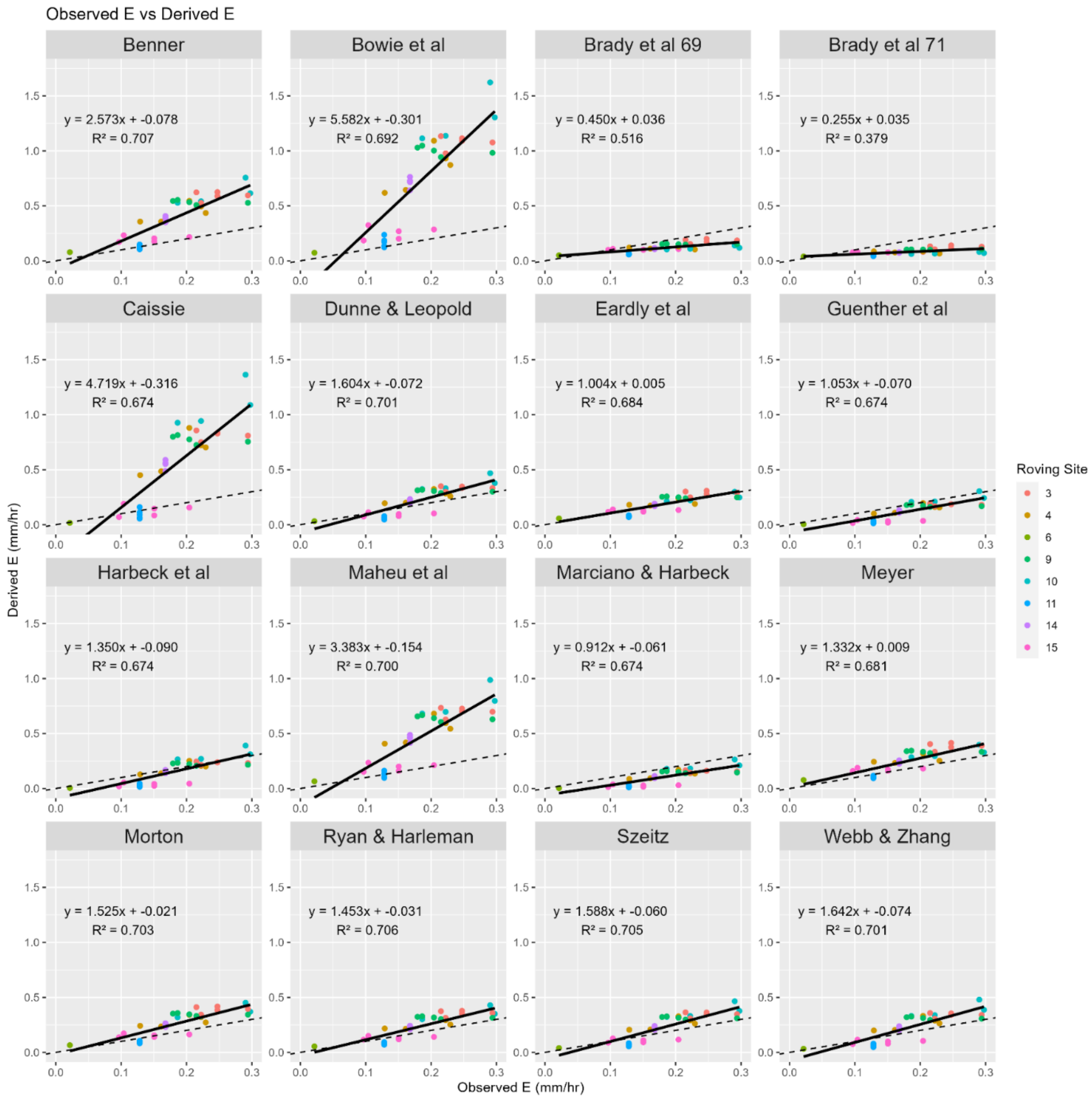

Figure 3-8 Observed evaporation rates from floating pan vs derived rates using Dalton style equation and empirically derived wind functions. Dotted line is 1:1 ratio.

As expected, wind functions derived from the evaporation rates observed in this study performed best in recreating observed evaporation rates (Figure 3-8 & Table 3-3). Performances elsewhere varied substantially, with wind functions from Bowie et al., (1985), Caissie (2016) and Maheu et al., (2014) producing overestimations of evaporation rates orders of magnitude larger than the observed rates. Of the remaining wind functions, those of Guenther et al., (2012) and Marciano & Harbeck (1952) both performed well, producing linear regression gradients close to one, albeit with both functions consistently underpredicting evaporation rates slightly.

Table 3-3 Root mean square error, standard deviation and bias of evaporation rates derived from Dalton style equations, with best performing equations highlighted green and well-performing equations highlighted yellow

Method	RMSE	SD	bias
Benner (2000)	0.253	0.188	0.212
Bowie et al (1985)	0.652	0.413	0.544
Brady et al. (1969)	0.078	0.039	-0.065
Brady et al. (1971)	0.114	0.026	-0.102
Caissie (2016)	0.477	0.354	0.37
Dunne & Leopold (1978)	0.083	0.118	0.04
This study	0.042	0.075	0.006
Guenther et al. (2012)	0.075	0.079	-0.061
Harbeck et al. (1958)	0.066	0.101	-0.026
Maheu et al. (2014)	0.347	0.249	0.285
Marciano & Harbeck (1952)	0.086	0.068	-0.077
Meyer (1942)	0.092	0.099	0.071
Morton (1983)	0.102	0.112	0.076
Ryan & Harleman (1973)	0.083	0.107	0.053
Szeitz (2019)	0.086	0.117	0.048
Webb & Zhang (1997)	0.088	0.121	0.045

The derived evaporation rates calculated using wind functions developed in this study had the smallest RMSE of all coefficients as well as the smallest bias (Table 3-3). The largest RMSE was produced using wind functions developed by Bowie et al., (1985). Bowie et al., (1985) also produced the largest bias of all coefficients. 11 of the 16 coefficients tested introduced positive biases, with Bowie et al., (1985) and Caissie (2016) wind functions introducing biases larger than the maximum observed evaporation rate.

3.4. Discussion

Management of river temperatures requires understanding of river heat and energy budgets and the consequences of different management actions (for example altering the river energy budget by planting trees). Process-based river temperature models can provide such understanding but require high-resolution hydro-meteorological data inputs, from which to derive heat and energy fluxes, which can be challenging to obtain at appropriate spatial and temporal scales. This study utilises uncommonly detailed continuous monitoring from 6 fixed AWS across 3 nested sub-catchments, supplemented by a further 15 roving AWS sites. Spatio-temporal variability in air temperature, relative humidity and wind speeds are visualised and used to inform approaches for scaling observations from individual sites to the sub-catchment scale, which are subsequently evaluated. Furthermore, given the importance of evaporation on river energy budgets, a floating evaporation pan was used to derive bespoke wind functions to calculate latent heat fluxes. These were then compared to observed evaporation rates and those generated using existing wind functions, thereby providing novel insights into the utility of different wind functions across environments. The findings build on earlier observational studies, explore opportunities for scaling and provide useful information to guide future monitoring efforts and identify areas of future research which are discussed below.

3.4.1. Characterising spatiotemporal variability in microclimate

The use of six stationary AWS in Chapter 2 identified spatiotemporal variability in air temperature, relative humidity and windspeed both within and between nested sub-catchments within the study area. The roving AWS introduced in this chapter provided temporally discrete observations of microclimate at fifteen sites across a longitudinal stream network at a novel sub-km resolution along the length of Clunie Water. These observations highlighted weak longitudinal patterns in microclimate at a daily temporal resolution including reduction in air temperatures and relative humidity with increasing elevation and an increase in wind speed with elevation. However, at the sub-daily scale, these patterns became more complex, likely as a result of the effects of site-specific landforms interacting with larger scale anabatic and katabatic winds.

Previous stream temperature studies which have measured microclimate at multiple locations have typically been limited to smaller reaches, making use of two or three locations within the given reach (Garner, et al., 2017; Leach & Moore, 2010). Where studies have discussed spatiotemporal variability, they have been within the context of land use, with locations typically being chosen to capture the influence of the presence and absence of riparian forests on microclimate. Where stated, these studies have shown varying magnitudes of differences in air temperatures (mean temperature differences of 0.65 °C across 5 km for Hannah et al., (2008), 2 °C across 700 m for Leach & Moore (2010)), but typically larger differences in windspeed (mean differences of ~2 m/s for both Hannah et al., (2008), and Leach & Moore (2010) (Hannah et al., 2008; Leach & Moore, 2010). Controlling for land-use, where no sites were dominated by riparian woodland, the results of this study show that spatiotemporal differences still occur within catchments with uniform land-use. Having elucidated further spatial complexity in microclimate patterns between fixed AWS, the roving AWS observations were incorporated into the validation of microclimate scaling methods.

3.4.2. Scaling microclimate

The surveying conducted with the novel roving AWS provided new insight into the nature of instantaneous differences in air temperature, relative humidity and wind speed along a river network at a spatial resolution and range which has not before been studied. The discontinuous nature of these data make inter-site comparisons more challenging but patterns still emerge when comparing with the reference site in the downstream reaches of Clunie Water.

3.4.2.1. Air temperature

As has been observed in previous catchment-wide studies, air temperatures typically decreases upstream with increasing altitude (Oke, 1987). This observation is physically grounded in the adiabatic lapse rate of the troposphere, wherein a parcel of air moving up through the troposphere and assuming not to exchange energy with the surrounding air, will use up thermally energy as it is greeted by lower atmospheric pressure and expands (Oke, 1987). However, as shown in both the validation against roving AWS data along the Clunie Water network and the leave one out cross-validation across the sub-catchments, the adiabatic lapse rate paired with observations at the downstream reference AWS site alone does not sufficiently account for air temperature patterns across the catchment, with this method underestimating air temperatures in the study area headwaters in the early mornings and overestimating by the afternoon. The biases introduced by the lapse rate method when validated again the stationary AWS were alone in the fact that they underestimated air temperatures for all Baddoch sites. This is likely due to the fact that the lapse rate does not account for valley orientation, which has an influence on the amount of solar radiation received and therefore air temperatures within headwater catchments. The Baddoch Burn is orientated in a southwest to northeast direction, which in a Scottish summer, would receive more energy from solar radiation than Clunie Water and Callater Burn in their respective south to north and southeast to northwest orientations (Jackson, et al., 2021).

For the four methods which utilised six stationary AWS for scaling, when validating against the stationary AWS data, all sites underestimated air temperatures for Clunie 2, the most downstream site. This would be expected as all other AWS are at higher altitudes so will typically have lower air temperatures. The same methods introduced small biases for the second and third Baddoch sites. Once more, this is to be expected for these sites are they are situated in close proximity to one another so have similar air temperatures as a result. The two streamwise methods introduced large biases when reproducing air temperature for the Callater site. This is also to be expected as this site is closest in a streamwise sense to the most downstream Clunie site, but is closer to the Clunie site further upstream when measuring Euclidean distance. The Callater site is more similar to the upstream Clunie site regarding elevation, so in pairing the Callater site with the upstream Clunie site, the Euclidean methods would be expected to outperform the streamwise methods.

3.4.2.2. Relative humidity

Large site-specific bias is observed in the results of the LOOCV, especially for sites within the Baddoch Burn. These sites, although close in proximity, showed large inter-site variations in relative humidity in the previous chapter. Such large variations in relative humidity have been observed in other studies, but these have been attributed to the presence and absence of riparian forests, which locally reduce air temperatures and increase relative humidity as a result (Spittlehouse et al., 2004). The differences in relative humidity observed within short distances in the Baddoch Burn do not correlate with significant differences in air temperature. With the scaling methods which utilise data from the six AWS relying on spatial proximity to scale, large biases will be introduced for these sites and demonstrates the need for high spatial resolution to well scale highly variable parameters. RMSE between sites was the most consistent between methods for relative humidity, with the single AWS method producing the largest RMSE for all Baddoch sites as well as Callater. Just as the bias was lower for the single AWS for predicting relative humidity because it did not include data from the other sites, this also caused the method to have the largest RMSE for most sites.

3.4.2.3. Wind speed

Where relative humidity showed large inter-site variations between sites in relatively close proximity, wind speed did not. These results are contrary to other stream energy balance studies comparing spatiotemporal wind speed variations. This is due to the typical study design wherein land-use and the presence or absence of riparian trees is treated as an independent variable between sites. The primary control of riparian trees on summer stream energy balances is the reduction in receipt of shortwave radiation. A secondary effect of the presence of trees is the reduction in latent heat exchange due to the reduction in wind speed (Hannah et al., 2008). As a result, when comparing with previous studies, inter-site differences in wind speed are substantially larger than those observed in this study (Hannah et al., 2008; Leach & Moore, 2010).

Sites adjacent to one another tended to share similar wind speed observations and as a result, scaling methods for wind speed introduced smaller biases for LOOCV, particularly for the two closest sites, Baddoch 2 and Baddoch 3. The single AWS method underestimated wind speeds for Baddoch 1, Callater and Clunie 1 sites. The previous chapter found that most sites within the study area experienced higher wind speeds than Clunie 2, the site used for the single AWS method. As a result, this method would be expected to underestimate for other locations. Likewise, other methods which incorporate the five other sites would typically underestimate for the Clunie 2 reference site, as was the case for three of these four methods.

3.4.3. Scaling limitations and development requirements

Results for the streamwise scaling methods were mixed, with the streamwise distances improving scaling predictions for some sites but worsening for others, which could be explained by streamwise distance matrix not accounting for flow direction. A potential improvement to be made in the calculation of streamwise distance matrices for nodes along these river networks could be to only incorporate AWS data in a downstream direction. However, introducing flow direction as a scaling constraint could potentially worsen the performance of streamwise distance scaling as it would not factor in anabatic winds which flow upstream, influencing summer daytime microclimate in an upstream direction, a common microclimate feature within this study area (Oke, 1987).

Due to limitations in land access permission, the roving AWS could only be installed along Clunie Water. As shown in this study as well as the previous chapter, the Baddoch Burn and Callater Burn sub-catchments can display different microclimate patterns to that of Clunie Water. For future studies, validation methods utilising the roving AWS would be more powerful if the roving AWS survey were extended along the Baddoch Burn and Callater Burn sub-catchments as opposed to just the Clunie Water mainstem.

3.4.4. Evaporation pan wind functions

The range of values for predicted evaporation rates between different wind functions were substantial (on occasion larger than the actual observed evaporation). With evaporative cooling being the largest energy sink for hot rivers during typical summer conditions (Dugdale, et al., 2018; Hannah & Garner, 2015; Webb & Zhang, 1997), the choice of wind function coefficients to use when building process-based river temperature models is very important.

Many of the wind functions developed for evaporation rates have been developed for lakes and cooling ponds in the USA (Table 3-1). With large lakes typically experiencing greater wind speeds than rivers, particularly lower order rivers, and having greater fetch distances, it could be assumed that coefficients derived in these conditions may not be transferrable to river environments. Over the last decade a number of studies have looked to address this, installing evaporation pans along river banks (Benner, 2000; Guenther, et al., 2012) as well as developing floating evaporation pans to observe evaporation rates at the river's air-water interface (Caissie, 2016; Maheu, et al., 2014; Szeitz & Moore, 2019).

When comparing the performance of wind functions developed from lake environments with those from river environments, there was no consistent pattern in recreating observed evaporation rates from this study, with some river-based coefficients performing worse than lake-based. The three coefficients which produced the largest overestimates of evaporation rates were those of Bowie et al., (1985), Caissie (2016) and Maheu et al., (2014). The coefficients developed in the two latter studies used floating evaporation pans on rivers. After the wind function coefficients developed in this study, the next-best performing coefficients were from Guenther et al., (2012) which were calculated from a land-based evaporation pan in a river environment.

These discrepancies are likely due to the nature of the river environments captured in these recent studies. The vast majority of sites visited in this study featured no riparian trees, as is representative of the catchment, whereas the wind functions tested here from the studies of Maheu et al., (2014) and Seitz & Moore (2019) are for forested rivers with canopy covers ranging from 30-90%. The sheltering provided from riparian canopies will have reduced wind speeds in these studies, with maximum wind speeds of 0.6 and 1 m/s respectively, contrasting with wind speeds of 7 m/s observed during evaporation surveys in this study. As well as impacting wind speeds, riparian vegetation will typically reduce air temperatures through shading and increase relative humidity above the river surface in the summer daytime. These influences on micrometeorology will have influences on resultant evaporation rates.

Nine of the 16 linear functions derived from the observed vs. derived evaporation rates for different wind function coefficients underestimated evaporation rates when rates were low and overestimated when rates were high. This characteristic was not associated with the environment in which the coefficients were derived. Although some of the wind functions performed poorly, ten of the 16 produced RMSE of under 0.1 mm hr^{-1} and 11 introduced biases of under 0.1 mm hr^{-1}, which indicates that many literature wind functions can be suitable for estimating evaporation rates in headwater stream environments. However, the choice of wind function is aided significantly by having observed evaporation rates to compare against.

3.4.5. Implications for future monitoring

The use of six stationary AWS in this study alongside the roving AWS has shown a degree of spatiotemporal variability within and between sub-catchments of a nested headwater catchment. These variations in air temperature, relative humidity and wind speed could not be effectively represented by a single AWS alone or with a single AWS twinned with a linear function of an environmental characteristic (lapse rate derived from elevation for air temperature). The use of multiple AWS in this study with the additional spatial resolution introduced with a novel roving AWS improved the characterising of microclimate across the study area.

Previous stream temperature study designs have typically had land-use as an independent variable, investigating the impacts of trees on riverine microclimate (Garner et al., 2017; Hannah et al., 2008; Leach & Moore, 2010). With the study area having predominantly uniform land-use with no riparian tree cover present at the six stationary AWS locations and very limited tree-cover present at roving AWS sites, this study has shown that microclimate can still vary considerably across space with uniform land-use. Future studies, particularly those working at scales larger than single stream reaches, should use multiple AWS where possible to capture this spatial complexity independent of land-use.

When scaling microclimate between point locations, inverse distance weighting using Euclidean distances was found to perform best when reproducing AWS observations. The value of this microclimate scaling should be assessed against conventional microclimate observation data in process-based stream temperature models to confirm whether scaling between point observations improves model performance in simulating stream temperatures at catchment scales.

When calculating latent heat fluxes, stream temperature models have historically used empirical wind functions from the literature, or calibrated within the range of literature values (Dugdale, et al., 2017). The use of a floating evaporation pan to provide observed evaporation rates for deriving wind functions identified a large potential source of error when representing latent heat fluxes, with literature wind function values providing a large range of resultant fluxes. Future studies looking to capture latent heat fluxes, particularly in unforested headwater streams which can observe high evaporation rates, should look to constrain wind function values with the use of observed evaporation rates within the given study area.

In an effort to reduce the uncertainty associated with wind functions in Dalton-style evaporation estimation, some studies utilise an alternative physically-based method referred to as the energy budget method (Dugdale et al., 2017). This method calculates evaporation rates as a function of heat transfer processes, but has a greater degree of complexity, with the potential to introduce further limitations if corresponding atmospheric data are not sufficiently detailed and accurate (Boyd & Kasper, 2003). Furthermore, a study directly comparing evaporation estimates from Dalton-style and energy budget methods found that at higher temporal resolutions such as those utilised in this study, the Dalton method outperformed the energy budget method (Meng et al., 2020). Future studies could look to replicate these findings within this study area.

3.5. Conclusion

In conclusion, the use of a novel roving AWS provided new insight into complexities of spatiotemporal patterns in microclimate at a new spatial scale along a river network. Using a single AWS to capture sub-daily spatiotemporal patterns in microclimate within and between temperate headwater catchments was found to be insufficient when accounting for introduced biases and the root mean square error of predicting microclimate within sub-catchments. The use of a floating evaporation pan for generating catchment-specific wind functions will have a large influence on estimating rates of river evaporation using the Dalton method, with many empirically-derived wind functions from the literature proving inappropriate, particularly for river environments in the absence of riparian canopies.

The use of these six stationary AWS alongside a novel roving AWS allowed for further increases in the spatial resolution of microclimate data, allowing for the scaling of said data from six points to observations at a novel resolution of 50m intervals along stream networks, which in turn led to improvements in the recreation of microclimate observations in a leave-one-out-cross-validation. Process-based stream temperature model accuracy is limited by a paucity of high resolution microclimate data, particularly in areas with high relief (Dugdale et al., 2017). The novel microclimate data structure created in this study is more spatially heterogeneous than the conventional nearest-neighbour microclimate observations typically used in process-based stream temperature models. Where single AWS are used, no spatiotemporal variability exists within the microclimate data; where multiple AWS are used, large step-changes occur between measurement points. Gradual changes in microclimate represented by the interpolation used for this study's novel microclimate dataset provided an improved representation of microclimate. As an input to process-based stream temperature models, this dataset may in turn improve the representation of the stream energy balance across space and time.

One of the largest challenges facing process-based stream temperature modelling efforts, particularly in temperate headwater environments, is the representation of latent heat fluxes.

These fluxes are controlled primarily by air and water temperatures, relative humidity and wind speed. The latter two controls are known to be highly spatiotemporally variable, making their estimation particularly challenging at the sub-daily scale. The representation of evaporation rates will have been improved with the use of the novel scaled microclimate dataset, but another limiting aspect of evaporation rate representation for the vast majority of stream temperature models which use Dalton-style evaporation rate equations is in the selection of wind functions. The use of a floating evaporation pan in this study provided a physical observation of evaporation rates against which literature wind functions were assessed. The wide range of results identified the inadequacy of relying solely on literature wind functions for representing evaporation rates in headwater riverine environments and the need to ground-truth such estimates with in-situ observations.

4. Investigating influence of microclimate scaling and in-situ wind function on the performance of process-based stream temperature models

Abstract:

Process-based stream temperature models are invaluable tools for studying stream thermal dynamics under climate change. These models simulate complex hydrometeorological and thermal processes, offering mechanistic insights into how riparian tree planting can mitigate current and future summer stream temperature increases. However, due to their data-intensive nature and the reliance on high-temporal-resolution micrometeorological data available only at point locations, their application has historically been limited to small spatial scales- typically reaches under 1km or sub-catchments under 30km². This limited scale often excludes the critical role of heat advection as cooled water flows downstream from forested to unforested reaches. Additionally, the use of empirical wind function coefficients for latent heat flux calculations introduces potential errors, further constraining model accuracy.

Within this context, Chapter 4 aims to elucidate the influence of novel scaled microclimate data developed in Chapter 3 on the performance of process-based models simulating stream temperatures for summer low-flow, high-temperature conditions across three sub-catchments of Clunie Water. Model outputs using the novel microclimate data scaled from six AWS are compared against other models using input data from a single AWS or a series of AWS applied using a conventional nearest-neighbour method. A second aim of the chapter is to assess the importance of characterising model evaporation rates using in-situ wind functions derived from floating evaporation pan observations. Models outputs using these bespoke wind functions will be compared with outputs using wind function values obtained conventionally through calibration within a range of literature values.

Results showed that model performances in all three sub-catchments improved when introducing additional data from AWS. Models in two of the three sub-catchments improved when using scaled micrometeorological data in place of the conventional nearest-neighbour data.

Chapter 4 also compared stream temperature model performances using bespoke wind function values derived from observed floating pan evaporation rates in Chapter 3 against wind function values calibrated within a range of empirical coefficients from the literature. The use of bespoke wind functions improved stream temperature model simulations in two of the three sub-catchments studied. In addition, current limitations in process-based stream temperature modelling are discussed, with suggestions made for future research within the field.

4.1. Introduction

Water temperature is a key variable in stream ecosystem functioning (Hannah & Garner, 2015). It influences riverine biogeochemical cycles as a control on primary production and ecosystem respiration (Allen, et al., 2005) and impacts cold water-adapted fish species at every stage of their life cycles (American Fisheries Society, 2009). Stream temperature regimes in the UK have a history of alteration in response to anthropogenic land use practices and river regulation (Hannah & Garner, 2015). Additionally, ongoing climate change will further impact thermal regimes of UK streams by altering the water surface energy fluxes and groundwater temperature (Schmutz & Sendzimir, 2018). Concerns are therefore growing over the potential impacts of climate change on the already declining status of Atlantic salmon (*Salmo* salar) in the UK (Soulsby et al., 2023; Hannah & Garner, 2015).During the European summer heatwave of 2018, Scotland observed abnormally high air temperatures and low stream discharges. In combination, these conditions resulted in 69% of Scottish rivers experiencing temperatures exceeding the 23 °C thermal stress threshold for Atlantic salmon. (Breau et al., 2012, Marine Scotland, 2019). The hottest days during this period had return periods of five to fifteen years, but UK climate projections (Met Office Hadley Centre, 2018) suggest that due to climate change, these conditions could be expected for every other year by 2100 (Undorf et al., 2020).

One option at for mitigating the impacts of climate change on summer stream temperatures is the planting of riparian trees to shade the stream channel, reducing the receipt of solar radiation and helping moderate water temperatures (Jackson, et al., 2018). Scotland's low forest cover of 18% (cf. European average of 38%; (European Environment Agency, 2019) means that many of its streams are exposed to high summer radiative forcing in the absence of riparian tree canopies, and are thus at an elevated risk of high summer stream temperatures. However, this absence of trees also means that there is an opportunity to mitigate elevated temperatures via tree planting campaigns. Resources for such campaigns are often limited, and there is therefore a need to develop planting prioritisation strategies to providing insight into where tree planting can have the greatest impact on mitigating high stream temperatures for the benefit of salmonid populations.

Large-scale statistical river temperature models (e.g. Jackson et al. 2018) represent a highly useful tool for highlighting areas at risk of ecologically-damaging elevated water temperatures under climate change (Marine Directorate, 2021) and thus prioritising general tree planting strategies across catchments. However, there is also a need for localised reach-scale guidance into how and where specific configurations of planting generates the greatest shading response (e.g. Jackson et al. 2021; Dugdale et al. 2024). Tools capable of informing these local planting strategies are typically underpinned by process-based models which calculate energy fluxes to simulate water temperature within individual river channels or reaches. While such models have provided highly useful insights into where limited tree planting resources should be positioned alongside a single channel to maximise apparent stream temperature reductions, the data-intensive nature of process-based river temperature models means that they cannot easily elucidate the cumulative thermal impacts of tree planting across multiple sub-catchments, if energy flux and microclimate data needed to drive the model are unavailable for these multiple sub-catchments.

Process-based stream temperature models conventionally use discrete point-based meteorological data as inputs, with most studies typically using one or two automated weather stations (AWS) to provide model input data across a limited space (Carrivick et al., 2012; Fabris et al., 2018; Shen et al., 2014). However, using six AWS across three nested catchments, the first research chapter showed that at the scale of these nested catchments, a single AWS would fail to capture the observed spatiotemporal variabilities in input energy fluxes across multiple catchments. While previous stream temperature modelling studies have documented how (often semi-conceptual) process-based models can make use of reanalysis data to produce simulations at larger scales (Gatien et al., 2023; Rincón et al., 2023; Shi et al., 2021; Spratt et al., 2024), this practise is unfeasible when investigating tree planting impacts on energy fluxes and stream temperature, as highly accurate/localised energy flux and microclimate data are required to illuminate the site-specific impacts of such planting. There is therefore a pressing need to develop methods capable of upscaling energy flux and microclimate inputs from discrete fixed AWSs across multiple sub-catchments, with a view to expanding the simulation of tree planting impacts on river temperature from single channels to entire headwaters.

The first research chapter also highlighted the substantial influence of the latent heat flux in limiting summer stream temperatures, with evaporation removing energy from the system at the air-water interface. However, representation of this energy flux within process-based stream temperature models has historically relied on model calibration within the bounds of literature coefficients derived from reservoirs and cooling ponds rather than rivers and streams

(Boyd & Kasper, 2003). Further improvements in stream temperature modelling could be made with the use of real-world latent heat flux observations.

Building on the results of the second research chapter, which showed how hydrometeorological data from these six fixed weather stations could be manipulated to produce a spatially-continuous dataset (with unique air temperature, relative humidity and wind speed estimates at a 50 m spatial resolution), the following study seeks to build process-based stream temperature models for three streams within a nested catchment and quantify the extent to which the use of these spatially-continuous inputs improve temperature model simulations in comparison to 'conventional' discrete inputs from spatially-isolated AWSs. This chapter also aims to understand the extent to which the addition of real-world latent heat flux observations (derived from a floating evaporation minipan) further improves model simulations in comparison to using wind functions established during model calibration. The specific objectives of this chapter are therefore as follows:

(i) build and calibrate process-based stream temperature models for three nested catchments capable of simulating water temperature with a degree of accuracy comparable to those achieved in similar studies (~ ± 1 °C).

(ii) compare the impact on model performance of driving a model using scaled microclimate data derived from a spatially-continuous dataset (Chapter 2) in comparison to 'conventional' microclimate data from isolated discrete AWS

(iii) understand whether model performance is further improved by the introduction of observed latent heat flux inputs from an evaporation minipan

4.2. Methodology

4.2.1. Study area

Clunie Water, Baddoch Burn and Callater Burn are spawning streams for Atlantic salmon located in the central Cairngorm Mountain range. Their catchments range in altitude from 338 to 1062 mAOD and span a combined area of 104 km^2. Clunie Water flows in a south-to-north direction, merging with the Aberdeenshire River Dee in Braemar. The Baddoch Burn and Callater Burn serve as a major tributaries, flowing from southwest-to-northeast and southeast-to-northwest respectively. The contributing catchments for these tributaries have areas of 23 and 35 km^2, respectively (Figure 4-1). Higher flows occur during autumn and spring due to seasonal precipitation and snowmelt, with lower flows observed in summer. Land cover primarily consists of open heather moorland used for sheep grazing, with two sections of pine plantation forest situated at the confluence of Clunie Water and Baddoch Burn and to the west of Clunie Water between its confluences with Baddoch Burn and Callater Burn. The local geology mainly comprises granite, low-permeability metamorphic rock overlain with peat, till,

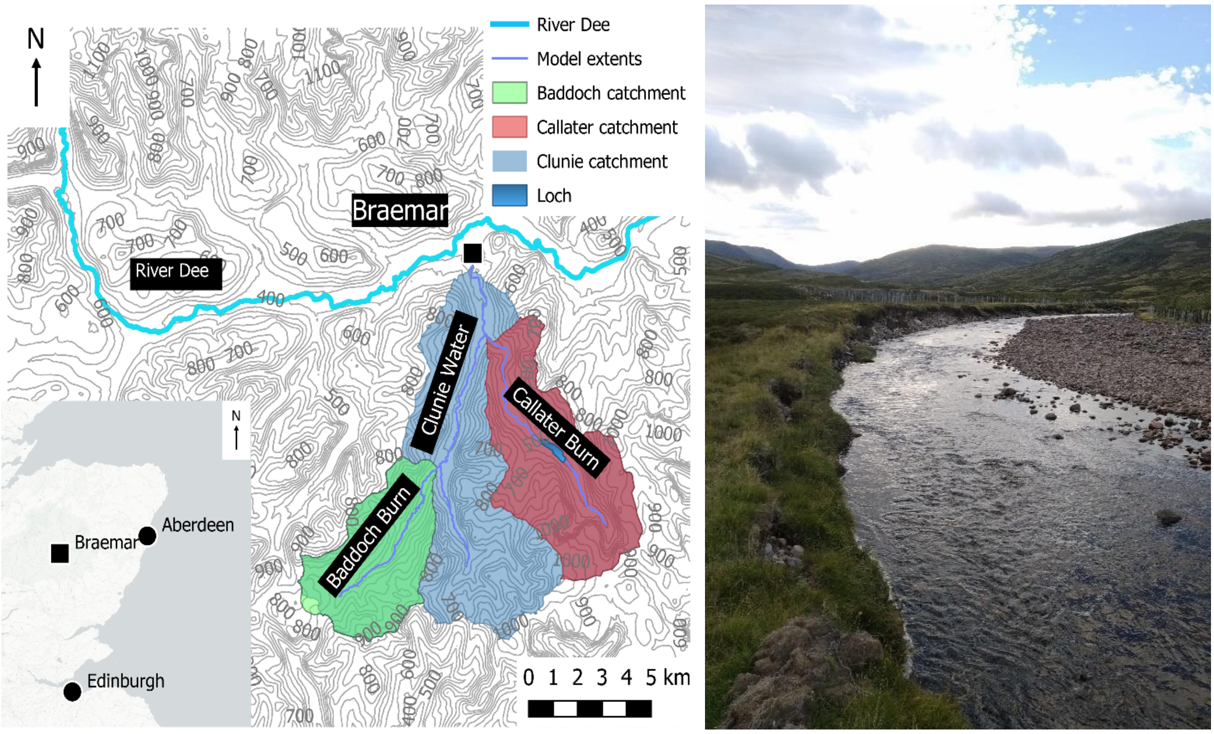

Figure 4-1 Map identifying location of Braemar within Scotland and locations of Clunie Water, Baddoch Burn and Callater Burn sub-catchments (left); and a photo displaying a typical representation of Clunie Water, with its open heather moorland and exposed sediment during low flows (right).

and glaciofluvial deposits. Callater Burn flows from Loch Callater, a shallow freshwater loch with a length of 1.6 km and an average depth of 3.7 m.

4.2.2. Stream temperature model

The model chosen for simulating water temperatures was a modified version of Heat Source 9.0.0.b19; a process-based temperature model developed at Oregon State University and used by the Oregon Department of Environmental Quality (Boyd & Kasper, 2003). The model simulates stream thermodynamics and hydraulic routing as a function of physically-derived energy fluxes (Equation 1). Where the original model uses a combination of a solar routine and observed cloudiness to calculate the radiative portion of the energy balance, our version had been modified to accept observed shortwave and longwave radiation from AWS installed within the study area.

In short, Heat Source simulates stream temperatures by calculating the net available energy to a stream at a given point as a function of the energy balance equation:

$$Qn = Qa + Q^{*} + Qe + Qh + Qbhf + Qf \qquad [1]$$

Where:

Qn is the total energy available to heat or cool a river.

Qa is advected heat from groundwater discharge, hyporheic exchange, tributaries, precipitation, and longitudinal advection.

*Q** is net radiation

Qe is latent heat

Qh is sensible heat

Qbhf is bed heat exchange

Qf is friction at the bed and banks

Within the Heat Source model, the latent heat flux is calculated as the sum of the sensible heat in evaporated water vapour and the product of the energy needed to change the state of water from liquid to gas (latent heat of vaporisation), density of water and the evaporation rate. The latent heat of vaporisation itself is a function of water temperature.

$$Qe = \rho H_2O \cdot L_e \cdot \overline{E} \qquad [2]$$

Where Qe is the latent heat flux, ρH_2O is the density of water, L_e is the latent heat of vaporisation and E is the evaporation rate.

The latent heat of vaporisation is in turn calculated as follows:

$$L_e = 1000 \cdot (2501.4 + (1.83 + T_w)) \quad [3]$$

There are a number of methods available for calculating the evaporation rate, but for the models used in this study, the following mass transfer method was used:

$$\overline{E} = f(\overrightarrow{W}) \cdot (e_s - e_a) \qquad [4]$$

where $f(\overrightarrow{W})$ is a wind function, e_s and e_a are saturation and actual vapour pressure.

The wind function is used to estimate the adiabatic portion of evaporation. The wind function is structured as follows:

$$f(\overrightarrow{W}) = a + b \cdot \overrightarrow{W} \qquad [5]$$

Where a and b are coefficients and $\overrightarrow{W}$ is wind speed (m/s) measured at 2 m above the water surface (Boyd & Kasper, 2003). A number of values for the wind function coefficients a and b exist within the current literature, having been developed through empirical study. Those assessed in this study, including the set of coefficients derived from evaporation pan observations in Chapter 3 can be seen in Table 3-1.

4.2.3. Model input data

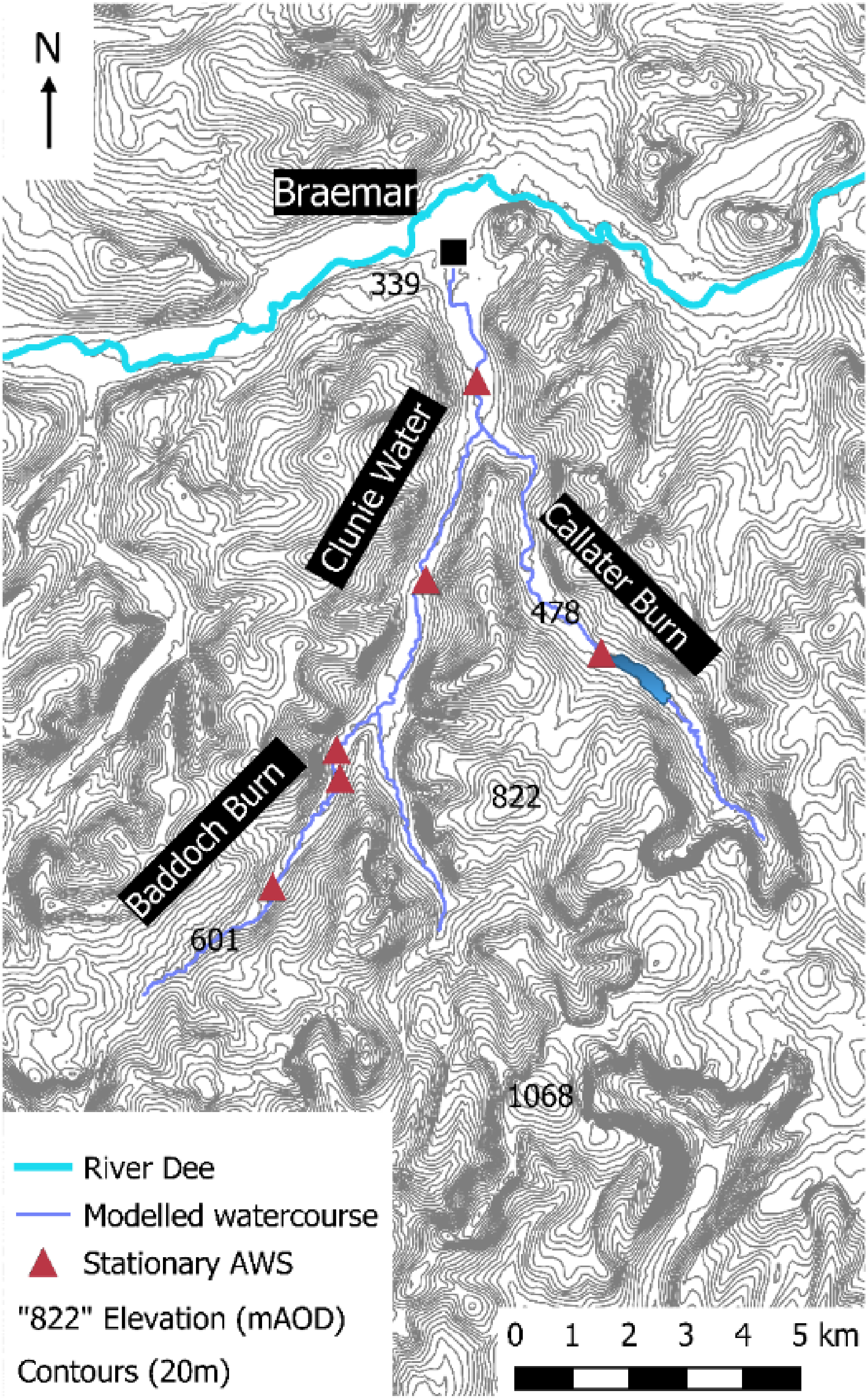

Figure 4-2 Stationary AWS locations

Heat Source employs finite difference steps for heat and mass transfer and flow routing. User-defined spatial and temporal resolutions affect model accuracy and computational efficiency (Boyd & Kasper, 2003). Our models used 50 m spatial steps and a one-minute temporal resolution, with hourly input data. These settings balanced accuracy and practical run times.

4.2.3.1. Microclimate and energy flux data

Data from six stationary AWS (Figure 4-2) recorded observations of input data needed to run Heat Source (incoming and reflected shortwave and longwave radiation, air temperature, relative humidity and wind speed) across the study sub-catchments. Three AWS were located along Baddoch Burn, two within Clunie Water and one at the top boundary of Callater Burn within 100 m of the outlet of Loch Callater. AWS were anchored to stream banks with sensors attached to a cross-arm extending out over the stream. AWS locations were selected to encompass variability in elevation, stream channel orientation, geomorphology and land use within the study area (as well as capturing the influence of Loch Callater on the thermal regime of Callater Burn and, subsequently, Clunie Water). Further information on the instrumentation used can be found in Table 2-2 of Chapter 2. Summer field data were collected at a 15-minute resolution between 21st June and 9th September 2022. Heat Source also requires cloud cover data as an input. Cloud cover was not recorded via the AWS, but was instead calculated using the following equation:

$$CC = \sqrt{1.54 \cdot \left(1 - \frac{Q_{sw\ observed}}{Q_{sw\ potential}}\right)} \qquad [6]$$

Where:

CC is cloud cover,

$Q_{sw\ observed}$ is the observed shortwave radiation,

$Q_{sw\ potential}$ is the maximum shortwave potential during cloudless conditions, calculated using Heat Source's inbuilt solar routine which generates shortwave solar radiation estimates for a given site based on the time of day and its longitude/latitude.

Heat Source's solar routine uses the Gregorian calendar corrected for daylight savings to calculate solar time relative to Earth. It then calculates the solar position relative to Earth through a number of astronomical parameters. The Earth's orbit is situated on the ecliptic plane and the tilt of its axis, known as the obliquity, is the angle between the equatorial and orbital planes. The Earth's eccentricity is the shape of its elliptical orbit, measuring how much it deviates from being circular. These parameters vary as a function of time, hence the need for calculating solar time.

Having calculated the solar time and position relative to Earth, latitude and longitude of the stream location are then used to estimate the intensity of incoming solar radiation. From the given latitude and longitude, the solar zenith angle can be calculated. This indicates the angle at which the sun's rays contact the Earth's surface. A smaller angle means the sun is overhead, resulting in higher solar radiation as the ray travels for a shorter distance through the Earth's atmosphere. Solar altitude, also determined by the stream's latitude, longitude and solar time, is the angular height of the sun above the horizon. A higher altitude results in more direct sunlight with a shortened path through the atmosphere. Using this combination of parameters, Heat Source's solar routine calculates potential shortwave radiation (Boyd & Kasper, 2003).

4.2.3.2. Microclimate data interpolation

In order to test the extent to which scaled microclimate inputs from a 50 m resolution dataset improved model performance against a model based on inputs from either a single weather station or the nearest AWS to each model node, three different microclimate data input types were tested: *Single AWS*, *Nearest AWS* and *Scaled Met*. The *Single AWS* model used observed microclimate and energy flux data taken from the furthest downstream AWS along Clunie Water. Observations from this site were directly input for all model nodes for the Clunie Water, Baddoch Burn and Callater Burn models. This data type was chosen to reflect the conditions commonly observed in stream energy balance studies, i.e. using a single observation point to capture microclimate to represent the study area. The most-downstream AWS was chosen as it is the most easily accessible of the six available sites and would typically be used in a study utilising a single site. The *Nearest AWS* model used data from all AWS available within each catchment, with each model node being assigned data from its nearest weather station (Figure 4-3a). This is the conventional method used by Heat Source to attribute microclimate inputs to model nodes. Finally, the *Scaled Met* model used inverse distance weighting (calculated using Euclidean distances between each 50 m model node and the six AWS) to generate interpolated values for the various microclimate inputs at each node (Figure 4-3b). Euclidean inverse distance weighting scaling was found to best represent air temperature, relative humidity and wind speeds across the study area throughout the summer of 2022 (Chapter 2).

Figure 4-3 identifies a range of differences in microclimate input when changing input data method from Nearest AWS per model to largest AWS weighting per model. Due to the higher density of instrumentation in the Baddoch Burn sub-catchment, differences are less notable, when compared with Clunie Water and Callater Burn. Model sensitivities to changes in input data may reflect these differences. Another cause for differing model sensitivity could be found in the stream order, with the larger Clunie Water showing less sensitivity to model input changes due to its greater thermal inertia as a result of larger discharges relative to Baddoch Burn and Callater Burn.

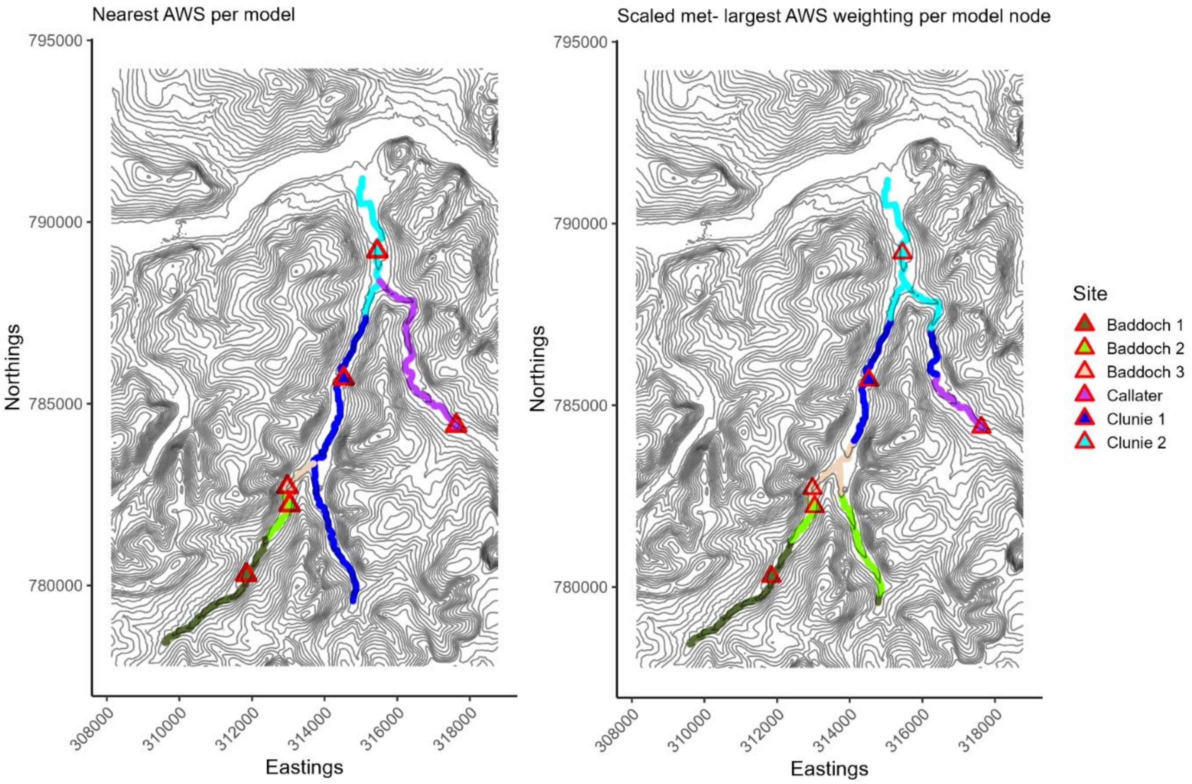

Figure 4-3 Attribution of met data from Nearest AWS and Scaled Met models

4.2.3.3. *Water temperature data*

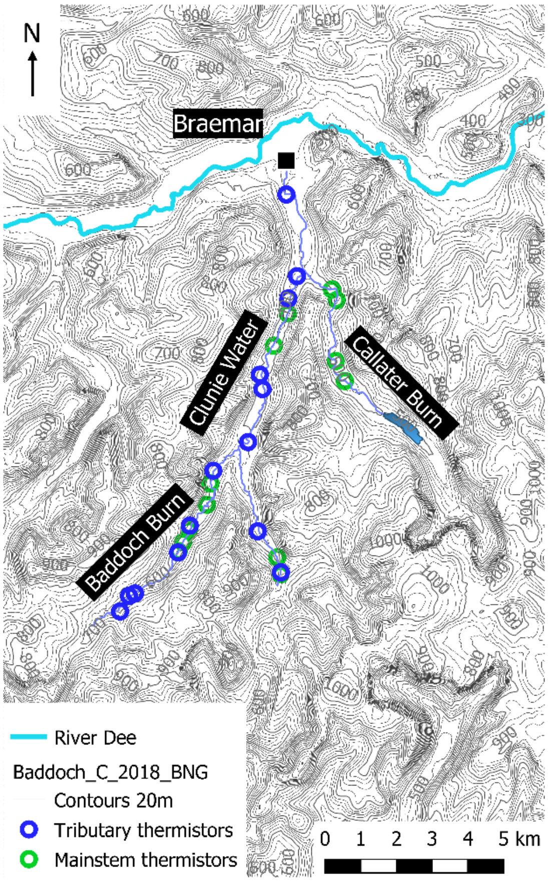

Figure 4-4 Mainstem and tributary temperature logger locations

Heat Source requires water temperature inputs as boundary conditions for the main stem and incoming tributaries. Water temperature was recorded at a 15-minute resolution using a series of 24 submerged Tinytag Aquatic-2 temperature loggers installed in both the main stem and tributaries of the Baddoch Burn and Clunie Water. Loggers were installed within Callater Burn, although due to land access constraints, no tributaries of Callater Burn could be instrumented. The loggers were corrected to a true temperature reference by the Marine Directorate Freshwater Fisheries Lab in accordance with the Marine Scotland – Science Laboratory Manual MFL 1000 (Marine Scotland - Science, 2019). Locations for logger installation prioritised well-mixed water in order to capture representative mean water column temperature and avoid the effect of localised thermal stratification which can occur in pools. Loggers were housed within white PVC tubing to reduce the influence of direct solar heating and were secured to a perforated steel angle inserted into the streambed. Data from loggers other than the three used to represent model boundary conditions or 14 used to represent tributaries were withheld from the model for use in the model calibration and validation processes. This left a total of ten mainstem loggers across the catchment to be used in the calibration and validation. The tributaries instrumented varied in size but mostly consisted of small streams fed by shallow sub-surface flows from peat deposits, with widths ranging from 0.3 m to 5.6 m and contributing catchment areas ranging from 0.69 km^2 to 8.79 km^2. See Table 4-1 for further information.

Table 4-1 Characteristics of tributaries instrumented with water temperature loggers

Tributary	**Location**	**Channel width (m)**	**Contributing catchment (km^2)**
Baddoch 1	Baddoch headwaters	1.8	2.05
Baddoch 2	Baddoch headwaters	3.9	2.93
Baddoch 3	Baddoch headwaters	1.3	0.69
Baddoch 4	Baddoch headwaters	5.2	4.83
Baddoch 5	Baddoch mid-reaches	1.4	2.22
Baddoch 6	Baddoch mid-reaches	3.8	5.77
Baddoch 7	Baddoch lower reaches	1.2	1.95
Clunie 1	Clunie headwaters	5.6	8.79
Clunie 2	Clunie headwaters	1.3	1.16
Clunie 3	Clunie mid-reaches	3.7	2.00
Clunie 4	Clunie mid-reaches	2.0	1.02
Clunie 5	Clunie mid-reaches	2.5	1.16
Clunie 6	Clunie mid-reaches	0.3	0.95
Clunie 7	Clunie mid-reaches	2.1	1.24
Clunie 8	Clunie lower reaches	0.3	0.73

Table 4-2 Microclimate and energy flux variables measured at stationary AWS

Variable	Instrument	Location	Instrument error
Stream temperature (Tw)	Gemini Tinytag Aquatic 2	0.05 m above streambed	±0.5 °C
Air temperature (Ta) and relative humidity (RH)	Vaisala HMP45C / Rotronic HC2S3 temperature and relative humidity probe	~1.50 m above stream surface	Temp ±0.2 °C, RH ± 3% / Temp ±0.1 °C, RH ± 0.8%
Wind speed (WS)	Vector Instruments A100R 3-cup anemometer	~1.50 m above stream surface	±1% + 0.1 m s−1
Incoming (Ks↓) and reflected (Ks↑) solar shortwave radiation	Skye SKS 1110 pyranometer	~1.50 m above stream surface	±5%
Net all-wave radiation (Q*)	Kipp & Zonen NR-LITE /NR-LITE2 net radiometer	~1.50 m above stream surface	±5%

4.2.3.4. Discharge data

Heat Source also requires stream discharge data at the upstream model boundaries and for tributaries. Two methods were used to generate discharge data. For the first method, stage gauge measurements recorded using a Marine Directorate gauging station located in the lower reaches of Baddoch Burn were converted to discharge using a discharge rating curve. The rating curve was developed by the Marine Directorate using 26 repeat discharge measurements taken using an acoustic doppler current profiler (ADCP) from 2011 to 2018, with measured discharges ranging from to 0.17 m^3s^{-1} to 4.84 m^3s^{-1}, then plotting against stage measured using a pressure transducer. Discharges calculated from observed stage during the study period were then scaled to model boundaries and tributary outflows using upstream catchment area weighting, following the approach of Dugdale et al. (2024). For the second gauging method, discharges were attained at model boundaries across a single day in June 2022 with characteristic low flows using the velocity area method applied to velocities collected in the field using an MFP51 impeller flowmeter. The observed stage gauge discharge for the period when the spot measurements were taken was then divided by said spot gauge discharges to produce a weighting factor. This weighting factor was then applied to the stage gauge discharge timeseries to generate model extent boundary condition discharges. During the model parameterisation process, discharges were allowed to vary within the range of values produced from the spot gauging and area weighting methods. Heat Source also allows for accretion flows to be included in the model. However, flow accretion surveys conducted along the mid reaches of Clunie Water indicated that flow accretion was negligible (within the margin of error for discharge measurement), so flow accretion inputs were not used for models in this study.

4.2.3.5. Hydromorphic data

A 5 m DTM was used to provide elevation data needed for calculation of topographic shading and channel gradient within the model (Landmap; GetMapping, 2023). Channel width data needed for Heat Source's hydraulic model component were digitised from orthophotos captured in summer 2018 and found to be good agreement with the channel widths measured in the field during the 2022 study period. However, due to the geomorphology of the study area, particularly that of Callater Burn, with its step-pool system and large areas of exposed sediment during summer low flows, there are limitations in using orthophotos to define channel widths. Because of this, when building models to simulate stream hydraulics, the initially-defined channel widths had room for adjustment (+/- 20%) in order to improve the simulation of observed point depths and velocities. Heat Source also allows for variability in thermal conductivity and diffusivity of streambed sediment, thickness of the hyporheic zone, percentage of the stream channel interacting with the hyporheic zone and porosity of bed sediment. With these parameters being highly spatially variable and very difficult to capture at catchment scales, they were parameterised within a given range of literature values measured in similar stream environments.

4.2.3.6. Evaporation data

The Heat Source model has two methods to choose from for calculating the latent (evaporation) heat flux: the Mass Transfer Method and the Combination Method. The former uses a Dalton style equation to estimate evaporation, incorporating wind functions as an empirical expression of the adiabatic portion of evaporation. The latter uses a more complex, physically-based equation involving net irradiance to capture the energy budget as well as mass transfer components of evaporation rates (Boyd & Kasper, 2003). Previous studies utilising these different methods have found conflicting results (Alazard et al., 2015; McJannet et al., 2013; Ouellet et al., 2014), and a subsequent literature review has suggested to only use the Combination Method where wind function coefficients are unavailable (Dugdale, et al., 2017). This study uses the Mass Transfer method to calculate the latent heat flux.

In order to determine whether observations of latent heat flux improved model performance over one where latent heat was estimated via calibration, an evaporation pan was built inspired by the methods outlined in Szeitz & Moore (2019). For further information on the evaporation pan design and how wind functions are used to calculate latent heat fluxes, see Chapter 3 Section 2.6, Evaporation pan methodology.

In conjunction with the evaporation pan, a roving AWS was built to measure microclimate at a series of locations along Clunie Water. Being easy to install and transport, the roving AWS was moved between a total of fifteen sites for 24-hour periods throughout the summer of 2022 to capture microclimate variability at a sub-km spatial scale. For further information on the roving AWS methodology, see Chapter 3 Section 2.2, Site Locations and Measurements.

The roving AWS was installed alongside the floating evaporation pan at six sites along Clunie Water to measure wind speeds alongside the pan's observed evaporation rates. Linear regression fitted between evaporation pan measurements and wind speeds recorded at the roving AWS were used to derive empirical wind function coefficients, which were then supplied to Heat Source to allow it to simulate realistic latent heat flux values. These field-derived wind functions are subsequently referred to as *Fixed* wind functions, allowing comparison against wind functions estimated via model calibration (hereafter referred to as *Parameterised* wind functions. Parameterised values of wind functions *a* and *b* were generated within a range of values empirically derived from the literature. For further information regarding these literature wind function values, see Chapter 3.

4.2.4. Model calibration and validation

Heat Source models were calibrated for each stream (Clunie Water, Baddoch Burn and Callater Burn) for a three-week period during the summer of 2022 (1^{st}-22^{nd} of July). During this period, mean, maximum and minimum air temperatures at the furthest downstream AWS were 14.9 °C, 27.9 °C and 6.2 °C respectively. Mean, maximum and minimum inflows at the upper boundary of Clunie Water were 0.31, 0.51 and 0.21 m^3s^{-1} respectively. The validation period consisted of 19 days from the 26^{th} of July to the 14^{th} of August. Mean, maximum and minimum air temperatures at the furthest downstream AWS were 13.8 °C, 24.5 °C and 3.9 °C respectively, with Clunie upper boundary inflows mean, maximum and minimum inflows of 0.28, 0.0.52 and 0.12 respectively.

These calibration and validation periods were chosen as they represent the high temperature, low flow conditions which characteristically cause stress to thermally sensitive fish species

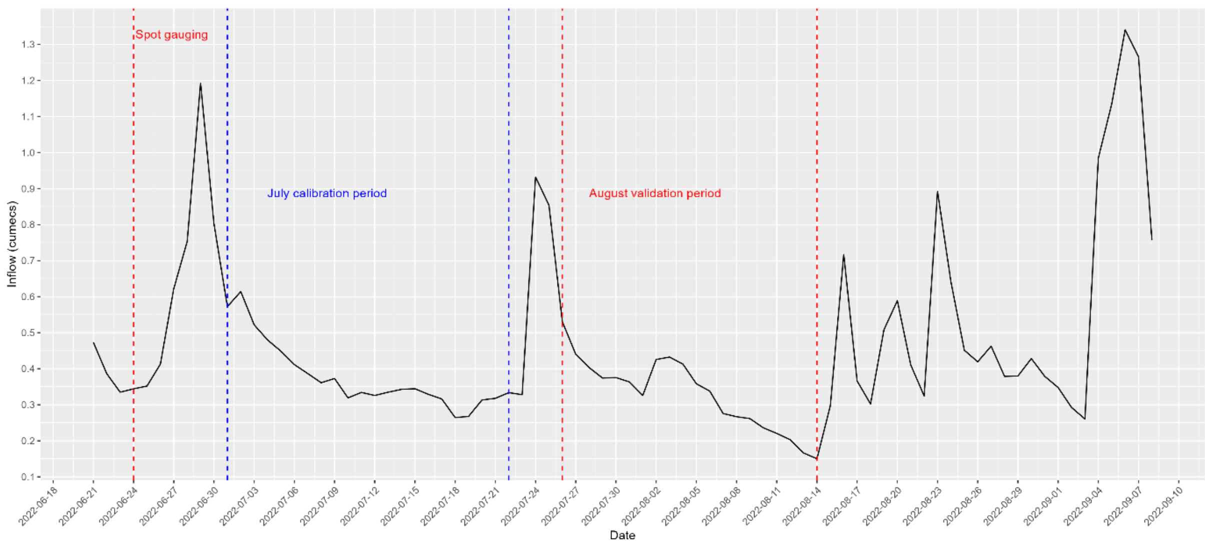

Figure 4-5 Baddoch stage gauge discharges during summer 2022 and the periods chosen for spot discharge gauging, model calibration and validation.

To calibrate model parameters, a Latin Hypercube-based sampling method was used to generate parameter values within a given range.

For the model calibration, a Latin hypercube-based set of 1000 parameter combinations (i.e. 1000 model iterations with different parameters) was created. The ranges of individual parameter values were constrained first by values observed in the literature, then second with a view to ensuring that the resultant simulated energy fluxes stayed within sensible limits (informed by comparable stream energy balance studies). Particular attention was paid to modelled turbulent fluxes due to the limited number of studies conducted in conditions with streams as exposed as those found in this study.

Model calibration was performed using the Heat Source models parameterised with the *Scaled Met* dataset as results from Chapter 3 showed that microclimate observations within the study area are best-represented spatiotemporally using Euclidean inverse-distance-weighting scaled data, as well as using the *Fixed* wind functions using evaporation rates observed from the floating evaporation pan (see section Chapter 3, section 3.3).

The 1000 parameter combinations were run for the three-week July calibration period for each of the three streams, and the RMSE of each model run recorded. The best performing parameter combinations were then run for the August validation period. The best-performing calibration parameter set did not always produce the best validation RMSE (showing some model parameter combinations to be overfitted to the calibration period), so the best performing 5% of models from the calibration period were then tested for the validation period and their calibration and validation RMSEs averaged. The parameter combinations with the lowest average RMSE were then selected as the best-performing models (Table 4-3). These parameter sets were then maintained for all subsequent model simulations (i.e. all tested input meteorological datasets and wind functions).

Table 4-3 Set of parameter values used in optimised Clunie, Baddoch and Callater Heat Source models. Initial ranges for discharge vary between models due to varying ratios of area-weighted discharges and velocity-area observed discharges.

Parameter	Clunie	Baddoch	Callater	Initial range	Source for constraint
Channel width factor	1.30	1.19	1.26	0.7 – 1.3	Malcolm & Dugdale, (2023)
Manning's n	0.21	0.20	0.51	0.05 - 0.5	(Constrained by model stability)
Sediment thermal conductivity (W m^{-1} $°C^{-1}$)	2.21	0.82	1.94	1 - 10	Sebok & Müller, (2019)
Sediment thermal diffusivity (m^{-2} s^{-1})	1.73 E-06	7.45 E-07	8.59 E-07	0.01 - 10 E-05	Cuthbert et al., (2010)
Sediment hyporheic thickness (m)	0.55	2.80	1.78	0 - 10	Malcolm & Dugdale, (2023)
Percentage hyporheic exchange (%)	0.17	0.41	0.4	0 -5	Schmadel et al., (2017)
Porosity	0.11	0.44	0.09	0 – 0.5	Wu & Wang, (2006)
Discharge factor	1.10	1.01	1.06	Clunie: 1 – 3.73 Baddoch: 1 – 1.56 Callater: 1 – 2.27	Weighting constrained by area weighting factor (1) and velocity-area gauging measurement (e.g. 3.73)

4.3. Results

4.3.1. Model calibration and simulated stream temperatures

4.3.1.1. Model calibration and validation

Heat Source models for Baddoch Burn, Callater Burn, and Clunie Water accurately reproduced stream temperatures during high-temperature, low-flow periods in July and August 2022. The mean RMSE across calibration and validation was 1.07 °C, with a mean bias of -0.16 °C. The Baddoch Burn model had the best calibration RMSE at 0.97 °C, while Callater Burn exhibited the smallest bias during calibration at 0.4 °C. In the validation period, Callater Burn achieved the lowest mean RMSE of 1.01 °C, and Baddoch Burn produced the smallest bias at -0.185 °C. Overall, models typically demonstrated smaller RMSE during calibration and smaller biases during validation. Further information on model performance is found in Table 4-4.

Table 4-4 Performance metrics of best-performing stream temperature models (best performing judged by smallest RMSE produced) after 1000 model runs using Scaled Met microclimate inputs and Fixed wind functions from evaporation pan observations

		Calibration (°C)			Validation (°C)		
		Clunie	Baddoch	Callater	Clunie	Baddoch	Callater
RMSE	Mean	1	0.97	1.19	1.11	1.13	1.01
	Min	0.35	0.62	0.97	0.44	0.87	0.97
	Max	1.61	1.36	1.32	1.67	1.37	1.07
Bias	Mean	-0.56	-0.45	0.4	-0.66	-0.185	0.5
	Min	-0.06	-0.16	0.17	0.05	-0.02	0.31
	Max	-1.13	-0.84	0.62	1.25	-0.49	0.68
SD	Mean	0.79	0.81	1.1	0.8	1.07	0.86
	Min	0.35	0.59	0.75	0.44	0.79	0.72
	Max	1.3	1.07	1.28	1.18	1.5	0.96

4.3.1.2. Spatial Tw prediction trends

The Clunie model showed increasing RMSE values downstream during both calibration and validation periods. Headwater predictions within 1 km of the boundary condition were accurate

(RMSE 0.35 °C and 0.44 °C for calibration and validation), but performance declined downstream (RMSE 1.33 °C and 1.38 °C after 11 km). RMSE increases and bias were linear downstream for both periods. Baddoch model predictions also became less accurate downstream during calibration (RMSE 0.62 °C upstream to 1.36 °C downstream), with a similar pattern in validation, except for some improvements between 4.35 km and 3.35 km upstream. Bias increased linearly downstream during calibration and most validation locations. Callater model predictions differed, showing no strong downstream trends. Both calibration and validation periods improved from the furthest upstream point to the second-most upstream, then decreased further downstream. Uniquely, validation periods produced better RMSE than calibration. However, bias still reduced downstream for both periods.

4.3.1.3. *Temporal Tw prediction trends*

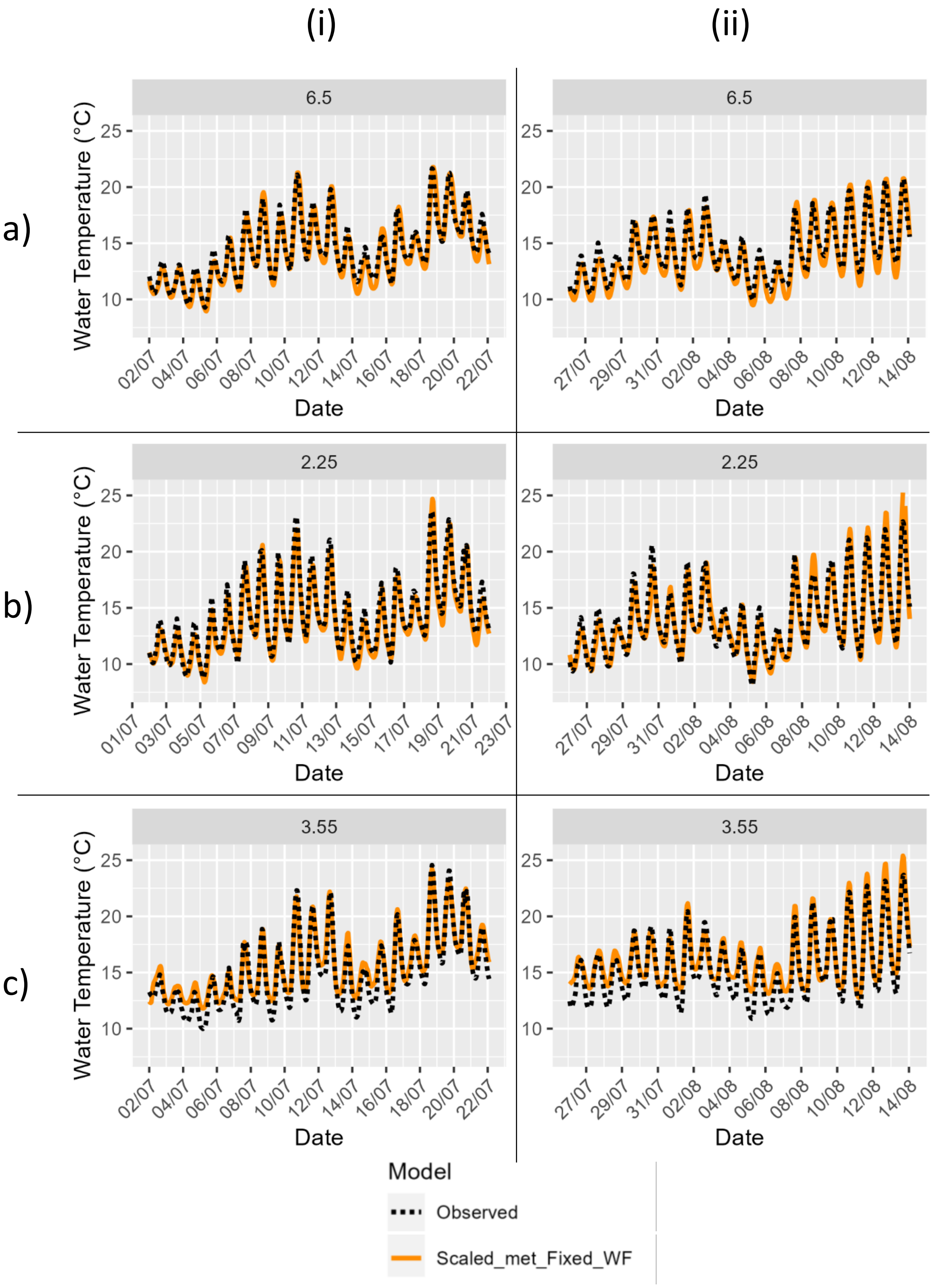

Figure 4-6 Timeseries plot of observed and predicted water temperatures at mid-stream locations for calibration (i) and validation (ii) periods for Clunie (a), Baddoch (b) and Callater models (c). Panel titles are the upstream distance along each model in km.

The Clunie, Baddoch, and Callater models showed varied behaviours in temperature prediction timings and amplitudes. Clunie experienced minor delays in peak temperatures in mid-reaches but early peaks further downstream, meaning the point at which the mid-reaches experienced their daily maximum temperatures occurred slightly later in simulated timeseries (e.g. daily maximum temperatures occurring at a given logger location simulated at 4pm where in reality the logger recorded its daily maximum temperature at 3pm) than in the observed data and slightly earlier in simulated timeseries for the lower reaches. Baddoch had minor delays in mid-reaches, continuing downstream. Callater consistently showed minor delays in both mid-reaches and downstream during calibration and validation. Clunie typically underpredicted temperatures in lower reaches, especially daily maxima, during calibration. This trend persisted in validation, with increased underprediction of daily minima. Baddoch similarly underpredicted temperatures, except for some warmer days when upstream predictions exceeded observed daily maxima. During the final validation week, daily maximum temperatures were overestimated in upper and mid-reaches but not in lower reaches. Callater accurately reproduced daily maxima throughout most periods but consistently overestimated daily minima. Improvements in minima predictions only occurred in the final five days of both calibration and validation periods.

4.3.1.4. Influence of meteorological inputs on model performance

Table 4-5 Mean root mean square error, bias and standard deviation between model calibration and validation periods for models using tiers of meteorological inputs.

Stream	Met input	RMSE	Bias	SD
Clunie	Single AWS	1.1	-0.55	0.96
	Nearest AWS	1.1	-0.61	0.92
	Scaled Met	1.09	-0.55	0.95
Baddoch	Single AWS	1.34	-0.56	1.21
	Nearest AWS	1.11	-0.53	0.97
	Scaled Met	1.08	-0.32	1.02

Callater	Single AWS	1.02	0.355	0.96
	Nearest AWS	0.985	0.36	0.92
	Scaled Met	1.02	0.465	0.9

Results of testing model performance under different meteorological inputs (i.e. *Single AWS, Nearest AWS and Scaled Met*) show that the source and type of meteorological data input has a notable input on temperature model performance. Across all three model catchments, the best performing meteorological input tier with regard to RMSE was the *Scaled Met* input. In terms of model bias, the *Scaled Met* input produces the best performance for two of the three catchments, these being Clunie and Baddoch, with the *Single AWS* meteorological input producing the smallest bias for Callater models and *Nearest AWS* producing the second smallest.

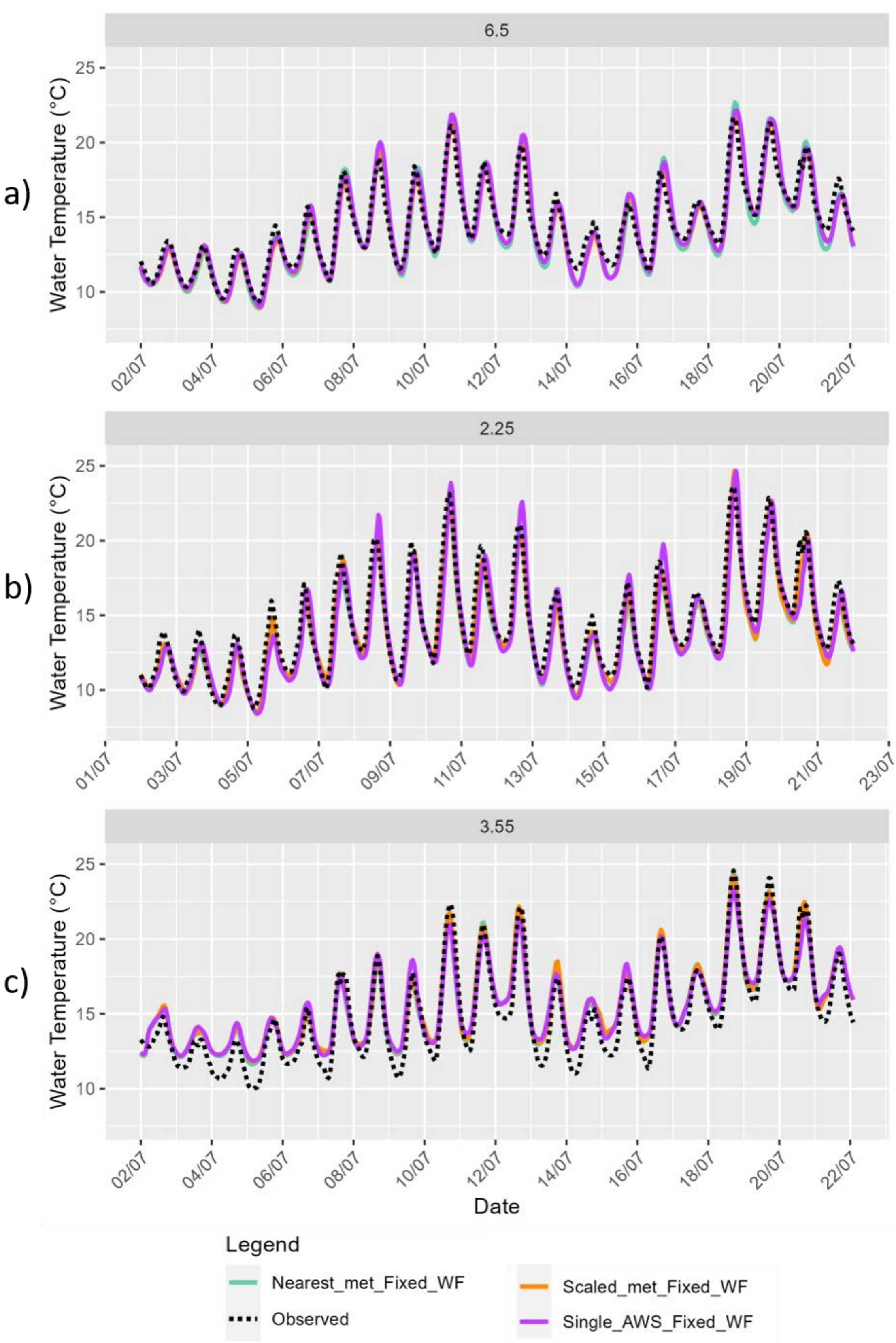

Figure 4-7 Influence of meteorological input on stream temperature model predictions for a) Clunie, b) Baddoch and c) Callater models.

Across Clunie, Baddoch, and Callater models, the impact of different meteorological inputs on stream temperature predictions varied. Generally, differences between model predictions using various meteorological inputs were often subtle, with all three input types producing similar stream temperature predictions throughout the modelling periods. The *Nearest AWS* input occasionally diverged from other inputs, sometimes underpredicting daily minima during calibration. This was particularly noticeable in the Clunie model, where it consistently produced lower daily minima, and overestimated daily maxima on five occasions. Baddoch models showed more marked differences between inputs compared to Clunie, with the *Single AWS* performing poorly, especially in the upper reaches. *Single AWS* and *Scaled Met* predictions were often more closely related, with *Nearest AWS* diverging at times. Callater models showed les influence than Baddoch models from changing meteorological inputs. The *Single AWS* input caused the largest changes, regularly underpredicting and occasionally overpredicting temperatures. A notable observation across all models was that differences between meteorological inputs were often less pronounced than differences between predictions and observations, particularly in downstream areas. However, this trend was less evident in Baddoch models, where inter-model differences were often larger than deviations from observed temperatures.

4.3.1.5. Influence of wind functions on model performances

Table 4-6 Mean root mean square error, bias and standard deviation between model calibration and validation periods for models using parameterised (param) wind functions and values fixed from evaporation pan observations (fixed).

Stream	Model inputs	RMSE	Bias	SD
Clunie	Scaled Met param WF	1.24	-0.78	0.98
	Scaled Met fixed WF	1.09	-0.55	0.95
Baddoch	Scaled Met param WF	1.27	-0.68	1.05
	Scaled Met fixed WF	1.08	-0.32	1.02
Callater	Scaled Met param WF	0.95	0.195	0.92
	Scaled Met fixed WF	1.02	0.465	0.9

Model responses to wind function inputs varied between catchments. All Clunie models improved regarding model rmse, bias and standard deviation with the use of fixed wind functions, whereas Baddoch and Callater models showed improved model rmse and bias with parameterised wind functions. Baddoch model standard deviation was also improved with the use of parameterised wind functions whereas Callater models using fixed wind functions showed superior standard deviations.

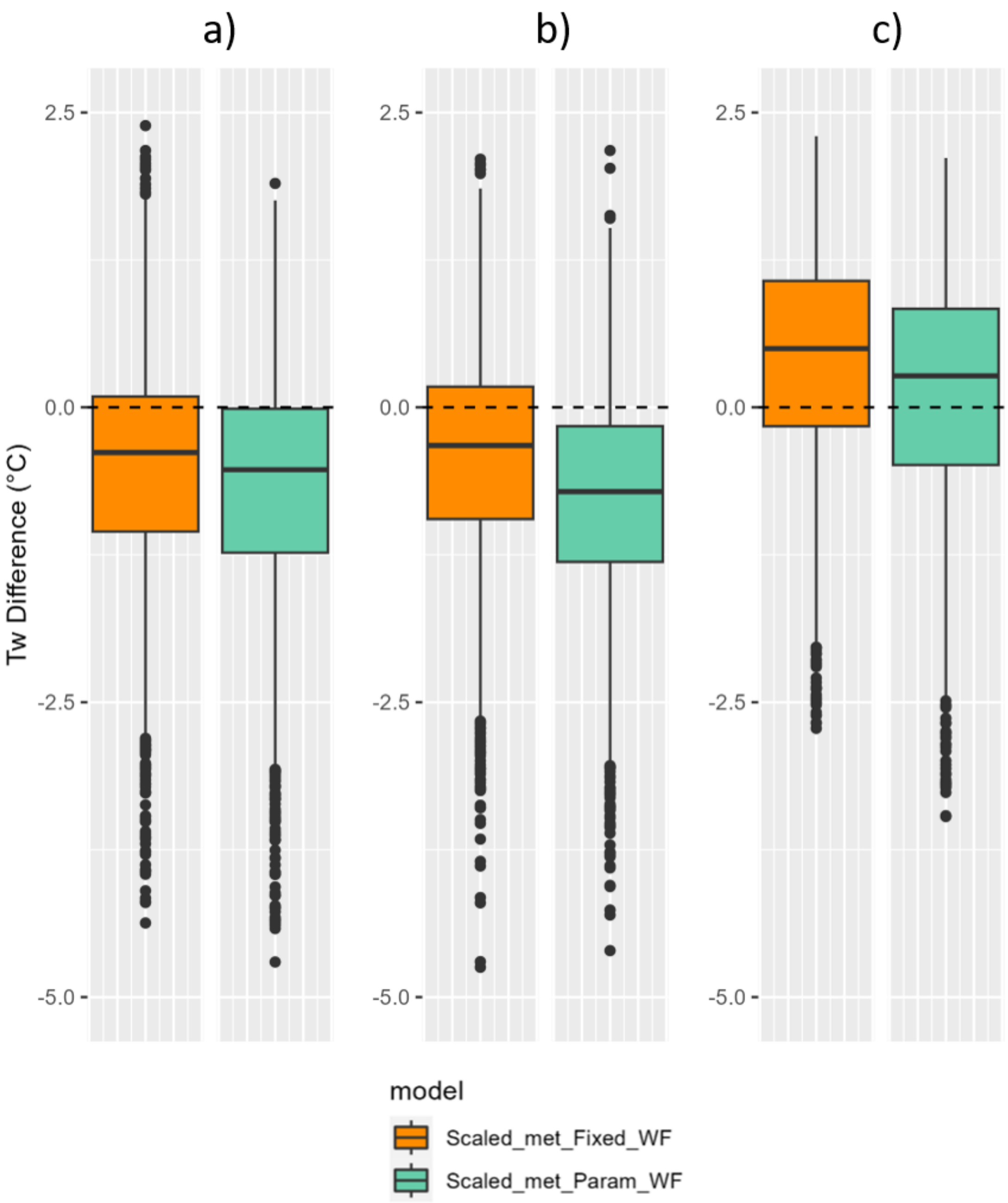

Figure 4-8 Influence of wind function input on stream temperature model predictions for a) Clunie, b) Baddoch and c) Callater models.

The impact of wind function inputs on stream temperature predictions varied across Clunie, Baddoch, and Callater models. For Clunie models, wind function choice had a stronger and more consistent impact than meteorological input choice, with fixed wind functions consistently outperforming parameterised ones. Fixed wind functions increased temperature predictions, especially downstream, improving performance metrics due to the models' tendency to underpredict temperatures. In Baddoch models, wind function choice had similar influence to meteorological input choice on model performance, with consistent differences in stream temperature outputs between fixed and parameterised wind functions across calibration and validation periods. However, differences between observed and predicted temperatures were greater than those between models using different wind functions, particularly for Callater models. Callater models showed less influence from wind function choice compared to meteorological inputs, especially regarding model bias. Fixed wind functions consistently produced higher temperatures than parameterised ones, resulting in worse model performances due to Callater models' tendency to overpredict daily minima. Overall, the impact of wind function choice varied across the three models, with Clunie and Baddoch displaying improvements in model performance when using fixed wind functions and Callater exhibiting deterioration.

4.4. Discussion

4.4.1. Model performance in comparison with previous studies

The models developed in this study achieved high calibration and validation accuracies of ≲1.1 °C. These results are comparable with other studies simulating thermal processes in rivers at hourly or sub-hourly timesteps. Dugdale et al., (2024) in their study using three AWS over 7 km of the Baddoch Burn over a one-month summer period achieved a mean RMSE of 1 °C using the same Heat Source model used in this study (Dugdale et al., 2024). Garner et al., (2014) achieved an RMSE of 1.1 °C in their study, once more utilising three AWS in a deterministic model developed by Moore et al., (2005) to simulate stream temperatures for a week-long period across a 1 km study reach of the Girnock Burn, another tributary of the Aberdeenshire Dee (Garner et al., 2014). Both of these studies utilised nearest-neighbour methods for apportioning observed microclimate data along a stream network. Hebert et al., (2015) achieved model RMSEs between 1.05 °C and 1.36 °C when predicting stream temperatures at two nested locations within a salmon river in New Brunswick, Canada, using a single AWS located 1 km from the first site and 7 km from the second site (Hebert et al., 2015).

The fact that studies utilising a single AWS can still achieve comparatively high levels of model accuracy when compared with the models built in this study identifies a potential issue in using RMSE alone to assess the performance of process-based stream temperature models. The fact that models using a single AWS can still achieve high accuracy with low RMSE whilst potentially insufficiently representing the catchment micrometeorology suggests that other model parameters may also be insufficiently represented, resulting in an equifinality issue where different combinations of parameter values produce similar model outputs.

4.4.2. Influences of meteorological inputs on model performance

This study investigated the response of stream temperature models to the influence of scaling meteorological data from point locations to a continuous network of meteorological observations. This study found that using scaled meteorological data improves the performance of stream temperature models when compared with point observations.

The comparison of meteorological inputs reveals distinct impacts on model performance for Baddoch, Callater, and Clunie models. For both Baddoch and Callater models, introducing meteorological observation data from their respective sub-catchments improved performance, with *Nearest AWS* models yielding smaller RMSE than the *Single AWS* models that relied on the downstream-most AWS from Clunie Water. This suggests that the AWS installed along Baddoch Burn and Callater Burn better represented the local meteorological conditions than the downstream Clunie AWS.

However, when comparing Clunie models using the *Single AWS* with those utilizing an additional AWS within the catchment (*Nearest AWS*), the increase in spatial resolution did not enhance model performance. In fact, Clunie models using *Nearest AWS* produced marginally larger RMSE and more negative bias than those using the *Single AWS*. The influence of the additional AWS was significant, as illustrated in Figure 4-3, indicating that its meteorological observations did not better represent those of the Clunie catchment compared to observations further downstream. This discrepancy is likely due to the additional AWS's location along a steep bank of a meandering reach of Clunie Water, which is downstream of a depression in local topography. Such positioning could contribute to localized cold air drainage, supported by observed air temperatures at this site, which recorded the lowest mean air temperatures across the study area. In contrast, sites along Baddoch Burn and Callater Burn were expected to have cooler mean air temperatures due to their greater elevation.

The use of *Scaled Met* meteorological inputs yielded further improvements compared to conventional *Nearest AWS* inputs used in previous studies. Not only did these inputs reduce model RMSE, but they also provided substantial reductions in model bias for both Clunie and Baddoch models. These results suggest that Scaled Meteorological input data better represent the microclimate of the study area, as they draw from all six stationary AWS within the catchment rather than just those within individual sub-catchments.

The responses of models to different tiers of meteorological inputs may be partially driven by the differing density of instrumentation within their sub-catchments. For Baddoch models, *Nearest AWS* utilized three AWS across 7.5 km of stream network, equating to one AWS per 2.5 km of stream length. In contrast, Clunie models had access to two AWS, while Callater models had one, resulting in one AWS per 7 km for Clunie and one per 6 km for Callater. Additionally, because Clunie Water is a larger stream than both Baddoch Burn and Callater Burn, its models would be expected to exhibit lower sensitivity to changes in input data due to greater thermal inertia.

In summary, while increasing spatial resolution of microclimate data generally improved model performance for Baddoch and Callater models, the unexpected response of Clunie when introducing a second AWS highlights the importance of careful placement of AWS. The *Scaled Met* approach proved most successful in accurately representing the microclimate of the study area by incorporating data from all available AWS.

4.4.3. Influences of wind function inputs on model performance

Heat Source uses a Dalton-style equation to calculate estimates of energy exchanges resulting from latent heat fluxes, which uses wind speed, actual vapour pressure, and saturation vapour pressure alongside empirically derived wind functions. This study derived its own wind functions from evaporation rate observations recorded using a floating evaporation pan and compared model performance using these coefficients with other values parameterised to each model within a range of other field-derived coefficients. As shown by Ouellet et al., (2014), this method can result in an overestimation of energy losses from evaporation.

Previous Heat Source modelling conducted within Baddoch Burn produced a negative bias throughout the study, particularly in locations further downstream. This negative bias was attributed in part to the aforementioned overestimation of evaporative losses whilst using the Dalton-style method, but in contrast to this study, wind function coefficients were only parameterised, with no observations of evaporation rates used within the field (Dugdale et al., 2024). In theory, the introduction of fixed wind functions derived from floating pan evaporation rate observations within the study area should have provided improved simulations of turbulent fluxes within models, improving their performances in comparison to parameterised wind functions. Results from the Clunie and Baddoch modelling efforts reflect this theory with fixed wind functions reducing RMSE and model bias across the board. However, for the Callater, the use of fixed wind functions actually reduced model performances, increasing RMSE and model bias.

An examination of why the fixed wind function worked worse than their parameterised counterparts within the Callater Burn reveals that the Callater Burn's model's parameterised wind functions had a shallower gradient and considerably larger intercept than the fixed versions, meaning evaporation from parameterised wind functions would be greater for almost all observed wind speeds than if using the fixed wind function. Only wind speeds in excess of 7 m/s produce greater evaporation rates for models utilising fixed wind functions. The evaporative flux is the primary energy sink during summer high temperature, low flow conditions, and the Callater models tested had positive biases across calibration and validation periods. As a result, the fixed wind functions (which limit the energy lost from evaporation), would ultimately worsen performances for Callater models. Had they been obtained, wind functions derived from evaporation rates within Callater Burn may have performed better than those transferred from observations in Clunie Water.

4.4.4. Limitations of model building and parameterisation process

Although the models developed in this study simulate stream temperature with a relatively high degree of accuracy (RMSE $\lesssim$ 1 °C, bias $\lesssim$ 0.5 °C), on many occasions during both calibration and validation periods in all three model networks, the differences between predicted stream temperatures from models using different meteorological and wind function inputs were smaller than the differences between these predicted temperatures and the observed temperatures. This suggests that the primary sources of error in the models lie outside the representation of microclimate and evaporation. There are a number of potential reasons for the deviations between observed and predicted temperatures.

Insufficient characterization of hydraulics as discharge data at model boundaries and tributary inflows and stream velocity along the network may contribute to downstream compounding errors in temperature predictions. Inaccurate hydraulics can affect the timing and amplitude of energy fluxes between the stream channel and the surrounding environment, potentially propagating and amplifying initial errors (Dugdale et al., 2024). The study area's geomorphology and low flow conditions resulted in exposed sediment at model boundaries, complicating discharge measurements. Two methods were used to capture discharges: contributing catchment area weighting and velocity area gauging weighting. The latter method can struggle with exposed boulders (Le Coz et al., 2012), while the former faces challenges during periods of low flows, especially for tributaries, as the precipitation-fed near-surface flows from the upstream contributing catchment reduce during dry periods (Gillet et al., 2021). Initial model runs used a discharge weighting factor for the top boundary discharge, with scaling factor values ranging from contributing catchment area weighting to the velocity area method observation weighting. Later iterations incorporated additional weightings for tributary inflows based on velocity area gauging observations, which improved model performances.

Although improvements were made in recreating observed boundary and tributary hydraulics, other obstacles arose in this area, particularly when generating inflows for Clunie models. Following an initial tributary catchment delineation using GIS spatial analysis of digital terrain models twinned with identification of existing tributaries in using high resolution orthophotos, fifteen major tributaries were identified for modelling along Clunie Water. Upstream tributaries were relatively simple to locate and instrument with temperature loggers in the field but further downstream, as anthropogenic activities became more prominent, identifying these tributaries became more challenging. As heather moorland was replaced by improved grasslands, a golf course and a series of roads, the introduction of land drains altered natural flow regimes decoupling the relationship between upstream contributing area and discharge. These features introduced additional uncertainty to the generation of tributary inflows, creating a further potential source of error to model hydraulics.

A number of potential sources of error arose when deriving wind functions using the floating evaporation pan. Firstly, a single pair of wind functions was derived from evaporation measurements taken between the hours of 12:00 and 16:00, when evaporation rates would be expected to be at their greatest. This time period was chosen because of this fact, as latent heat fluxes will typically have their greatest influence on the energy balance of a stream in summer low flow conditions during this time. However, by using a single period for deriving wind functions, this methodology does not incorporate cooler periods of the day where the latent heat flux would be less influential on energy balances, or potentially become a source of energy through condensation.

In addition to the temporal constraints on evaporation observations, spatial constraints were also imposed on the use of the floating evaporation pan. Due to land access limitations, observations were only collected along Clunie Water, with no observations made from Baddoch Burn or Callater Burn. Although other phenomena are likely the cause for the relatively poor performances of models using fixed wind functions for modelling Callater Burn, no comparisons can be made between wind functions derived in different catchments and no conclusions can be made on the transferability of the fixed wind functions between catchments.

Another challenge to model development in this region of the Cairngorms, as outlined by Dugdale et al. 2024, is the introduction of error from stream temperature logger installation. If installed in stratified sections of rivers or in areas where they become stranded during low flows, their temperature records will not reflect true observed temperatures (Dugdale et al., 2024).

A second challenge arising from logger placement in these environments is the influence of hyporheic exchange. In parameter sensitivity analyses, the parameter governing hyporheic zone contribution was found to have a substantial impact on predicted temperatures and thus model performance. Although the Heat Source model allows for hyporheic exchange to vary from node to node, without observations of these spatially heterogeneous exchanges, a single continuous value was chosen to represent this exchange. The final hyporheic exchange values chosen following the calibration process produced models which best-represented observed stream temperatures along the entire network, but due to the localised nature of hyporheic exchange, the values chosen may not have represented the local conditions at logger installation locations.

Another source of model error is the inadequate representation of geomorphological parameters. Although the models do encapsulate spatial variability in stream azimuth and incision, channel gradient and elevation, the absence of (spatially-explicit) data on some hydromorphic parameters (e.g. sediment thermal conductivity and diffusivity, thickness of the hyporheic layer, percentage of the water column exchanging with the hyporheic zone and streambed porosity mean that these values were held as fixed values across each model and derived via calibration. In reality, these parameters will vary spatially and, in some cases, temporally. No model can perfectly capture the complexities of the natural environment and must always incorporate assumptions (Westhoff et al., 2011) but due to the high levels of complexity in these upland headwater catchments alongside the systemic and sometimes compounding error observed in these stream temperature models, further improvements in model performance could be attained through categorising the geomorphology of sub-sections of stream networks in order to assign more spatially-explicit parameter values.

4.4.5. Areas for future research

To increase the analytical power of results from this study, one area for further research would be to standardise the number of instruments per unit distance of the stream network within a study. Changes to model performance in response to meteorological input data were largest for Baddoch Burn, which was the most heavily instrumented sub-catchment with a total of three AWS installed at a density of one AWS per 2.5 km of stream. Responses of Clunie Water and Callater Burn to input data may have been larger if they had also been instrumented to the same density. However, with Clunie Water being larger than both Baddoch Burn and Callater Burn, the influence of input meteorological data on model performance may still have been muted relative to other sub-catchments due to the increased thermal capacity of the larger stream (Leach, et al., 2023).

Further insight into the impacts of wind function choice in stream temperature model performances may been gleaned by increasing both the spatial and temporal observations of evaporation rates within the study area. Due to land access constraints, this study only conducted evaporation rate observations using the floating evaporation pan along reaches of Clunie Water, with no observations made in the Baddoch Burn and Callater Burn. With additional labour resources, instantaneous evaporation rates could be measured within the three sub-catchments, providing directly comparable evaporation rates in different environments subject to the same prevailing climate conditions.

Little was known of the groundwater regime and hyporheic exchange within the study area, with the flow accretion surveys conducted across a limited area observing no substantial sub-surface flow accretion. To provide more confidence in flow accretion representation, flow accretion surveys could be conducted across a more extensive region of the study area, including sub-catchments. To further constrain parameter values dictating hyporheic exchange in future models, a series of tracer injection and monitoring studies could be conducted to provide observations of hyporheic exchange within the study area.

Finally, further insight into interactions between parameterised values for model inputs would be gleaned from increasing the number of calibration runs. Dugdale et al., (2024) used a similar method to calibrate and validate their Heat Source models and found that parameter values began to stabilise when submitted to 10,000 model iterations. Due to constraints around time, processing power and available computer memory, the calibration process for model parameter combinations in this study was limited to 1,000 iterations. Inspection of our calibration results suggested a high degree of equifinality when generating models with low RMSE scores, with many different combinations of parameter values resulting in similarly well-performing models. With additional time and computing resources available, increasing the number of iterations from 1,000 to 10,000 or more would have likely resulted in improved parameterisation.

4.5. Conclusion

This study further develops the existing literature for building process-based stream temperature models. Stream temperature simulations across three sub-catchments were improved by incorporating additional microclimate data from automatic weather stations within sub-catchments. Simulations within two of the three sub-catchments were further improved by scaling microclimate observations from discrete point locations to a novel spatially continuous dataset at a 50m resolution. The study also found that using wind function coefficients derived from observed evaporation in the field also improved model performances for two of the three sub-catchments, identifying improvements in evaporation process representation through constraining wind functions with in-situ evaporation observations whilst also showing limitations in transferability of wind functions between sub-catchments. Despite generating high accuracy in reproducing observed stream temperatures, all models tested in this study displayed predicted temperatures which diverged from observations, with some sub-catchments performing more strongly than others. It is suggested here that many of these divergences are likely caused by the model representation of streambed and hyporheic zone characteristics. Another cause is likely the imbalance of instrumentation between sub-catchments with some having a higher density of automatic weather stations than others. Future studies should incorporate evenly-spaced weather stations across study areas to resolve this, whilst also looking to sub-categorise reach geomorphology along a model network to capture spatial heterogeneity in streambed and hyporheic zone characteristics.

5. Integration of nested process-based river temperature models to understand the effects of contrasting riparian tree planting strategies on reducing river temperatures: implications for management.

Abstract

Summer stream temperatures are expected to increase in response to climate change with negative consequences for species adapted to living in cold water habitats, including ecologically, culturally and financially important species such as Atlantic salmon and brown trout. Many of the UK's headwater streams have little or no shading from tree cover due to over grazing. This leaves streams exposed to shortwave radiation, enhanced warming and higher maximum temperatures under current and future climate. Riparian tree planting is one of the few management actions able to reduce stream temperatures and mitigate some of the effects of temperature rises. However, the practice is expensive and logistically challenging due to the issue of heavy grazing in many Scottish headwaters requiring the erection and maintenance of substantial fencing to protect trees. There is therefore a need to improve understanding of the impacts of riparian planting on summer stream temperatures to ensure that trees are planted where they can have the greatest benefits for management. Previous studies have shown that planting riparian woodland alongside narrower headwater streams, with lower water volumes and higher residence times has the greatest effects on river temperature. However, it remains uncertain which planting strategies are likely to be most effective in cooling larger downstream rivers.

In this study, three nested process-based stream temperature models are integrated to assess the effects of contrasting riparian tree planting strategies on spatio-temporal variability in thermal regime. By integrating multiple models, it was possible to assess the effects of riparian

tree planting in both tributaries and larger downstream rivers incorporating effects of advected heat.

Consistent with previous studies, our findings show that the greatest reductions in maximum stream temperatures across an entire 104 km^2 network can be achieved by planting the most upstream areas. However, stream temperature reductions from headwater riparian planting also declined in a downstream direction, particularly in response to substantial tributary inflows. Maximum stream temperature reductions in the larger downstream river reaches and at the lower extent of the model domain were achieved by planting at the lower end of the study area. Our investigation highlights the need to carefully consider management objectives when devising riparian tree planting strategies with constrained resources.

5.1. Introduction

Stream temperature is one of the most important abiotic controls on stream ecosystem composition and functioning (Borgwardt et al., 2020). As well as acting as a primary control on gross primary production and ecosystem respiration (Allen, et al., 2005), it influences all aspects of the life cycle of cold-water-adapted fish species (American Fisheries Society, 2009), controlling spawning location and timing, embryo development and hatching, feeding, growth and productivity (Fenkes et al., 2016; Jonsson, 2023). In the UK, salmonid populations are impacted by a number of pressures, including poor water quality from agricultural runoff and sewage discharges and habitat degradation from historic river regulation (Cefas, 2022; Scottish Government, 2022). However, there is also increasing concern over rising stream temperatures associated with rising air temperatures and changes to catchment hydrology, both governed by climate change. Rising stream temperatures have the potential to reduce the thermal suitability of riverine habitats for salmonids (Arevalo et al., 2021; Bernthal et al., 2023; Borgwardt et al., 2020; Pohle et al., 2019; Schneider et al., 2013) and could act synergistically with other pressures such as excess nutrients (Johnson et al., 2024).

The UK is characterised by low forest cover, with woodlands making up only 13% of total land use, significantly lower than the European average of 46% (Forest Research, 2023). Many of the UK's headwaters have limited tree cover, exposing rivers to high incoming solar radiation resulting in elevated summer stream temperatures (Dugdale et al., 2024). Riparian tree planting is one of the few management options proven to reduce stream temperatures. In some circumstances, reintroducing riparian woodland can shade streams, reducing the receipt of shortwave radiation and in turn, reducing extreme high temperatures (Benyahya et al., 2012; Broadmeadow et al., 2011; Dugdale et al., 2024; Fabris et al., 2018; Garner et al., 2014a, 2017; Hannah et al., 2008; Imholt et al., 2013; Jackson et al., 2021b; Malcolm et al., 2004b, 2008a). However, tree planting and associated fencing to reduce grazing can be expensive and logistically challenging. Consequently, there is a need for continued improvement in the understanding of the effects of riparian tree planting on thermal regime to inform and target management intervention. Given the scientific interest and management imperative for new information, there have been a growing number of studies investigating the effects of riparian tree planting on river temperatures in recent years (Dugdale et al., 2024; Fabris et al., 2018; Garner et al., 2014a, 2017; Hannah et al., 2008; Imholt et al., 2013; Jackson et al., 2021b; Leach & Moore, 2010; Malcolm et al., 2008a).

There are typically two types of models which can be used to assess the impacts of riparian planting on stream temperatures: statistical models and process-based models. Statistical models work by fitting statistical links between observed stream temperatures and a number of covariates seen to relate to stream temperatures (Benyahya et al., 2007). Compared to process-based models, statistical models need relatively little input data and as a result, can be easily implemented at large spatial scales. However, they do not directly relate to the processes governing stream temperature and therefore require interpretation when assessing outputs. They are also generally poor at identifying site-specific effects of woodland on stream temperatures and typically apply mean values to the effects of cooling. They also don't typically address the cumulative spatial effects of riparian canopies as cooled water is advected downstream (Webb et al., 2008).

Process-based stream temperatures offer an alternative approach for assessing the effects of riparian woodland on river temperature. These models simulate the energy fluxes between a stream and its environment based on physical processes and principles. In addition, specific fluxes can be modified to explore hypothetical scenarios affecting the energy budget (Dugdale, et al., 2017). As streams typically increase in width with distance downstream, the ability of riparian trees to effectively shade streams diminishes, leaving larger areas of water surface exposed to solar radiation (Hebert et al., 2011). In addition, water volume and stream velocity also tend to increase with distance downstream. Taken together, these factors suggest that stream temperature reductions from riparian planting are likely to be larger when focused on smaller headwater streams (Jackson et al., 2021a).

However, there remains substantial interest in understanding whether temperature extremes in larger rivers could be moderated by reducing temperatures in the contributing tributaries (Fuller et al., 2022) and over what spatial scales (e.g. local thermal refugia or reach scale reductions (Rutherford, et al., 2004)). Previous studies employing process-based models to investigate the effects of riparian woodland on river temperature have often focussed on management scenarios in single study catchments with limited spatial extents (typically under 30 km^2) where small tributary inflows are not the target of management action. Consequently, further work is required to understand the potential importance of advected heat in management scenarios focussed on tributary streams as water flows from smaller sub-catchments to larger mainstems.

Given this context, the current study aims to integrate nested process-based stream temperature models to investigate the effects of contrasting riparian restoration strategies on the spatio-temporal variability of river temperatures at different spatial scales.

The specific objectives are to:

i. Integrate three separate process-based stream temperature models to understand and predict stream temperature across a large (104 km^2) sub-catchment of the Aberdeenshire River Dee, Scotland;
ii. Introduce a series of spatially varying riparian tree planting scenarios into the integrated stream temperature model;
iii. Characterise steam temperature changes resulting from contrasting riparian tree planting strategies aggregated across the study and at catchment outlets.

5.2. Methods

The following methods section briefly discusses the study site, stream temperature model used, the hydrometeorological data inputs, and how the baseline model was calibrated and validated. For more detail on these methods, see Chapter 4. The methods section then describes how the model represents riparian trees, the descriptive data used to capture tree characteristics within the study area, how these tree characteristics are read into the model and how their presence influences solar radiation receipt at the channel surface. The choices of riparian planting scenarios for testing are then discussed along with the reasoning behind their choosing. Finally, the methods section ends by outlining how stream temperature reductions in scenario model outputs are quantified, specifying how changes in energy receipt at the stream surface and stream temperature changes at point and network scales are calculated.

5.2.1. Study site, stream temperature model and input data

Clunie Water, Baddoch Burn and Callater Burn are spawning streams for Atlantic salmon located in the central Cairngorm Mountain range. Their catchments range in altitude from 338 to 1062 mAOD and span a combined area of 104 km^2. Clunie Water flows in a south-to-north direction, merging with the Aberdeenshire Dee in Braemar. The Baddoch Burn and Callater Burn serve as a major tributaries to the Clunie Water, flowing from southwest-to-northeast and southeast-to-northwest respectively. The contributing catchments for these tributaries have areas of 23 and 35 km^2, respectively. The Baddoch Burn - Clunie Water confluence is situated at an upstream distance of 9.45 km and the Callater Burn- Clunie Water confluence occurs further downstream at an upstream distance of 3.4 km. (For further information on the study area, see chapter 4, section 2.1 Study Area).

The stream temperature model chosen for simulating water temperatures was a modified version of Heat Source 9.0.0.b19; a process-based temperature model developed at Oregon State University and used by the Oregon Department of Environmental Quality (Boyd & Kasper, 2003). For further information on the stream temperature model, see chapter 4, section 2.2 Stream Temperature Model. For information on the microclimate, energy flux, water temperature, discharge, and hydromorphic data used in the modelling process, see Chapter 4, section 2.3- Model input data.

Heat Source calculates evaporation rates using a Dalton-style equation, involving the difference between the saturation vapour pressure at the water surface temperature and the actual vapour pressure of air above the water surface together with derived constants related to wind speed, referred to as “wind functions”.

Wind functions for the Clunie and Baddoch models were developed from observed evaporation rates from a floating evaporation pan in Chapter 3, section 3.5, Deriving Wind Functions from Observed Evaporation. For the Callater model, the wind functions derived from evaporation pan observations performed poorly, likely due to the absence of evaporation rate observations within the Callater sub-catchment. In this instance, wind function values were parameterised during the model calibration process, calibrating within a range of existing empirically derived values from the literature. For further information, see Chapter 4, section 2.3.6, Evaporation data.

5.2.1.1. Riparian tree data and model representation

To simulate the influence of riparian trees on stream energy budgets Heat Source uses a series of transects radiating from a central stream node, with each point along a transect having a tree height, canopy density and canopy overhang value associated with it (Figure 5-2). Where a tree was not present at a given point, the height being zero negates the influence of canopy overhang or canopy density values. Here eight transects were chosen to represent riparian trees, with transects running at a 45-degree angle from the last (see figure 5-2, right panel for representation of transects). Each transect consisted of five data points each spaced 5 m apart, making the length of a total transect 25 m. Each tree in models was allocated an overhang of 2.5 m and a canopy density of 70%, meaning in models, 70% of incoming solar radiation would not pass through the canopy to the stream water surface. Heights for mature conifer and deciduous trees were 30 m and, 15 m respectively. These values were chosen to reflect the existing commercial conifer plantation within the study area (~30 m in height) as well as a mean of typical tree heights expected of mixed native deciduous species which are typical of a semi-natural forest site in the region (birch, rowan and alder) (Dugdale et al., 2018). The overhang of 2.5 m was chosen as an approximation of half of the crown diameter at maturity for these tree species (Evans et al., 2015). They were also chosen for consistency with previous modelling within the study area (Dugdale et al., 2024).

In some circumstances points along the transects extending outwards from each model stream node would be unsuitable for tree planting; for example, within the model's wetted width or situated on gravel bars. Gravel bars were digitised and combined with wetted widths to identify areas deemed unsuitable for planting. This process can be observed in Figure 5-2.

5.2.1.2. Model influence of riparian trees

Heat Source calculates the influence of riparian trees on the stream energy balance as follows. Direct beam and diffuse solar radiation is routed through the transect zones from the outermost to innermost, with direct sunlight being attributed from the transect direction closest to the solar azimuth. For example, if the sun is at 231°, the southwest transect at an angle of 225° will be used. Shadows cast from each land cover node are calculated as a function of the solar altitude and azimuth in combination with the physical attributes of the tree represented within a given land cover node. When the model determines a tree is shading the channel, it calculates the reduction of incoming radiation using Beer's Law, the path length through the planting zone, stream orientation, solar altitude and azimuth, as described in Boundary Layer Climates (Boyd & Kasper, 2003; Oke, 1987). This process is repeated through each node in the land cover transect.

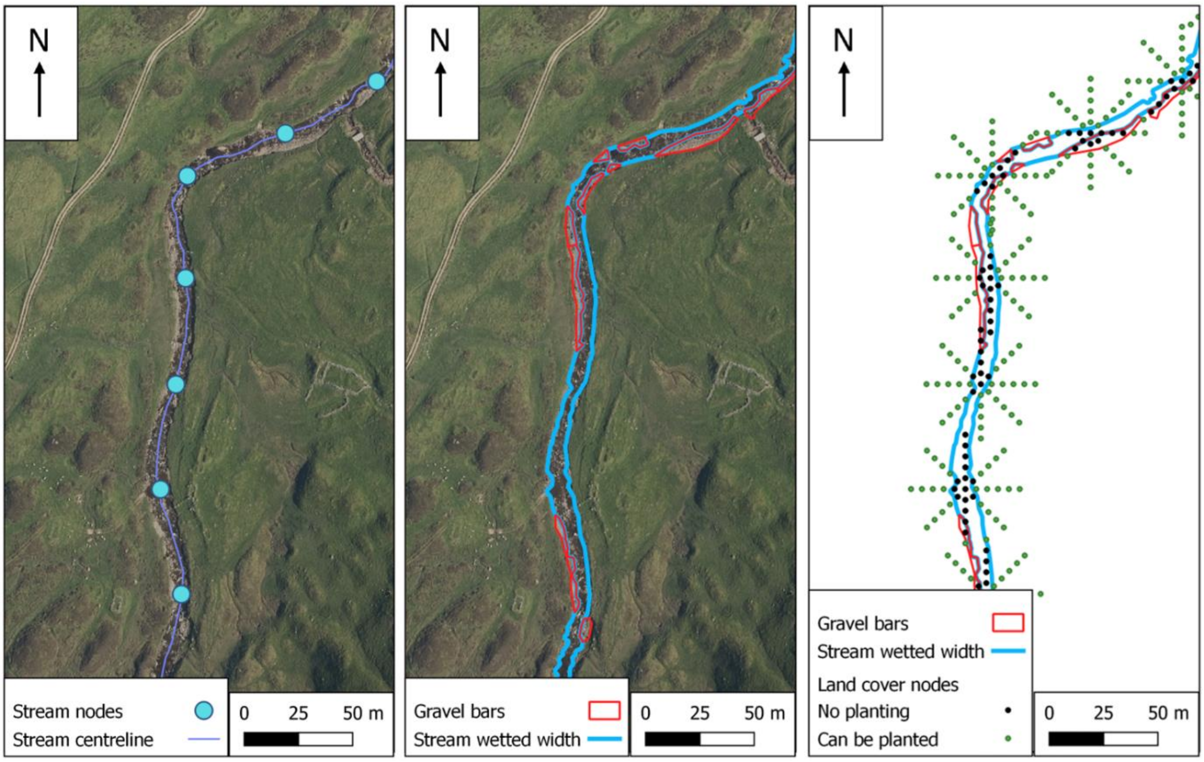

Figure 5-1 Land cover node generation and identification of areas suitable for riparian planting

5.2.2. Baseline model implementation and calibration/validation

Baseline models for Baddoch Burn, Callater Burn and Clunie Water were calibrated and validated for a three-week period in July 2022 and a 19-day period in July-August 2022 respectively (See Chapter 4, section 2.4, Model Calibration and Validation). Baseline models

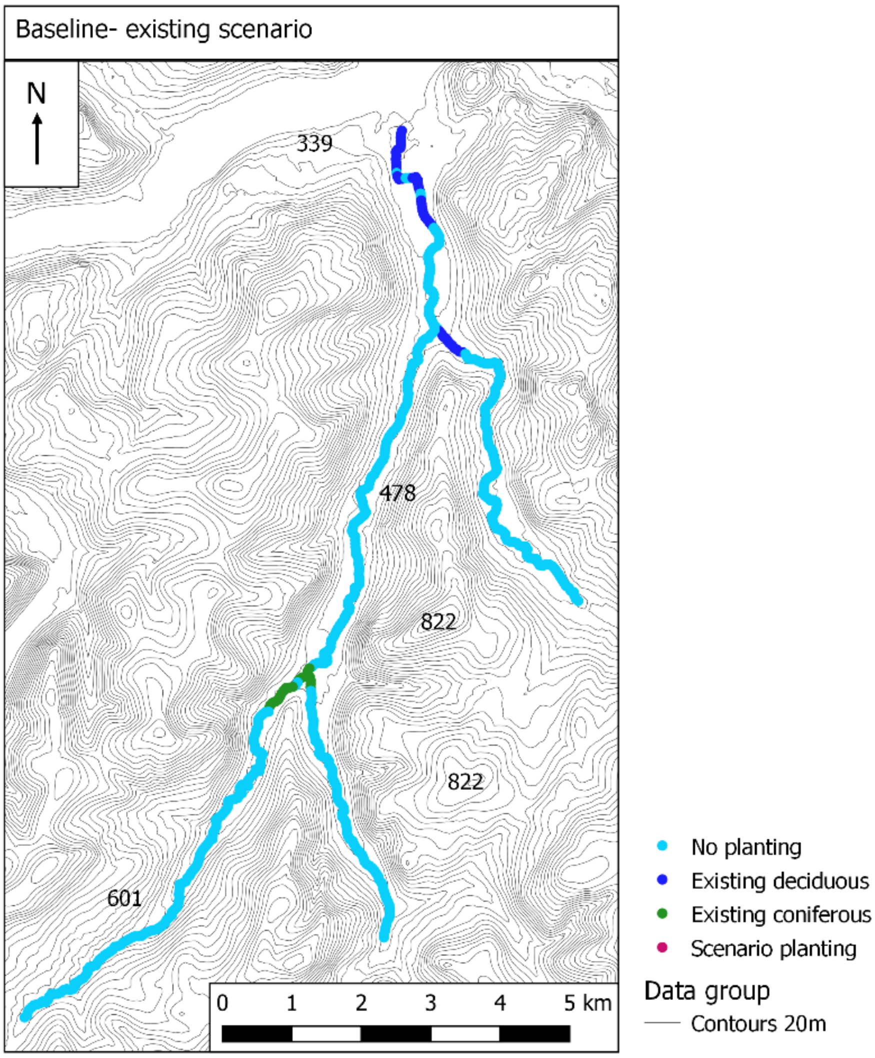

Figure 5-2 Existing riparian trees included in baseline model

used land cover data representing the existing riparian land use within the study area. These areas consisted of a small plot of conifer plantation at the Baddoch Burn-Clunie Water confluence, a small number of deciduous trees in the lower reaches of Callater Burn and sporadic groupings of deciduous trees in the lower Clunie Water. Areas of existing trees (Figure 5-3) were digitised as polygons using a combination of orthophotos and satellite imagery from Google Earth (Google, 2024).

Hydraulic and aforementioned geomorphological model parameters were constrained using values from the literature (See Table 4-3 in Chapter 4, section 2.4, Model Calibration and Validation). Manning's n values were constrained within a range of values which were unrealistic for the site's morphology but supported model stability. Although Manning's n values were unrealistic, model hydraulics were tested against point observations during the study period to ensure realistic flow velocities and depths. A Latin hypercube sampling method was used to generate 1,000 representative combinations of parameter values which were subsequently run through the Heat Source model. Simulated water temperatures from each parameter combination were compared to observed stream temperatures (for more information on the model calibration and validation process, see Chapter 4, section 2.4, Model Calibration and Validation) to identify the best performing parameter combinations based on a combination of RMSE , bias and standard deviation. Final baseline models achieved a high degree of accuracy across the calibration and validation periods (RMSE $\lessapprox$ 1 °C, bias $\lessapprox$ 0.5 °C), providing a reliable baseline against which to assess the potential influence of contrasting riparian planting scenarios. For further information on baseline models, see Chapter 4.

To investigate the effects of riparian tree planting in tributaries (Baddoch Burn and Callater Burn) on downstream river temperatures (Clunie) a nested modelling approach was implemented whereby simulated outlet temperatures from the Baddoch and Callater were used as inflow boundary conditions to the Clunie Water model. Spatially distributed temperature monitoring data from sub-catchment main stems (i.e. those not used to represent model boundary conditions or tributaries) were used for model calibration and validation.

5.2.3. Planting scenarios

All riparian planting scenarios, assumed a fixed resource of 6 km of trees. This allowed the outcomes of a range of highly contrasting planting scenarios to be explored, while at the same time ensuring a sufficiently large effect on stream temperature to be detected. Existing deciduous trees and conifer trees were allocated a height of 15 m and 30 m respectively. Any new riparian planting, assumed a conservative uniform tree height of 15 m. All riparian trees were allocated a canopy overhang of 2.5 m and a canopy density of 70%. Table 1 describes each planting scenario, with following sections expanding on these descriptions.

Table 5-1Description of model planting scenarios

Model	**Planting scenario**
1	Planting the upper 6 km of Baddoch Burn only
2	Planting the total 6 km of Callater Burn only
3	Planting the upper 6 km of Clunie Water only
4	Planting the mid 6 km of Clunie Water only
5	Planting the bottom 6 km of Clunie Water only
6	Planting the upper 2 km of each sub-catchment (Baddoch, Clunie and Callater)
7	Planting the mid 2 km of each sub-catchment (Baddoch, Clunie and Callater)
8	Planting the bottom 2 km of each sub-catchment (Baddoch, Clunie and Callater)
9	Planting 2 km spread evenly across each sub-catchment (1 in 4 Baddoch nodes, 1 in 7 Clunie nodes and 1 in 3 Callater nodes)

10	Planting the areas in receipt of the greatest incoming SW radiation

5.2.3.1. Single sub-catchment planting

The first set of planting scenarios explored the effects of riparian planting on stream temperature using a single 6 km river reach. This involved three planting scenarios focussed on the top of each sub-catchment (Baddoch, Clunie, Callater), and two further scenarios focussed around the middle and lower end of the Clunie. (Scenarios 1 to 5 in Figure 5-4). Because the Callater Burn (below Loch Callater) was <6 km in length (5.9 km), the whole channel was included in this planting scenario.

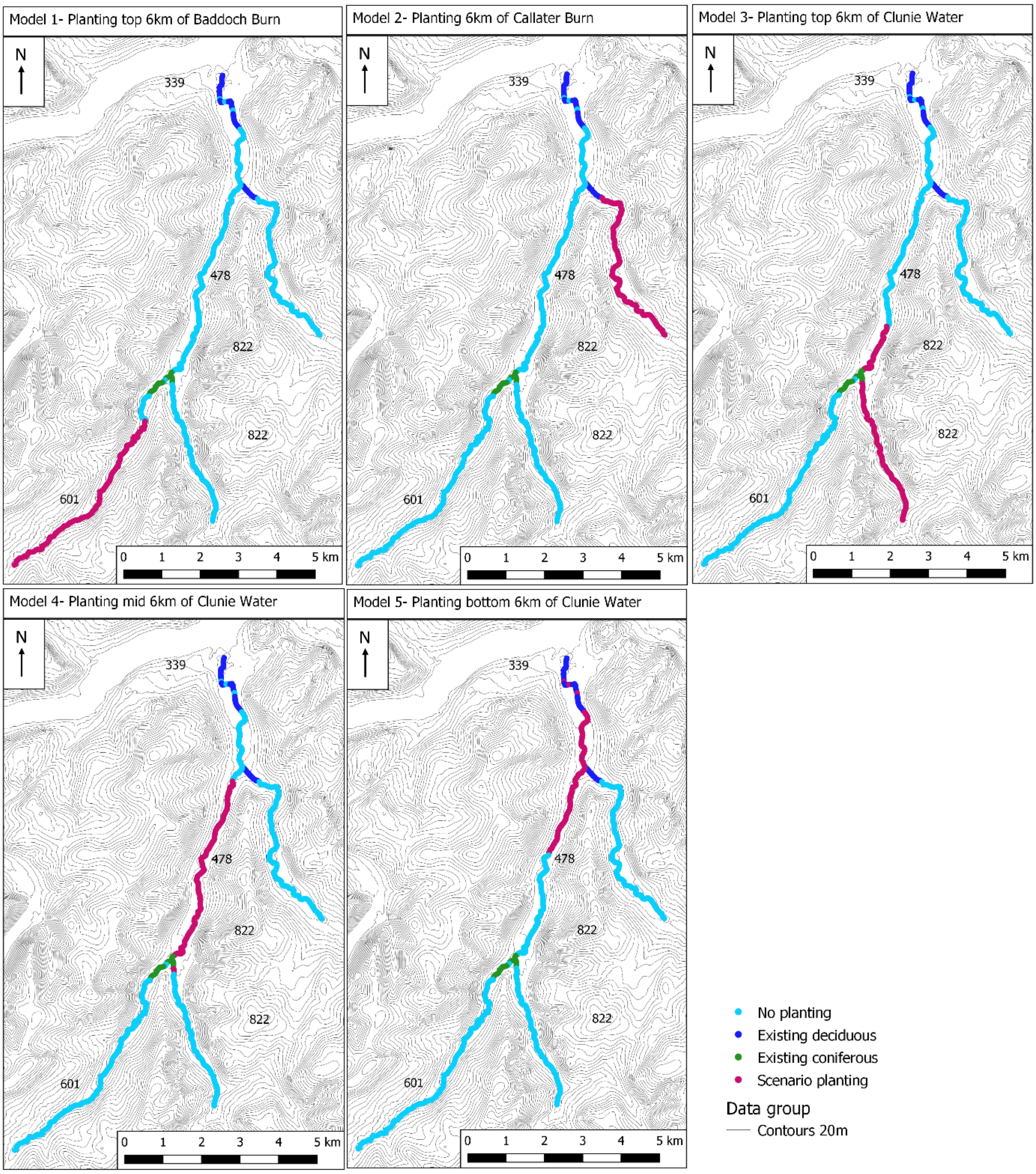

Figure 5-3 Single-catchment planting scenarios, planting 6km zones of riparian trees

5.2.3.2. *Multi-catchment planting*

The second set of scenarios involved distributing the same 6 km of riparian planting across three continuous 2 km planting zones, distributed across the three sub-catchments. Three scenarios were explored whereby the 2 km riparian planting zones were distributed in the upper, middle and lower reaches of each sub-catchment (Models 6-8, Figure 5-5).

5.2.3.3. *Intermittent planting*

The third planting scenario distributed riparian planting into small equally spaced intervals within each sub-catchment, with an equal allocation (2 km total) of planting in each sub-catchment. This resulted in riparian planting at every one in three 50 m stream nodes along Callater Burn, one in every four along Baddoch Burn and one in every seven along Clunie Water (Model 9 in Figure 5-5). This scenario attempted to simulate the type of planting being undertaken by some river managers in Scotland where landowners continue to prioritise the unimpeded movement of deer across the landscape.

5.2.3.4. *Highest solar receipt planting*

The final scenario prioritised riparian planting to areas of the stream network in receipt of the greatest solar radiation, having accounted for riparian topography and associated shading. The 6 km of planting was then split between these 120 nodes. Of these locations, 61 were within the Callater sub-catchment, 55 were within Baddoch and only four were within Clunie Water. This planting scenario is displayed in Model 10 in Figure 5-5. This simulation was intended to replicate the prioritisation approach advocated by the England's "Keeping Rivers Cool" project led by the Environment Agency (Environment Agency, 2016).

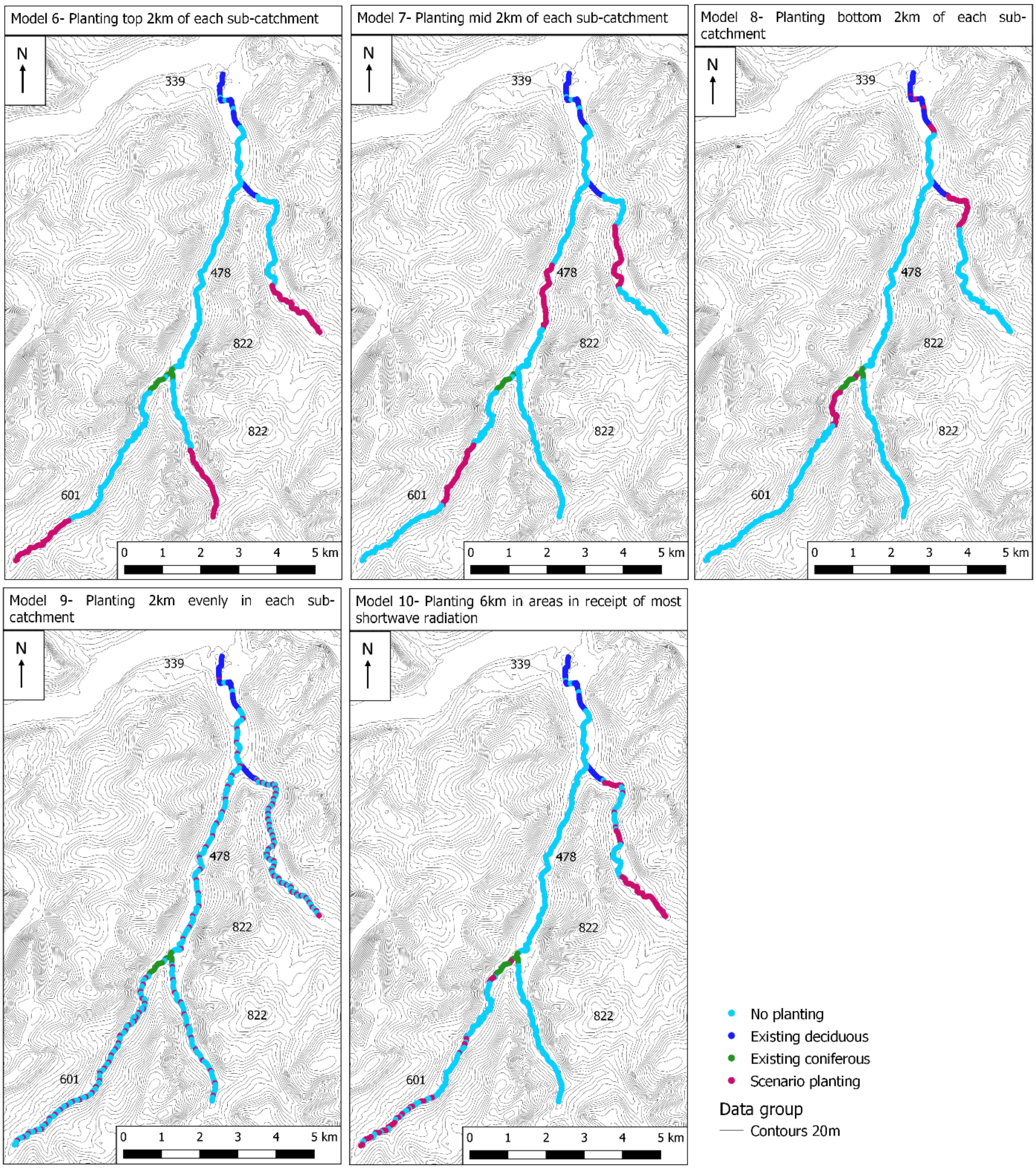

Figure 5-4 Multi-catchment planting scenarios, planting riparian trees in each of the three sub-catchments

5.2.4. Quantifying effects of riparian planting on stream temperature

The reduction in shortwave radiation resulting from introduced shading from riparian planting is the driver of temperature reductions in the model scenarios simulated. As such, the first results compare changes to received shortwave radiation between planting scenarios. The metric used to capture changes in received shortwave radiation is MJ/m^2 and is calculated as the difference in total received shortwave radiation in W/m^2 at a given model node between baseline and planting scenario models over the three-week simulation period multiplied by 3600 to give J/m^2 and divided by 1,000,000 to give MJ/m^2. It does not refer to the total reduction of received shortwave radiation at a given stream node, but a spatially averaged measure of reduced radiation. To calculate total reduction in received shortwave radiation, this value would need to be multiplied by the stream channel width at the given node.

Simulated stream temperatures were compared between baseline and scenario models to assess the effects of riparian tree planting. To characterise cumulative changes in stream temperature across the entire stream networks, the Area Under Curve (AUC) metric described by Dugdale et al., (2024) was applied. This method seeks to aggregate temperature differences across space by calculating the integral of a maximum stream temperature long profile, quantifying the “area under the curve” of a stream’s long profile. If simulated stream temperatures from the planting scenarios are lower across the river network than those observed in the baseline scenario, then the AUC value will also be lower, providing a single overall metric of spatially varying effects. The smaller the AUC value, the lower the temperatures across the stream network (Dugdale et al., 2024).

The metric “Degree Hours” was used to aggregate differences in stream temperature effects between baseline and treatment scenarios over time. This was calculated as the cumulative difference in temperature at a given location between baseline and scenario models. Degree hours for each scenario were visualised in a spatial plot to provide an indication of where and when river temperatures varied as a result of tree planting (Malcolm et al., 2019). This is a useful metric for studying stream temperatures within an ecological context as, by accounting for both duration and magnitude of temperature change, it quantifies changes to the total thermal load experienced at a given location which can be of ecological significance, particularly for Atlantic salmon (Dugdale et al., 2016). Additional context was then provided for the degree hours metric, wherein the number of degree hours stream reaches in the baseline scenario spent above a 23 °C threshold (the temperature which triggers a stress response in juvenile salmon) were calculated, then compared with degree hours of reaches under each planting scenario.

For each model node changes in daily maximum (ΔTw_{max}) and mean stream temperatures (ΔTw_{mean}) were calculated thereby characterising changes to both average and extreme temperatures. These metrics were applied to the outlets of each sub-catchment (Baddoch Burn and Callater Burn) as well as the outlet of the total study area (Clunie Water) to assess the influences of planting on stream temperatures at the most downstream points in each sub-catchment and the total model space.

In order to visualise timings and amplitudes of changes in stream temperature across the entire catchment between baseline and planting scenario models, spatiotemporal water temperature plots were generated, as used in Garner et al., (2017) and Fabris et al., (2018).

5.3. Results

The following results section describes the influence of contrasting riparian tree planting scenarios on the receipt of shortwave radiation, patterns of stream temperature response at sub-catchment outlets and whole study area scales, and the influence of heat advection on these patterns.

5.3.1. Influence of planting location on receipt of shortwave radiation

Stream temperatures were altered in this study primarily as a result of reductions in shortwave radiation receipt by stream channels due to shade introduced from riparian planting. A summary of shortwave radiation reductions resulting from each planting scenario can be found in Chapter 5 Appendix. The table in this appendix displays means and standard deviations of shortwave radiation reductions associated with each planting scenario (MJ/m^2). Changes in stream temperature between baseline and scenario models primarily reflected reductions in shortwave radiation receipt due to shading by riparian trees and subsequent downstream effects due to advection (See Figure 5-6). The largest reduction in shortwave radiation occurred in the headwaters of Baddoch Burn with one node receiving a cumulative reduction of 246 mJ/m^2 of shortwave radiation received over the 3-week model period (Models 1, 6 and 10). The smallest reductions in shortwave radiation were in the lower reaches of Clunie Water, with some nodes experiencing a reduction of less than 2 mJ/m^2 throughout the model period (Models 3, 4 and 9). The planting scenario which resulted in the largest reduction in cumulative shortwave radiation receipt was Model 1, with a mean reduction of 26.53 MJ/m^2 across the system. Model 5 produced the smallest mean reduction across the system, with a reduction of 15.44 MJ/m^2. These findings show that larger reductions in shortwave radiation receipt can typically be achieved by planting in headwaters. However, there are site-specific exceptions, for example, planting in the lower 2 km of Baddoch Burn results in larger reductions in shortwave radiation receipt than planting in the mid-reaches (Model 8 and 7). The model node receiving the maximum reduction in shortwave radiation for each planting scenario increased with increases in mean shortwave radiation reduction, with a minor outlier presented in the Model_8 scenario, wherein a relatively small mean reduction in shortwave radiation coincided with one of the larger maximum reductions.

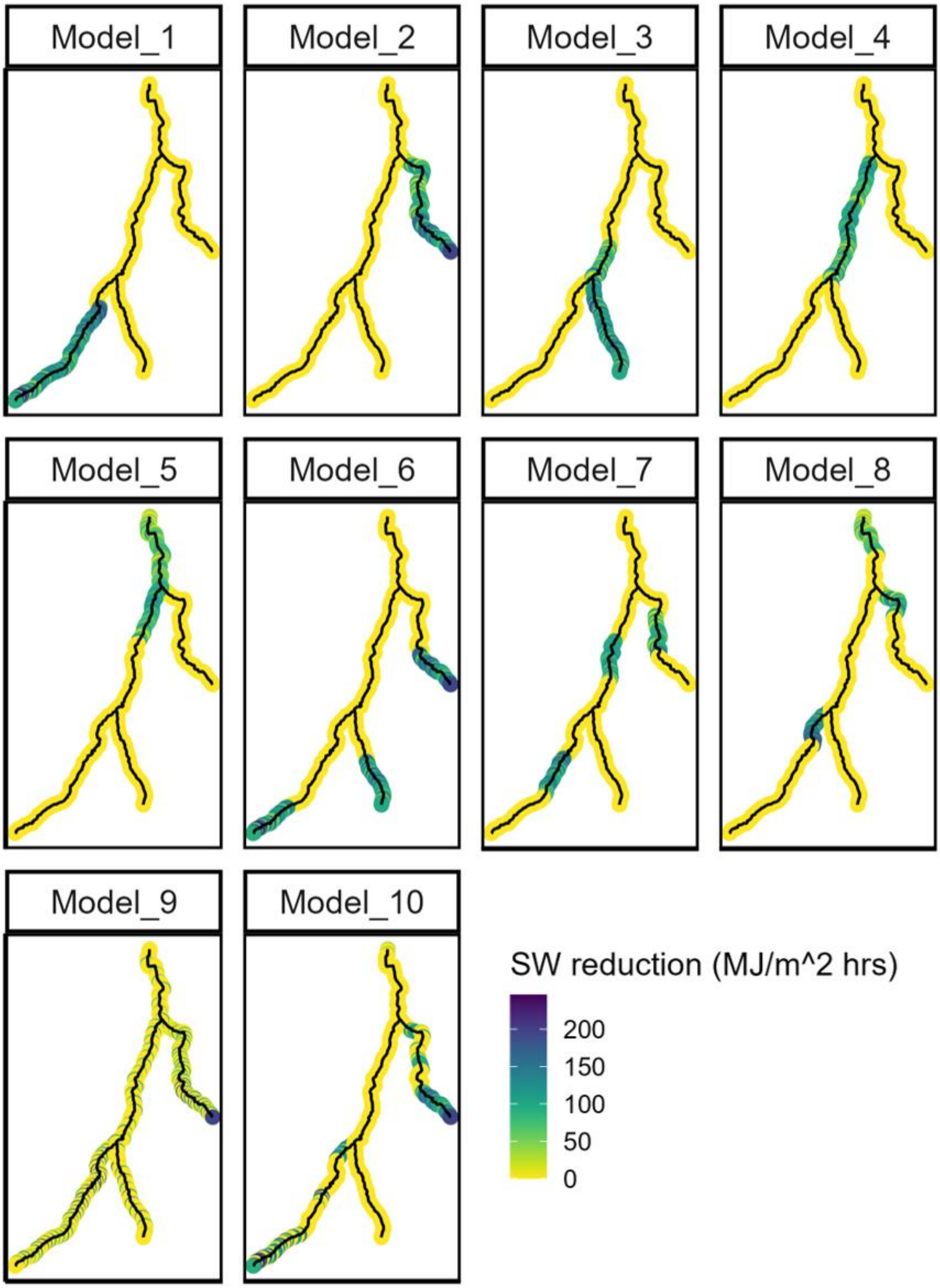

Figure 5-6 Temporal cumulation of reduction in shortwave radiation (MJ/m^2) received by the stream channel as a result of riparian planting.
Models 1 and 2 are 6km of planting in Baddoch and Callater sub-catchments; models 3, 4 and 5 and 6km of planting in the upper, mid- and lower reaches of all three sub-catchments; model 9 is 2km evenly spaced across each sub-catchment and model 10 is 6km of planting in the areas in receipt of most shortwave radiation

5.3.2. Sub-catchment-scale and study area stream temperature reductions

Table 2 displays the change in the area under curve metric (AUC) for each planting scenario in reference to the baseline Δ AUC (°C km) and the sum of the three area under curve difference values for each stream (∑ Δ AUC (°C km)), with the latter metric indicating the study stream temperature reduction achieved by each planting scenario across the entire study area.

Table 5-2 Sub-catchment and total study area changes in AUC for each planting scenario. Models 1 and 2 are 6 km of planting in Baddoch and Callater sub-catchments; models 3, 4 and 5 and 6 km of planting in the upper, mid-reaches and lower Clunie Water; models 6, 7 and 8 are 2 km of planting in the upper, mid- and lower reaches of all three sub-catchments; model 9 is 2 km evenly spaced across each sub-catchment and model 10 is 6 km of planting in the areas in receipt of most shortwave radiation.

Planting scenario	Sub-catchment	Sub-catchment Δ AUC (°C km)	Study area ∑ Δ AUC (°C km)
Model 1	Baddoch	26.81	28.27
	Callater	-	
	Clunie	1.45	
Model 2	Baddoch	-	16.02
	Callater	14.72	
	Clunie	1.3	
Model 3	Baddoch	-	13.65
	Callater	-	
	Clunie	13.65	
Model 4	Baddoch	-	9.95
	Callater	-	
	Clunie	9.95	
Model 5	Baddoch	-	7.03
	Callater	-	
	Clunie	7.03	
Model 6	Baddoch	8.21	21.9
	Callater	8.2	
	Clunie	5.49	
Model 7	Baddoch	8.73	16.87
	Callater	4.36	
	Clunie	3.78	
Model 8	Baddoch	3.71	11.67
	Callater	2.21	
	Clunie	5.74	
Model 9	Baddoch	7.61	17.94
	Callater	4.64	
	Clunie	5.68	
Model 10	Baddoch	10.29	22.2
	Callater	9.3	
	Clunie	2.61	

Model 1 produced the largest stream temperature reduction across the whole study area, with a change in AUC of 28.27 °C km. Of the ten planting scenarios, model 5, (single 6 km in the lower reaches of Clunie Water), produced the smallest change in AUC of 7.03 °C km.

When considered at across the entire study area, planting scenarios focussed on upstream areas in the headwaters generally resulted in larger maximum stream temperature reductions than planting in mid- or lower reaches. This is observed most clearly when comparing planting of a single 6 km zone in the Clunie headwaters (Model 3), with mid- (Model 4) and lower reaches (Model 5). Model 3 produced the largest $\sum \Delta$ AUC of 13.65 °C km, compared to 9.95 °C km and 7.03 °C km for models 4 and 5 respectively. The same patterns were observed when planting 2 km at the top (Model 6), mid- (Model 7) and bottom (Model 8) reaches of each sub-catchment, producing respective $\sum \Delta$ AUC of 21.9 °C km, 16.87 °C km and 11.67 °C km. The exception to this rule was the Baddoch Burn where planting in the mid-reaches (8.73 °C km) resulted in slightly larger effect than planting the upper reaches (8.21 °C km).

The greater effects of upstream planting scenarios on stream temperature can also be seen in the degree hour difference plots (Figure 5-7). For example, the spatial extent and magnitude of negative values in Model 3 were considerably greater than those observed in Model 4 and 5. Similarly Model 6 had greater negative effects on cumulative temperatures than Models 7 or 8. These patterns were similar to those shown for the reduction in shortwave radiation (Figure 5-6).

Additional context to the degree hours of planting scenarios is provided in Figure 5-8. Here the “Baseline” panel illustrates the degree hours spent above the 23 °C threshold at which juvenile salmon display stress responses to stream temperature (Breau et al., 2012). The remaining panels display the changes in degree hours spent above the 23 °C threshold. The middle reaches of Callater Burn and the majority of Baddoch Burn both exceed this threshold during the three week July modelling period, whereas Clunie Water did not. As a result, Models 3, 4 and 5 which only introduce riparian trees along Clunie Water do not reduce the time spent exceeding the threshold. Within this context, models 1, 9 and 10 produce the largest reductions in degree hours above the threshold, with mean reduction of 0.69, 0.66 and 0.57 °C hrs respectively. Of the models which enacted a change on the threshold (excluding models 3, 4 and 5), models 8 and 2 produced the smallest responses, with mean reductions in degree hours of 0.08 and 0.17 °C hrs respectively.

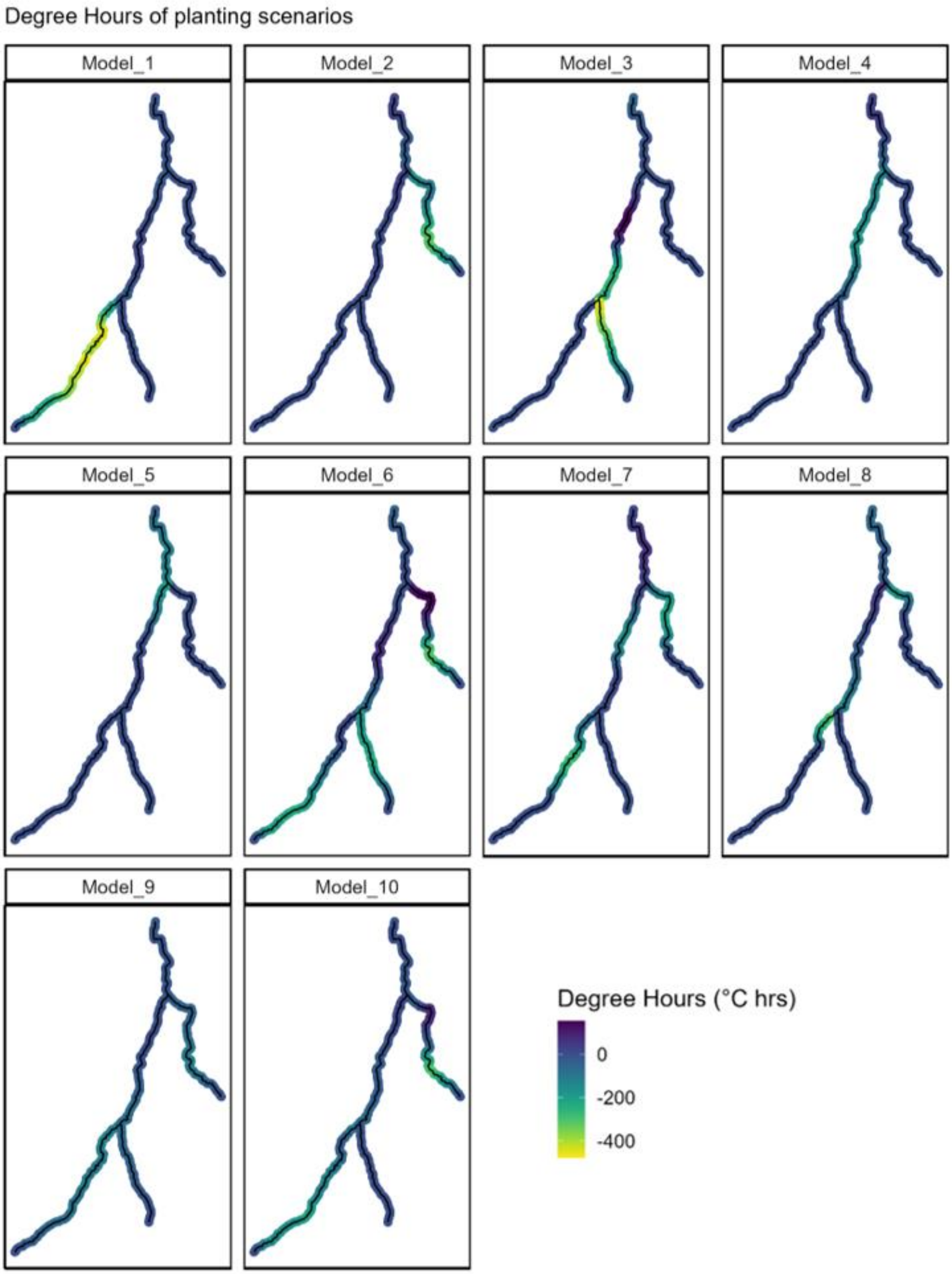

Figure 5-7 Degree hours of planting scenarios across the study area network in relation to baseline models. Models 1 and 2 are 6km of planting in Baddoch and Callater sub-catchments; models 3, 4 and 5 and 6km of planting in the upper, mid-reaches and lower Clunie Water; models 6, 7 and 8 are 2km of planting in the upper, mid- and lower reaches of all three sub-catchments; model 9 is 2km evenly spaced across each sub-catchment and model 10 is 6km of planting in the areas in receipt of most shortwave radiation.

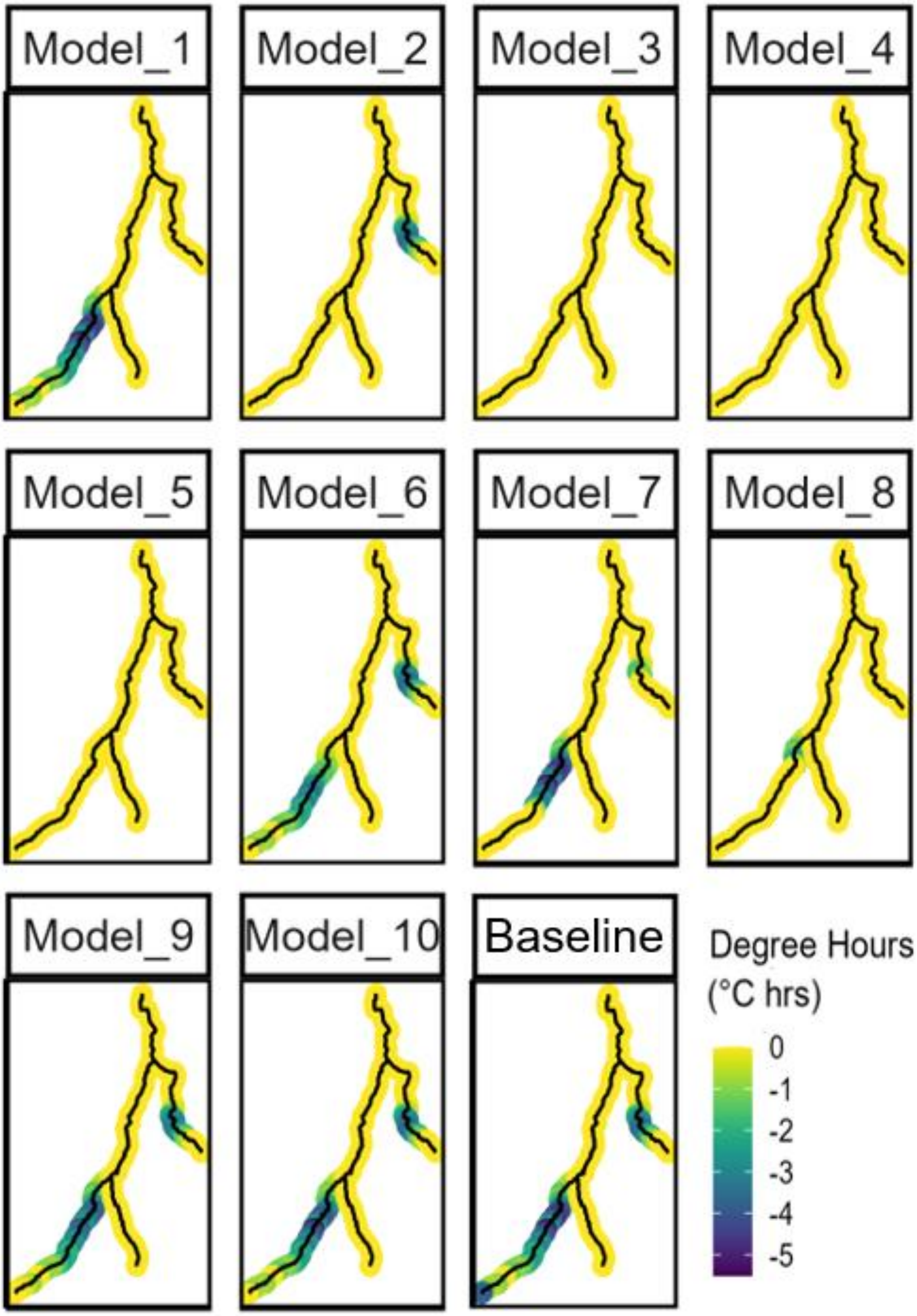

Figure 5-8 Reduction in degree hours spend above a 23 degree C threshold. Baseline panel identifies areas where 23 degree threshold was exceeded and the number of degree hours spent above said threshold.

5.3.3. Catchment outlet stream temperature reductions

Table 5-3 Planting scenario model outlet temperature reductions.
Models 1 and 2 are 6 km of planting in Baddoch and Callater sub-catchments; models 3, 4 and 5 and 6 km of planting in the upper, mid-reaches and lower Clunie Water; models 6, 7 and 8 are 2 km of planting in the upper, mid- and lower reaches of all three sub-catchments; model 9 is 2 km evenly spaced across each sub-catchment and model 10 is 6 km of planting in the areas in receipt of most shortwave radiation.

Planting scenario	Stream	Baseline Tw mean	Scenario Tw mean	Δ Tw mean	Baseline Tw max mean	Scenario Tw max mean	Δ Tw max
Model 1	Baddoch	14.01	13.29	-0.72	17.11	15.85	-1.26
	Callater	15.07	15.07	-	17.26	17.26	-
	Clunie	14.52	14.44	-0.08	16.14	16.15	0.01
Model 2	Baddoch	14.01	14.01	-	17.11	17.11	-
	Callater	15.07	14.36	-0.71	17.26	15.77	-1.49
	Clunie	14.52	14.34	-0.19	16.14	15.97	-0.17
Model 3	Baddoch	14.01	14.01	-	17.11	17.11	-
	Callater	15.07	15.07	-	17.26	17.26	-
	Clunie	14.52	14.39	-0.13	16.14	16.18	0.04
Model 4	Baddoch	14.01	14.01	-	17.11	17.11	-
	Callater	15.07	15.07	-	17.26	17.26	-
	Clunie	14.52	14.25	-0.27	16.14	15.81	-0.33
Model 5	Baddoch	14.01	14.01	-	17.11	17.11	-
	Callater	15.07	15.07	-	17.26	17.26	-
	Clunie	14.52	14.11	-0.41	16.14	15.25	-0.89
Model 6	Baddoch	14.01	13.94	-0.07	17.11	17.09	-0.02
	Callater	15.07	14.84	-0.23	17.26	17.14	-0.12
	Clunie	14.52	14.41	-0.11	16.14	16.17	0.03
Model 7	Baddoch	14.01	13.76	-0.25	17.11	16.72	-0.39
	Callater	15.07	14.85	-0.22	17.26	16.7	-0.56
	Clunie	14.52	14.34	-0.18	16.14	16.03	-0.12
Model 8	Baddoch	14.01	13.29	-0.72	17.11	15.68	-1.43
	Callater	15.07	14.78	-0.29	17.26	16.51	-0.75
	Clunie	14.52	14.23	-0.29	16.14	15.64	-0.51
Model 9	Baddoch	14.01	13.65	-0.36	17.11	16.37	-0.74
	Callater	15.07	14.85	-0.22	17.26	16.8	-0.46
	Clunie	14.52	14.35	-0.17	16.14	15.98	-0.17
Model 10	Baddoch	14.01	13.53	-0.48	17.11	16.3	-0.81
	Callater	15.07	14.65	-0.42	17.26	16.59	-0.67
	Clunie	14.52	14.36	-0.17	16.14	16.05	-0.09

Riparian planting was able to reduce mean temperatures (Δ Tw mean) at sub-catchment outlets by a greater amount in the Baddoch and Callater Burns than in Clunie Water (See Table 5-3).The largest reductions in mean temperatures observed at Baddoch Burn and Callater Burn outlets were 0.72 °C and 0.71 °C respectively, compared to only 0.41 °C at the outlet of Clunie Water. The three planting scenario models delivering the greatest reductions in mean temperatures at sub-catchment outlets all involved planting a single reach of 6 km within the same sub-catchment (Model_1 for Baddoch Burn, Model_2 for Callater Burn, Model_5 for Clunie Water).

In contrast to AUC, the largest reductions in temperature at the sub-catchment outflows were observed for scenarios where planting was closest to the outlets. This is illustrated by comparing mean temperatures for models 3-5 where 6 km of trees were planted in the upper (Model 3), mid- (Model 4) and lower reaches (Model 5) of the Clunie, reduced mean outlet temperatures by 0.13 °C, 0.27 °C and 0.41 °C respectively. A similar pattern can be observed for the Baddoch (Models 6, 7 and 8), where 2 km of trees in the upper, middle and lower reaches resulted in mean stream temperature reductions at the outlet of 0.07 °C, 0.25 °C and 0.72 °C respectively. In contrast, planting in the mid-reaches of the Callater Burn (Model 7) resulted in smaller mean temperature reductions at the outlet (0.22 °C) than planting in the upper (0.23 °C, Model 6) or lower catchment (0.29 °C, Model 8). Planting 6 km of the Callater Burn resulted in mean stream temperature reductions of 0.17 °C for the Clunie Water outlet, more than twice that achieved from the equivalent planting on the upper Baddoch Burn (0.08 °C).

The various planting scenarios had similar effects of maximum stream temperatures (Δ Tw max), at sub-catchment outlets as they did for mean temperatures, with greatest reductions where planting was closest to the outlets. One surprising observation to come from the scenario testing was an increase in mean daily maximum temperatures at the Clunie outlet in response to planting in the Baddoch (Models1, 3, 6). These scenarios increased mean maximum daily temperatures at the outlet by between 0.01 °C and 0.04 °C. These models also coincided with the smallest reductions in mean temperatures at the Clunie Water outlet.

5.3.4. Influence of heat advection on stream temperature responses

A comparison of Figures 5-6 and 5-7 readily identifies that changes in shortwave radiation alone do not drive the observed differences in the spatial distribution of stream temperature changes between baseline and planting scenarios. The effects of water volume and advected heat are illustrated more clearly in Figure 5-9 which shows the spatiotemporal variability in simulated river temperatures between the baseline model and Model 1 (planting 6 km of the upper Baddoch) together with their instantaneous differences. The effects of riparian planting are greatest in the middle and lower riparian planting areas (Fig. 8i right hand panel), but continue in a downstream direction beyond the planting declining with distance. Upon reaching the larger Clunie catchment (0.73 m^3s^{-1}) the temperature effects from Baddoch (0.3 m^3s^{-1}) are substantially reduced (Fig. 8 ii right hand panel). Temperature reductions are further reduced at the confluence with the Callater (0.59 m^3s^{-1}). Another observation illustrated in this figure is that the largest reductions in stream temperature between baseline and scenario models occur on the days with the largest net receipt of energy, as seen in the middle "Q" column.

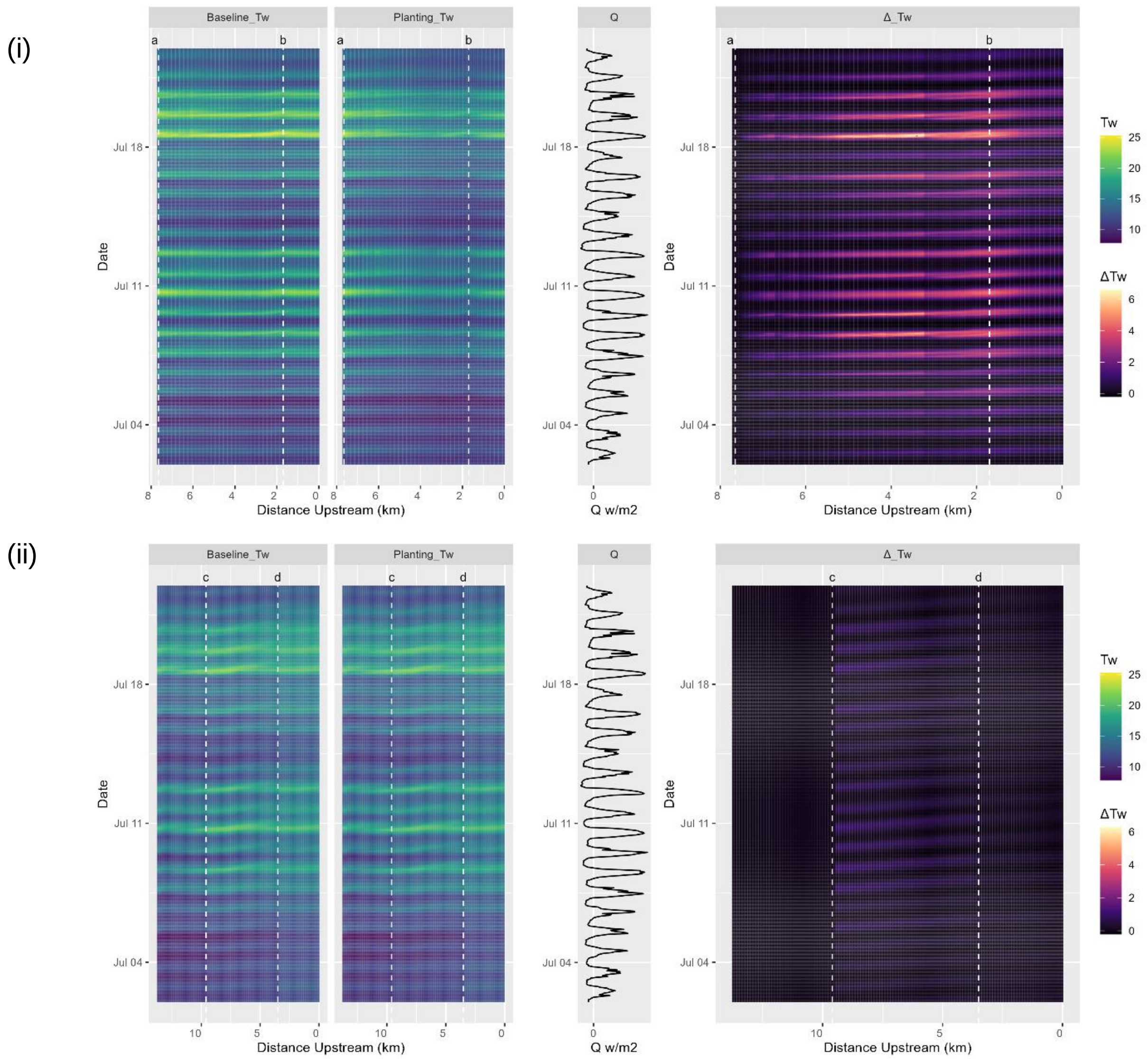

Figure 5-9 Spatiotemporal distribution of water temperatures across (i) Baddoch Burn and (ii) Clunie Water in response to planting 6km of Baddoch Burn in Model 1 planting scenario. The blue and green panels on the left hand side show spatiotemporal stream temperatures in baseline and planting scenarios. The central panel depictsa timeseries of total energy exchange (W/m2) occurring at the Clunie Water outlet for the baseline simulation. The black and purple panels on the right hand side depict differences in stream temperature between baseline and Model 1 planting scenarios. "a" and "b"annotations in the plots on the first row indicate the beginning and ending of introduced planting in Baddoch Burn; "c" and "d" indicate Baddoch Burn and Callater Burn tributaries along Clunie Water.

5.4. Discussion

This study used nested process-based temperature models to investigate the effects of alternative riparian tree planting strategies on river temperature regime across the Clunie water, a large sub-catchment of the Aberdeenshire Dee, Scotland. In contrast to previous studies, the modelling approach enabled the effects of riparian tree planting in tributaries to be investigated in larger downstream rivers, addressing issues of advected heat. The modelling suggests that the greatest overall benefits of riparian tree planting for reducing river temperatures occurs where this planting is targeted towards smaller upstream catchments. However, riparian planting continued to have a notable effect on river temperatures even in larger (5^{th} Strahler order) streams towards the bottom of the Clunie model domain and the greatest effects at sub-catchment outflows were obtained where riparian planting is focussed locally. This has potential consequences for decision making where managers are aiming to create localised thermal refugia at the confluence of tributaries with larger rivers. Models 9 (equally distributed small planting enclosures) and 10 (planting targeted to areas with high shortwave receipt) performed reasonably well at the scale of the whole study site (i.e. overall temperature reductions), although less well than the scenarios focussed on the upper Baddoch (Model 1). However, as Model 9 does not distinguish between smaller and larger streams, it is unclear whether this finding would transfer to larger spatial scales associated with greater water volumes and shorter residence times. These issues are discussed in further detail below.

5.4.1. Effects of planting on sub-catchment outflows

This study is one of a limited number of investigations into stream temperature which use process-based models at similar scales. Previous research using process-based stream temperature models has typically focused on simulating the effects of riparian tree planting at reach-scales (Abdi & Endreny, 2019; Fabris et al., 2018; Fuller et al., 2022; Garner et al., 2014b) and at most, single sub-catchments (Dugdale et al., 2024; Fabris et al., 2018). By increasing the scale of modelling from reach and sub-catchment to the integrated nested catchment, this study has been able to assess the cumulative effects of riparian planting on stream temperatures downstream in larger mainstem rivers.

Simulations within this study have estimated that the planting scenarios tested can provide the sub-catchment outlets of Baddoch Burn and Callater Burn a mean summer temperature reduction of 0.72 °C and 0.71 °C with reductions in summer daily maxima of 1.26 °C and 1.49 °C. Lower mean and maximum reductions of 0.41 °C and 0.89 °C are achievable for the outlet of the larger mainstem, Clunie Water. Although it is difficult to compare findings with those from other studies where model network and riparian planting extents are dissimilar, these findings are largely similar with other studies into the effects of riparian planting on stream temperatures. Studies within the Girnock Burn, another headwater tributary of the Aberdeenshire Dee, found mean temperature reductions of 0.66 °C between forested and unforested models of a 2.2 km stretch of Girnock Burn over a seven-day model period, wherein the existing riparian canopy which covered the majority of the site was removed for the unforested model (Dugdale, et al., 2019). Maximum temperature reductions of up to 2 °C were observed when comparing two-week simulations of an unforested Girnock Burn to one with riparian planting simulated along the majority of its ~9 km mainstem (Fabris et al., 2018). In a five-day simulation during July 2012, Bond et al., found partial reforestation of a 1 km reach of the Salmon River in northern California, USA, reduced mean stream temperatures by 0.11-0.12 °C per km, with full restoration achieving mean reductions of 0.26-0.27 °C. However, these reforestation metrics did not explicitly state the lengths of riparian planting introduced to the models, making direct comparison on influences of riparian planting difficult. Lee et al., (2012) modelled the influences of riparian planting on reducing maximum stream temperatures in a 4 km reach of ChiChiaWan Creek, a salmon stream in central Taiwan. Here they tested four scenarios where trees were targeted in isolation on the west, the east bank, the upstream half and the downstream half of the reach, as well as vegetative shading angles of 50° and 70°. For the warmest stream temperature month, across the four km of reach they observed mean reductions in daily maxima ranging from 0.38 to 0.58 with a vegetative shading angle of 50°, with reductions increasing by a further ~0.2 °C when increasing to 70° shading angles.

Dugdale et al., (2024) developed models for the Baddoch Burn sub-catchment, which used 3 km of riparian planting in a number of scenarios. Their planting scenarios observed mean temperature changes at the outlet ranging from 0.41 °C to 0.61 °C, reductions in daily maxima of 1.04 °C to 1.40 °C and reductions in AUC of 2.9 °C km to 14.9 °C km associated with the 3 km of riparian planting. This is broadly comparable with the 3.71 °C km to 10.29 °C km observed in this study. Because similar studies introduce varying degrees of planting in streams with different geomorphological and hydrological conditions, direct comparisons between absolute temperature reductions are difficult. Also, these studies are conducted at daily or weekly timescales, wherein for temperate headwater streams, microclimate can be highly variable (Dugdale et al., 2019, 2024; Fabris et al., 2018; Fuller et al., 2022; Garner et al., 2017; Webb & Zhang, 1999). This will have significant impacts on the stream energy balance over a short study period and, in turn, impact the stream temperature values generated (Rincón et al., 2023). For example, the highly spatiotemporally variable climate metric of cloud cover over a number of days drastically impacts the primary source of stream heating in the amount of shortwave solar radiation received (Boyd & Kasper, 2003).

Although absolute values may be difficult to compare between studies, the spatial and temporal patterns in stream temperature response to different riparian planting scenarios can be compared. The observation that localised planting provided the greatest reduction in temperatures at catchment outlet than planting further upstream were in agreement with Dugdale et al., (2024) for the same study location and model. Although temperature reductions immediately downstream from a given planting zone were typically larger when planting upstream in the Dugdale et al., (2024) study, these reductions were found to diminish with distance downstream. As a result, although producing smaller stream temperature responses immediately downstream, the lower reaches of Baddoch Burn saw larger stream temperature reductions from local planting (Dugdale et al., 2024). The same phenomenon was observed in this study for Baddoch Burn, Callater Burn and Clunie Water.

5.4.2. Effects of planting on stream temperatures across the study area

Planting in upstream locations resulted in larger reductions in stream temperature across the whole study than the same sized resource planted further downstream. This is consistent with previous studies conducted in the same catchment (Dugdale et al., 2024). It is also consistent with previous work by Jackson et al., (2021), which assessed the effects of riparian planting on stream temperatures across a range of channel gradients, widths, orientations and Strahler river orders (as a proxy for water volumes and residence times) with a simplified reach scale model. The study concluded that riparian planting has a greater influence on stream temperature in headwaters where channels are narrow and susceptible to shading, but also where water volumes are low and residence times higher than downstream locations (Jackson, et al., 2021). Lee et al., (2012), although not incorporating an AUC metric to quantify stream temperature effects along a network, discussed the role of heat advection on cooling downstream reaches. They also found upstream riparian planting to be more effective in the narrower upstream channels, with this reduced stream temperature then advecting along the stream network. Johnson and Wilby (2015) also observed this same phenomenon. Using an air temperature – water temperature logistic regression model, they studied the effects of riparian planting along the Rivers Dove and Manifold in the Peak District, UK. Linking temperature reduction resulting from riparian planting to heat capacity, their findings concluded that in the catchment headwaters, 0.5 km of riparian shade could reduce stream temperatures by 1 °C at 11am on the 15th day of July. To achieve the same stream temperature reduction in the lower reaches where the thermal capacity was three times as large as upstream, 1.1 km of riparian planting was required.

5.4.3. Transferability of findings and implications for river management

Previous studies have suggested that planting riparian trees to reduce temperatures in sub-catchments could have benefits for larger rivers downstream (Malcolm et al., 2008b). However, subsequent investigations have shown that although stream temperatures in headwaters may be more responsive to riparian shading, benefits are reduced with distance downstream, especially in the presence of larger water volumes in the receiving waters and any tributary inflows (Dugdale et al., 2024; Fuller et al., 2022).

By incorporating the sub-catchment outlets of Baddoch Burn and Callater Burn as tributaries into the larger Clunie Water, this study further highlights the influence of discharge and advected heat upon stream temperature reduction. Consistent with previous reach scale studies (Jackson et al., 2021), the current investigation again highlighted the overriding influence of water volumes and residence times on channel shading effects. This was observed in Model 1 (Figure 5-9), where the given Baddoch planting scenario produced the largest observed temperature reductions at a given point within the greater study area, with these reductions occurring at 3.3 km upstream from the Baddoch outlet in the afternoon of the day with the largest net energy receipt in the study period. As this cooled water was advected from Baddoch Burn into Clunie Water, the cooling effect was immediately substantially reduced and not observed at the Clunie Water outlet. Alternatively, prioritising all of the available 6 km of riparian planting at the Clunie Water outlet resulted in the largest stream temperature reduction for the outlet itself.

A key consideration for river managers looking to implement riparian planting scenarios for stream temperature reductions in catchments at the scale investigated here is where they would like to see the stream temperature reductions. If the goal is to produce the largest total reduction for stream temperature across the network, this can be achieved by planting in headwaters, but if the cooling of specific locations is the aim, the results of this study suggest planting in close proximity to the target location is most likely to yield the best results at this scale. However, when looking to reduce stream temperatures in larger Strahler order streams, there will come a point where this is no longer the case. This is due to the typical increases in stream channel width and thermal capacity alongside the reduction in residence time as stream Strahler order increases rendering localised riparian planting in larger systems less influential on stream thermal regimes.

5.4.4. Limitations and opportunities for future work

The key finding from this study is that, at the catchment size investigated here (104 km^2), to maximise stream temperature reductions at a point with a large discharge, channel width and thermal capacity (Clunie Water outlet), the most effective planting scenario is still to plant locally to the target location. Planting further upstream produced larger stream temperature reductions immediately downstream of planting, but these reductions in stream temperature diminished when advected downstream.

However, the same processes that have been shown to produce larger immediate stream temperature reductions when planting in smaller headwater streams; largely large effective shading, large stream residence time and small thermal capacity, are the opposite (reduced effective shading, reduced residence time and large thermal capacity) in higher stream orders than Clunie Water to the extent that localised planting is no longer effective (Jackson et al., 2021a; Johnson & Wilby, 2015). To further assess these relationships, and elucidate the point at which stream temperature reductions from localised planting are less effective than temperature reductions from advected cooling as a result of upstream planting, future work should look to further increase the spatial scale of modelling efforts.

The thermal regime of Callater Burn was substantially different to those of the Baddoch Burn and Clunie Water. This was due primarily to the presence of Loch Callater, a shallow loch immediately upstream of the Callater Burn where the upstream model boundary is located. Lakes and reservoirs have been shown to regulate downstream river temperatures, buffering diurnal ranges, or even increasing temperatures in summer months due to thermal stratification (Bois et al., 2023). Future stream temperature modelling would benefit from improved understanding of the effects of standing water on downstream temperatures under different climatological and hydrological conditions. This could be investigated by installing dataloggers at different depths within the loch and coupling physically based models of thermal variability in standing waters (Noori et al., 2019) with the sort of stream temperature model employed in this study. By increasing the modelling extent upstream of Loch Callater and instrumenting the loch itself, future modelling studies could also assess the influence of riparian planting on loch, lake and reservoir temperatures.

Another limitation of this study is the characterisation of energy exchanges at the water-streambed interface. During low-flow, high-temperature summer conditions, factors such as hyporheic flow can have a considerable impact on stream temperatures in smaller headwater streams (Faulkner et al., 2020). The models used in this study developed parameter values associated with water-streambed energy fluxes through a process of calibration within a range of reasonable values observed from the literature. Future models simulating summer stream temperatures could look to further constrain these values with the use of field observations of hyporheic exchange including the use of tracer tests, hydrometric methods using piezometers or broader geophysical understanding. Such studies could build on the work conducted by Richardson et al., (2016), where tracer dilutions methods were explored for measuring discharge in steep mountain streams, with breakthrough curves differing between different sites despite observing similar discharges.

The Heat Source model used within this study is the best available for simulating the effects of riparian tree planting on stream temperatures (Dugdale, et al., 2017). However, there are still limitations associated with this model. One such limitation is that the Heat Source model is only capable of simulating a single stream channel. Stream braiding occurs in many of the reaches along the modelled sub-catchments particularly during the low flow conditions modelled in this study. By splitting a single channel into multiple channels, braiding can increase the surface area of the air-stream surface interface (Piegay, et al., 2006). Thus, these braiding locations may experience large amounts of solar forcing and thus may also benefit more than expected from riparian planting. In addition, where perennial islands exist between braids, there is an opportunity for increased shading from a single tree when planted on an island between braids as it can provide shade to two channels at different times of the day. The development of stream temperature models capable of capturing braiding may provide further insight into these potential benefits.

Because the Heat Source model is not coupled with a hydrological model to simulate catchment hydrology, our modelling study was limited to specific periods of observed low flow discharges. Using a coupled hydrological-stream temperature model such as that used in Fabris et al., (2018), future studies would be able to test the responses of stream temperature to riparian planting across a number of flow conditions. A further avenue of potential study would be to adapt microclimate inputs to assess the response of riparian tree planting strategies to future climate scenarios. Coupling the stream temperature model with a hydrological model could provide further insight in this effort as climate change will impact the hydrological cycle, and in turn, baseflow generation.

The primary function of heat source as a stream temperature model is to simulate the impacts of riparian planting on the receipt of solar radiation. Riparian planting also influences turbulent heat fluxes by reducing wind speeds and increasing relative humidity. Although Heat Source has routines to simulate the effect of riparian trees on these fluxes (Boyd & Kasper, 2003), the author is unaware of any existing studies which test the accuracy of these simulations. An assessment of the energy lost to the latent heat flux within this study showed changes following the introduction of trees occurred at a gradual rate, with losses reducing as a function of stream temperature changes rather than as a response to reduced wind speeds or increased relative humidity, as was shown in a 2008 study conducted in the nearby Girnock Burn (Hannah et al., 2008). Further improvements in model performance could be achieved by assessing the accuracy of Heat Source in recreating observed turbulent fluxes in the field.

5.5. Conclusion

This study supports and builds on the existing evidence base used by environmental scientists and river managers investigating the effects of riparian tree planting on summer stream temperatures within the context of climate change. By expanding model extents from the single sub-catchment to a larger nested catchment, the study provides new insights into the influence of advection within and between sub-catchments on thermal responses of streams to riparian planting. Consistent with the findings of previous studies, riparian planting was shown to have a larger impact on stream temperatures immediately downstream when planting upper reaches than when planting lower reaches (Dugdale et al., 2024; Jackson et al., 2021a). At the scale of the study area, maximum stream temperature reductions along the network were larger when planting upper reaches than planting lower reaches.

However, at the scale of catchment studied here (104 km^2), when targeting stream temperature reductions in the larger downstream reaches, where riparian planting is considered to be less effective, this study found that planting in the immediate vicinity still produced the largest stream temperature reductions for larger reaches, with the stream temperature reductions from planting further upstream diminishing as they are advected along the network. Further investigations into this phenomenon are needed in order to deduce the catchment scale at which stream temperature reductions from localised riparian planting in larger mainstems are less substantial than the temperature reductions advected from planting further upstream.

6. Synthesis, implications and future research opportunities

The research presented in this thesis was driven by the concerns of scientists and fisheries managers that climate change will reduce the thermal suitability of habitats for freshwater fish that are adapted to cool conditions, in particular salmonids such as the Atlantic salmon (Scottish Government, 2022). The management of riparian woodland and abstractions are the only two management actions that are proven to be capable of managing thermal extremes (White et al., 2023). However, previous process-based modelling has shown that the riparian shading becomes less effective in reducing river temperatures as rivers become larger (Jackson et al., 2021). This has led some practitioners to consider whether the best way to protect larger rivers from high temperatures might involve planting tributary streams, relying on cool inflows from these streams to reduce temperatures in the larger rivers. This thesis addressed these questions by increasing the spatial scale of process-based stream temperature models, to improve our understanding of the cumulative effects of energy exchange processes on river temperature along a stream network. In doing so it provides new insights as to the effects of upstream riparian tree planting on downstream water temperatures within the context of climate change. In pursuing this overall research objective, it was necessary to overcome a number of technical and scientific challenges relating to the characterisation of energy exchange processes, upscaling data from point locations to network scales and the application of process-based models which are not generally suited to more complex interacting and nested networks.

Specific objectives within the thesis were as follows:

(1) To identify spatiotemporal variability in stream energy fluxes governing water temperatures at the catchment scale making use of high spatial and temporal resolution hydrometeorological data within nested catchments (Chapter 2)

(2) To scale conventional hydrometeorological data from point locations along stream networks, creating spatiotemporally continuous datasets for use in process-based stream temperature modelling (Chapter 3)

(3) To examine the representation of the latent heat flux in conventional stream energy balance and temperature model studies by constraining evaporation rates to field-observations (Chapter 3)

(4) To investigate spatiotemporal patterns in energy fluxes and how they cumulatively impact downstream water temperatures using process-based stream temperature models (Chapter 4)

(5) To compare the benefits of contrasting riparian planting strategies in mitigating extreme high summer stream temperatures using hierarchically nested process-based stream temperature models (Chapter 5)

The thesis follows a four-stage research design to address four related research objectives, which build in spatial scale. In Chapter 2, a classic point energy balance study was undertaken at six sites within a nested headwater catchment. This chapter identified the spatiotemporal variability in stream energy fluxes governing water temperature at a large sub-catchment scale, making use of detailed hydrometeorological data within nested catchments. It also identified the challenges associated with deriving the latent heat flux in dynamic headwater stream environments; a flux which acts as an important energy sink, particularly during summer low-flow, high-temperature conditions in exposed moorland catchments. A key challenge surrounding the calculation of this energy flux is in the choice of existing literature wind function coefficients which are used to calculate the adiabatic portion of evaporation. In Chapter 3, hydrometeorological data from the six fixed weather station locations were scaled from point locations to the whole stream network, creating a continuous spatiotemporal dataset of selected climate determinands that could be used to parameterise process-based stream temperature models. A number of scaling methods were tested using a combination of leave-one-out-cross-validation from the six weather station sites, and comparisons to data from a novel roving automatic weather station which was deployed across the study area. The challenge of deriving latent heat fluxes was also addressed in Chapter 3, where a floating evaporation pan provided observed evaporation rates in the field, against which field-derived wind function coefficients were generated. In Chapter 4, scaled meteorological datasets were used to parameterise three nested process-based stream temperature models. The resulting model performance was then tested against models using conventional (single location) hydrometeorological datasets. The performance of models utilising field-derived wind functions from the floating evaporation pan was also compared with models using wind functions parameterised from a range of values existing in the literature. In Chapter 5, the best-performing models from Chapter 4 were combined in series (Baddoch and Callater models provided tributary input values to the Clunie) to investigate the effects of contrasting riparian tree planting strategies on river temperature through a simulation exercise involving multiple planting scenarios. Ten different planting scenarios were explored to compare the efficacy of alternative riparian planting strategies in mitigating extreme high summer stream temperatures.

6.1. Research overview and synthesis

6.1.1. Characterising spatiotemporal variations in microclimate and stream energy fluxes within and between nested catchments

The fundamental controls on stream temperature are well understood in isolation. As hierarchical systems, stream temperatures have first-order controls in the form of the initial headwater temperature as a result of the water's source (groundwater, snowmelt, surface water) and the hydrological and climate forcing of regional climate which control the downstream increases or decreases in temperature as energy is exchanged between the stream and the local environment (Hannah & Garner, 2015). The response of stream temperature to the regional climate is then governed by second and third order controls within a given catchment, including the features of the riparian environment which influence shortwave and longwave radiation receipt, wind speed and relative humidity (Hannah et al., 2008), and reach scale geomorphology governing hyporheic exchange and local hydraulics respectively (Leach et al., 2023). Although these phenomena are understood, they do not influence stream temperatures in isolation but by complex interactions across space and time. As a result, research is ongoing to improve our understanding of these spatiotemporal interactions and how they combine to determine stream temperatures (Dugdale et al., 2024; Garner et al., 2017).

A number of stream energy balance studies have quantified energy exchanges between streams and their surroundings in temperate stream environments, with such studies typically utilising two or three AWS either within a single catchment (Hannah et al., 2008; Leach & Moore, 2010; Macdonald et al., 2014) or across separate catchments (Dugdale et al., 2018; Webb & Zhang, 1997). Although studies have been conducted across different spatial and temporal scales, a number of patterns still emerge ((Dugdale et al., 2018; Garner et al., 2014a, 2017; Hannah et al., 2004, 2008; Leach & Moore, 2010; Webb & Zhang, 1999). Typically, during the summer, the air-water interface experiences the larger exchanges in energy between the stream and the environment than the water-streambed interface, with solar radiation acting as the largest source of energy to the stream system. Riparian woodland is known to be a strong control on river energy budgets, substantially altering radiative and latent heat fluxes. Previous observational studies have typically attempted to isolate the effects of land use by comparing locations with different riparian characteristics, while at the same time controlling for other variables e.g. altitude, discharge, channel orientation etc (Hannah, et al., 2008; Garner, et al., 2017; Dugdale, et al., 2018).

Although these studies have provided valuable insights as to the effects of riparian woodland on stream energy exchange, there have been fewer studies of spatiotemporal variability within single land use categories. The only stream temperature study to date which has compared stream energy fluxes across sites without riparian canopies present is Webb & Zhang (1997). However, these inter-site variabilities cannot be analysed within the context of landscape characteristics as observations were taken over discontinuous timeframes. To scale microclimate variability across the spatial domain of interest for this study, it was first necessary to improve understanding of the spatiotemporal variability in microclimate and energy fluxes within and between nested sub-catchments.

In Chapter 2 of this thesis, stream microclimate, heat exchange and dynamics were characterised across the 104 km^2 study space with the use of six stationary AWS, providing a novel spatial resolution for point energy balances within and between nested catchments. The investigation found that although their magnitude may be less pronounced than between forested and unforested locations, there remains substantial inter-site variability at the spatial scales investigated. The study also suggested some structure within the observed variability which correlated with landscape controls. However, these correlations did not have the sufficient statistical power to scale energy fluxes using the environmental characteristics. Although the observations did not provide a basis for scaling directly against environmental variables, they provided important context for future process-based stream temperature modelling. Specifically, for study areas of ~100 km^2 investigations should not assume uniform microclimate even in the presence of uniform land use. There are still substantial variations across the catchment which would not be captured with the use of a single AWS and these variations, in turn, cause spatiotemporal variations in stream energy fluxes, particularly the latent heat flux. Within the context of summer stream temperatures, this finding is of particular importance. As was found in other similar studies, the latent heat flux acts as a significant and often the largest energy sink in temperate streams.

6.1.2. Scaling microclimate observations from point locations to across stream networks

River temperature models have been developed to improve understanding of the processes governing spatiotemporal patterns in stream temperature. Statistical models take observations of water temperatures and relate them to landscape and other variables (e.g. discharge, air temperature) that directly or indirectly influence stream temperature (Jackson et al., 2018). In doing so, they can infer the drivers of variability in stream temperature. Needing relatively few data inputs, these models can be deployed at large spatial scales (Benyahya et al., 2007). Although they can infer drivers of variability, they are unable to determine the specific energy transfer mechanisms which have caused observed temperature changes (Dugdale et al., 2017). Process-based stream temperature models work by simulating the physical processes controlling stream temperature. In doing so, they can provide information on the mechanisms driving stream temperatures. However, they are data intensive and highly parameterised, needing continuous monitoring locations such as AWS installations to provide a series of microclimate and physiological inputs to models. The number of monitoring locations is typically limited, especially in remote locations due to the financial and logistical challenges associated with deployment. Where studies look to incorporate the nearest microclimate data from distant locations, this can act as a source of significant error, failing to accurately represent conditions within a given study area (Dugdale, et al., 2017). As a result, process-based stream temperature studies have typically been limited to reach and sub-catchment scales, with the representation of contributing tributaries simplified to boundary conditions (Dugdale et al., 2018; Fabris et al., 2018; Hebert et al., 2011; Leach & Moore, 2010).

Chapter 3 of this thesis aimed to address the issue of microclimate variability in process-based stream temperature modelling by building on the observations gathered in the six-point energy balance study in Chapter 2, and introducing additional microclimate observations using a novel roving AWS. The additional 15 roving AWS locations were placed along a longitudinal gradient covering the spatial extent of the large mainstem stream within the catchment (Clunie Water) for discrete 24-hour periods, with each location within <1 km of the next. Chapter 3 aimed to incorporate the stationary and roving datasets to generate a novel continuous microclimate dataset along the stream network of the study area, with unique microclimate represented at 50m intervals.

The data gathered by the six stationary AWS were then scaled across the study area using *Nearest Fixed* and *Inverse Distance Weighting* methods with distances calculated first using Euclidean distance and second by streamwise distance. As far as the authors are aware, this is the first instance of scaling microclimate observations using a leave-one-out-cross-validation, with the only previous study scaling AWS data utilising a simple linear interpolation (Garner et al., 2014). These scaled data were tested first in reproducing the observed data from the 15 roving AWS sites along the Clunie Water stream network and then by reproducing observations from the six stationary AWS sites using a leave-one-out-cross-validation method. The study found that the best-performing method for scaling microclimate within the study area was the *Inverse Distance Weighting* method using Euclidean distances. Unsurprisingly, both scaling methods were found to improve upon the use of a single AWS for capturing spatiotemporal variations in microclimate across the catchment.

Chapter 2 identified the potential error associated with capturing representative riverine conditions when calculating the latent heat flux using the mass transfer method. This method utilises wind function coefficients to estimate the adiabatic portion of evaporation, with the majority of values in the literature being derived from studies investigating latent heat fluxes in reservoirs and power station cooling ponds in the mid- to late 20th century (Bowie et al., 1985; Morton, 1983). More recently, studies have since been conducted using floating evaporation pans to provide in-field observations of evaporation rates in rivers to constrain wind function values (Maheu et al., 2014; Szeitz et al., 2020). However, these studies have been conducted in catchments with mature riparian forests and as a result, may not represent the open moorland environment investigated in this study. With this in mind, Chapter 3 used a floating evaporation pan to inform and constrain wind function coefficients for the study area. These wind functions were then compared with literature values to assess their performance in recreating observed floating pan evaporation rates. Observed evaporation rates from the floating evaporation pan ranged from 0.02 – 0.3 mm/hr. The majority of evaporation rates generated using literature coefficients were within the bounds of 0-0.5 mm/hr but some produced rates which exceeded 1 and even 1.5 mm/hr. If stream energy balance studies were to incorporate these poor performing wind functions, estimates of energy lost via the latent heat flux would be two to three times larger than those observed within this study. This further emphasises the importance of choice of wind function coefficients for estimating latent heat fluxes.

In Chapter 4, the scaled microclimate data and field-derived wind functions were incorporated into three separate process-based stream temperature models to assess their influence on model performance when simulating observed stream temperatures for a low-flow, high-temperature three-week scenario recorded during July 2022. Models using the novel scaled microclimate data were compared with conventional discrete data from the six stationary AWS as well as models using a single AWS. For all three sub-catchments models using the six AWS performed better than using the single AWS, highlighting the importance of using multiple AWS to capture spatiotemporal variations in microclimate data to inform process-based stream temperature modelling. For two of the three models, the use of scaled microclimate produced further improvements in model performances when compared to conventional discrete data for two of the three models. This result provides further support for the use of Euclidean *Inverse Distance Weighting* as a method for the improvement of representation of microclimate for stream temperature modelling along a stream network. The field-derived wind functions were tested against parameterised wind function coefficients generated within a range of literature values. Once more, models for two of the three sub-catchments showed improved performance when using field-derived wind function coefficients in simulating observed stream temperatures. Consistent with previous studies, these results support the notion that the estimation of latent heat fluxes in stream environments can be improved with the introduction of field-derived wind functions from floating evaporation pans (Maheu et al., 2014), with this study expanding the environmental range from forested stream reaches to those of open moorland and grassland.

6.1.3. Using novel scaled microclimate in stream temperature models to assess the impacts of riparian stream planting within and between nested catchments

Riparian tree planting is one of a small number of options available to stream management as a mitigation action against increasing summer stream temperatures in response to climate change (Environment Agency, 2016). However, in UK uplands it is an expensive and labour-intensive practice, due primarily to the necessary construction and maintenance of large fences to protect juvenile trees from grazing pressures. As a result, with limited resources, stream managers need to find the most effective riparian planting methods for reducing stream temperatures. Process-based modelling studies to date have identified a number of best-practice actions for reducing stream temperatures with riparian planting (Christopher Rutherford et al., 2018; Fabris et al., 2018; Garner et al., 2017; Jackson et al., 2021a) but due to their limited spatial extent, any effects of advection have been limited within the single reach, with no investigation of the fate of locally influenced stream temperatures as they flow further downstream and into larger mainstems. This could be a highly important factor when looking to reduce temperatures in larger streams, where riparian shading is considered less effective. Due to increased channel widths, effective shading from trees is reduced and with reduced residence times and increased thermal capacity, the reduction in received shortwave radiation is seen to have less of an influence on stream temperatures Jackson et al., 2021). In these instances, it is thought that the best option could be to plant further upstream in smaller tributaries to have cooled water advecting downstream to the larger system (Lee et al., 2012). However, with the limited spatial extent of most previous process-based stream temperature studies, the role of advection in determining stream temperature reductions in larger mainstem rivers is largely unknown. In order to build the evidence base for stream management decisions regarding best practice in riparian planting, there is a need to increase the scale at which planting scenarios are modelled in process-based stream temperature studies, incorporating the impacts of planting in headwaters and tributaries on the fate of stream temperatures further downstream in larger mainstems.

Within this context, Chapter 5 increased the scale of a process-based stream temperature model from the individual sub-catchment scale to a novel nested catchment scale, incorporating the influence of planting scenarios in headwaters and major tributaries of a fifth order river. With its novel nested structure, the model simulations incorporated the influence of advection both within and between nested sub-catchments to investigate the effects of riparian planting in headwaters and tributaries on stream temperatures in downstream mainstems. The scenarios assessed the influence on stream thermal regimes of targeting 6 km of riparian planting as a single zone at the headwaters, mid reaches and lower reaches of the larger mainstem, a single 6 km zone in each of the mainstem's largest tributaries, three sets of 2 km planting zones along the mainstem and tributaries in combination, intermittent planting along each sub-catchment and finally, targeting planting in the areas in highest solar radiation receipt.

The modelling study found that larger instantaneous reductions in stream temperature were achieved by planting in smaller headwaters. These findings were consistent with previous process-based stream temperature studies (Dugdale et al., 2024; Jackson et al., 2021), and statistical model studies (Johnson & Wilby, 2015), which have identified that as stream order increases: (1) channel widths typically increase, resulting in less effective shading from riparian planting; (2) thermal capacity increases, making temperatures of larger streams less responsive to reductions in incoming solar radiation; and (3) residence time decreases, giving parcels of water less time to be influenced by local changes in radiative forcing (Jackson et al., 2021).

Planting in headwaters also resulted in the largest reductions in mean daily maximum stream temperatures along the stream network, measured using an “Area Under Curve” (AUC) metric. This finding was also in agreement with previous studies (Dugdale et al., 2024; Lee et al., 2012). However, the reductions in stream temperature resulting from planting headwaters diminished as the cooled water advected downstream, with cooled water being exposed to warmer waters at confluences with unplanted sub-catchments. The scenario where a single upstream tributary (Model 1- Baddoch Burn) was planted produced the largest temperature reduction at a sub-catchment outlet and also the largest network-scale stream temperature reduction. But when this cooled water advected downstream, it had very little effect on stream temperatures at the outlet of the larger mainstem (Clunie Water). The planting scenario which was found to produce the largest stream temperature reduction at the outlet of the larger mainstem was that which planted a single 6 km zone locally to said mainstem (Model 5). Planting scenarios representing common practice methods used in UK uplands (intermittent planting to avoid excluding deer from large areas of land) and existing recommendations from the Environment Agency (targeting areas in receipt of largest incoming solar radiation) also performed reasonably well in reducing stream temperatures at the network scale but were less effective for reducing stream temperatures at outlets.

The findings of this modelling study identified that the scale at which local riparian planting is less effective at cooling temperatures at larger mainstems than planting in headwaters and smaller tributaries had not yet been reached. Although the largest immediate stream temperature reductions were achieved by planting further upstream, localised planting in the larger fifth order Clunie Water stream, with a contributing catchment area of 104 km^2 was found to be the most effective method for reducing stream temperatures in the larger mainstem itself due to the diminishing of cooled water as it advected downstream.

6.2. Implications for stream management

Understanding current and future variability in river thermal regime is an area of active research globally (Van Vliet et al., 2013). Studies have often focused on understanding risks of high river temperatures (Gallagher et al., 2022; Isaak et al., 2012; Otero et al., 2014), especially given concerns of rising river temperatures under climate change (Wanders et al., 2019). Riparian tree planting is one of few management options for protecting rivers and fisheries from high temperatures (Dugdale, et al., 2018; Hannah, et al., 2008; Jackson, et al., 2021; Garner, et al., 2014). Consequently, there are a number of studies which have looked to understand the effects of riparian woodland (Bond et al., 2015; DeWalle, 2008; Dugdale et al., 2018, 2024; Fuller et al., 2022; Garner et al., 2017; Imholt et al., 2013; Johnson & Wilby, 2015; Leach & Moore, 2010; Malcolm et al., 2008a; Roth et al., 2010; Swartz et al., 2020).

Research has shown that riparian woodland typically reduces temperature most where rivers can be fully shaded by riparian trees and water volumes low and residence times are high (Jackson et al., 2021a; Lee et al., 2012). Consequently, riparian woodland creation is often targeted in smaller tributary streams, rather than larger mainstem rivers. However, larger rivers can experience high river temperatures, thus there remains a need to understand how temperatures can be moderated in these locations (Malcolm et al., 2008a). Previous studies have suggested planting smaller upstream reaches and tributaries of larger mainstem streams, cooling the larger systems downstream with cooled water advected from the upstream planting (Hannah, et al., 2008). An area of particular interest is thus the potentially important role of advection of cooled waters following riparian planting, where tributaries subsequently converge with larger rivers.

To explore the spatial scales of heat advection, this study increased the scale of process-based stream temperature models from the reach and sub-catchment scale to the intermediate nested catchment scale by combining three sub-catchment models into a single model, simulating the effects of riparian planting scenarios across a 104 km^2 total model extent.

The study found that riparian planting provided the most effective shading to channels in smaller headwaters , with planting in the lower reaches being least effective with increased channel widths (Chapter 5). In terms of producing the largest total reduction in mean and maximum stream temperatures across the study area, planting in headwaters was also the most effective strategy, with cooled water advecting downstream, influencing water temperatures across a larger spatial scale (Chapter 5).

As stream Strahler order increases, typically so too does channel width, stream thermal capacity and velocity (Gleason, 2015), which reduces the impact of riparian planting on stream temperatures (Jackson, et al., 2021). With the lower reaches of the Clunie Water representing a larger mainstem, this findings of this study agree with previous studies wherein riparian planting has less of an effect on stream temperatures when planting downstream (Dugdale et al., 2024; Fuller et al., 2022). However, the rivers in this study area are not large enough to represent the mainstem rivers at which thermal refugia are typically explored (Wawrzyniak et al., 2016) and where riparian tree planting is not usually targeted. At the scale of this study, local planting was still found to be most effective, with stream temperature reductions from upstream planting diminishing as they were advected downstream. As a result, there is a need to further increase the spatial scale at which riparian planting scenarios, with the objective of reducing temperatures and larger rivers and generating of thermal refugia, are modelled (see future work). Such research would allow quantification of point at which the stream temperature reductions resulting from localised planting in large mainstems are smaller than the reductions observed from cooled water advected from upstream. This will help to extend the evidence base to inform management decisions in larger rivers, within the context of mitigating elevated summer stream temperatures.

6.3. Future research

Table 6-1 Summary table of key research priorities

Priority	**Summary**
1	Adding wind direction to microclimate analysis could help to provide temporally varying relationships for scaling microclimate between upper and lower stream reaches, accounting for anabatic and katabatic winds.
2	Further increase the deployment of floating evaporation pans for constraining river evaporation rates, increasing the environmental ranges where they've been used (currently Canada and Scotland) to inform future process-based stream temperature studies in other environments.
3	Assess the performance of Heat Source in simulating the influence of riparian planting on air temperature, relative humidity and wind speed and compare with other process-based models.
4	Integrate shading routine of the Heat Source model with another stream temperature model which is more suitable for simulating low-flow conditions in smaller headwater streams.
5	Couple the Heat Source model with a hydrological model and incorporate the additional influences of riparian tree planting on stream temperatures resulting from changes to catchment hydrology.

6	Couple the Heat Source model with a hydrological model to generate future hydrological scenarios within the context of climate change (e.g. more extreme low-flow conditions associated with hydrological drought).
7	Continue studies modelling the effects of riparian planting but in larger stream orders with the aim of identifying the scale at which localised riparian planting in larger mainstems is no longer more beneficial for locally reducing stream temperatures in large streams than planting further upstream.
8	Investigate the effects of heat advection on the development of thermal refugia for the benefit of salmonid populations in larger mainstem rivers.
9	Investigate the potential winter increases in stream temperature as a result of riparian tree planting and any negative impacts this might have on the survival of salmon ova.

The novel application of spatially nested process-based river temperature models (Chapter 4) provides improved understanding of spatial variability in heat advection processes. When combined with spatially scaled fluxes (Chapter 2) and varying riparian woodland characteristics (Chapter 5 scenario testing) it is possible to provide improved understanding of the effects of riparian woodland on river temperature across different spatial scales. Nevertheless, knowledge gaps remain and there are a number of opportunities for further development, which are highlighted in this section.

Chapters 2 and 3 of this study identified spatiotemporal variability of microclimate and stream energy fluxes both within and between nested catchments, using these data to build spatially continuous scaled microclimate. Diurnal dynamics were observed in these data, thought to be driven in part by anabatic and katabatic winds. Future studies looking to scale microclimate across catchment scales could further investigate diurnal trends thought to be influences by anabatic and katabatic winds by incorporating wind vanes into microclimate data collection.

Adding wind direction to analysis could help to provide temporally varying relationships for scaling microclimate between upper and lower stream reaches.

The use of a floating pan to provide field observations of evaporation rates in this study identified literature wind function coefficients as a potential source of error when estimating latent heat fluxes using the mass transfer method. Alternative physically-based evaporation routines exist which do not use wind functions, but their accuracy in representing evaporation has varied (McJannet et al., 2013). With this flux often acting as the primary limit to stream warming during low-flow high-temperature summer conditions, its accurate representation is paramount in stream temperature studies. With the use of floating evaporation pans proving successful in a handful of sites limited to western Canada (Szeitz & Moore, 2020) and now Scotland, there is a need to further increase the deployment of this method for constraining evaporation rates, increasing the environmental range in which it is used so as to inform future process-based stream temperature studies in other environments.

The choice of stream temperature model to use in a given study significantly impacts the representation of the latent heat flux. This study used a single process-based stream temperature model to simulate the effects of riparian planting scenarios on reducing stream temperatures within and between nested catchments. The model was chosen as it had successfully simulated summer stream temperatures within the study region with a high accuracy (RMSE < 1 °C) and also featured a comprehensive shading routine to simulate the effects of riparian planting on stream channel solar radiation receipt (Dugdale et al., 2024). Riparian planting has also been shown to influence air temperature, relative humidity and wind speeds at stream channels (Hannah et al., 2008), with all of these metrics influencing rates of latent heat flux. The Heat Source model applies a routine to account for reductions in wind speed as a result of sheltering provided by riparian trees (Prandtl's universal velocity distribution law (Dingman, 2002)), but, as far as the authors are aware, the accuracy with which the model captures the influence of trees on latent heat fluxes remains untested. Future studies could assess the performance of Heat Source in simulating this influence, comparing results with those produced by other process-based stream temperature models.

Although performing strongly with regard to simulating the effects of riparian planting on radiative forcing, the Heat Source model often became unstable when recreating observed hydraulics in this study area. Heat Source hydraulic simulations use St-Venant equations, which have been shown to struggle under low flow conditions, particularly in wide and shallow reaches where roughness heights are high relative to stream depths (Marcus et al., 1992). To combat this, the Heat Source models used unrealistically high Manning's n values in order to generate models stable enough to run for the given simulation periods. Where discharges increased substantially following precipitation events, the models became unstable and would not run and as a result, the influence of temporally variable discharges on summer stream temperatures was not incorporated into this study. Future work could look to integrate the shading routine of the Heat Source model with another stream temperature model which is more suitable for simulating low-flow conditions in smaller streams.

Recent studies have successfully integrated physically-based hydrological models with heat transfer models allowing for the simulation of discharge as well as stream temperature (Fabris et al., 2018). Hydrological models use climatology and land use controls to simulate rainfall-runoff dynamics and generate lateral inflows to streams as a result of the interactions of precipitation with the environment as it travels towards the given stream (Flood Estimation Handbook, 1999). Trees influence the generation of lateral inflows through multiple mechanisms: their canopies enhance interception of precipitation and increase evapotranspiration (Breil et al., 2021), while their root systems create macropores that boost infiltration rates, collectively reducing surface runoff (Revell et al., 2022). These interactions can, in turn, influence baseflow generation which influences stream temperature regimes, especially in low-flow high-temperature summer conditions (Hemr et al., 2024). By coupling

Heat Source with a hydrological model, the additional influences of riparian tree planting on stream temperatures resulting from changes to catchment hydrology can be investigated to further develop the evidence base on which to inform land management practices.

Coupling Heat Source with a hydrological model also presents an opportunity to expand this modelling study to investigate the effects of riparian planting in future climates. As well as directly influencing stream temperatures with changes to microclimate, climate change can also indirectly influence UK stream temperatures through disrupting the hydrological cycle (Hannah & Garner, 2015). Coupling with a hydrological model would allow stream temperature models to generate future hydrological scenarios as well as future microclimate scenarios in which to test the influence of riparian planting on stream temperatures.

Chapter 5 showed that at this scale of study area (104 km^2), the largest instantaneous reductions in stream temperature immediately downstream of planting were achieved by planting in smaller headwater and tributary channels. However, when targeting the cooling of larger mainstems, maximum reductions in both mean and daily maximum stream temperatures were achieved following localised riparian planting. To inform riparian planting strategies for targeting cooling in stream orders larger than those investigated in this study, further modelling incorporating larger stream orders is required in order to identify the scales at which localised riparian planting in larger mainstems is no longer more beneficial for locally reducing stream temperatures in large streams than planting further upstream.

This study elucidated the influence of heat advection in reducing summer stream temperatures following the riparian planting of tributaries and mainstem streams. This was undertaken within the context of mitigating stream temperature increases for the benefit of thermally sensitive salmonids. During high summer temperatures, these salmonids avoid heat stress in areas of cold water referred to as thermal refugia (Breau et al., 2012). Future work could investigate the additional benefits to salmonid populations in larger mainstems by further analysing the spatial extent and duration of stream temperature reductions resulting from riparian planting of headwaters and tributaries. Within the context of reducing thermal stress on salmonids, future studies into the reductions of stream temperatures resulting from riparian planting scenarios could be linked to thermal targets and strategies appropriate to the survival and health of salmonids, thus linking the physical and ecological dimensions of stream thermal regimes.

This thesis focused on the effects of riparian tree planting on the reduction of stream temperatures in summer conditions. Studies encompassing annual stream temperatures have observed warming effects during winters in temperate streams, thought to be due to the reduction in energy losses from net radiation and evaporation (Hannah et al., 2008). Recent investigations into salmonid populations in the UK suggested a reduction in recruitment in 2016 coincided with unusually warm winter temperatures (Gregory et al., 2020). Future studies into the effects of riparian tree planting on stream thermal regimes could investigate the potential winter increases in stream temperature as a result of riparian tree planting and any negative impacts this might have on the survival of salmon ova.

6.4. Final comments

This body of research has explored the complex spatiotemporal dynamics of microclimate, energy fluxes and stream temperature in a nested headwater catchment, emphasising the importance of microclimate representation in stream temperature modelling. The research demonstrates that substantial inter-site variabilities in stream energy balances exist when controlling for land-use, highlighting the need for more nuanced approaches to understanding these systems and challenging the adequacy of using a single weather station to represent the dynamic microclimate of a headwater catchment.

The research introduces innovative techniques to enhance microclimate representation at the catchment scale, including the use of inverse distance weighting between sites and site-specific wind functions. These methods proved more effective in reproducing catchment scale microclimate and recreating observed evaporation rates compared to those found in existing literature.

By increasing the spatiotemporal scale of process-based stream temperature models and incorporating scaled microclimate inputs data, the research demonstrates improved stream temperature model performance. However, the effectiveness of field-derived wind functions varied between sub-catchments, indicating the need for site-specific considerations. The research culminates in the successful integration of sub-catchment stream temperature models into a single continuous model, capturing the downstream advection of stream temperatures from tributaries into larger mainstems. Within this context, the study assesses the impact of various riparian planting scenarios on stream temperatures, finding that, at this study area scale, planting at sub-catchment outlets produced the largest temperature reductions at those specific points, while upstream planting resulted in the most significant temperature reductions across the entire study area network. This comprehensive research provides valuable insights into the complexities of stream temperature dynamics and offers improved methodologies for modelling and managing these ecosystems, as well as identifying potential areas of further investigation to continue building an evidence base for river management decisions to protect salmonid habitats.

References

Abdi, R., & Endreny, T. (2019). A river temperature model to assist managers in identifying thermal pollution causes and solutions. *Water (Switzerland)*, *11*(5). https://doi.org/10.3390/w11051060

Alazard, M., Leduc, C., Travi, Y., Boulet, G., & Ben Salem, A. (2015). Estimating evaporation in semi-arid areas facing data scarcity: Example of the El Haouareb dam (Merguellil catchment, Central Tunisia). *Journal of Hydrology: Regional Studies*, *3*, 265–284. https://doi.org/10.1016/j.ejrh.2014.11.007

Allen, A. P., Gillooly, J. F. & Brown, J. H., (2005). Linking the global carbon cycle to individual metabolism. *Functional Ecology,* 19(2), pp. 202-213.

American Fisheries Society, (2009). Coldwater Fish in Rivers. In: S. A. Bonar, W. A. Hubert & D. W. Willis, eds. *Standard Methods for Sampling North American Freshwater Fishes.* Bethesda: American Fisheries Society, pp. 139-158.

Arevalo, E., Maire, A., Tétard, S., Prévost, E., Lange, F., Marchand, F., Josset, Q., & Drouineau, H. (2021). Does global change increase the risk of maladaptation of Atlantic salmon migration through joint modifications of river temperature and discharge? *Proceedings of the Royal Society B: Biological Sciences*, *288*(1964). https://doi.org/10.1098/rspb.2021.1882

Benner, D. A., (2000). Evaporative heat loss of the Upper Middle Fork of the John Day River, Northeast Oregon (master's thesis). *Oregon State University.*

Benyahya, L., Caissie, D., St-Hilaire, A., Ouarda, T. B. M. J., & Bobée, B. (2007). A Review of Statistical Water Temperature Models. In *Canadian Water Resources Journal* (Vol. 32, Issue 3, pp. 179–192). https://doi.org/10.4296/cwrj3203179

Benyahya, L., Caissie, D., Satish, M. G., & El-Jabi, N. (2012). Long-wave radiation and heat flux estimates within a small tributary in Catamaran Brook (New Brunswick, Canada). *Hydrological Processes*, *26*(4), 475–484. https://doi.org/10.1002/hyp.8141

Bernthal, F. R., Seaman, B. W., Rush, E., Armstrong, J. D., McLennan, D., Nislow, K. H., & Metcalfe, N. B. (2023). High summer temperatures are associated with poorer performance of underyearling Atlantic salmon (Salmo salar) in upland streams. *Journal of Fish Biology*, *102*(2), 537–541. https://doi.org/10.1111/jfb.15282

Bond, R. M., Stubblefield, A. P., & Van Kirk, R. W. (2015). Sensitivity of summer stream temperatures to climate variability and riparian reforestation strategies. *Journal of Hydrology: Regional Studies*, *4*, 267–279. https://doi.org/10.1016/j.ejrh.2015.07.002

Bois, P., Beisel, J. N., Cairault, A., Flipo, N., Leprince, C., & Rivière, A. (2023). Water temperature dynamics in a headwater forest stream: Contrasting climatic, anthropic and geological conditions create thermal mosaic of aquatic habitats. *PLoS ONE*, *18*(2 February). https://doi.org/10.1371/journal.pone.0281096

Borgwardt, F., Unfer, G., Auer, S., Waldner, K., El-Matbouli, M., & Bechter, T. (2020). Direct and Indirect Climate Change Impacts on Brown Trout in Central Europe: How Thermal Regimes Reinforce Physiological Stress and Support the Emergence of Diseases. *Frontiers in Environmental Science*, *8*. https://doi.org/10.3389/fenvs.2020.00059

Bowie, G. L., Mills, W. B., Porcella, D. B., Campbell, C. L., Pagenkopf, J. R., Rupp, G. L., Johnson, K. M., Chan, P. W. H., Gherini, S. A., Chamberlin, C. E., & Barnwell, T. 0. (1985). *RATES, CONSTANTS, AND KINETICS FORMULATIONS IN SURFACE WATER QUALITY MODELING (SECOND EDITION)*.

Boyd, M. & Kasper, B., (2003). *Analytical Methods for Dynamic Open Channel Heat and Mass Transfer: Methodology for heat source model Version 7.0,* Portland: Oregon Department of Environmental Quality.

Branch, R., Spittlehouse, D. L., Adams, R. S., & Winkler, R. D. (2004). *Forest, Edge, and Opening Microclimate at Sicamous Creek-Research Report 24*. http://www.for.gov.bc.ca/hfd/pubs/Docs/Rr/Rr24.htm

Breau, C. (2012). *Knowledge of fish physiology used to set water temperature thresholds for in-season closures of Atlantic salmon (Salmo salar) recreational fisheries*. www.dfo-mpo.gc.ca/csas-sccs

Breil, M., Davin, E. L., & Rechid, D. (2021). What determines the sign of the evapotranspiration response to afforestation in European summer? *Biogeosciences*, *18*(4), 1499–1510. https://doi.org/10.5194/bg-18-1499-2021

Broadmeadow, S. B., Jones, J. G., Langford, T. E. L., Shaw, P. J., & Nisbet, T. R. (2011). The influence of riparian shade on lowland stream water temperatures in southern England and their viability for brown trout. *River Research and Applications*, *27*(2), 226–237. https://doi.org/10.1002/rra.1354

Burton, T. M. & Likens, G. E., (1973). The Effect of Strip-Cutting on Stream Temperatures in the Hubbard Brook Experimental Forest, New Hampshire. *BioScience,* 23(7), pp. 433-435.

Caissie, D., (2006). The thermal regime of rivers: a review. *Freshwater Biology,* 51(8), pp. 1389-1406.

Caissie, D., (2016). River evaporation, condensation and heat fluxes within a first-order tributary of Catamaran Brook (New Brunswick, Canada). *Hydrological Processes,* 30(12), pp. 1872-1883.

Carrivick, J. L., Brown, L. E., Hannah, D. M., & Turner, A. G. D. (2012). Numerical modelling of spatio-temporal thermal heterogeneity in a complex river system. *Journal of Hydrology*, *414–415*, 491–502. https://doi.org/10.1016/j.jhydrol.2011.11.026

Cefas. (2022). *Assessment of Salmon Stocks and Fisheries in England and Wales*.

Comer-Warner, S. A., Romeijn, P., Gooddy, D. C., Ullah, S., Kettridge, N., Marchant, B., Hannah, D. M., & Krause, S. (2018). Thermal sensitivity of CO2 and CH4 emissions varies with streambed sediment properties. *Nature Communications*, *9*(1). https://doi.org/10.1038/s41467-018-04756-x

Cuthbert, M, Mackay, R, Durand, V, Aller, M-F, Greswell, R & Rivett, M (2010), 'Impacts of river-bed gas on the hydraulic and thermal dynamics of the hyporheic zone', *Advances in Water Resources*, vol. 33, no. 11, pp. 1347-1358. https://doi.org/10.1016/j.advwatres.2010.09.014

Delpla, I., Jung, A. v., Baures, E., Clement, M., & Thomas, O. (2009). Impacts of climate change on surface water quality in relation to drinking water production. In *Environment International* (Vol. 35, Issue 8, pp. 1225–1233). Elsevier Ltd. https://doi.org/10.1016/j.envint.2009.07.001

DeWalle, D. R. (2008). Guidelines for riparian vegetative shade restoration based upon a theoretical shaded-stream model. *Journal of the American Water Resources Association*, 44(6), 1373–1387. https://doi.org/10.1111/j.1752-1688.2008.00230.x

Di Cecco, G. J. & Gouhier, T. C., (2018). Increased spatial and temporal autocorrelation of temperature under climate change. *Sci Rep,* 8(14850).

Dugdale, S. J., Bergeron, N. E., & St-Hilaire, A. (2013). Temporal variability of thermal refuges and water temperature patterns in an Atlantic salmon river. *Remote Sensing of Environment*, 136, 358–373. https://doi.org/10.1016/j.rse.2013.05.018

Dugdale, S. J., Hannah, D. M. & Malcolm, I. A., (2017). River temperature modelling: A review of process-based approaches and future directions. *Earth Science Reviews,* Volume 175, pp. 97-113.

Dugdale, S. J., Malcolm, I. A. & Hannah, D. M., (2024). Understanding the effects of spatially variable riparian tree planting strategies to target water temperature reductions in rivers. *Journal of Hydrology,* 635(131163).

Dugdale, S. J., Malcolm, I. A., & Hannah, D. M. (2019). Drone-based Structure-from-Motion provides accurate forest canopy data to assess shading effects in river temperature models. *Science of the Total Environment*, *678*, 326–340. https://doi.org/10.1016/j.scitotenv.2019.04.229

Dugdale, S. J., Malcolm, I. A., & Hannah, D. M. (2024). Understanding the effects of spatially variable riparian tree planting strategies to target water temperature reductions in rivers. *Journal of Hydrology*, *635*. https://doi.org/10.1016/j.jhydrol.2024.131163

Dugdale, S. J., Malcolm, I. A., Kantola, K. & Hannah, D. M., (2018). Stream temperature under contrasting riparian forest cover: Understanding thermal dynamics and heat exchange processes. *Science of the Total Environment,* Volume 610-611, pp. 1375-1389.

Dugdale, S.J., Franssen, J., Corey, E., Bergeron, N.E., Lapointe, M. and Cunjak, R.A. (2016), Main stem movement of Atlantic salmon parr in response to high river temperature. *Ecol Freshw Fish*, 25: 429-445. https://doi.org/10.1111/eff.12224

Durance, I. & Ormerod, S. J., (2009). Trends in water quality and discharge confound long-term warming effects on river macroinvertebrates. *Freshwater Biology,* 54(2), pp. 388-405.

Elliott, J. M., & Elliott, J. A. (2010). Temperature requirements of Atlantic salmon Salmo salar, brown trout Salmo trutta and Arctic charr Salvelinus alpinus: Predicting the effects of climate change. *Journal of Fish Biology*, *77*(8), 1793–1817. https://doi.org/10.1111/j.1095-8649.2010.02762.x

Environment Agency. (2016). *Keeping Rivers Cool: A Guidance Manual Creating riparian shade for climate change adaptation*.

European Environment Agency, (2019). *The European environment- state and outlook 2020: Knowledge for transition to a sustainable Europe,* Copenhagen: European Environment Agency.

European Union, (1992). *Council Directive 92/43/EEC of 21 May 1992 on the conservation of natural habitats and of wild fauna and flora,* Brussels: European Union.

Evans, E. C., McGregor, G. R. & Petts, G. E., (1998). River energy budgets with special reference to river bed processes. *Hydrological Processes,* 12(4), pp. 575-595.

Evans, M.R., Moustakas, A., Carey, G., Malhi, Y., Butt, N., Benham, S., Pallett, D. and Schäfer, S., (2015). Allometry and growth of eight tree taxa in United Kingdom woodlands. Scientific Data, 2(1), p.150006

Fabris, L., Malcolm, I. A., Buddendorf, W. B., & Soulsby, C. (2018). Integrating process-based flow and temperature models to assess riparian forests and temperature amelioration in salmon streams. *Hydrological Processes*, *32*(6), 776–791. https://doi.org/10.1002/hyp.11454

Faulkner, B. R., Brooks, J. R., Keenan, D. M., & Forshay, K. J. (2020). Temperature decrease along hyporheic pathlines in a large river riparian zone. *Ecohydrology*, *13*(1). https://doi.org/10.1002/eco.2160

Feller, M. C., (1981). EFFECTS OF CLEARCUTTING AND SLASHBURNING ON STREAM TEMPERATURE IN SOUTHWESTERN BRITISH COLUMBIA. *Journal of the American Water Resources Association,* 17(5), pp. 863-867.

Fenkes, M., Shiels, H. A., Fitzpatrick, J. L., & Nudds, R. L. (2016). The potential impacts of migratory difficulty, including warmer waters and altered flow conditions, on the reproductive success of salmonid fishes. *Comparative Biochemistry and Physiology -Part A: Molecular and Integrative Physiology*, *193*, 11–21. https://doi.org/10.1016/j.cbpa.2015.11.012

Flood Estimation Handbook (1999). Centre for Ecology and Hydrology, Wallingford, Oxfordshire (formerly the Institute of Hydrology). December 1999. ISBN 0 948540 94 X.

Forest Research. (2023). *Provisional Woodland Statistics 2023*.

Fuller, M. R., Leinenbach, P., Detenbeck, N. E., Labiosa, R., & Isaak, D. J. (2022). Riparian vegetation shade restoration and loss effects on recent and future stream temperatures. *Restoration Ecology*, *30*(7). https://doi.org/10.1111/rec.13626

Gallagher, B. K., Geargeoura, S., & Fraser, D. J. (2022). Effects of climate on salmonid productivity: A global meta-analysis across freshwater ecosystems. *Global Change Biology*, 28(24), 7250–7269. https://doi.org/10.1111/gcb.16446

Garner, G., Malcolm, I. A., Sadler, J. P. & Hannah, D. M., (2017). The role of riparian vegetation density, channel orientation and water velocity in determining river temperature dynamics. *Journal of Hydrology,* Volume 553, pp. 471-485.

Garner, G., Malcolm, I. A., Sadler, J. P., & Hannah, D. M. (2014). What causes cooling water temperature gradients in a forested stream reach? *Hydrology and Earth System Sciences*, *18*(12), 5361–5376. https://doi.org/10.5194/hess-18-5361-2014

Garner, G., Malcolm, I. A., Sadler, J. P., & Hannah, D. M. (2017). The role of riparian vegetation density, channel orientation and water velocity in determining river temperature dynamics. *Journal of Hydrology*, *553*, 471–485. https://doi.org/10.1016/j.jhydrol.2017.03.024

Gatien, P., Arsenault, R., Martel, J. L., & St-Hilaire, A. (2023). Using the ERA5 and ERA5-Land reanalysis datasets for river water temperature modelling in a data-scarce region. *Canadian Water Resources Journal*, *48*(2), 93–110. https://doi.org/10.1080/07011784.2022.2113917

Georges, B. et al., (2021). Which environmental factors control extreme thermal events in rivers? A multi-scale approach (Wallonia, Belgium). *PeerJ,* Volume 9.

Gillet, M., Le Gal La Salle, C., Ayral, P. A., Khaska, S., Martin, P., & Verdoux, P. (2021). Identification of the contributing area to river discharge during low-flow periods. *Hydrology and Earth System Sciences*, *25*(12), 6261–6281. https://doi.org/10.5194/hess-25-6261-2021

Gleason, C. J. (2015). Hydraulic geometry of natural rivers: A review and future directions. *Progress in Physical Geography*, *39*(3), 337–360. https://doi.org/10.1177/0309133314567584

Google, (2024). *Google Maps.* [Online]

Available at: https://maps.google.com

[Accessed 12 August 2024].

Gregory, S. D., Bewes, V. E., Davey, A. J. H., Roberts, D. E., Gough, P., & Davidson, I. C. (2020). Environmental conditions modify density-dependent salmonid recruitment: Insights into the 2016 recruitment crash in Wales. *Freshwater Biology*, *65*(12), 2135–2153. https://doi.org/10.1111/fwb.13609

Guenther, S. M., Moore, R. D. & Gomi, T., (2012). Riparian microclimate and evaporation from a coastal headwater stream, and their response to partial-retention forest harvesting. *Agricultural and Forest Meteorology,* Volume 164, pp. 1-9.

Gurney, W. S. C., Bacon, P. J., Tyldesley, G., & Youngson, A. F. (2008). Process-based modelling of decadal trends in growth, survival, and smolting of wild salmon (Salmo salar) parr in a Scottish upland stream. *Canadian Journal of Fisheries and Aquatic Sciences*, *65*(12), 2606–2622. https://doi.org/10.1139/F08-149

Hannah, D. M., Malcolm, I. A., Soulsby, C., & Youngson, A. F. (2004). Heat exchanges and temperatures within a salmon spawning stream in the Cairngorms, Scotland: Seasonal and sub-seasonal dynamics. *River Research and Applications*, *20*(6), 635–652. https://doi.org/10.1002/rra.771

Hannah, D. M. & Garner, G., (2015). River water temperature in the United Kingdom: Changes over the 20th century and possible changes over the 21st century. *Progress in Physical Geography,* 39(1), pp. 68-92.

Hannah, D. M., Malcolm, I. A., Soulsby, C., & Youngson, A. F. (2008). A comparison of forest and moorland stream microclimate, heat exchanges and thermal dynamics. *Hydrological Processes*, *22*(7), 919–940. https://doi.org/10.1002/hyp.7003

Hannah, D. M., Webb, B. W. & Nobilis, F., (2008). River and stream temperature: Dynamics, processes, model and implications - preface. *Hydrological Processes,* Volume 22, pp. 899-901.

Harbeck, G. E., Kohler, M. A., & Koberg, G. E. (1959). *Water-Loss Investigations: Lake Mead Studies*.

Hebert, C., Caissie, D., Satish, M. G., & El-Jabi, N. (2011). Study of stream temperature dynamics and corresponding heat fluxes within Miramichi River catchments (New Brunswick, Canada). *Hydrological Processes*, *25*(15), 2439–2455. https://doi.org/10.1002/hyp.8021

Hemr, O., Kupec, P., Čech, P., & Deutscher, J. (2024). The response of forested upland micro-watersheds to extreme precipitation in a precipitation abundant year. *Theoretical and Applied Climatology*, *155*(4), 2627–2640. https://doi.org/10.1007/s00704-023-04766-w

Hrachowitz, M. et al., (2010). Thermal regimes in a large upland salmon river: a simple model to identify the influence of landscape controls and climate change on maximum temperatures. *Hydrological Processes,* 24(23), pp. 3374-3391.

Imholt, C., Soulsby, C., Malcolm, I. A., & Gibbins, C. N. (2013). Influence of contrasting riparian forest cover on stream temperature dynamics in salmonid spawning and nursery streams. *Ecohydrology*, *6*(3), 380–392. https://doi.org/10.1002/eco.1291

IPCC, (2014). *Climate Change 2014: Synthesis Report. Contribution of Working Groups I, II and III to the Fifth Assessment Report of the Intergovernmental Panel on Climate Change,* Geneva: IPCC.

Isaak, D. J. et al., (2018). Global warming of salmon and trout rivers in the Northwestern U.S.: road to ruin or path to purgatory? *Transactions of the American Fisheries Society,* 147(3), pp. 566-587.

Isaak, D. J., & Young, M. K. (2023). Cold-water habitats, climate refugia, and their utility for conserving salmonid fishes. *Canadian Journal of Fisheries and Aquatic Sciences*, 80(7), 1187–1206. https://doi.org/10.1139/cjfas-2022-0302

Jackson, F. L. et al., (2016). Development of spatial regression models for predicting summer river temperatures from landscape characteristics: implications for land and fisheries management. *Hydrological Processes,* Volume 31, pp. 1225-1238.

Jackson, F. L. et al., (2018). A spatio-temporal statistical model of maximum daily river temperatures to inform the management of Scotland's Atlantic salmon rivers under climate change. *Science of the Total Environment,* Volume 612, pp. 1543-1558.

Jackson, F. L., Hannah, D. M., Fryer, R. J., Millar, C. P., & Malcolm, I. A. (2017). Development of spatial regression models for predicting summer river temperatures from landscape characteristics: Implications for land and fisheries management. *Hydrological Processes*, *31*(6), 1225–1238. https://doi.org/10.1002/hyp.11087

Jackson, F. L., Hannah, D. M., Ouellet, V., & Malcolm, I. A. (2021). A deterministic river temperature model to prioritize management of riparian woodlands to reduce summer maximum river temperatures. *Hydrological Processes*, *35*(8). https://doi.org/10.1002/hyp.14314

Johnson, M. F., & Wilby, R. L. (2015). Seeing the landscape for the trees: Metrics to guide riparian shade management in river catchments. *Water Resources Research*, *51*(5), 3754–3769. https://doi.org/10.1002/2014WR016802

Johnson, M. F., Albertson, L. K., Algar, A. C., Dugdale, S. J., Edwards, P., England, J., Gibbins, C., Kazama, S., Komori, D., MacColl, A. D. C., Scholl, E. A., Wilby, R. L., de Oliveira Roque, F., & Wood, P. J. (2024). Rising water temperature in rivers: Ecological impacts and future resilience. *Wiley Interdisciplinary Reviews: Water*, *11*(4). https://doi.org/10.1002/wat2.1724

Jonsson, B. (2023). Thermal Effects on Ecological Traits of Salmonids. In *Fishes* (Vol. 8, Issue 7). Multidisciplinary Digital Publishing Institute (MDPI). https://doi.org/10.3390/fishes8070337

Kedra, M., (2020). Regional Response to Global Warming: Water Temperature Trends in Semi-Natural Mountain River Systems. *Water,* 12(1).

Landmap; GetMapping, (2023). *GetMapping 5 m resolution Digital Terrain Model (DTM) for Scotland,* Fleet: NERC Earth Observation Data Centre (NEODC).

Le Coz, J., Camenen, B., Peyrard, X., & Dramais, G. (2012). Uncertainty in open-channel discharges measured with the velocity-area method. *Flow Measurement and Instrumentation*, *26*, 18–29. https://doi.org/10.1016/j.flowmeasinst.2012.05.001

Leach, J. A. & Moore, R. D., (2010). Above-stream microclimate and stream surface energy exchanges in a wildfire-disturbed riparian zone. *Hydrological Processes,* 24(1), pp. 2369-2381.

Leach, J. A. et al., (2022). A primer on stream temperature processes. *WIREs Water,* 10(4), p. e1643.

Leach, J. A., & Moore, R. D. (2010). Above-stream microclimate and stream surface energy exchanges in a wildfire-disturbed riparian zone. *Hydrological Processes*, *24*(17), 2369–2381. https://doi.org/10.1002/hyp.7639

Leach, J. A., Kelleher, C., Kurylyk, B. L., Moore, R. D., & Neilson, B. T. (2023). A primer on stream temperature processes. *Wiley Interdisciplinary Reviews: Water*, *10*(4). https://doi.org/10.1002/wat2.1643

Lee, T. Y., Huang, J. C., Kao, S. J., Liao, L. Y., Tzeng, C. S., Yang, C. H., Kalita, P. K., & Tung, C. P. (2012). Modeling the effects of riparian planting strategies on stream temperature: Increasing suitable habitat for endangered Formosan Landlocked Salmon in Shei-Pa National Park, Taiwan. *Hydrological Processes*, *26*(24), 3635–3644. https://doi.org/10.1002/hyp.8440

Lim, W.H., Roderick, M.L., Hobbins, M.T., Wong, S.C., Groeneveld, P.J., Sun, F. and Farquhar, G.D. (2012) 'The aerodynamics of pan evaporation', Agricultural and Forest Meteorology, 152, pp. 31-43.

MacDonald, R. J., Boon, S., Byrne, J. M. & Silins, U., (2014). A comparison of surface and subsurface controls on summer temperature in a headwater stream. *Hydrological Processes,* 28(1), pp. 2338-2347.

Malcolm, I. A., & Dugdale S. J., (2023) *Personal communication*, [25th February 2023].

Maheu, A., Caissie, D., St-Hilaire, A. & El-Jabi, N., (2014). River evaporation and corresponding heat fluxes in forested catchments. *Hydrological Processes,* 28(1), pp. 5725-5738.

Malcolm, I. A. et al., (2008). The influence of riparian woodland on stream temperatures: implications for the performance of juvenile salmonids. *Hydrological Processes,* 22(1), pp. 968-979.

Malcolm, I. A., Hannah, D. M., Donaghy, M. J., Soulsby, C., & Youngson, A. F. (2004). Influence of riparian woodland on spatial and temporal variability of stream water temperatures in an upland salmon stream. In *Hydrology and Earth System Sciences* (Vol. 8, Issue 3).

Malcolm, I. A., Millidine, K. J., Glover, R. S., Jackson, F. L., Millar, C. P., & Fryer, R. J. (2019). Development of a large-scale juvenile density model to inform the assessment and management of Atlantic salmon (Salmo salar) populations in Scotland. *Ecological Indicators*, *96*, 303–316. https://doi.org/10.1016/j.ecolind.2018.09.005

Malcolm, I. A., Soulsby, C., Hannah, D. M., Bacon, P. J., Youngson, A. F., & Tetzlaff, D. (2008). The influence of riparian woodland on stream temperatures: Implications for the performance of juvenile salmonids. *Hydrological Processes*, *22*(7), 968–979. https://doi.org/10.1002/hyp.6996

Marine Directorate, (2021). *Salmon fishery statistics: 2020, ISBN: 978100049529,* Edinburgh: Scottish Government.

Marine Directorate, (2021). *Scottish Government: Riaghaltas na h-Alba.* [Online]
Available at: https://www.gov.scot/publications/scotland-river-temperature-monitoring-network-srtmn/

Marine Directorate, (2022). *Scottish wild salmon strategy, ISBN: 9781802016451,* Edinburgh: Scottish Government.

Marine Scotland - Science, (2019). *Field Temperature Datalogger Calibration, Deployment, Retrieval and Data Storage (not accredited),* Pitlochry: Scottish Government.

Marine Scotland, (2019). *Topic Sheet Number 143: Summer 2018 River Temperatures,* Edinburgh: Scottish Government.

McJannet, D. L., Cook, F. J., & Burn, S. (2013). Comparison of techniques for estimating evaporation from an irrigation water storage. *Water Resources Research*, *49*(3), 1415–1428. https://doi.org/10.1002/wrcr.20125

Meng, X., Liu, H., Du, Q., Xu, L., & Liu, Y. (2020). Evaluation of the performance of different methods for estimating evaporation over a highland open freshwater lake in mountainous area. *Water (Switzerland)*, *12*(12), 1–22. https://doi.org/10.3390/w12123491

Met Office Hadley Centre, (2018). *UKCP18 Probabilistic Climate Projections,* Reading: Centre for Environmental Data Analysis.

Met Office, (2023). *What is UKCP?* [Online]
Available at: https://www.metoffice.gov.uk/research/approach/collaboration/ukcp/about/what-is-ukcp

Milner, N. J., Solomon, D. J., & Smith, G. W. (2012). The role of river flow in the migration of adult Atlantic salmon, Salmo salar, through estuaries and rivers. *Fisheries Management and Ecology*, *19*(6), 537–547. https://doi.org/10.1111/fme.12011

Montgomery, D. R. (1999). Process domains and the River Continuum. *Journal of the American Water Resources Association*, *35*(2), 397–410. https://doi.org/10.1111/j.1752-1688.1999.tb03598.x

Morton, F. I. (1983). OPERATIONAL ESTIMATES OF AREAL EVAPOTRANSPIRATION AND THEIR SIGNIFICANCE TO THE SCIENCE AND PRACTICE OF HYDROLOGY. In *Journal of Hydrology* (Vol. 66).

NIST/SEMATECH (2024) 'Loess (aka Lowess)', in e-Handbook of Statistical Methods, 4.1.4.4. Available at: http://www.itl.nist.gov/div898/handbook/pmd/section1/pmd144.htm (Accessed: 12 December 2024).

Noori, R., Tian, F., Ni, G., Bhattarai, R., Hooshyaripor, F., & Klöve, B. (2019). ThSSim: A novel tool for simulation of reservoir thermal stratification. *Scientific Reports*, *9*(1). https://doi.org/10.1038/s41598-019-54433-2

North Atlantic Salmon Conservation Organization, (2020). *Plan of Action for the Application of the Precautionary Approach to the Protection and Restoration of Atlantic Salmon Habitat,* Edinburgh: NASCO.

Oke, T. R., (1987). *Boundary Layer Climates.* 2nd ed. Abingdon: Routledge.

OSPAR, (2015). *OSPAR Commission.* [Online]
Available at: https://www.ospar.org/organisation [Accessed 18 October 2024].

Otero, J., L'Abée-Lund, J. H., Castro-Santos, T., Leonardsson, K., Storvik, G. O., Jonsson, B., Dempson, B., Russell, I. C., Jensen, A. J., Baglinière, J. L., Dionne, M., Armstrong, J. D., Romakkaniemi, A., Letcher, B. H., Kocik, J. F., Erkinaro, J., Poole, R., Rogan, G., Lundqvist, H., … Vøllestad, L. A. (2014). Basin-scale phenology and effects of climate variability on global timing of initial seaward migration of Atlantic salmon (Salmo salar). *Global Change Biology*, *20*(1), 61–75. https://doi.org/10.1111/gcb.12363

Ouellet, V. & Caissie, D., (2023). Towards a better understanding of the evaporative cooling of rivers: case study for the Little Southwest Miramichi River (New Brunswick, Canada). *Canadian Water Resources Journal,* 48(2), pp. 189-205.

Ouellet, V., Secretan, Y., St-Hilaire, A., & Morin, J. (2014). Water temperature modelling in a controlled environment: Comparative study of heat budget equations. *Hydrological Processes*, *28*(2), 279–292. https://doi.org/10.1002/hyp.9571

PACEC. (2017). An Analysis of the Value of Wild Fisheries in Scotland Final Report. www.pacec.co.uk

Piegay, H., Grant, G., Nakamura, F. & Trustrum, N., (2006). Braided River Management: from Assessment of River Behaviour to Improved Sustainable Development. In: I. Jarvis, ed. *Braided Rivers: Process, Deposits, Ecology and Management.* s.l.:International Association of Sedimentologists.

Pohle, I., Helliwell, R., Aube, C., Gibbs, S., Spencer, M., & Spezia, L. (2019). Citizen science evidence from the past century shows that Scottish rivers are warming. *Science of the Total Environment*, *659*, 53–65. https://doi.org/10.1016/j.scitotenv.2018.12.325

Revell, N., Lashford, C., Rubinato, M., & Blackett, M. (2022). The Impact of Tree Planting on Infiltration Dependent on Tree Proximity and Maturity at a Clay Site in Warwickshire, England. *Water (Switzerland)*, *14*(6). https://doi.org/10.3390/w14060892

Richardson, M., Moore, R. D. (Dan), & Zimmermann, A. (2017). Variability of tracer breakthrough curves in mountain streams: Implications for streamflow measurement by slug injection. *Canadian Water Resources Journal*, *42*(1), 21–37. https://doi.org/10.1080/07011784.2016.1212676

Rincón, E., St-Hilaire, A., Bergeron, N. E., & Dugdale, S. J. (2023). Combining Landsat TIR-imagery data and ERA5 reanalysis information with different calibration strategies to improve simulations of streamflow and river temperature in the Canadian Subarctic. *Hydrological Processes*, *37*(10). https://doi.org/10.1002/hyp.15008

Roon, D. A., Dunham, J. B., & Groom, J. D. (2021). Shade, light, and stream temperature responses to riparian thinning in second-growth redwood forests of northern California. *PLoS ONE*, *16*(2 February). https://doi.org/10.1371/journal.pone.0246822

Roth, T. R., Westhoff, M. C., Huwald, H., Huff, J. A., Rubin, J. F., Barrenetxea, G., Vetterli, M., Parriaux, A., Selker, J. S., & Parlange, M. B. (2010). Stream temperature response to three riparian vegetation scenarios by use of a distributed temperature validated model. *Environmental Science and Technology*, 44(6), 2072–2078. https://doi.org/10.1021/es902654f

Rutherford, C. J., Marsh, N. A., Davies, P. M. & Bunn, S. E., (2004). Effects of patchy shade on stream water temperature: how quickly do small streams heat and cool? *Marine and Freshwater Research,* Volume 55, pp. 737-748.

Rutherford, Christopher J., Meleason, M. A., & Davies-Colley, R. J. (2018). Modelling stream shade: 2. Predicting the effects of canopy shape and changes over time. *Ecological Engineering*, *120*, 487–496. https://doi.org/10.1016/j.ecoleng.2018.07.008

Schmadel, N.M., Ward, A.S. and Wondzell, S.M., (2017). Hydrologic controls on hyporheic exchange in a headwater mountain stream. *Water Resources Research*, 53(7), pp.6260-6278.

Schmutz, S., & Sendzimir, J. (2018). *Aquatic Ecology Series Volume 8: Riverine Ecosystem Management Science for Governing Towards a Sustainable Future*. http://www.springer.com/series/5637

Schneider, C., Laizé, C. L. R., Acreman, M. C., & Flörke, M. (2013). How will climate change modify river flow regimes in Europe? *Hydrology and Earth System Sciences*, *17*(1), 325–339. https://doi.org/10.5194/hess-17-325-2013

Scottish Government. (2022). *Scottish Wild Salmon Strategy*.

Sebok, E. and Müller, S. (2019): The effect of sediment thermal conductivity on vertical groundwater flux estimates, Hydrol. Earth Syst. Sci., 23, 3305–3317, https://doi.org/10.5194/hess-23-3305-2019

Shen, H., Cunderlik, J., Godin, G., Coombs, A., Rimer, A., & Dobrindt, I. (2014). Thermal Effects of the Proposed Water Reclamation Centre Discharge on the East Holland River. *Journal of Water Management Modeling*. https://doi.org/10.14796/JWMM.C366

Shi, X., Sun, J., & Xiao, Z. (2021). Investigation on river thermal regime under dam influence by integrating remote sensing and water temperature model. *Water (Switzerland)*, *13*(2). https://doi.org/10.3390/w13020133

Sinokrot, B. A. & Stefan, H. G., (1993). Stream temperature dynamics: measurements and modeling. *Water Resources Research,* 29(7), pp. 2299-2312.

Song, C. et al., (2018). Continental-scale decrease in net primary productivity in streams due to climate warming. *Nature Geoscience,* Volume 11, pp. 415-420.

Soulsby, C., Tetzlaff, D., & Malcolm, I. A. (2023). *Six decades of ecohydrological research connecting landscapes and riverscapes in the Girnock Burn, Scotland: Atlantic salmon population and habitat dynamics in a changing world*. https://doi.org/10.22541/au.170067435.59383187/v2

Spratt, R., Vazquez, J., & Carroll, D. (2024). A Synoptic-Scale Comparison of Satellite Yukon River Mouth Temperature to In-Situ and Reanalysis Data During 2003–2020. *IEEE International Geoscience and Remote Sensing Symposium*, 5883–5888. https://doi.org/10.1109/igarss53475.2024.10640625

Strøm, J. F., Ugedal, O., Rikardsen, A. H., & Thorstad, E. B. (2023). Marine food consumption by adult Atlantic salmon and energetic impacts of increased ocean temperatures caused by climate change. *Hydrobiologia*, *850*(14), 3077–3089. https://doi.org/10.1007/s10750-023-05234-2

Swartz, A., Roon, D., Reiter, M., & Warren, D. (2020). Stream temperature responses to experimental riparian canopy gaps along forested headwaters in western Oregon. *Forest Ecology and Management*, *474*. https://doi.org/10.1016/j.foreco.2020.118354

Swift, L. W. & Messer, J. B., (1971). Forest cuttings raise temperatures of small streams in the southern Appalachians. *Journal of Soil and Water Conservation.*

Szeitz, A. J. & Moore, R. D., (2019). Predicting evaporation from mountain streams. *Hydrological Processes,* Volume 34, pp. 4262-4279.

The River Dee Trust, (2020). *River Dee 2020-2025 Fisheries Management Plan,* Aboyne: The River Dee Trust.

Thorstad, E. B., Bliss, D., Breau, C., Damon-Randall, K., Sundt-Hansen, L. E., Hatfield, E. M. C., Horsburgh, G., Hansen, H., Maoiléidigh, N., Sheehan, T., & Sutton, S. G. (2021). Atlantic salmon in a rapidly changing environment—Facing the challenges of reduced marine survival and climate change. *Aquatic Conservation: Marine and Freshwater Ecosystems*, *31*(9), 2654–2665. https://doi.org/10.1002/aqc.3624

Trimmel, H., Weihs, P., Leidinger, D., Formayer, H., Kalny, G., & Melcher, A. (2018). Can riparian vegetation shade mitigate the expected rise in stream temperatures due to climate change during heat waves in a human-impacted pre-alpine river? *Hydrology and Earth System Sciences*, *22*(1), 437–461. https://doi.org/10.5194/hess-22-437-2018

Tyldesley, E., Banas, N. S., Diack, G., Kennedy, R., Gillson, J., Johns, D. G., & Bull, C. (2024). Patterns of declining zooplankton energy in the northeast Atlantic as an indicator for marine survival of Atlantic salmon. *ICES Journal of Marine Science*, *81*(6), 1164–1184. https://doi.org/10.1093/icesjms/fsae077

Undorf, S., Allen, K., Hagg, J., Li, S., Lott, F. C., Metzger, M. J., Sparrow, S. N., & Tett, S. F. B. (2020). Learning from the 2018 heatwave in the context of climate change: are high-temperature extremes important for adaptation in Scotland? In *Environmental Research Letters* (Vol. 15, Issue 3). Institute of Physics Publishing. https://doi.org/10.1088/1748-9326/ab6999

Vagheei, H., Laini, A., Vezza, P., Palau-Salvador, G., & Boano, F. (2023). Climate change impact on the ecological status of rivers: The case of Albaida Valley (SE Spain). *Science of the Total Environment*, *893*. https://doi.org/10.1016/j.scitotenv.2023.164645

van Vliet, M. T. H. et al., (2013). Global River Discharge and Water Temperature under Climate Change. *Global environmental change: human and policy dimensions,* 23(2), pp. 450-464.

van Vliet, M. T. H., Thorslund, J. & Strokal, M., (2023). Global river water quality under climate change and hydroclimatic extremes. *Nature Reviews: Earth & Environment,* Volume 4, pp. 687-702.

Wawrzyniak, V., Piégay, H., Allemand, P., Vaudor, L., Goma, R., & Grandjean, P. (2016). Effects of geomorphology and groundwater level on the spatio-temporal variability of riverine cold water patches assessed using thermal infrared (TIR) remote sensing. *Remote Sensing of Environment*, *175*, 337–348. https://doi.org/10.1016/j.rse.2015.12.050

Webb, B. W. & Zhang, Y., (1997). Spatial and seasonal variability in the components of the river heat budget. *Hydrological Processes,* 11(1), pp. 79-101.

Webb, B. W. et al., (2008). Recent advances in stream and river temperature research. *Hydrological Processes,* 22(7), pp. 902-918.

Webb, B. W., & Zhang, Y. (1999). Water temperatures and heat budgets in Dorset chalk water courses. *Hydrological Processes*, *13*(3), 309–321. https://doi.org/10.1002/(SICI)1099-1085(19990228)13:3<309::AID-HYP740>3.0.CO;2-7

Webb, B. W., (1996). Trends in stream and river temperature. *Hydrological Processes,* 10(1), pp. 205-226.

Westhoff, M. C., Bogaard, T. A., & Savenije, H. H. G. (2011). Quantifying spatial and temporal discharge dynamics of an event in a first order stream, using distributed temperature sensing. *Hydrology and Earth System Sciences*, *15*(6), 1945–1957. https://doi.org/10.5194/hess-15-1945-2011

White, J. C., Khamis, K., Dugdale, S., Jackson, F. L., Malcolm, I. A., Krause, S., & Hannah, D. M. (2023). Drought impacts on river water temperature: A process-based understanding from temperate climates. *Hydrological Processes*, 37(10). https://doi.org/10.1002/hyp.14958

Wu, W. & Wang, S.S., (2006). Formulas for sediment porosity and settling velocity. *Journal of Hydraulic Engineering*, 132(8), pp.858-862.

Chapter 2 Appendix

AWS sensor calibration

Sensors were first calibrated at the University of Birmingham prior to installation. These sensors were calibrated within groups of sensor type. For instance, first the thermistors used for measuring stream temperature were cross-calibrated together. Then the air temperature and relative humidity probes would be cross-calibrated. This involved wiring every sensor of a given type (e.g. 12x thermistors) into a single Campbell Scientific CR1000 data logger for testing. It was later found that a bias could potentially be introduced with the use of a different CR1000 data logger. As a result, when each AWS had been uninstalled from the study area, they were cross-calibrated once more at the University of Birmingham, but this time they were wired into the specific data logger they had been associated with in the field in order to account for this potential bias.

Cross calibration methods

For the cross-calibration, sensors were tested in a number of ways. Thermistors were placed in a beaker and filled with cold water at a temperature of 7 °C, then left in a warm room to increase in temperature to the room temperature of 15 °C over a period of six hours (see Figure 1). Observed temperatures at a 2-minute temporal resolution were then plotted in a timeseries and underwent a visual inspection. Of the 12 sensors tested, one was removed from the analysis as erroneous due to its persistent deviation from the remaining 11 sensor readings, with deviations greater than the ± 0.2 °C margin of instrument error associated with the thermistor. This deviation was not associated with the data logger used as each logger had four thermistors wired into it and the remaining three thermistors in this data logger showed strong agreement with means. The mean of the remaining thermistor readings was then used as the reference temperature against which RMSE, bias and standard deviation values of each sensor were calculated (see Table 1). These were found to be within the aforementioned margin of error so no correction factors were applied to these sensors.

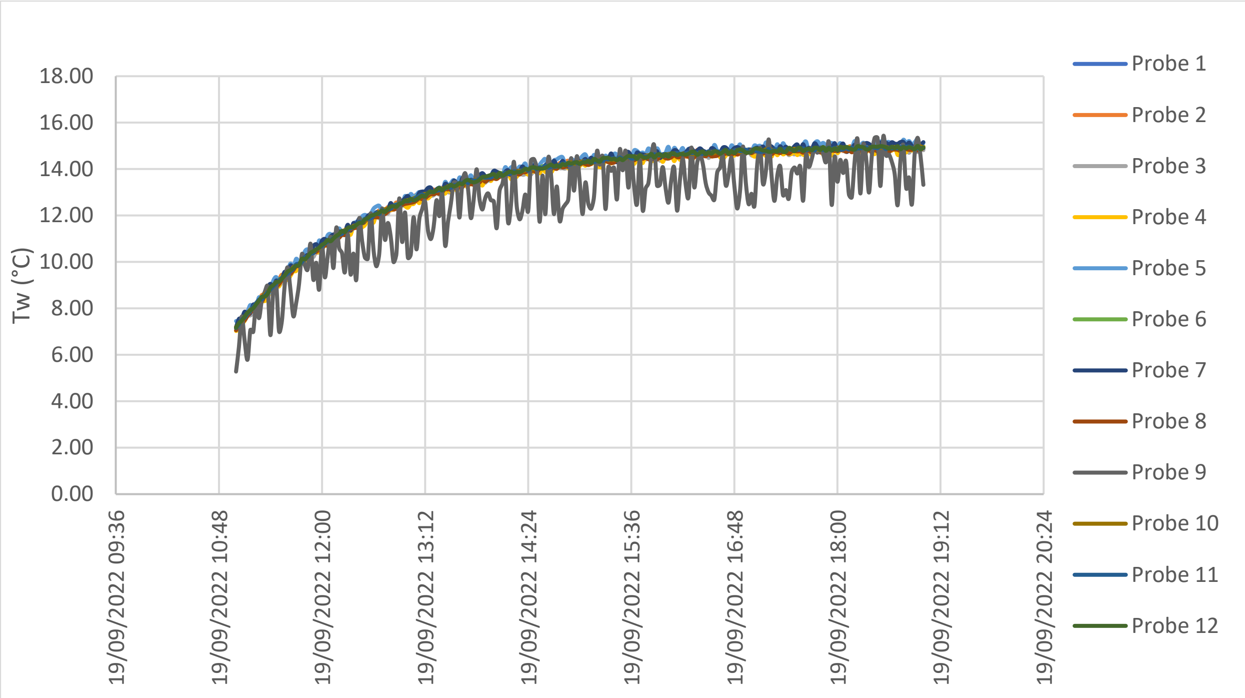

Figure 1 Thermistor calibration timeseries. Probe 9 was removed from the calibration process following visual inspection.

Wind speeds were measured using Vector Instruments A100R 3-cup anemometers. For the cross-calibration, as with the thermistors, these anemometers were tested indoors. Four sensors were tested at three distances from an electric fan at a set speed; first at 10cm from the fan, then at 20cm and finally at 30cm. Sensors were kept at each distance for a total of twenty minutes, with recordings taken at two minute intervals. Following a visual inspection of timeseries, no sensors were deemed to produce erroneous readings. The anemometers were found to show very strong agreement with a mean RMSE value calculated against the sensor mean of 0.02 ms^{-1}, well within the ± 0.1 ms^{-1} associated with the sensors (see Figure 2 and Table 1). As a result, no correction factors were applied to these sensors.

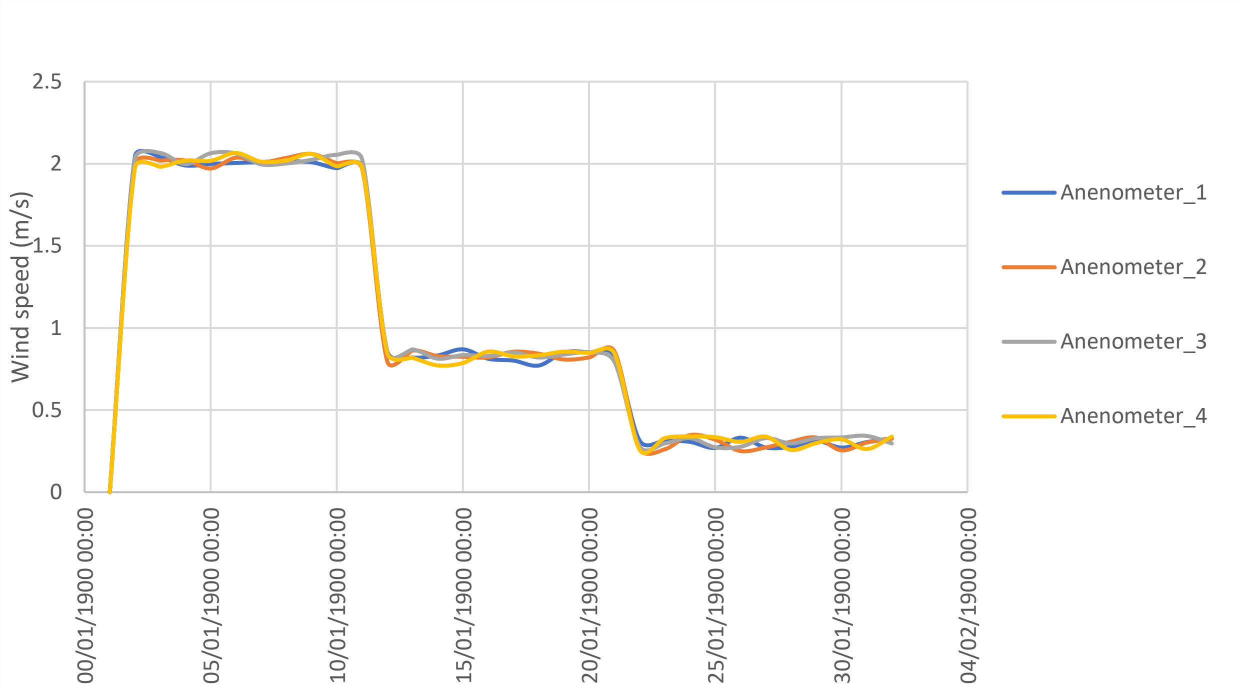

Figure 2 Anemometer calibration timeseries

Three Hukseflux HFP01 heat flux plates were cross calibrated within a laboratory environment, with each sensor placed on a uniform workbench surface over a one hour period. Each sensor had a unique multiplier associated with it, with these multipliers input into the CR1000 logger programme. Observations showed strong agreement with mean RMSE of 0.03 Wm^{-2} (see Figure 3 and Table 1). No further correction factors were applied to the sensors.

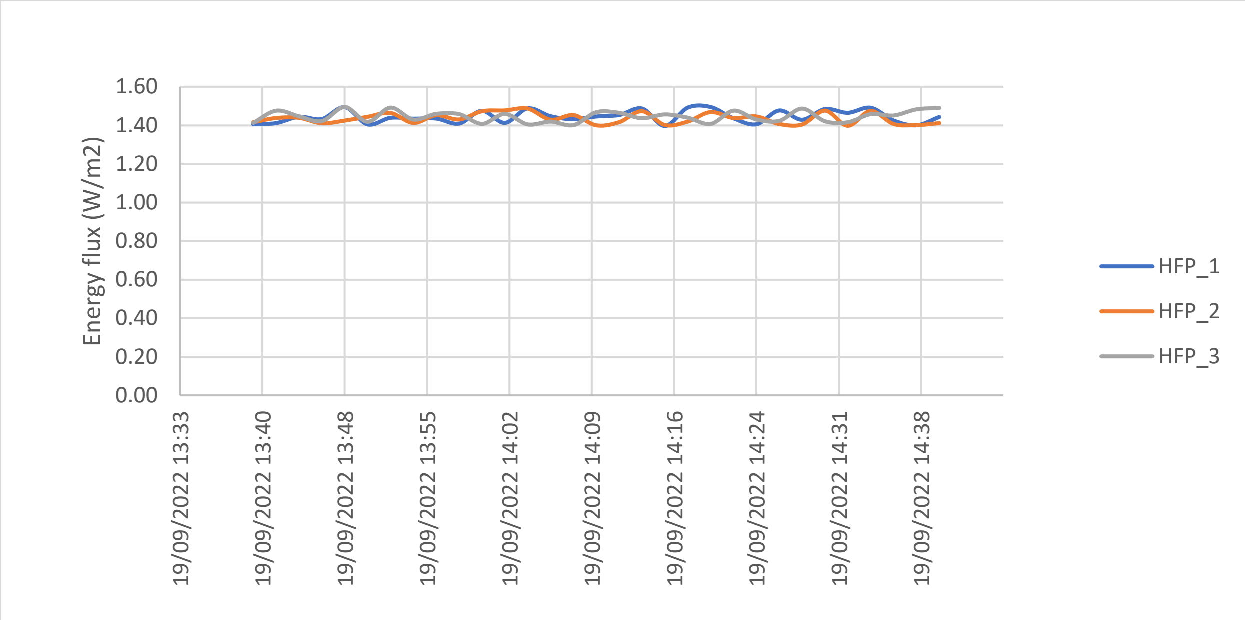

Figure 3 Heat flux plate calibration timeseries

Four air temperature and relative humidity sensors were cross-calibrated by installing along a single cross arm in the open air outside a University of Birmingham laboratory for a period of 18 days measuring at 15-minute intervals. Two of the sensors were Rotronic HC2S3 sensors and two were Vaisala HMP45C sensors. The probes showed strong agreement with one another for air temperature, with the newer Rotronic sensors showing slightly tighter grouping than Vaisala probes, but both models remaining within their advertised degrees of accuracy. Agreement was also found between sensors for relative humidity observations (see Figures 4, 5 and Table 1).

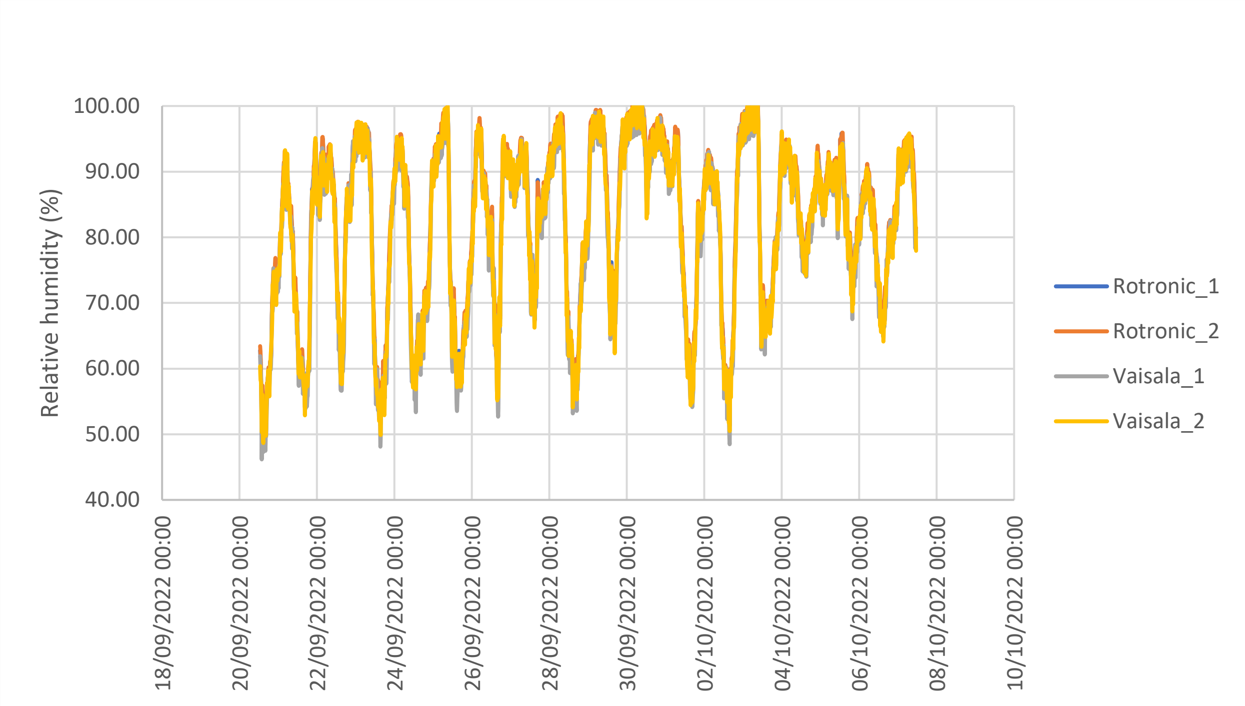

Figure 4 Relative humidity calibration timeseries

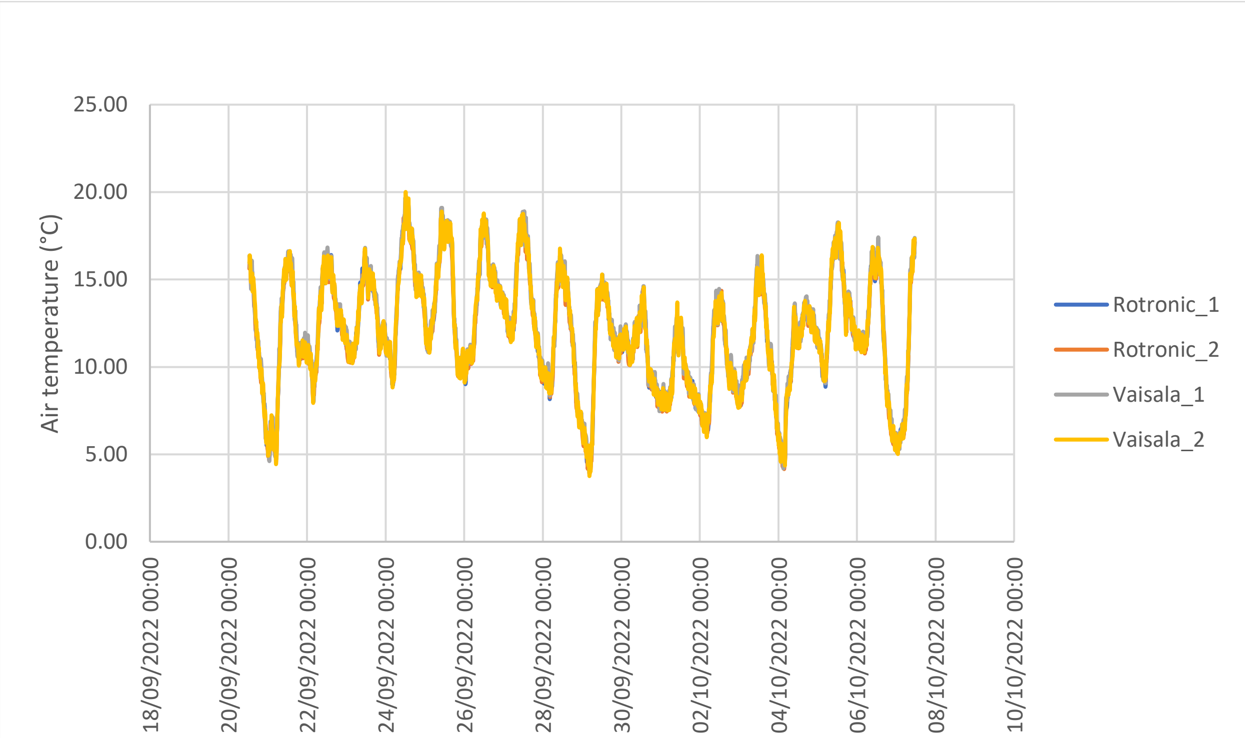

Figure 5 Air temperature calibration timeseries

During the same 18-day period, eight Skye SKS 1110 pyranometers were cross-calibrated alongside the air temperature and relative humidity probes. Due to a limited number of available sensor arms, for the first eight days of the 18 day period, four pyranometers were tested. These were then switched out for the four remaining pyranometers for the final ten days. Readings from these sensors had a systematic bias introduced for the mid to late morning and the late afternoon to early evening, associated with shading introduced from a fence to the east of the sensors and a treeline to the west. The fence and trees would begin to shade some pyranometers before others. When these short periods in the morning and evening were removed from analysis, sensors showed strong agreement with deviations from the mean falling within the 5% error margin associated with sensors (see Table 1). No correction factors were applied.

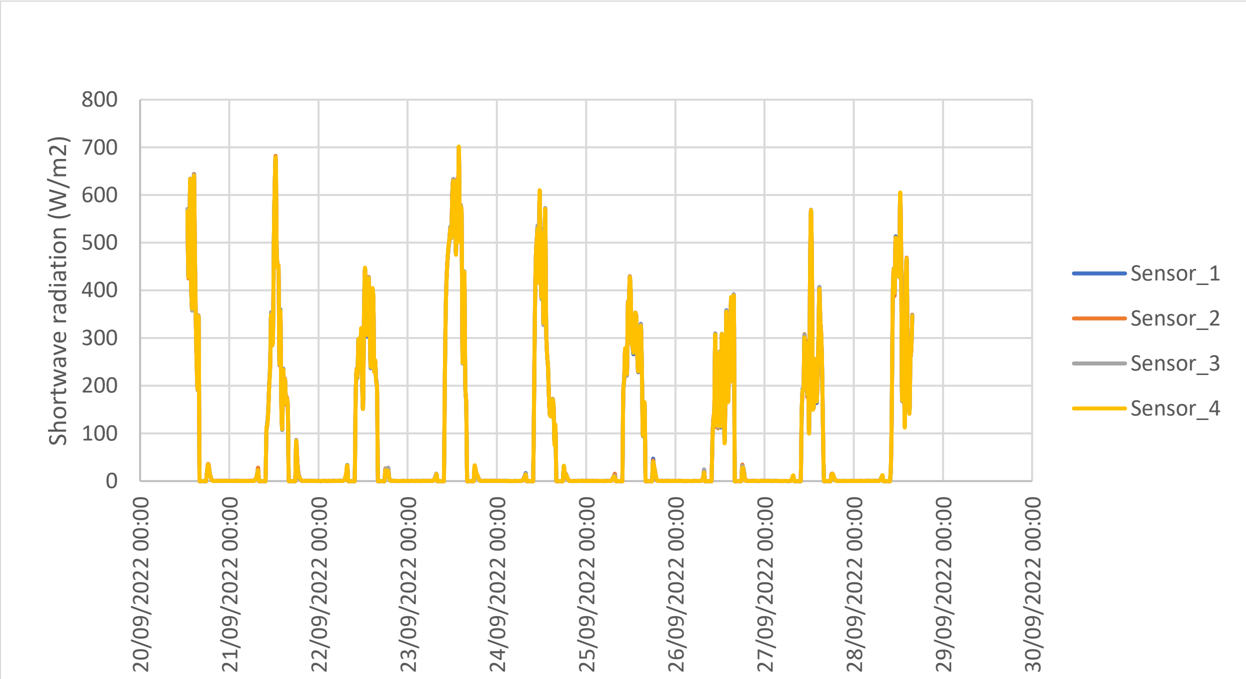

Figure 6 Pyranometer calibration timeseries (first four sensors)

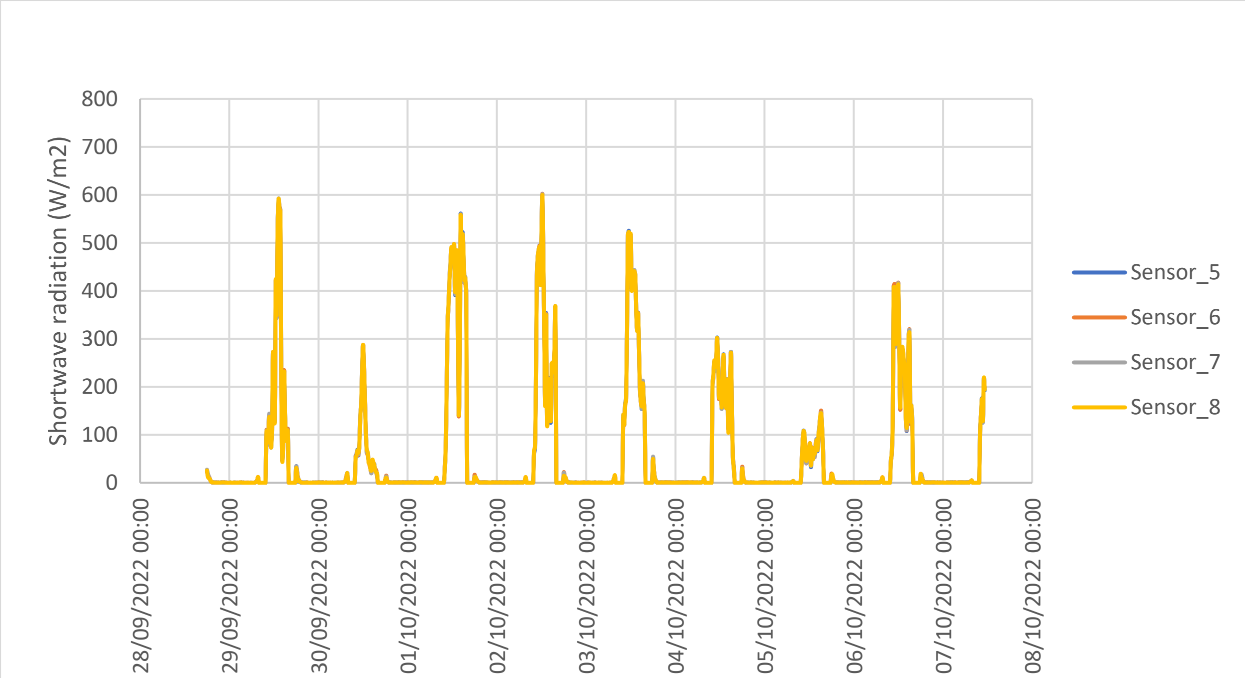

Figure 7 Pyranometer calibration timeseries (second four sensors)

Four Kipp and Zonen NR Lite- 2 net radiometers were also cross-calibrated for the 28-day period alongside pyranometers and air temperature and relative humidity probes. Each net radiometer had a unique factory-set calibration coefficient associated with it, which was input into the CR1000 logger code. As with the pyranometers, observations from the net radiometers experienced a systematic bias associated with shade introduced by a fence and tree line adjacent to sensors. The same treatment was applied to these sensors, after which, mean deviations for each sensor fell well within the 5% error of margin associated with the sensors (see Table 1). No further correction factors were applied to these sensors.

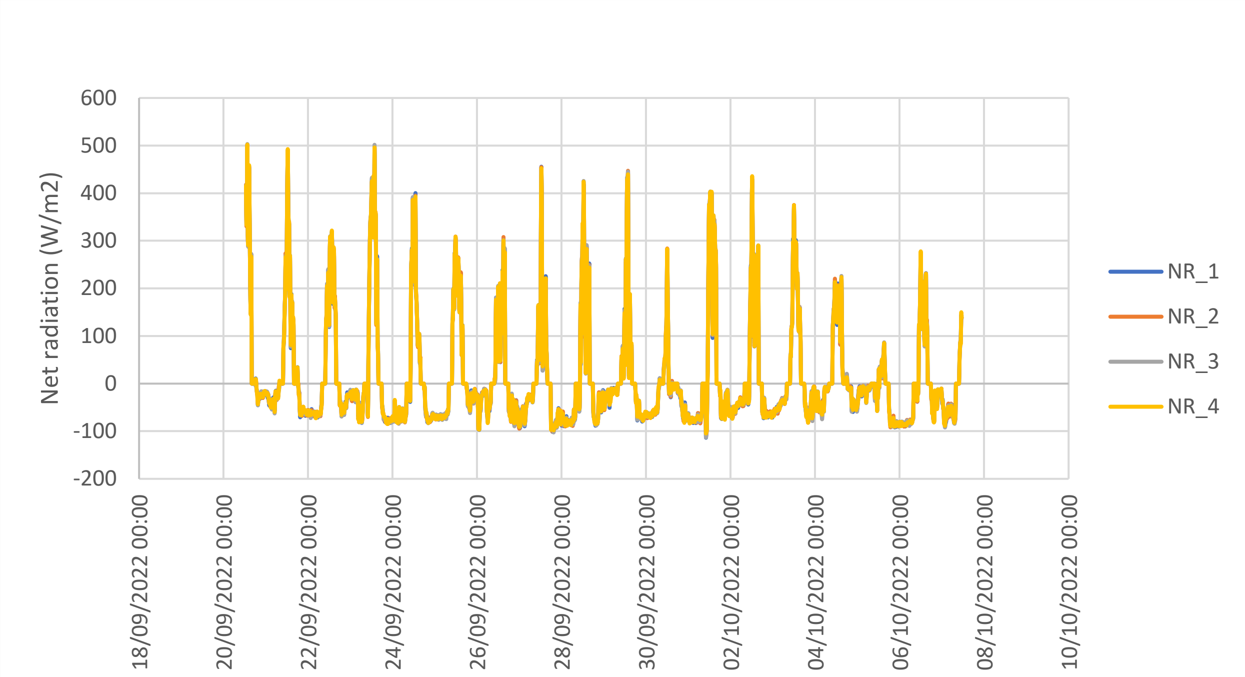

Figure 8 Net radiometer calibration timeseries

Table 1 Mean and range of RMSE, bias and standard deviation between sensors. The reference value against which said parameters are calculated is the mean of sensors, with the erroneous thermistor omitted from thermistor calculations.

Sensor	**Mean and range of RMSE**	**Mean and range of bias**	**Mean and range of SD**
Thermistor	0.09 °C (0.05 to 0.18)	0.05 °C (- 0.1 to 0.15)	0.03°C (0.01 to 0.06)
Anemometer	0.02 m/s (0.01 to 0.05)	0.01 m/s (-0.02 to 0.02)	0.01 m/s (0.01 to 0.02)
Heat flux plate	0.03 W/m2 (0.02 to 0.05)	0.01 W/m2 (-0.02 to 0.02)	0.01 W/m2 (0.01 to 0.02)
Relative humidity probe	1.48 % (0.76 to 2.86)	1.00% (-1.97 to 1.96)	0.48 % (0.31 to 0.98)
Air temperature probe	0.15°C (0.11 to 0.18)	0.05°C (- 0.15 to 0.11)	0.04°C (0.03 to 0.07)
Pyranometer	3.30 W/m2 (2.17 to 5.42)	2.03 W/m2 (-4.34 to 4.01)	1.5 W/m2 (1.14 to 3.08)
Net radiometer	4.34 W/m2 (3.21 to 7.46)	2.60 W/m2 (-5.03 to 4.14)	2.36 W/m2 (1.03 to 4.49)

Chapter 3 appendix

Table 1 Roving AWS site characteristics. Elevation was measured using a 5m DTM, stream widths and incisions were measured on site with a tape measure and comments on exposed sediment size and riparian trees were observed upon roving AWS installation

Roving Site	Elevation (mAOD)	Stream width (m)	Stream incision (m)	Degree/ size of exposed sediment	Riparian trees
1	500	6.2	3	High/ boulder	NA
2	472	5.2	< 0.5	High/ boulder	NA
3	450	6.4	< 0.5	High/ boulder	NA
4	431	8.5	< 0.5	High/ cobble	NA
5	412	7	1	High/ cobble	NA
6	400	10.4	< 0.5	High/ cobble	NA
7	392	20	< 0.5	Moderate/ v. coarse gravel	NA
8	388	11.5	< 0.5	Low/ v. coarse gravel	NA
9	381	16.5	1	NA	Mature deciduous, north (far) bank
10	376	16.2	1	NA	NA
11	372	14.1	1	NA	NA
12	361	10.6	1	High/ v. coarse gravel	NA
13	352	15.1	1	NA	NA
14	345	19.4	< 0.5	High/ v. coarse gravel	NA
15	339	16.7	< 0.5	High/ bedrock	Mature deciduous, west (near) bank

Table 2 Tabulated mean and standard deviation of observed differences in RH (relative humidity), Ta (air temperature) and Ws (wind speed) between the Clunie 2 reference site and Roving AWS sites

Metric	Roving Site	Mean difference	SD difference
RH	1	9.92	11.49
RH	2	5.35	3.77
RH	3	5.38	3.47
RH	4	4.54	3.00
RH	5	5.29	5.12
RH	6	4.88	3.10
RH	7	-0.96	3.86
RH	8	4.29	5.24
RH	9	6.31	2.80
RH	10	8.46	4.59

RH	11	5.01	1.95
RH	12	5.65	2.91
RH	13	0.08	2.58
RH	14	4.88	2.10
RH	15	5.34	4.32
Ta	1	-0.35	3.39
Ta	2	0.78	0.88
Ta	3	0.49	1.05
Ta	4	0.42	0.54
Ta	5	0.56	0.52
Ta	6	0.06	0.32
Ta	7	0.41	0.87
Ta	8	0.39	0.39
Ta	9	0.25	0.58
Ta	10	-0.13	0.86
Ta	11	0.17	0.29
Ta	12	0.03	0.76
Ta	13	-0.07	0.60
Ta	14	0.02	0.26
Ta	15	-0.18	0.94
Ws	1	0.32	0.73
Ws	2	0.24	0.79
Ws	3	0.16	0.67
Ws	4	0.36	0.95
Ws	5	1.05	0.67
Ws	6	-1.16	0.83
Ws	7	1.09	0.86
Ws	8	0.70	0.76
Ws	9	0.64	0.73
Ws	10	0.27	1.82
Ws	11	0.38	0.63
Ws	12	0.82	0.47
Ws	13	0.98	0.83
Ws	14	0.67	0.76
Ws	15	1.44	0.87

Chapter 5 appendix

Table 1 Mean and maximum reductions in shortwave radiation within each riparian planting scenario

Scenario	**Mean shortwave radiation reduction (MJ/m2)**	**SD shortwave radiation reduction (MJ/m2)**
Model_1	26.53	246
Model_2	19.69	197.36
Model_3	22.49	202.54
Model_4	18.86	190.74
Model_5	15.44	145.28
Model_6	26.4	246
Model_7	20.8	189
Model_8	19.28	213.48
Model_9	20.68	196.11
Model_10	25.11	246